The Dissertation Committee for Rahul Kumar Certifies that this is the approved version of the following dissertation:

Enhanced Oil Recovery of Heavy Oils by Non-Thermal Chemical Methods

Committee:

Kishore K. Mohanty, Supervisor

Gary A. Pope

Mojdeh Delshad

Upali Weerasooriya

Keith Johnston

Enhanced Oil Recovery of Heavy Oils by Non-Thermal Chemical Methods

by

Rahul Kumar, B.Tech., M.S.Che.E.

Dissertation

Presented to the Faculty of the Graduate School of

The University of Texas at Austin

in Partial Fulfillment

of the Requirements

for the Degree of

Doctor of Philosphy

The University of Texas at Austin

May 2013

Dedication

Dedicated to my parents for their love and support throughout my life.

Acknowledgements

I would like to express my sincere thanks to my supervisor, Dr. Kishore K. Mohanty for his tremendous support and constant encouragement, both personal and academic, throughout my studies at the University of Texas at Austin. His guidance and advice are greatly appreciated. I would like to extend my thanks to Dr. Gary Pope and Dr. Upali Weerasooriya for their advice on this project.

My special thanks to Dr. Eric Dao for helping me throughout my research work and always being ready to answer my questions and concerns. I wish to thank my colleagues Abhishek Gaurav, Himanshu Sharma, Gaurav Sharma, Peila Chen, Shashvat Doorwar, Ming Gu and Chie Kozaki for extending their help and cooperation to me and making my graduate life a memorable one.

I would also like to acknowledge Dr. Stephanie Adkins, Jith Liyange, Sriram Solairaj and Dr. Do Hoon Kim for their help and valuable advice on this project, Christopher Britton for helping me with the analytical measurements, Glen Baum and Gary Miscoe for helping me to install the experimental equipment and Roger Terzian for his help with the computer and the necessary softwares.

Finally I would like to thank my parents and all my friends for providing me the strength and moral support I always needed for getting me through a very special phase of my life.

Enhanced Oil Recovery of Heavy Oils by Non-Thermal Chemical Methods

Rahul Kumar, Ph.D.

The University of Texas at Austin, 2013

Supervisor: Kishore K. Mohanty

It is estimated that the shallow reservoirs of Ugnu, West Sak and Shraeder Bluff in the North Slope of Alaska hold about 20 billion barrels of heavy oil. The proximity of these reservoirs to the permafrost makes the application of thermal methods for the oil recovery very unattractive. It is feared that the heat from the thermal methods may melt this permafrost leading to subsidence of the unconsolidated sand (Marques 2009; Peyton 1970; Wilson 1972). Thus it is necessary to consider the development of cheap non-thermal methods for the recovery of these heavy oils.

This study investigates non-thermal techniques for the recovery of heavy oils. Chemicals such as alkali, surfactant and polymer are used to demonstrate improved recovery over waterflooding for two oils (A:10,000cp and B:330 cp). Chemical screening studies showed that appropriate concentrations of chemicals, such as alkali and surfactant, could generate emulsions with oil A. At low brine salinity oil-in-water (O/W) emulsions were generated whereas water-in-oil (W/O) emulsions were generated at higher salinities. 1D and 2D sand pack floods conducted with alkali surfactant (AS) at different salinities demonstrated an improvement of oil recovery over waterflooding. Low salinity AS flood generated lower pressure drop, but also resulted in lower oil recovery rates. High salinity AS flood generated higher pressure drop, high viscosity

emulsions in the system, but resulted in a greater improvement in oil recovery over waterfloods.

Polymers can also be used to improve the sweep efficiency over waterflooding. A 100 cp polymer flood improved the oil recovery over waterflood both in 1D and 2D geometry. In 1D geometry 1PV of polymer injection increased the oil recovery from 30% after waterflood to 50% OOIP. The tertiary polymer injection was found to be equally beneficial as the secondary polymer injection. It was also found that the combined application of AS and polymer did not give any major advantage over polymer flood or AS flood alone.

Chemical EOR technique was considered for the 330cp oil B. Chemical screening studies showed that microemulsions could be generated in the system when appropriate concentrations of alkali and surfactant were added. Solubilization ratio measurement indicted that the interfacial tension in the system approached ultra-low values of about 10^{-3} dynes/cm. The selected alkali surfactant system was tested in a sand pack flood. Additionally a partially hydrolyzed polymer was used to provide mobility control to the process. The tertiary injection of ASP (Alkali-Surfactant-Polymer) was able to improve the oil recovery from 60% OOIP after the waterflood to almost 98% OOIP.

A simple mathematical model was built around viscous fingering phenomenon to match the experimental oil recoveries and pressure drops during the waterflood. Pseudo oil and water relative permeabilities were calculated from the model, which were then used directly in a reservoir simulator in place of the intrinsic oil-water relative permeabilities. Good agreement with the experimental values was obtained.

For history matching the polymer flood of heavy oil, intrinsic oil-water relative permeabilities were found to be adequate. Laboratory data showed that polymer viscosity

is dependent on the polymer concentration and the effective brine salinity. Both these effects were taken into account when simulating the polymer flood or the ASP flood.

The filtration theory developed by Soo and Radke (1984) was used to simulate the dilute oil-in-water emulsion flow in the porous media when alkali-surfactant flood of the heavy oil was conducted. The generation of emulsion in the porous media is simulated via a reaction between alkali, surfactant, water and heavy oil. The theory developed by Soo and Radke (1984) states that the flowing emulsified oil droplets clog in pore constrictions and on the pore walls, thereby restricting flow. Once captured, there is a negligible particle re-entrainment. The simulator modeled the capture of the emulsion droplets via chemical reaction. Next, the local water relative permeability was reduced as the trapping of the oil droplets will reduce the mobility of the water phase. This entrapment mechanism is responsible for the increase in the pressure drop and improvement in oil recovery. The model is very sensitive to the reaction rate constants and the oil-water relative permeabilities.

ASP process for lower viscosity 330 cp oil was modeled using the UTCHEM multiphase-multicomponent simulator developed at the University of Texas at Austin. The simulator can handle the flow of three liquid phases; oil, water and microemulsion. The generation of microemulsion is modeled by the reaction of the crude oil with the chemical species present in the aqueous phase. The experimental phase behavior of alkali and surfactant with the crude oil was modeled using the phase behavior mixing model of the simulator. Oil and water relative permeabilities were enhanced where microemulsion is generated and interfacial tension gets reduced. Experimental oil recovery and pressure drop data were successfully history matched using UTCHEM simulator.

Table of Contents

List of Tables

List of Figures

CHAPTER 1: INTRODUCTION

1.1 MOTIVATION

The age of cheap oil is over. (World Energy Outlook 2010). The energy price is a combined result of the energy demand and supply. The future price depends on the rising energy needs of the ever growing world population and the diminishing production from hydrocarbon reservoirs. Figure 1.1 compares the energy price steadily rising for at least two energy policy scenarios. In the 'new policies' scenario, where both the existing policies and the declared intentions of the governments are taken into account, energy prices are projected to rise steadily from 2010 to 2035, though not as fast as they would if only the current government policies are taken into account. Only in the 450 scenario, where it is assumed that the future government policies will aim to restrict the concentration of greenhouse gases in the atmosphere to 450 parts per million of CO_2 equivalent and global temperature rise to 2^0C, the energy prices may remain stable.

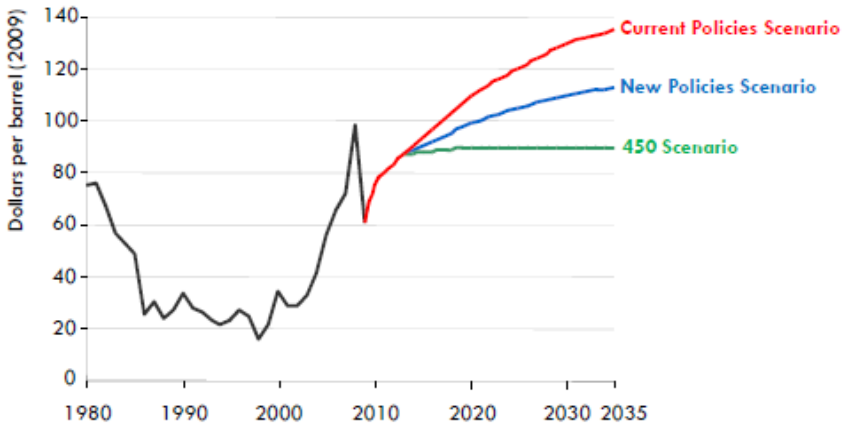

Figure 1.1: Crude oil price steadily rising 2010 onwards under current energy policies scenario. *Source: World Energy Outlook 2010*

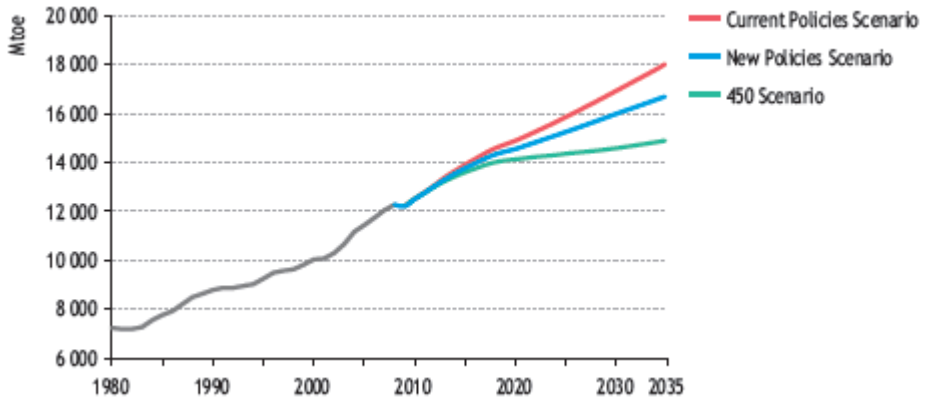

Figure 1.2: World energy demand by scenario. *Source: World Energy Outlook 2010*

Figure 1.2 indicates that the energy demand will continue to rise in all the different scenarios. While the increasing energy demand can be met in part by developing renewable energy sources, fossil fuels will still play a major role in meeting the energy demands. However the conventional oil reserves are expected to decline as the companies and governments go after the easy oil before opting for more difficult oil. As the production of conventional oil declines around 2020 there will be a need to develop unconventional oil (heavy oil, bitumen and shale oil) resources economically so as to meet the energy demands of the world.

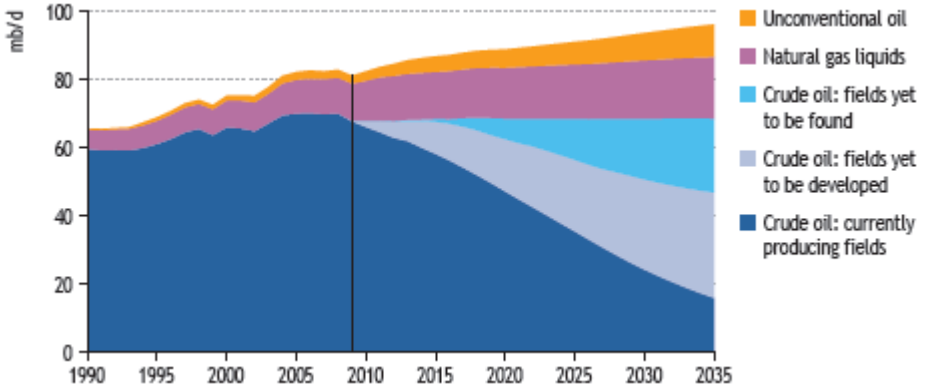

Figure 1.3: World oil production. *Source: World Energy Outlook 2010*

DOE estimates that the USA heavy oil resource is approaching 100 billion barrels of OOIP. Around 80 billion barrels of this heavy oil is concentrated in the states of California, Alaska and Wyoming. (DOE office of Petroleum Reserves-Strategic Unconventional Fuels, Jun 2007).

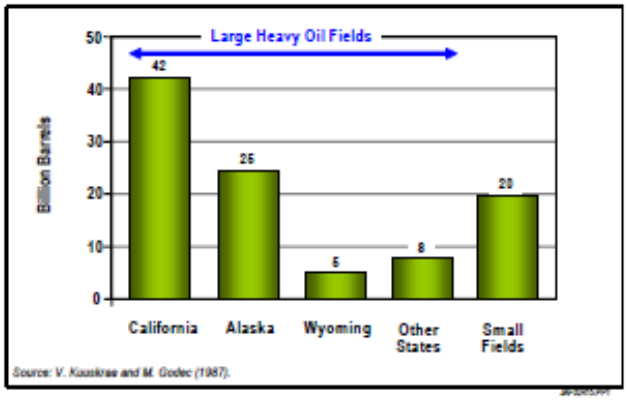

Figure 1.4: Distribution of US heavy oil resources. *Source: DOE Report 2007*

Developing the suitable technology to tap into this heavy oil resource successfully will prove very beneficial for the future energy demands. The north slope of Alaska contains about 20 billion barrels of viscous oil in the reservoirs of Ugnu, West Sak and the Shraeder Bluff reservoirs. These reservoirs overlie the already producing reservoirs of Kuparuk and the Milne Point (Hallam and Plekenbrock 1992) and underlie the permafrost. The application of the thermal methods such as steam flooding, SAGD etc. is a natural choice for improving the recovery of these viscous oils. The proximity of these shallow reservoirs to the permafrost makes the application of thermal methods for the oil recovery very unattractive. It is feared that the heat from the thermal methods may melt this permafrost leading to subsidence of the unconsolidated sand (Marques 2009; Peyton 1970; Wilson 1972). Thus it is necessary to consider the development of cheap nonthermal methods for the recovery of the viscous oils

Conventional oil reservoirs are often developed (or depleted) through waterflooding the reservoir. The recoveries obtained are about 30-40% at the field scale and can be as high 60-70% at the laboratory scale. Waterflood application for the heavy oil, albeit possible is expected to suffer from lower oil recoveries both at the laboratory scale and the field scale (Jennings 1996, Kumar et.al. 2005, Miller 2006, Bryan et.al. 2008) due to a large contrast in viscosities between water (1 cp) and the heavy oil (>10,000 cp) leading to poor sweep efficiency.

One method of improving the sweep of the heavy oil without injecting any heat into the reservoir is to use chemicals such as alkali and surfactant. Laboratory tests have shown that the chemicals have the potential of generating emulsions between oil and water. Several studies have shown that the emulsions, either generated in situ or injected externally have the tendency to block the swept out pores and divert the flow to the bypassed region. On the other hand, in some other situations emulsions help to entrain the oil into the flowing aqueous phase. Both the conditions lead to improved sweep after waterflooding.

Polymers have been widely used in the petroleum industry to improve the sweep of the oil during a waterflood or a chemical flood. The heavy oil reservoirs suffer from poor sweep efficiencies and viscous fingering effects due to very large viscosity ratios. The use of polymers will reduce the viscosity ratio and may help in improve the sweep of the waterflood.

1.2 OBJECTIVE OF THE RESEARCH

The present study aims to study the benefits of using alkali, surfactant and polymer for enhancing the recovery of the heavy oil. Some specific objectives can be summarized as:

1. To evaluate whether alkali and surfactant have the potential to generate emulsions with the heavy oil. Conditions are evaluated which generate Oil in Water (O/W) emulsions as opposed to the (W/O) Water in Oil emulsions. Brine salinity was found to be a key factor responsible for controlling the specific emulsion type in the system.
2. To evaluate the benefits and drawbacks of the O/W emulsions and W/O emulsions in improving the heavy oil recovery. Here the displacement experiments are conducted under different conditions of brine salinity. Different salinities result in different kinds of emulsions in-situ. Details of the experiments and the results are given in Chapter 4.
3. To evaluate the role of polymer for improving the sweep efficiency over waterflooding. Polymer injection is considered in the secondary and the tertiary mode. The displacement experiments have been conducted both in 1D and 2D geometry. The 2D geometry is chosen to better understand the role of polymers in improving the areal sweep efficiency.
4. To model and simulate the experiments to better understand the mechanisms responsible.

1.2 DESCRIPTION OF CHAPTERS

The dissertation is divided into a total of 6 chapters. Chapter 2 gives a literature review on chemical flooding in general. Special emphasis is given to the use of alkali, surfactant and polymer for the improvement in oil recovery over waterflooding. The chapter discusses the subject matter on emulsions and microemulsions. The Chapter 3 gives the description of materials used and the methodologies adopted for conducting the research. The

Details of the experiments conducted for this research are given in Chapter 4. The chapter examines the research objectives set a forth. The development and testing of the alkali surfactant systems for two heavy oils is given in separate sections. The chemical screening studies are followed by the sand pack floods. Chapter 5 discusses the development of the mathematical models and the simulations conducted to history match the experimental results. Different simulation techniques are used for the two heavy oils. The simulations help in the better understanding the mechanisms that are involved in the recovery process. On the basis of the experimental results, some conclusions were drawn from this study. These are summarized in the Chapter 6. Recommendations for the future work, which can enhance the knowledge and understanding of the subject matter, are also discussed.

CHAPTER 2: LITERATURE SURVEY

Chemical EOR (Enhanced Oil Recovery) processes have gained attention in the last few decades owing to the improvement in oil recovery provided over waterflooding. These processes involve the use of chemicals such as alkali, surfactant and polymer for enhancing the recovery of oil over waterflood. Surfactants reduce the interfacial tension between oil and water, as a result of which the capillary forces impeding the flow of oil droplets through the reservoir, gets reduced and additional oil can be mobilized. Alkali reacts with the organic acids in the crude oil to generate in-situ soaps which work alongside surfactants in reducing the interfacial tension. A water soluble polymer is often injected either by itself or with the alkali surfactant solution to make the injected phase more viscous. This aids in improving the mobility contrast of the process and achieving higher oil recovery rates. The present chapter reviews the development of the chemicals EOR processes over the last few decades.

The chapter is divided into several sections. The first section describes the role of alkalis in generating in situ emulsifying agents and aid in oil recovery. The second section reviews the use of polymers in the petroleum industry for providing a better mobility control to the displacement process. In the third section, the benefit of using a combination of all the chemicals is discussed. This process is usually referred to as the ASP (Alkali Surfactant Polymer) process where microemulsions, with ultra-low interfacial tensions are generated. The last section describes the phenomena of viscous fingering which occurs in cases where viscous oils are displaced by low viscosity driving fluids such as water or solvents.

2.1 IMPROVED OIL RECOVERY BY USING ALKALI

The potential of alkali in improving the oil recovery was realized as early as 1917 (Squires, 1917). He found out that the displacement of oil by water can be made more complete by adding alkali to the water. Atkinson (1926) discovered that when strong alkalis such as caustic soda (NaOH), soda ash (Na_2CO_3) or caustic potash (KOH) are used to treat the oil bearing sands; it is easier to remove the oil completely from the sands in a shorter period of time than otherwise. He concluded that the application of alkalis has made it easier to overcome the forces of adhesion, capillarity and viscosity which retain the oil to the oil wet sands. Nutting (1925) described the role of alkali salts such as sodium carbonate and sodium silicate in improving the performance of the waterflood. He however discouraged the use of strong alkalis for field use as these alkalis would react too fast with the crude oil and thus be used up before being transported over sufficient enough distances in the reservoir. Some of the other early authors also found improvements in oil recovery with different alkalis. However, the underlying mechanisms by which alkalis help to improve the oil recovery were not clearly understood. Squires did not provide any reason for his observations. Atkinson pointed out that the alkali treatment could be helping in overcoming the forces of adhesion and capillarity. He seems to be talking about wettability change and interfacial tension reduction as the main mechanisms. Nutting, on the other hand identified wettability alteration to a more favorable water wet state to be a main mechanism. Subkow (1942) claimed that the action of alkali on bitumen resulted in a low interfacial tension and led to a subsequent entrainment of bitumen in the flowing aqueous phase. He also described the reaction between the naturally occurring acids in the crude oil with the injected alkali producing in-situ soaps which act as emulsifying agents. He mentioned that the solute (alkali in this case) could be as low as 0.1% to as high as 2-3% for formation of the

proper kind of emulsion. Using too high an alkali concentration could produce the inverted emulsion or an emulsion requiring highly rigorous treatment to yield the original bitumen.

2.1.1 Main Mechanisms

Johnson (1976) summarized the main mechanisms enhanced oil recovery by alkaline flood. These were:

1) Emulsification and entrainment
2) Wettability reversal (oil wet to water wet state)
3) Wettability reversal (water wet to oil wet state)
4) Emulsification and Entrapment

Emulsification and entrainment:

Subkow (1942) claimed that the injected alkali could react with the acids in the bitumen and produce in situ soaps acting as the emulsifying agents. These agents were helpful in entraining the bitumen in the flowing aqueous phase. However it was also suggested that for the formation of the desired Oil in Water (O/W) emulsions it is necessary that the alkali concentration lies in a certain range.

Reisberg and Doscher (1956) also emphasized the formation of the O/W emulsions as a result of the lowering of the interfacial tension as the basic mechanism responsible for the production of the Ventura crude oil as an emulsion in the caustic solution. However they also warned that the alkali adsorption, reaction with the rock and the displacement of the connate water could result in the alkali front falling behind the oil water displacement front. This could delay the recovery of any additional oil till several pore volumes of the alkali have been injected.

Wettability reversal (Oil wet to a water wet state)

Wagner and Leach (1959) found out in laboratory experiments that the wettability of the rock could be altered from oil wet to water wet state by the action of pH altering agents such as alkali, acids and some salts. The oil recovery improved and the producing WOR could be lowered by this action. They argued that the alteration of the wettability to a more water wet state lowers the water relative permeability and increases the oil relative permeability. This leads to an improvement in the mobility ratio between oil and water. For the cases where viscous fingering is occurring, the wettability reversal can lower the WOR for some time until it inevitably rises again. Mungan (1966), Cooper (1971) and Ehrlich *et.al.* (1974) also observed the improvement in oil recovery due to wettability reversal mechanism.

Wettability reversal (water wet to an oil wet state)

Cooke *et.al.* (1974) found out the reservoir rock wettability can also change from water wet to an oil wet state by sodium hydroxide if proper conditions of salinity, pH and temperature are maintained. Simultaneous generation of in situ soaps by reaction of alkali and the petroleum acids leads to ultralow interfacial tensions. The wettability alteration converts the discontinuous non wetting residual oil to a continuous wetting phase which can now flow rather than getting trapped. The low interfacial tension in conjunction with the wettability reversal to an oil wet state generates the Water in Oil (W/O) emulsion. The emulsion droplets tend to block flow and induce the high pressure gradients in the regions where they form. The high pressure gradients in turn overcome the capillary forces already weakened by the low interfacial tension. Hence, very low residual oil saturations could be obtained.

Emulsification and entrapment

Jennings *et.al.* (1974) found in their lab experiments that in some cases where the interfacial tension is low enough and the residual oil can be emulsified in situ, the emulsion droplets moving downstream with the caustic solution may get entrapped by the pore throats which are small enough for the emulsion droplets to pass through. The mobility of the water phase is thus lowered which improves the vertical and the areal sweep efficiencies. Hence in waterfloods of the viscous oil where the sweep efficiency is poor due to by passing, entrapment of the emulsion droplets can provide a potential solution. McAuliffe (1973a, 1973b) showed evidence suggesting that the oil recovery could be improved by injecting oil in water (O/W) emulsion in a very similar way as with the emulsions generated in situ. Dranchuk *et.al.* (1974) working with the viscous Lloydminster crude oil reported the generation of O/W emulsions in situ and lowering of the water relative permeability during displacement.

It is generally agreed that for the caustic flooding to work successfully by a particular mechanism, the crude oil should have sufficient organic acids which can react with the pH altering agents such acid or alkali and produce soaps (Johnson, 1976; Jennings *et.al.*, 1974). The chemical composition of the water phase also plays an important role in determining the success of the caustic flood. Presence of significant amounts of divalent ions such as Ca^{2+} and Mg^{2+} in the caustic slug may lead to precipitations. Thus presence of divalent ions in the caustic slug should be avoided. The rock reactivity with alkali is important for the favorable changes in wettability. Too much consumption of alkali on the rock can delay the alkali front and can even render the alkali process ineffective. The size of the alkali slug should be decided taking the adsorption effects into consideration. Alkali concentration in the slug should be selected based on the recovery mechanism to be used. Johnson (1976) pointed out that low alkali

concentrations ranging from 0.1 to 0.5wt% was generally sufficient for emulsification mechanisms whereas higher concentrations ranging from 0.5 to 3% or even higher might be required for the wettability reversal mechanisms. Symonds *et.al.* (1991) conducted alkali flooding on the Wainright crude oil (408.3 cp, 941 kg/m3) in a sandpack at alkali concentrations of 0.1wt% and 0.01wt%. Based on the observations of the oil recovery and the effluent concentrations, they suggested that emulsification and entrainment was the dominant mechanism when the alkali concentration was 0.1wt% whereas emulsification and entrapment was the mechanism when a low alkali concentration of 0.01wt% was used.

The generation of in situ emulsions in the porous media is an important aspect of the alkali flooding. This aspect of alkali flooding has been explored in the present study. In the next section a literature review on emulsions has been presented. The factors which influence the type of emulsion are discussed along with some of the key properties.

2.1.2 Emulsions

Definition

Emulsions, also called macroemulsions are dispersions of one liquid into another liquid immiscible with the first liquid. Alvorado and Marsden (1979) describe the role of a third component called emulsifier in the generation and sustenance of an emulsion. The emulsifier should (1) decrease the interfacial tension between the two immiscible liquids, thus enabling the generation of an interface between the two fluids and (2) stabilizing the generated interface against forces of coalescence. The oil water emulsions can be of three kinds:

a) Oil in Water (O/W) emulsions: These emulsions consist of droplets of oil dispersed in the external water phase. In general the viscosity of these emulsions is higher than the water phase but lower than the constituent oil phase.
b) Water in Oil (W/O) emulsions: These emulsions are generated by the droplets of water dispersed in the oil phase. In general the viscosity of these emulsions is higher than the oil phase.
c) Multiple or complex emulsions

Factors influencing the type of emulsion

Generation of one particular type of emulsion as opposed to the other depends on the number of factors. As a thumb rule, when one phase is present in a very small volume as compared to the other phase, the phase with a smaller volume becomes the dispersed phase (Kokal, 2002). Other important factor to consider is the property of the emulsifier (usually surfactant or a mixture of surfactants). Bancroft's rule states that the phase in which the surfactant is more soluble forms the continuous phase (Ruckenstein, 1996) and the other phase becomes the droplet phase. Sun and Shook (1995) discuss the stability of O/W emulsions. These emulsions are stabilized by the hydrophilic character of the surfactants. The hydrophilic and the hydrophobic character of the surfactant is determined by the polarity of the surfactant molecule; the relation between the contribution of the polar head group and the non-polar hydrophobic tail. Ottewill (1967) suggested that longer ethylene oxide chains would enhance the hydrophilic character of the surfactant. Inversion of an O/W emulsion to a W/O emulsion may occur if the balance between the hydrophilic and the hydrophobic character of the surfactant is reversed. This may happen when either the temperature of the mixture is raised (Winsor, 1954 and

Shinoda, 1967) or the amount of electrolytes dissolved in the aqueous phase is increased (Salager *et.al.*, 2000).

Viscosity of Emulsion

The viscosity of emulsion is often higher than the viscosity of the continuous phase. O/W emulsions have a viscosity which is higher than the aqueous phase but much lower than the oil phase. W/O emulsions, on the other hand have a higher viscosity than the oil itself. Kokal (2002) have identified the factors which determine the viscosity of the emulsions. These include:

1) Viscosities of oil and water
2) Volume fraction of the dispersed phase
3) Shear rate
4) Temperature
5) Droplet size distribution

Due to the low viscosity of the O/W emulsions, these have been used in the pipeline technology in order to transport heavy oil crudes. Sun and Shook (1995) gave emphasis on avoiding the inversion of emulsions at any time in the pipeline flow as these would cause extraordinarily high pressure drops. However there are a few examples of W/O emulsions as viscosity enhancing agents in the oil industry.

Stability of Emulsions

Kokal (2002) identified emulsions as thermodynamically unstable systems where there is a natural tendency for the droplets to come together and coalesce over a period of time. This phenomenon is thermodynamically favored as it reduces the interfacial energy of the system. However, most emulsions are stable for a period of time, in other words they are said to possess kinetic stability. Emulsions which are stable only for a few minutes are

called loose emulsions. Emulsions stability can be increased by adding emulsifiers such as surfactants. Some emulsifiers like asphaltenes are naturally occurring in the crude oil. Emulsifiers tend to increase the kinetic stability of the emulsions so that they can remain stable over days, weeks or even months. These emulsions were called tight emulsions by Kokal (2002).

Emulsion Flow

McAuliffe (1973) depicts the flow of emulsions in the porous media with the help of a cartoon of an oil droplet flowing through a pore constriction. The size of the pore constriction is smaller than the droplet size. Moreover the capillary pressure at the leading portion of the droplet is higher than the capillary pressure at the trailing edge due to a difference in the radii of curvature and hence an external pressure is required to force the droplet through the pore. This is called Jamin effect (Jamin, 1861) and becomes more significant as the concentration of droplets in the aqueous phase increases.

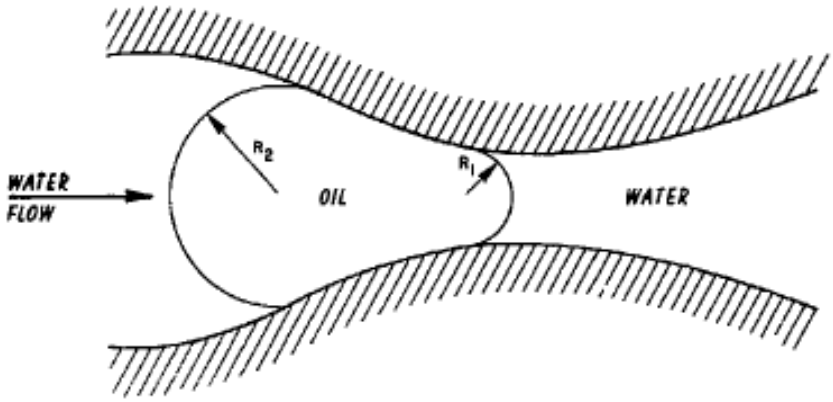

Figure 2.1: An oil droplet entering the pore constriction (Jamin, 1861)

When the droplet sizes are slightly higher than the pore throat constrictions, they can block off the high permeability zones or the swept out zones after a waterflood.

Emulsions can also restrict the flow in the viscous fingers formed after the waterflood of viscous oils. Due to this kind of restriction, the injected fluid has a chance to flow into a less permeable or a bypassed zone, thus increasing the sweep efficiency of the process. This mechanism is known as the emulsification with entrapment. The experiments conducted by McAuliffe (1973) also indicated that the oil in water emulsions could reduce the water permeability if the absolute permeability were less than 2 darcies and that the permeability reduction effect was retained even after several pore volumes of water was injected.

On the other hand if the emulsion droplets are smaller than the pore throat constriction sizes, another mechanism called emulsification with entrainment is dominant. Here instead of blocking the pores, the emulsion droplets are produced as oil in water emulsions themselves. Soo and Radke (1984) applied the filtration model to predict the flow of dilute O/W emulsions in the porous media.

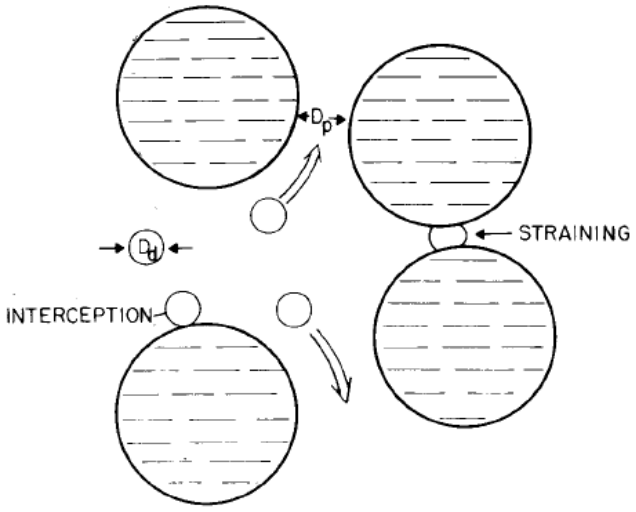

Figure 2.2: The mechanism of the dilute emulsion flow in the porous media by Soo and Radke (1984)

Figure 2.2 illustrates the flow of a dilute emulsion as visualized by the filtration theory. Droplets larger than the pore throat sizes clog those constrictions. This capture mode is called straining. Additionally droplets smaller than the pore sizes may also get captured on the pore walls by Vander Walls forces. This capture is called interception. The overall effect is the decrease in the water permeability in the flooded pores and thus the diversion of the fluid to the low permeability or the bypasses zones. The model for the droplet capture and the permeability reduction was coupled with the classical Buckley-Leverett two phase flow model in order to predict the transient displacement calculations.

2.1.3 Field tests

Johnson (1976) has summarized the results of various alkali flood field trials. Alkali concentrations of 2-3 wt% were used. The oil cuts increased from 5-6 % OOIP to 9-17 % OOIP as a result of alkali treatment. However, the field tests described is for lighter oils with the highest oil viscosity being 40 cp.

2.2 IMPROVED OIL RECOVERY BY USING POLYMER

Waterflooding of the viscous oils and heavy oils leave behind a large amount of oil unswept due to the adverse impact of viscous fingering. Presence of the reservoir heterogeneity further hampers the oil recovery. Reducing the mobility ratio holds the key to improving the oil recovery. The beneficial impact of using a viscous water slug and reducing the mobility ratio of the displacement process was realized by early authors (Aronofsky, 1952; Dyes *et.al.* (1952) and Barnes (1962)). Moreover for heavy oil reservoirs where applying thermal methods may pose environmental problems, polymers can be safely used to improve the oil recovery.

Detling (1944) was one of the early researchers who proposed increasing the viscosity of water to improve the mobility ratio of the process. Pye (1964) and Sandiford

(1964) established that the mobility of water can be reduced efficiently by adding a small quantity of a water soluble polymer. Since then a large number of laboratory and field studies have appeared in the literature Jewett and Schurz (1970) reviewed the application of polymer in 61 field projects. Chang (1978) and Needham and Doe (1987) also presented excellent reviews on the status of polymer application and its future potential.

2.2.1 Polymer Types and Main Properties

There are generally two types of polymer used in petroleum industry: a synthetic polymer, partially hydrolyzed polyacrylamide; and a biopolymer, xanthan gum. Each has its own advantages and disadvantages.

Polyacrylamides are manufactured by polymerization of acrylamide monomer. A polyacrylamide having higher molecular weight can produce higher viscosity and resistance factor, but it is more susceptible to mechanical degradation. Since polyacrylamide adsorbs strongly onto rock surface, the polymer is usually partially hydrolyzed to reduce adsorption. A partially hydrolyzed polyacrylamide is produced by converting some of the amide groups (NH_2) to carboxyl groups (COO-). The fraction of the converted amide group is defined as the degree of hydrolysis, usually ranging from 15% to 35%. Higher degree of hydrolysis can reduce the adsorption of polymer on solid surface, and increase viscosity in fresh water. But the polyacrylamide with higher degree of hydrolysis will be more salt sensitive. In high salinity environment, the polyacrylamide molecules may change from somewhat distended to nearly spherical shape, resulting in dramatically decrease in viscosity

Xanthan gum is produced from a fermentation process. The main advantages of xanthan gum are the insensitivity to salinity and tolerance to mechanical shearing. The

stiffness of xanthan gum molecule provides higher viscosity even in high salinity brine which makes it resistant to shear degradation.

2.2.2 Polymer rheology

Polymer solutions are generally non-Newtonian fluids. For very low to moderate shear rates, polymers exhibit a shear thinning behavior. Power-law model is commonly used to represent its rheological property in the shear thinning regime. (Green and Willhite, 1998):

$$\mu = K\dot{\gamma}^{(n-1)} \tag{2.3}$$

where μ is apparent viscosity, *K* is power-law constant, *n* is power-law exponent, and γ& is shear rate.

Overall rheological behavior of the polymer solution over a wide range of shear rates may be modeled using the Carreau model (Eqn 2.4).

$$\frac{\mu-\mu_\infty}{\mu_o-\mu_\infty} = \left(1+\left(\frac{K}{\mu_o}\right)^{\left(\frac{2}{n-1}\right)}\dot{\gamma}^{\,2}\right)^{\left(\frac{n-1}{2}\right)} \tag{2.4}$$

Where K is the consistency index and n is the power law exponent.

2.2.3 Polymer flow in porous media

In this section some definition and terms pertaining to the polymer flow in the porous media are explained

Resistance Factor

Resistance factor is defined (Pye, 1964) as the ratio of brine mobility before polymer injection to the mobility of polymer solution:

$$F_r = \frac{\lambda_w}{\lambda_p} = \frac{K_w/\mu_w}{K_p/\mu_p} \tag{2.1}$$

where *K*w is permeability to water at residual oil saturation measured before the injection of polymer solution, *K*p is permeability to polymer solution at residual oil saturation measured when polymer solution is flowing in a porous medium, μw and μp are viscosity of water and polymer solution, respectively.

Resistance factor is a measure of mobility ratio reduction. It is determined from core flooding tests. If water and polymer solution are injected at the same constant flow rate, the resistance factor can be determined by the ratio of the pressure drop during polymer flowing in a porous medium to that before the injection of polymer solution.

Residual Resistance Factor

Residual resistance factor is defined (Jewett and Schurz, 1970) as the ratio of brine mobility before contact with polymer to the brine mobility after all mobile polymer has been displaced out of pore space:

$$F_{rr} = \frac{\lambda_w}{\lambda_{wp}} = \frac{K_w}{K_{wp}} \qquad (2.2)$$

where λwp and *K*wp are brine mobility and permeability to brine, respectively, measured at residual oil saturation after contact with polymer solution. λw and *K*w have the same meaning as those in Equation (2.1).

Residual resistance factor is defined to describe the permeability reduction after the application of polymer solution. Smith (1970) referred it as the "permeability reduction".

Polymer retention

Retention of polymer in reservoir rocks is caused by physical adsorption on rock surface and mechanical entrapment in small pores (Gogarty, 1967; Willhite and Dominquez, 1976). Part of the retained polymer can be removed by the injecting water, but the release rate is very low. The negatively charged carboxyl group on partially

hydrolyzed polyacrylamide can reduce adsorption because the reservoir rock surface is negatively charged. Adsorption increases with increasing water salinity (Smith, 1970; Szabo, 1975), and retention in reservoir conditions is less than that measured in laboratory (Maerker, 1973).

Polymer molecules are larger than some pore throats. When flow in porous rock, polymers do not invade all the pore spaces swept by brine. The part of pore space that polymer cannot go through is called inaccessible pore volume which was first reported by Dawson and Lantz (1972). The inaccessible pore volume can be as low as 1% to 2%, and as high as 25% to 30%, depending on the polymer and porous medium (Green and Willhite, 1998). Retention tends to reduce the advancing velocity of polymer slug, while inaccessible pore volume tends to increase the slug moving velocity. The two effects can partly or fully offset.

2.2.4 Mechanisms of polymer flooding

Needham and Doe (1987) summarized three mechanisms of oil recovery improvement by polymer flooding: increasing oil fractional flow, decreasing water-oil mobility ratio and diverting water to un-swept region. Essentially, polymers help in increasing the oil recovery by improving the sweep efficiency of the displacement process.

From simple Darcy's law equation on neglecting the capillary pressure gradient, the fractional flow of oil phase can be derived as:

$$f_o = \frac{1}{1+\frac{\mu_o K_w}{\mu_w K_o}} \qquad (2.5)$$

On adding polymer, viscosity of the aqueous phase increases. Additionally polymers can also reduce the water relative permeability when they flood a zone. Both of these effects

lead to an increase in the oil fractional flow. This effect is more pronounced in the early stages of the flood when the oil saturation is high and the oil is still mobile.

Mobility ratio is directly related to sweep efficiency. The relationship between the areal sweep efficiency and mobility ratio has been extensively studied (Craig, 1955, 1971; Caudle and Witte, 1959). Area sweep efficiencies at breakthrough and at any given volume of water injection decrease with increasing water-oil mobility ratio. Polymer flooding reduce mobility ratio through increasing the water viscosity and decreasing permeability to water which are the same effects as described above.

In the case of heterogeneous reservoir, water preferentially flow through high permeability region, leaving large amount of oil untouched. Therefore, it is more important to divert the injecting fluid to the un-swept region. Crosslinked polymers can reduce the permeability of the high permeable zone in situ. A polymer solution and a crosslinking agent are injected to high permeable or fractured regions. The reaction of polymer and crosslinker produces a viscous gel, a fluid with extremely high apparent viscosity. This process significantly reduces the permeability in the crosslinking-treated region, and results in long lasting residual resistance factor. The subsequently injected water will be diverted to the un-swept or partially-swept regions, and oil recovery is greatly improved.

2.2.5 Field trials of polymer flooding

Jewett and Schurz (1970) presented a summary of the 61 different polymer field trials. The polymer used in all the projects was estimated to be about 95% of the entire polymer injected for mobility control till date. Reservoirs with a wide range of conditions and different fluid properties were considered. The highest oil viscosity for which successful application was possible was 126 cp. Polymer slug sizes in the successful

projects ranged between 7 % PV to 33 % PV. Smaller slug sizes were tested but without any significant success. Application in average permeabilities ranging from 20 md to 2300 md gave good results. Lower permeability application was discouraged.

Needham and Doe (1987) reviewed 27 polymer flooding projects, and found that the average oil recovery increment was around 8.0% of original oil in place (OOIP), with a highest value of 30.0% OOIP. 23 out of 27 projects were essentially secondary operations, initiated at WOR < 10. The average amount of polymer injected was about 0.011 kg/m^3 of reservoir. Four were tertiary applications, initiated at WOR of 30 to 100. The average amount of polymer injected was about 0.018 kg/m^3 of reservoir with an average of 1.8 % OOIP as the incremental oil recovery. On the basis of the data, it was concluded that the secondary injection of polymer has four times the potential for oil recovery than a tertiary polymer injection. Secondly, a tertiary polymer injection required about 6 times the polymer for a barrel of oil than the secondary injection. Most of the projects involved lower than 400 ppm of calcium in the injected water, which was well within the tolerance limit of the HPAM polymer.

The largest commercial scale polymer flooding project has been conducted in Daqing oilfield, China. Industrialized polymer flooding treatment started in 1995. The oil recovery increment by polymer flooding was more than 12% OOIP. Both displacement efficiency and volumetric sweep efficiency were increased by polymer flooding. The viscoelasticity of the polymer solution contributed to the increase in displacement efficiency. Field experience showed that the lower the oil saturation was at the start of polymer flooding, the less effective the polymer treatment would be in terms of oil production increase and water cut decrease.

2.2.6 Polymer Flooding for Heavy Oil

Traditionally, polymer flooding is not recommended for reservoirs with oil viscosity in excess of 200 cp. This is because the high oil viscosity will necessitate the use of very high concentration polymer solutions to achieve any significant reduction in water mobility. This will cause problems with the injection and increase significantly the cost of chemicals. Early tests on Lloydminster crude oil (Miller, 1987) failed because of the high crude oil viscosity and incompatibility of the polymer with the formation brine. However in recent years, the interest in the polymer flooding of the heavy oil has been revived due to high oil prices making it economically feasible to inject large and concentrated polymer slugs. Wang and Dong (2007, 2009 a) conducted the polymer flooding in tertiary mode and found out that an optimum value of the polymer viscosity exists for a particular oil viscosity at which the oil recovery is a maximum. Wassmuth *et. al.* (2007) conducted laboratory studies of polymer flooding using three different oils ranging in viscosity from 280 to 1,600 mPa.s. The concentration of polymer solution was 1,500 ppm. The incremental oil recoveries ranged from 16% to 23% OOIP after at least one pore volume of water injection.

2.3 IMPROVED OIL RECOVERY BY ALKALI-SURFACTANT-POLYMER FLOODING

In the present section, a synergistic effect of alkali, surfactant and polymer is discussed which can aid in enhancing the recovery of oil. Alkali is used to generate in situ soaps by reacting with the acids in the crude oil or serve to limit the adsorption of surfactants by raising the pH of the system. The use of all the three chemicals in the injected slug is termed as ASP flooding. This section summarizes the development of ASP flooding.

2.3.1 Main mechanisms

Surfactants, either externally added or formed in-situ are responsible for lowering the interfacial tension between oil and water. The reduction of IFT by alkali surfactant flooding is the main mechanism for the improvement of oil recovery. It leads to an increase in the capillary number of the system which further leads to a reduction in the residual oil saturation

$Nc = \frac{\mu v}{\sigma}$; Nc = Capillary number; σ = IFT (2.6)

The effect is usually captured in a capillary desaturation curve (CDC) as shown in figure 2.3. (Stegemeier, 1977; Lake, 1989). Low IFT increases the capillary number to 1E-6 to 1E-2 and brings down the residual oil saturation to near zero values. In addition, ultra-low IFT (~10^{-3} dynes/cm) produces a thermodynamically stable phase called a microemulsion inside the porous media. Under certain conditions of salinity, etc. the microemulsion phase can coexist with the oil and the water phases. Having a low enough IFT between oil and microemulsion as well as between water and microemulsion is important for an efficient displacement. This condition is called the condition of optimal IFT and is the most sought after in the microemulsion floods.

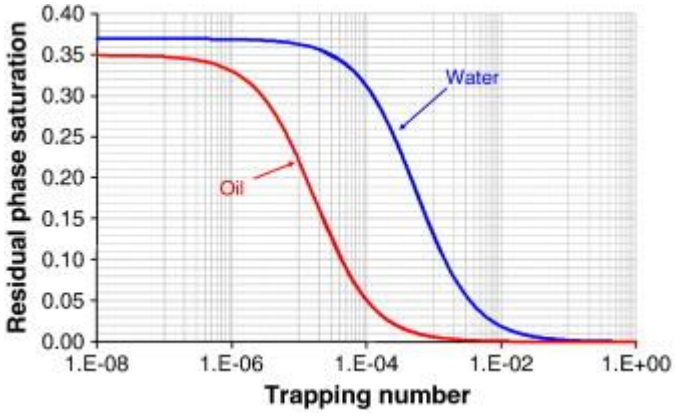

Figure 2.3: Capillary desaturation curve (Stegemeier, 1977)

In the next section, an overview of the microemulsions is provided.

2.3.2 Microemulsions

Definition

Hoar and Schulman (1943) introduced the term 'microemulsion'. They used the term to describe the transparent or translucent system obtained by the titration of an ordinary emulsion having a milky appearance with an alcohol of medium sized carbon chain. These alcohols were later referred to as co surfactants or co solvents. Microemulsions were also referred to as 'solubilized micellar solutions' by some authors (Palit, Moghe and Biswas, 1959).

Bourrel and Schechter (1988) defined microemulsions as thermodynamically stable phases formed under certain conditions when oil, water and surfactant are mixed together. A sharp distinction was drawn between the microemulsions and emulsions (macroemulsions). Emulsions are thermodynamically unstable (although they may be kinetically stable) with droplet sizes larger than 0.1 μm because of which these are milky rather than transparent or translucent. The droplet sizes of emulsions are a function of time and grow with time until the emulsion coalesces completely together. Microemulsions are thermodynamically stable and the droplet sizes are independent of time. They are independent of the order of mixing and return to their original state when subjected to perturbations in temperature, etc.

Microemulsion phase behavior

Winsor (1954) identified three types of microemulsion systems depending upon the process variables. Type I or II- microemulsion is obtained when the net surfactant is soluble in the aqueous phase. The oil droplets are solubilized in water with the help of the hydrophilic surfactant. When reverse micellization occurs, Type II or II+ system is

obtained. Here the surfactant is hydrophobic in nature and solubilizes the water in the oil phase. Type III or bi continuous microemulsions are obtained in some situations where both oil and water get solubilized in the micelle phase. Type III microemulsion region is also the region of optimum IFT. Reed and Healy (1975) stated that the microemulsion phase transitions may occur as a result of the changes in salinity, temperature, concentrations of surfactant and co solvent and the dissolved solids in the aqueous phase. Next the effect of some of the parameters on the phase behavior is analyzed.

Effect of salinity

It was found that the microemulsion phase behavior transitions from lower to middle to upper phase as the salinity of the system is increased. Due to the transition of the microemulsion phase abrupt changes in the microemulsion viscosity was observed which was found to be correlated to the microemulsion phase volume. The IFT and the solubilization parameter were found to be dependent on the salinity.

As shown in the figure 2.4, both IFTs (oil-microemulsion and water-microemulsion) exist only in the three phase region. At lower salinities Type I region exists where $\Upsilon mw = 0$ and Υmo decreases with salinity. For higher salinities Type II region exists where $\Upsilon mo = 0$ and Υmw increases with increasing salinity. In the three phase region both the IFTs exist simultaneously. The salinity at which both the IFTs are lowest is called the optimal salinity and the corresponding IFTs are called the optimum IFTs. The authors state the ultra-low values of both the IFTs are desired so that the immiscible microemulsion slug may effectively displace oil at the flood front and be effectively displaced by chasing brine at the rear end.

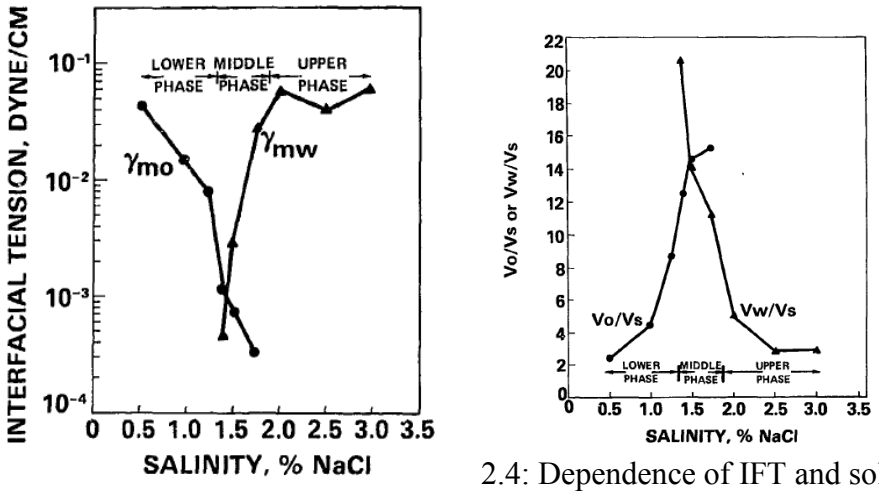

Figure 2.4: Dependence of IFT and solubilization ratio (V/Vs) with salinity (Reed and Healy, 1975)

Effect of surfactant structure

The surfactant structure was also found to play a major role in the phase behavior. The authors investigated the effect of the carbon chain length of an alkyl orthoxylene sulfonic acid. The results are displayed in figure 2.5. On increasing the carbon chain length, the optimal salinity reduced because of the surfactant becoming more hydrophobic.

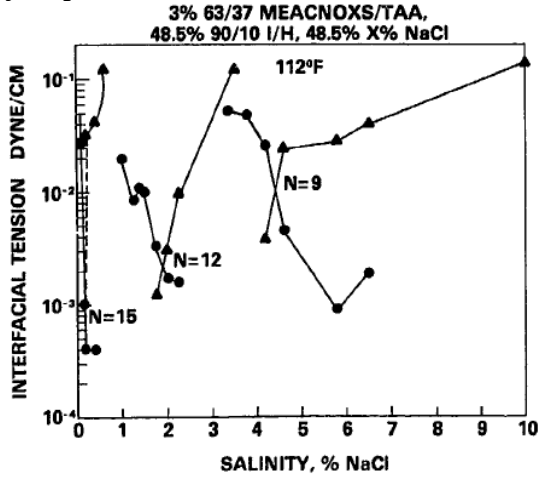

Figure 2.5: Effect of the surfactant structure on the phase behavior (Reed and Healy, 1975)

It was also found that the optimal IFT reduced when the carbon chain length was increased. The results were explained on the basis of the cohesive energy ratio.

For the particular surfactant the optimal salinity was found to increase with temperature. This is particular of the anionic surfactants where higher temperature leads to a greater solubility in the aqueous phase. However, the converse is true for the non-ionic surfactants. Salagar *et. al.* (2000) presented results where the partition coefficient of an octylphenol ethoxylate surfactant was studied with temperature and the number of the ethoxylate groups in the surfactant structure. Figure 2.6 depicts the results. The figure shows that as the number of the EO groups in the chain increases the partition coefficient (Cw/Co) increases indicating that the surfactant is becoming more hydrophilic in character. However for the same number of EO groups, an increase in temperature from 25C to 55C decreased the partition coefficient. The trend is typical of most of the non-ionic surfactants.

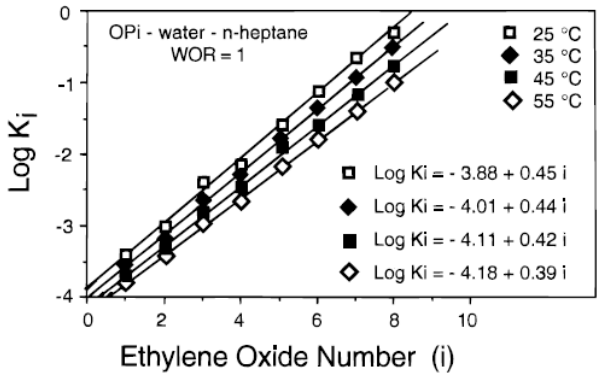

Figure 2.6: Dependence of the partition coefficient of octylphenol ethoxylate with the number of EO groups at different temperatures (Salagar *et.al.* 2000)

Effect of adding a co-solvent or a co-surfactant

Alcohols, also referred as co solvents are added to the surfactant formulation to improve its performance. Co solvents inhibit the formation of viscous emulsions, gels and

liquid crystals and promote rapid equilibration. Co solvents can also prove helpful in obtaining clear, transparent and aqueous stable surfactant mixtures at optimum conditions (Sahni *et.al.* 2010). In the study a water soluble co solvent TEGBE was used to increase the water solubility of the surfactant mixture and making the aqueous phase clearer as shown in Figure 2.7. Many authors have studied the effect of adding co solvents to the surfactant formulation in the phase behavior experiments.

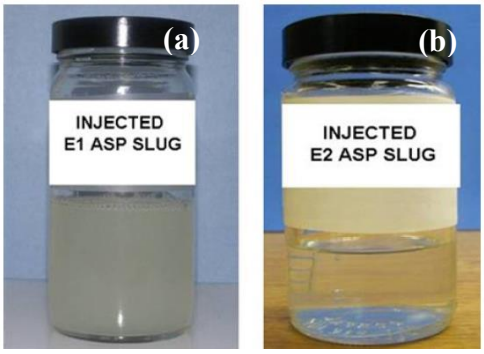

Figure 2.7: (a) cloudy surfactant solution without the co solvent and (b) clear surfactant solution with the co solvent (Sahni *et.al.* 2010)

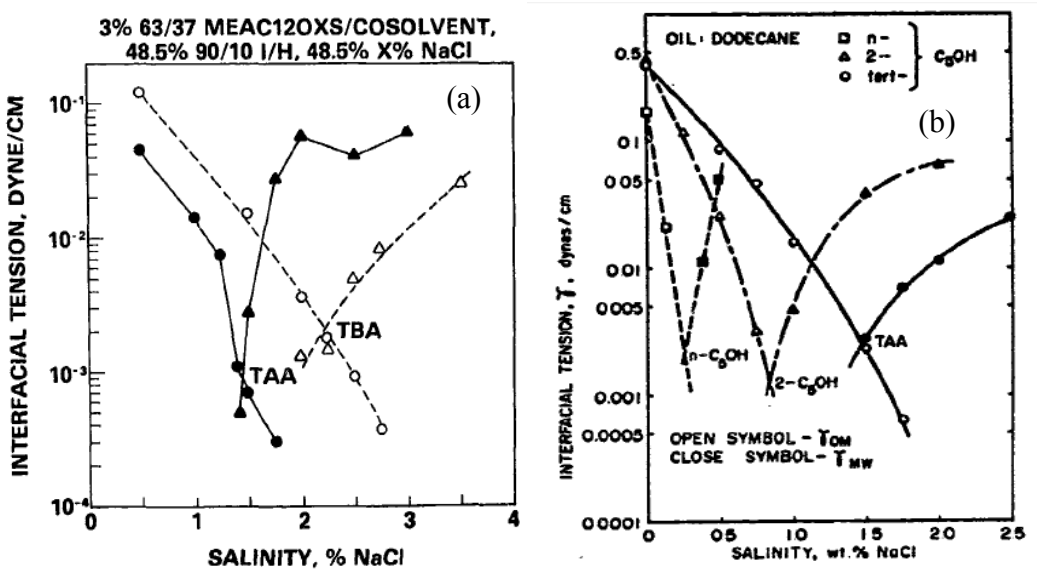

Figure 2.8: Effect of alcohol on IFT (a) increasing MW of alcohol (b) increasing the branching in alcohol (Reed and Healy, 1975; Hseih and Shah, 1977)

Jones and Dreher (1975) found that addition of oil soluble and water insoluble alcohol promotes higher water solubilization whereas the reverse is true for the water soluble alcohols. Reed and Healy (1975) compared the IFT characteristics with two alcohols TBA (Tertiary Butyl Alcohol) and TAA (Tertiary Amyl Alcohol) having a higher molecular weight than the TBA. A higher molecular weight alcohol decreased the optimal salinity and the optimal interfacial tension of the system. Hsieh and Shah (1977) found that unlike the straight chain alcohols, the branched alcohols tend to be more hydrophilic. The optimal salinity increased and the phase behavior tended to shift to Type I system.

Due to the benefit of adding co solvents to the surfactant system and their influence on the IFT phase behavior studies have to be conducted extensively in order to choose the optimum concentrations of different chemicals. More recently, Levitt *et.al.* (2006) investigated the use of SBA (Secondary Butyl Alcohol) and IPA (Iso Propyl Alcohol) and found IPA to perform better for the light oils. Flatten *et.al.* (2008) found both SBA and IBA (Iso Butyl Alcohol) to show good performance but preferred IBA because of its low cost for high salinity, high temperature and light oil reservoirs. Jackson (2006) and Zhou *et.al.* (2008) developed formulations using EGBE (ethylene glycol monobutyl ether), DGBE (diethylene glycol monobutyl ether) and TGBE (triethylene glycol monobutyl ether) as co solvents. Sahni *et.al.* (2010) also investigated the use of several co solvents for six different oils.

Effect of EACN of the oil

The surfactant phase behavior was also found to be dependent on the properties of oil. The effect was coined in the term EACN (equivalent alkane carbon number). The term was introduced by Cayias *et.al.* (1975). They found that the interfacial tension of the

crude oils can be modeled by the alkanes ranging up to nonane. Crude oils with high EACN numbers or in other terms heavier crudes required higher equivalent weight surfactants for achieving low IFTs.

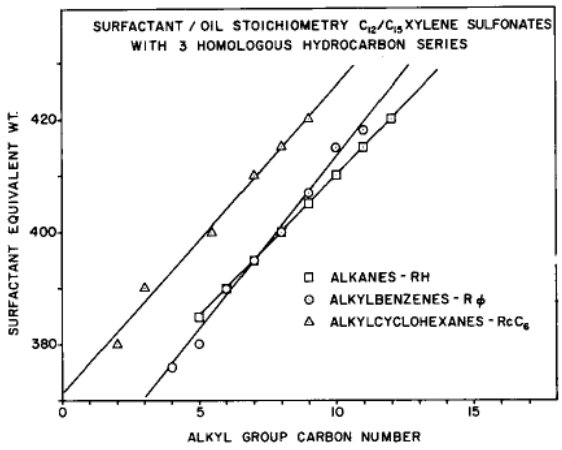

Figure 2.9: Variation of surfactant equivalent weight required for optimal IFT as a function of hydrocarbon EACN (Cayias *et.al*., 1975)

Sriram *et.al.* (2012) stated that with the invention of complex structure surfactants this relationship is quite complex. The surfactant hydrophobicity is dependent on many other factors such as the number of EO/PO groups, temperature, etc. rather than just the equivalent weight. Hence, although the large equivalent weight surfactants may be the first guess as appropriate surfactants for heavier oils, it's the surfactant structure which should play a major role in the final decision. However the concept of EACN is proving helpful in making surrogate oils. Research is on to compensate the loss of solution gas from the crude oil by adding an alkane in appropriate proportion so that the EACN of the surrogate oil becomes equal to the original live crude oil. The results of the phase behavior of this new surrogate oil will now be representative of the live crude oil.

Effect of pressure

Skauge and Fotland (1986) found experimental evidence suggesting that the pressure of the system affects the phase behavior. The results are plotted in figure 2.10. The effect of pressure is produced due to the higher compressibility of the oil phase as compared to the aqueous phase. This is the reason for a change in oil-microemulsion IFT variation with pressure. Initially the samples were Type II systems. An increase in pressure caused the changes in IFT and the system approached Type III behavior and further migrated to Type I system for even higher pressures. Figure 2.10 (b) indicates that a higher pressure required a higher optimal salinity as the system has the tendency to become Type I with an increase in pressure.

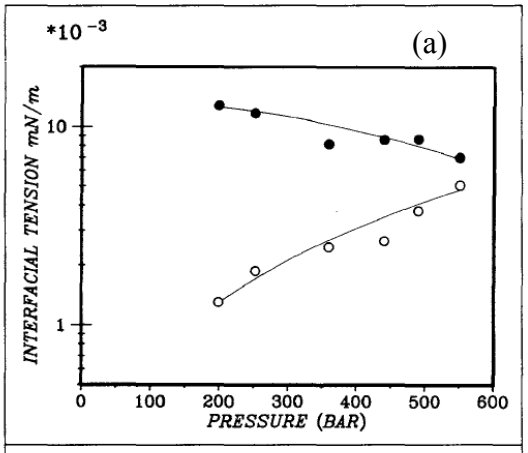

Fig. 8—IFT as a function of pressure for the SDBS system at a salinity of 2.93 wt%. Upper curve is the microemulsion/water interface, and lower curve is the microemulsion/oil interface. This sample is initially a WII + microemulsion. Viscosities are 0.8 (oil), 1.4 (microemulsion), 1 mPa·s (brine).

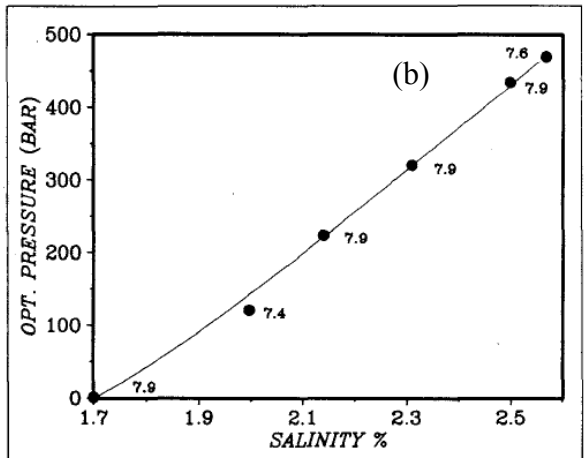

Fig. 14—Optimal pressure as a function of salinity for TBPE at 20°C. Numbers at each point are the solubilization parameter at the optimum.

Figure 2.10: (a) Effect of pressure on the phase behavior (b) relationship of optimal salinity and pressure (Skauge and Fotland, 1986)

Effect of adding alkali

Nelson *et.al.*(1984) introduced the concept of the co-surfactant enhanced alkali flooding where the synergy of alkali and a hydrophilic surfactant was used for EOR. In

this case it was found out that the alkali can influence the phase behavior as well by generating soaps by reacting with the petroleum acids in the crude oil. Soaps act as in situ surfactants and aid in lowering the IFT. However, it was realized that the optimal salinity of the soap is very low which would necessitate the use of low alkali concentrations. This was a problem since the alkali consumption by rock made the propagation very slow. It was found that the addition of a hydrophilic surfactant can solve this problem by increasing the optimal salinity of the soap-surfactant mixture. The phase behavior results were plotted in the form of activity diagrams and phase volume diagrams. The phase behavior was investigated at different oil concentrations. This is because the concentration of the generated soap and hence the hydrophilic hydrophobic balance of the total surfactant mixture was found to vary with the oil concentration.

2.3.3 Recent developments in alkali surfactant polymer flooding

The earlier work presented above demonstrated the efficiency of the alkali surfactant flooding in improving the oil recovery and reducing the residual oil saturation to near zero. In the following decades many research groups focused on developing alkali surfactant systems for different kinds of oil and various reservoir conditions. Recent research has led to the development of surfactant systems suitable for high salinity and carbonate environments (Levitt et al., 2009; Barnes et. al., 2008; Hirasaki et al., 2008; Adibhatla & Mohanty, 2008). Several ASP field tests have also confirmed that the residual oil can be displaced by the use of alkaline-surfactant-polymer system (Falls *et al.*, 1992; Reppert *et. al.*, 1990). In particular, the ASP field test in the Daqing field recovered about 20% additional OOIP after waterflooding (Shutang *et. al.*, 2010).

Alkaline-surfactant-polymer techniques have been studied for mostly light oils in the past (Nelson 1978; Pope 2008). Here we extend its application to the viscous oil reservoirs.

Polymer floods have been considered for viscous oil reservoirs for a long time (Seright 2010, Wassmuth et. al. 2007), but they do leave behind a residual oil saturation. Alkali surfactant formulations have been recently developed for a few viscous oils (Yang *et. al*. 2010), where the remaining oil saturations have been reduced to very little. Adkins *et.al*. (2010) developed the novel Guerbet Alkoxy Sulfate surfactants as a substitute for large hydrophobe surfactants needed for high EACN crude oils at high temperature and high salinity. Liyange *et.al.* (2012) talk about the attaching a large number of EO and PO groups to a large hydrophobe such as TSP (tristyrylphenol) to yield a surfactant suitable for high EACN crudes. In this study, we develop an alkaline-surfactant-polymer formulation for viscous oil of 330 cp at 75F. The high viscosity of the crude oil suggests that surfactants with large hydrophobes might be the best choice. However we have made use of the fact that this oil is active (TAN = 1.47 mg KOH/g oil) and have used alkali for producing hydrophobic soap and a commercially available non-ionic hydrophilic surfactant (TDA 30EO) to achieve the desired hydrophilic lipophilic balance. The low temperature and low salinity of the formation water enabled us to use sodium carbonate as an alkali without any precipitation problems.

2.3.4 Field tests of alkali and alkali surfactant floods

Numerous cases of successful alkali surfactants floods have appeared in the literature. Alkali flooding is an extremely complex process because of the interplay of different mechanisms in a particular application. Falls *et.al.* (1994) demonstrated a surfactant alkali flooding viable in recovering waterflood residual oil from the sandstone reservoirs in the near offshore Gulf of Mexico. The oil viscosity was 2.8 cp at reservoir conditions. Alkali concentration of 2.2 wt% was used with a mixed surfactant concentration of 0.6 wt%. The process was able to recover 38% of the waterflood

residual oil with almost 100% displacement efficiency. Other field trials have reported success with the ASP (Alkali Surfactant Polymer) flooding (French, 1996; Li *et.al.*, 2003; Kumar *et.al.,* 2012).

2.3.5 Chemical floods for heavy oil

There has been a limited application of alkali and surfactant chemicals for improving the recovery of the heavy oil. Subknow (1942) patented the idea of injecting caustic alkalis to emulsify and produce the bitumen as an emulsion in the water phase. The reaction of caustic alkalis and the organic acids in the bitumen could produce soaps which served the dual purpose of lowering the interfacial tension and emulsifying bitumen in water. Jennigs *et.al.* (1974) conducted the alkali flood of 187 cp heavy oil at the laboratory scale. They found out that a low concentration of alkali 0.05 wt% to 0.5 wt% could emulsify the oil in situ. The in situ emulsions plugged up the water channels formed due to viscous fingering during the prior waterflood. The result was improved areal and vertical sweep efficiency with a simultaneous increment in oil recovery and lowering of the WOR. Several studies also talk about the potential of alkalis and surfactants in order to enhance the performance of steam flooding for heavy oil (Okoye and Tiab, 1982; Shedid and Abbas, 2000). Chiwetelu (1994) studied the feasibility of employing various alkaline agents for the enhanced oil recovery of the Saskatchewan heavy oil reservoirs. The tests were conducted on the same oil at two temperatures of 25C and 65C. The viscosity of the oils at these temperatures was 474 cp and 45.6 cp respectively. The alkali floods conducted with 0.05 wt% resulted in the incremental oil recoveries of 42.4 % and 7.3 % at 25C and 65C respectively. Symonds *et.al.* (2002) conducted alkali flooding on the Wainright crude oil (408.3 cp, 941 kg/m3) in a sandpack and observed an increase from 53% OOIP oil recovery after waterflooding to about 75%

OOIP after alkali flooding. Thomas *et.al.* (1999) conducted surfactant flood on Senlac heavy oil (2048 cp at 25C and 219 cp at 52C). Experiments were conducted at two temperatures of 25C and 52C using 1000ppm concentration of surfactant. The surfactant flood at 25C produced 39% of total oil as opposed to the waterflood recovery of 34% at the same temperature. At 52C the oil production by surfactant flood was 53%, an increase of 6% recovery over waterflood. More recently, research on the application of alkali and surfactants for the heavy oil recovery has been conducted at University of Regina and University of Calgary. Bryan and Kantzas (2007) emulsified heavy oil (11,000 cp) in water using a combination of alkali and surfactant. On conducting the AS injection after the waterflood 40% improvement in oil recovery was observed. They suggested emulsification and entrapment along with the lowering of the interfacial tension to be the dominant mechanism.

2.4 VISCOUS FINGERING IN POROUS MEDIA

2.4.1 Viscous fingering in immiscible flows

General concepts

When the oil is displaced from the porous media by water having a viscosity quite lower than that of oil, the oil water interface becomes unstable and breaks up into 'fingers'. Engelberts and Klinkerberg (1951) observed viscous fingers in the sand pack when they used oil of viscosity 24 times or more than the displacing immiscible fluid. They also deduced from the lab experiments that for higher viscosity ratios, the displacement experiments had to be continued to a higher WOR (300-500) to reach the ultimate recovery than for the viscosity ratios not too high than unity. Van Meurs (1957) also observed the viscous fingering phenomena in their transparent three dimensional models for oil water viscosity ratio of 80.

Buckley and Leverett (1942) had presented a 1D displacement theory that could calculate the oil water relative permeability curves from the lab data of oil recovery. The theory assumes that a sharp front exists between the oil and the invading water. Thus it was questioned whether such a theory could be used to calculate the relative permeabilities in cases where the oil water front is in fact not sharp but has perturbations. There was a need to come up with a better mathematical model which could take into account the formation and transport of viscous fingers.

Van Meurs (1957) made first such attempt to incorporate the viscous fingering mechanism into the 1D displacement model. The model was a simplified version of the complex fingering phenomenon. The viscous fingers were assumed to have formed from the moment the water enters the oil reservoir. From then on they would transport in the porous medium without undergoing any changes in their shapes and sizes. In order to make the analysis even simpler the presence of oil in the fingers is assumed to not hinder the flow of water inside the fingers. In other words a linear relationship was established between the water relative permeability and saturation. The model, though very simple and ideal was a motivation for further studies on viscous fingering. The idealized model was based on the observations of the viscous fingers during oil water displacement experiments.

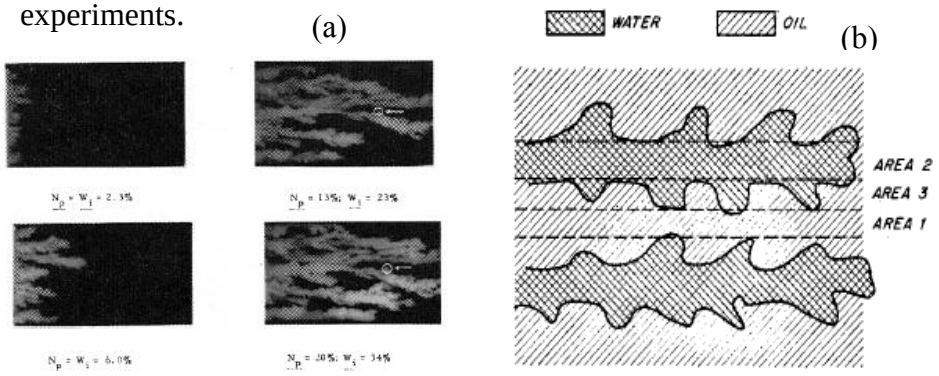

Figure 2.11: Snap of the idealized model used to calculate the oil recovery performance (Van Meurs, 1957)

Several studies were conducted in the next few years trying to come with analytical solutions which could predict the onset of viscous fingering. It was recognized that small instabilities always exist at the oil water interface due to random perturbations. With time these can be dampened out or can grow further to become viscous fingers. Thus in order to predict the onset of viscous fingering in a particular system it is essential to understand the factors which could lead the interfacial instabilities to grow with time.

Saffman and Taylor (1958) studied the growth of interfacial instabilities in a Hele Shaw cell. He identified that the interface may become unstable to small perturbations and the amplitude of such deviations grows exponentially with time if

a) The flow is directed from a less viscous fluid to a more viscous fluid or
b) Higher density fluid from the top flows downwards through a lower density fluid.

They also derived a relationship between the critical wavelength 'lcrit' of the interfacial disturbances and the other pertinent variables such as fluid viscosities and densities and interfacial tension. It was found out that interfacial tension is a dampening factor which prevents the wavelengths below lcrit to grow with time.

Chouke *et.al.* (1958) derived the similar expression for the critical wavelength λ_c in a porous media.

$$\lambda_c = 2\pi \left[\frac{\sigma^*}{\left(\frac{\mu_2}{k_2} - \frac{\mu_1}{k_1} \right)(U - U_c)} \right]^{1/2} \qquad (2.6)$$

From the expression it is clear that factors responsible for making the oil water interface more unstable to disturbances are larger difference between oil and water viscosity and a higher volumetric velocity 'U'. Presence of interfacial tension between oil and water

serves to make the interface stable to small perturbations essentially increasing the critical wavelength.

Haan (1959) studied the effect of the flow rate on the oil recovery by linear displacement experiments. At very low flow rates the capillary forces dominated the viscous forces and small immobile oil pockets were formed resulting in low oil recoveries. With increase in flow rates the size of the oil pockets decreased and the oil recoveries increased accordingly. With still higher flow rates, the oil recoveries decreased again owing to viscous fingering. The number of fingers increased with flow rate, in accordance with the instability theory of Chouke and Saffman and Taylor. Rachford (1964) extended the Chouke's theory of instability to account for the saturation transition zone behind the flood front in a water wet system. Peters and Flock (1981) extended the Chouke's theory of instability for cylindrical coordinate system. They calculated an instability number Isc and stated that onset of interfacial instability occurs when the value of this number is higher than 13.56. Experimental observation suggested that the oil recovery decreases in the range $13.56 < Isc < 1000$. They also introduced a wettability number which had to be experimentally determined for different wettability states. The instability number predicted the onset of instability in an oil wet medium to occur at a lower rate than water wet medium. That the wettability of the medium influences the width of the individual fingers was experimentally verified by Stokes *et.al.* (1986). The observed finger width was comparable with the pore size if the displaced fluid (oil) wetted the medium. On the other hand if the displacing fluid wetted the medium, the finger width was observed to be much larger than the pore size.

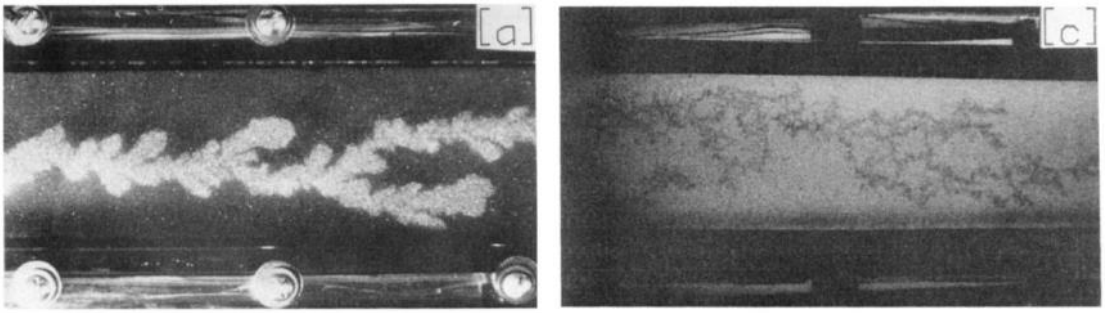

Figure 2.12: Adverse mobility displacement (a) wetting phase water displacing non wetting phase oil (c) non wetting phase oil displacing wetting phase mixture of water and glycerol (Stokes *et.al*., 1986)

Bentsen and Saeedi (1981) found out that for adverse mobility ratios, the displacement process can be represented adequately by the linear 1D displacement theory only if the stability criterion of Peters and Flock is satisfied. Yortsos and Huang (1986) and Yortsos, Huang and Chikhliwala (1984) conducted a linear stability analysis of immiscible displacement relaxing the abrupt interface assumption of Peters and Flock (1981) and Chouke *et.al.* (1958). Before introducing the interfacial perturbations, it was assumed that sufficient time has elapsed that a steady travelling wave solution (Buckley-Leverett type distribution) has been established. From the different experimental observations and linear stability analysis it is clear that viscous fingering is indeed a very complex process involving a number of parameters. These parameters play a major role in determining the final shape of the pattern formed. Efforts were made to incorporate these parameters in dimensionless numbers called stability numbers. The parameters included fluid mobilities (kri/μi), the flow rate, interfacial tension (liquid-liquid displacement) or surface tension (air-liquid displacement), medium heterogeneity and wettability. The linear stability theories were useful in predicting the wavelength and behavior of viscous fingers at early times. Riaz and Tchelepi (2005) employed high accuracy numerical methods (spectral methods) to analyze the non-linear evolution of

viscous fingers. Comparison with the linear stability analysis found good agreement at early times. However the two theories differ from each other at later times in that the nonlinear analysis predicted a finger shielding mechanism to become dominant decreasing the finger wave number. Riaz and Tchelepi (2006) further extended the stability analysis to determine the role of different relative permeability curves on the viscous fingering phenomenon.

Viscous fingering as a fractal phenomenon

In the late 1980s, several authors started viewing viscous fingering as a fractal phenomenon. Fractals occur in nature in a variety of systems (Mandelbrot, 1982; Brady and Ball, 1984; Avnir *et.al.*, 1984; Matsushita *et.al.*,1984) when the randomizing effects dominate over the stabilizing effects. Fractals are described as self-similar objects; which means they are either exactly the same or nearly the same at different scales. Nittmann *et.al.* (1985) conducted one of the earliest studies on the fractal nature of the viscous fingers in a Hele Shaw cell.

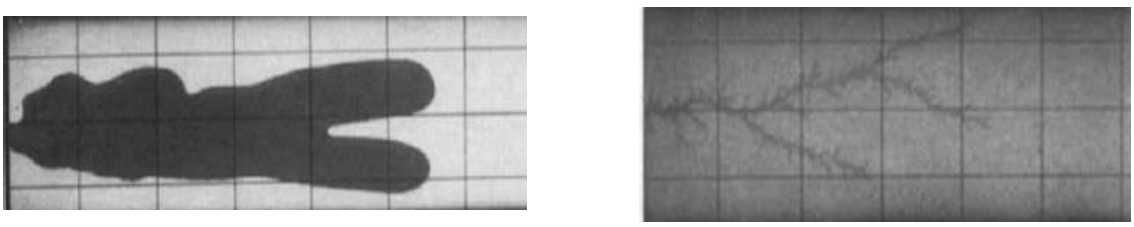

Figure 2.13: Viscous finger formation in a Hele Shaw cell (a) water being injected into oil (b) water being injected into 1000 cp polymer solution (Nittmann *et.al.,* 1985)

They argued that in order to generate fractal structures, the stabilizing effects of interfacial tension should be minimized so that the random effects can dominate. To achieve this purpose, they filled the Hele Shaw cell with a viscous polymer solution and

injected water into it. Their mathematical analysis showed that the viscous fingers formed could be analyzed using the concept of self-similarity or fractals. For this particular case the fractal dimension was found to be 1.40±0.04.

The fractal growth phenomenon was explained by the DLA (Diffusion Limited Aggregation) mechanism (Witten and Sanders, 1981; Witten and Sanders, 1983; Stanley, 1985). DLA is the process by which a particle undergoing a random walk due to Brownian motion cluster together to form aggregates of such particles. Paterson (1984) realized the analogy of the DLA mechanism with the two phase fluid flow in a porous media where one phase has a much larger viscosity than the other fluid and there is a sharp transition zone between the two fluids. DLA simulations in a 5 spot geometry lattice structure could generate viscous fingers. However it was recognized that the simulations do not hold good if the viscosity of one fluid is not negligible as compared to the other.

Maloy *et.al.* (1985) studied the radial displacement of immiscible fluids in a 2D random porous media. They also observed the fractal structure of the viscous fingers instead of the smooth broad fingers observed in the Hele Shaw cells. The fractal structures were found to have a dimension of 1.62±0.04 consistent with the results of a DLA simulation.

Ferer *et.al.* (1995) employed the pore scale simulations to study the flow behavior of different viscosity fluids in a square lattice model. It was observed that in the limit of very large viscosity ratio (~10,000) the pore scale simulations indicated the fractal nature of the flow. However for finite viscosity ratios it was observed that although the flow was fractal at the initial stages but became compact (or linear) on a characteristic time scale that increases with the viscosity ratio. Observations from the pore scale simulations

demonstrated that when the flow is nonlinear or fractal, the fractional flows and relative mobilities depend on both saturation and time.

Simple models to incorporate viscous fingering effects

Many authors have tried to develop simple methodologies for modeling the viscous fingering in the porous medium. The simplest approach is to model the unstable displacement experiments with the help of pseudo relative permeabilities. Sufi *et.al.* (1982) reported the effect of flow rates on the oil water relative permeability curves. The oil relative permeability showed a slight increase while the water relative permeability showed a marked increase with the flow rate and consequently with the instability number. Lefebvre de Prey (1973) found out that on increasing the viscosity of one phase, the relative permeability of the other phase declines. Amaefule and Handy (1981) showed that decreasing the oil water IFT reduces the oil relative permeability and increases the water relative permeability. Peters and Khataniar (1987) conducted a thorough study of dynamic relative permeability curves for different instability numbers and concluded that in general oil relative permeability decreases and the water relative permeability increases as the degree of instability increases. It is important to understand that no fundamental explanation has been provided for the respective observations. The pseudo relative permeability curves, in fact combine all the complexities of the unstable flows into a single parameter. Different systems thus can show different behaviors with the input parameters.

Unlike the relative permeability curves inferred by dynamic displacement tests, those inferred by the steady state methods were found to be independent of the flow rate and viscosity ratio. (Osaba *et.al.*, 1951; Claude *et.al.*, 1951; Sandberg *et.al.*, 1958). This

is expected as steady state measurements do not involve a displacement process and hence do not suffer from the problem of instability.

Analytical models to model immiscible viscous fingering

In this section, different viscous fingering models available in the literature are presented. Due to the complex nature of the instability phenomenon, the models analyze the growth of cross sectional average properties with time and space. The treatment makes the analyses simpler, at the same time reasonable conformance to the experimental data is ensured. Sigmund *et.al.* (1988) conducted the physical displacements in a bead pack and observed that the amplitude/frequency of the wave like fingers that form depend upon the flow rate and the mobility ratio. For analysis, the front shapes were digitized and an RMS (Root Mean Square) finger size was calculated. The results displayed that the RMS finger size for different rates of displacement increases linearly with time. A modified Buckley-Leverett model was presented where instead of using the exact position of saturation, an average position of the cross sectional averaged saturation was used. The model could reproduce adequately some of the key experimental findings. Hughes and Murphy (1987) developed an analytical model which could be used for calculating the pseudo relative permeabilities useful for describing the average properties of the unstable immiscible flows. In general, the calculation of pseudo relative permeabilities enables one to use conventional reservoir simulator with relative permeabilities replaced by the pseudo values.

2.8.2 Viscous fingering in miscible flows

General Concepts

Similar to the immiscible floods in the porous media, significant instabilities can also arise in case of miscible floods. Miscible floods are conducted by injecting a low

viscosity solvent, in either gas or liquid phase which is at least partially miscible with the oil at the reservoir temperature and pressure. Due to miscibility, the viscosity of the oil gets reduced as a result of which the oil becomes more mobile. However when a solvent displaces a viscous oil significant instabilities may occur leading to the development of viscous fingering (Perkins *et.al,*. 1965). The perturbation theory developed for miscible floods has indicated the manner in which the fingers will initiate and grow (Perrine 1961). One of the outcomes from this study was the concept of a minimum slug size needed for the stable displacement along with the requirement of miscibility and avoiding viscous fingering. Gardner and Ypma (1984) used the unpublished work of Chouke in which small perturbations were introduced at the interface which was assumed to be sharp. Constant injection of solvent was also taken as a simplifying assumption. The theory predicted that the interfacial instabilities would readily grow into viscous fingers for higher oil viscosity, higher fluid injection rate and a lower diffusion rate.

Claridge (1978) found out that the length of the transition zone predicted by stability theory of Chouke and Perrine was pessimistic. He proposed a new stability theory for the design of the viscosity graded slugs in a miscible flood. The theory was based on the repeated application of the Koval factor.

Lee *et.al.* (1984) conducted a linear perturbation analysis without the assumption of the quasi steady state concentration profile by previous authors. Dispersion as a function of the displacement velocity was used in the analysis. Due to the time dependent treatment of the flow equations, the critical wavelength and the critical injection rate (injection rate above which the interface becomes unstable) were found to increase with time. This means that as the injection proceeds, the injection rate can be gradually increased without causing instability. It was also shown that for laboratory core floods, a threshold time is reached after which the process becomes unconditionally stable

regardless of how high the injection rate is. Another outcome of the analysis was the role of longitudinal and transverse dispersion in controlling the fingers. The transverse dispersion was shown to be more effective than the longitudinal dispersion in smearing out the fingers; however a non-zero longitudinal dispersion is necessary for the transverse dispersion to be effective.

Coskuner and Bentsen (1987) extended the Chouke's theory to account for an appropriate boundary condition at the side walls. All the three dimensions were considered, first one being the principal flow direction and the other two the transverse directions. The modification allowed the authors to assign different values to the transverse and the longitudinal dispersion. It was now possible to derive the lower and the upper bounds of the length of the graded viscosity region. Tan and Homsy (1986) employed a quasi-steady state approximation to the evolution of the base state of concentration and velocity with time. The consequence was that in the model the base state evolved very slowly with respect to the growth of disturbances. This approximation could make the prediction of the growth rate of disturbances easier. Apart from the stability analysis in the rectilinear flow, Tan and Homsy (1987) conducted the stability analysis on the radial flow problem as well.

Tan and Homsy (1988) also undertook the study of the non-linear behavior of viscous fingering in which the Fourier spectral method was used for numerical simulation. For shorter durations the wavelength of the viscous fingers and the growth rate was in close agreement with the previously developed linear stability theory. However for longer times, the nonlinear characteristics of the fingers such as shielding and tip splitting became important. It was shown that the transverse dispersion aids in the evolution of the nonlinear characteristics of the fingers.

Simple models for miscible viscous fingering flows

The linear stability theories on miscible viscous fingering serve the purpose of determining the conditions under which such fingering may occur for a particular system. However once fingering occurs, it is also important to develop models which can predict the oil recoveries and the pressure drop with reasonable accuracy and without much computational effort.

Koval (1963) used the 1D fractional flow (Buckley and Leverett, 1942) to describe the viscous fingering flow. The solvent fractional flow was treated in the same manner as the immiscible displacement theory, with the relative permeability proportional to the solvent and the oil volume fractions. They assumed that channeling and the longitudinal dispersion can be combined into one factor called the heterogeneity factor. A fourth order power law viscosity mixing model was used to determine the effective viscosity of the oil solvent mixture. Koval used a value of 0.22 for the solvent concentration as an assumption. A Koval factor was then defined as the product of the heterogeneity factor and the viscosity factor. It was then used in the 1D fractional flow theory to determine oil recoveries and pressure drop for the system.

Todd and Longstaff (1972) modified the viscosity mixing model of Koval. They argued that in a numerical simulator, the final mix viscosity in a grid block can either be a result of negligible mixing due to a very small dispersion coefficient or complete mixing due to a large dispersion coefficient. A factor 'ω' was used as a weighting parameter between negligible mixing and complete mixing for a grid block. The effective viscosities calculated in this manner can then be used in the 1D fractional flow equations to predict the performance of the miscible flood.

However, Fayers (1988) argued that both the Koval model and the Todd and Longstaff model of the viscous fingering cannot in principle be extended to the 2D or 3D.

The viscous fingers are continuous in the principal direction of motion but not in the transverse direction. Thus effectively at a particular cross section, the effective mobilities of oil and solvent are different inside the fingered region than outside the fingered region. To address this issue, Feyers proposed a model where it was assumed that the fingers occupy a finite fraction of the total flowing cross section. The model assumes a sharp transition between the leading edge of the finger and the bulk oil region. Owing to lateral dispersion the fingers eventually broaden until eventually they occupy the entire cross sectional width and the oil displacement efficiency approaches 100%. A fingering function was used to describe this behavior. This model was shown to have the ability to reproduce the experimental observations of the miscible viscous fingering fairly well.

Finite difference simulation of miscible viscous fingering

For complex problems and reservoir scale studies neither the analytical methods nor the empirical models are adequate. Finite difference simulations are undertaken for this situation. Peaceman and Rachford (1962) conducted one such study where the finite difference scheme in a 40 by 20 grid was used to solve a PDE system to describe the miscible displacement of oil by a relatively low viscosity solvent. The numerical simulation method proved helpful in studying the role of the reservoir inhomogeneities and the influence of diffusion and gravity segregation on the development and propagation of viscous fingers. In order to initiate fingering, small random spatial perturbations were introduced in the permeability field.

Earlier detailed simulations of unstable miscible flows were conducted on coarse grids (Claridge, 1972; Gardner and Ypma, 1984; Geordano and Salter, 1984). These studies thus were limited in their capability to throw light on the very detailed and fine structures of the viscous fingers. Viscous fingers occur as a combination of several

different wavelengths as described by the instability theories of miscible and immiscible viscous fingering. The grid size is expected to strongly influence the wavelengths which will grow further with time and the ones which eventually will dampen out with time. Use of the coarse meshes tend to dampen out the small wavelengths of the viscous fingers due to the effects of dispersion and diffusion while the use of fine meshes tend to retain them.

Christie and Bond (1987) conducted a study of viscous fingers on a fine mesh of 130 by 130. The use of the fine meshes was important to study the evolution of the non-linear structures of the viscous fingers at later times. Use of fine mesh however, increase the computational effort and thus may not be possible to be undertaken for a reservoir scale simulation. Settari and Karcher (1985) discuss the grid orientation effects which may alter the results in a miscible or an immiscible unstable flow. Using finer grids can mitigate the grid orientation problem although impractically large number of grids is needed for this purpose. Other methods such as (1) variational approximations (2) modification of interblock transmissibilities and (3) use of nine point finite difference operators have been used in case of unstable miscible and immiscible flows.

CHAPTER 3: MATERIALS AND METHODOLOGY

The current research tests the applicability of chemical EOR method involving the application of alkali, surfactant and polymer in improving the recovery of heavy oil. A comprehensive approach has been adopted to study the proposed chemical EOR procedure. This approach involves the selection of the alkali and surfactant concentration through the test tube experiments, 1D tertiary sand pack floods with the selected chemicals, 2D sand pack floods to study the sweep improvement and mathematical modeling and simulation to understand the mechanisms involved. The current chapter describes the materials used in the research and the methods adopted for conducting calculations.

3.1 MATERIALS

3.1.1 Formation and Injection Brine

The concentration of the formation and the injection brine are kept the same for all the experiments. The reservoir has a lower salinity compared to the conventional reservoirs. The reservoir salinity of 20,000 ppm brine is comprised primarily of NaCl. The salt was provided by the Fisher Chemicals.

3.1.2 Alkali

The role of the alkali in the present research is to react with the organic acids in the crude oil to produce in situ soaps. The soaps then act as in situ emulsifying agents. Due to the absence of the divalent ions in the injection or the formation brine, Na_2CO_3 was used as the alkali for this study. The alkali was procured in the amorphous form from the Fisher Chemicals.

3.1.3 Surfactants

Surfactants work alongside in situ generated soaps in lowering the IFT (Interfacial Tension) and promoting the formation of oil water emulsions. Different surfactants were tried in the test tube experiments out of which we had selected Novel TDA 30EO (Tri Decyl Alcohol 30 Ethoxylate) non-ionic surfactant provided by Sasol for further experiments. The selection of this particular surfactant was based on the promising results shown in the emulsion screening tests with the heavy oil. The adsorption of the non-ionic surfactants on the sand occurs due to the Van der Walls forces rather than the ionic forces responsible in the case of anionic and cationic surfactants. In the case of sand packs the adsorption of the anionic surfactant on the surface is expected to be lower than the non-ionic surfactants. The adsorption needs to be studied for proper design of the process.

The hydrophilicity of this non-ionic surfactant is provided by the ethoxylate groups present in the structure. The hydrophobic carbon chain consists of thirteen carbon atoms. This surfactant has an activity of 100% and is solid at room temperature.

3.1.4 Polymer

Polymers serve to improve the mobility contrast between the oil and water so that the sweep efficiency of the process is improved and the adverse effects of viscous fingering can be countered. Hydrolyzed polyacrylamides (HPAM) are commonly used in the oil industry for this purpose. HPAM is soluble in water due to a negative charge on its structure from the hydrolysis reaction. A high molecular weight HPAM Flopaam^{TM} 3630S (MW=18 million Daltons) procured from SNF was used in this study.

3.1.5 Crude Oil

The crude oils were obtained from a reservoir in the North Slope of Alaska. The table below lists their viscosities and acid numbers.

Crude Oil	Viscosity (cp)	Acid Number (mg KOH/g oil)
Heavy Oil (Oil A)	~10,000 cp	3.54
Viscous Oil (Oil B)	~ 330 cp	1.47

Table 3.1: Properties of the crude oils used

The viscosity values are mentioned at the room temperature of 75F which falls in the temperature range encountered in the reservoir (45-85F). The acid number of the crude oils makes them a good candidate for the alkali application.

3.1.6 Reservoir sand

Reservoir sand gotten from the North Alaskan Slope was used for all the experiments. This sand was wet packed in the 1D column and the 2D cells for flow experiments. Because of the unconsolidated nature of the pack, the permeability of these packs was in the range of 20-25 Darcies.

3.2 EXPERIMENTAL EQUIPMENT

3.2.1 Core Flood Experimental Equipment

Steel tubes

The steel tubes were provided by Autoclave Engineers. They were used as 1D columns with the reservoir sand packed into them. These steel tubes are 0.67 inches in diameter and 3ft in length. Due to the large aspect ratio, flow experiments conducted with these can be expected to be 1D in character.

Stainless Steel Accumulators

The stainless steel transfer cylinders commonly called accumulators were used in order to pump fluids such as oil and polymer into the sandpack. These accumulators were purchased from the Core Laboratories. They contain a floating piston which prevents the two fluids to come in contact with each other. In order to pump oil or polymer into the sandpack, the accumulators were mounted vertically and a mineral oil was pumped into one end, pushing the piston inside and consequently the other fluid (oil or polymer) out into the sandpack.

Pumps

Teledyne ISCO 500D syringe pumps were used to pump the fluids into the desired experimental equipment. These pumps have a volume of 507 ml and can withstand a pressure of 3750 psi.

For brine/Alkali surfactant flood the pumps injected the fluid directly into the sandpack whereas for the oil/polymer injection operations the pumps were used to inject the mineral oil into the steel accumulators.

Pressure Transducers

Pressure transducers were used to record the pressure drop between the inlet and the outlet of the sandpack. They were purchased from Honeywell and a proper range was selected (0-300 psi) to ensure that an appropriate precision in the pressure measurements be maintained. The pressure transducers convert the measured pressure drop into a voltage signal and send that signal to a Data Acquisition Card (DATAQ) where it is converted into the digital format. The digital voltage data are now send to the desktop computer where they are logged into a spreadsheet file. In order to convert the raw

voltage data back into the pressure drop readings, a calibration curve between pressure drop and recorded voltage was generated before starting the flow experiments.

2D cells

Two kinds of 2D cells were used for the experiments, one made from the plastic material and the other made from the steel material. The cells have a length and width of 10 inches. The thickness of the plastic 2D cell is 0.5 inches and that of the steel cell is 1 inches. The plastic cell was used to enable the visual observation of the flood fronts which was not possible in the steel cell. However the use of the plastic cell was discontinued because of its low operating pressure which led to cracks developing on it. The steel cell had a higher operating pressure and an option of providing an overburden pressure leading to tight sandpacks.

Fraction Collector

A Retriever 500 fraction collector was used to collect the effluent samples from the sandpack at regular time intervals.

3.2.2 Analytical Instruments

Conductivity Meter

An Oakton Con 510 meter was used to measure the conductivity of the samples for the brine tracer test. This meter can measure up to 5 different measurement ranges with auto ranging capability which automatically detects and promptly switches to the appropriate range. Meter has an inbuilt automatic temperature compensation which compensates for any minor temperature fluctuations.

Viscometer

Brookfield DVII+ viscometer was used to measure the sample viscosity as a function of the shear rate. The viscometer uses the cup and cone geometry. The sample size was 1 ml. The sample is loaded in the cup and the instrument motor rotates the cone which contacts the fluid in the cup. The speed of rotation of the cone also called spindle is converted to the shear strain. The torque required to rotate the fluid at that particular speed is measured and converted to a viscosity value. Measurements at different speeds of rotation generate the viscosity-shear rate curve. The instrument is simple to operate but can only measure viscosity at applied shear strains higher than $1s^{-1}$.

Rheometer

For more precise measurements the bulk viscosity measurements were conducted using the AR-G2 rheometer provided by TA instruments. The instrument works on a similar principle as the viscometer but is more robust in terms of the operation. Shear strain values as low as $0.01s^{-1}$ can be used for viscosity measurements. The instrument comes with three geometries catering to different needs. Cone and plate geometry was widely used in this study. 0.6 ml of sample volume is required for this geometry. In addition to viscosity, the instrument can also measure the detailed rheology.

Microscope

A Nikon microscope was used to get a magnified image of the emulsion droplets for their typical droplet sizes.

HPLC

High Performance Liquid Chromatography (HPLC) was used to determine the surfactant concentration in the effluent samples. The instrument measures the retention time of a particular component in the mobile phase. A calibration curve between the

component concentration and retention time was generated before the actual measurements.

3.3 METHODOLOGY

3.3.1 Test tube experiments for Heavy Oil (Oil A)

Test tube experiments were conducted on the heavy oil in order to determine the concentration of the alkali and surfactant which would produce oil water emulsions. Different hydrophilic surfactants were tested in our lab to identify those which can form low viscosity (order of a few centipoises) oil-in-water (O/W) emulsions with the reservoir oil. Surfactant concentration was fixed in the initial screening tests. These tests were carried out at a constant WOR (water-to-oil ratio) of 9:1 and at the reservoir salinity. Bryan and Kanzas (2007) list the requirements for the formation of O/W in the bulk liquid study. Out of the two liquids, the phase with a higher volume is more likely to become a continuous phase. If the total surfactant is more soluble in one phase, that phase is likely to become the continuous phase. Taking these rules of thumb into consideration, the WOR of 9:1 was chosen and a hydrophilic surfactant was added along with alkali which would generate soap.

Because of the absence of divalent ions, sodium carbonate (Na_2CO_3) was chosen as the alkali. Surfactant and alkali were added to the NaCl brine and then mixed with reservoir oil in glass vials. The samples were mixed thoroughly and allowed to stand for 1 week or more to allow the phases to separate at the room temperature, ~75^0F. The amount of the emulsion phase was observed. The nature of the emulsions was determined by dissolving a droplet of the emulsion in DI water and toluene. In the case of O/W emulsion, the droplet dissolved in DI water but did not dissolve in toluene. The opposite is observed in the case of W/O emulsions. In some cases, the viscosity of the emulsion

phase was measured by a cup and cone Brookfield DVII+ viscometer. This mixture was further tested at different WORs and salinities in order to understand the emulsion behavior under varying conditions.

The figure below shows an example of an emulsion generated by the action of alkali and surfactant.

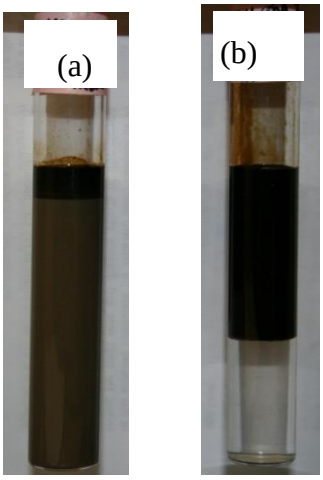

Figure 3.1: Example of emulsions generated for different WORs (a) O/W emulsion (b) W/O emulsion

3.3.2 Test tube experiments for Viscous Oil (Oil B)

For the lower viscosity oil surfactant screening experiments were conducted to identify the surfactant-alkali combinations which could generate large oil and water solubilizations and thus ultra-low interfacial tensions (IFT). These experiments are also performed at a temperature of 75F. Due to the high organic acid content of this crude oil (1.47 mg KOH/100 g oil), an alkali was used to generate in situ soaps. For the viscous oil, we were interested in producing microemulsions unlike that of the heavy oil. Nelson and Pope (1978) found out that the equilibrium phases in test tube studies are representative of the phases produced in the core flow experiments. Nelson et.al. (1984) proposed a combination of alkali and a hydrophilic surfactant be used for getting

optimum IFT in the region where the alkali concentration is high enough for it to propagate satisfactorily through the reservoir. Formation brine has low salinity (20,000 ppm NaCl) and negligible divalent ions such as calcium and magnesium; thus sodium carbonate is used as the alkali. In addition to the alkali, a synthetic non-ionic surfactant was added to bring the optimum salinity to the desired level. The in situ generated soap lowers the requirement of the externally added surfactant. The amount of in situ generated soaps is in turn dependent on the volume ratio of water and oil (WOR) in the system (Nelson 1978). Prescribed amounts of water, oil, alkali, and surfactant were mixed at different water-to-oil ratio (WOR) and the volumes of equilibrium phases were read. These volumes were thereafter used for calculating the solubilization ratios of oil and water. In a single test, the concentrations of NaCl and surfactant were kept constant and the alkali concentration was increased in steps. Higher alkali concentrations ensure the formation of more soap on one hand and increase the total electrolyte concentration on the other hand.

The activity diagram was then constructed showing the Type I, II or III regions at different WOR. Samples were equilibrated in test tubes (not pipettes) because the viscosity of the oil was quite high.

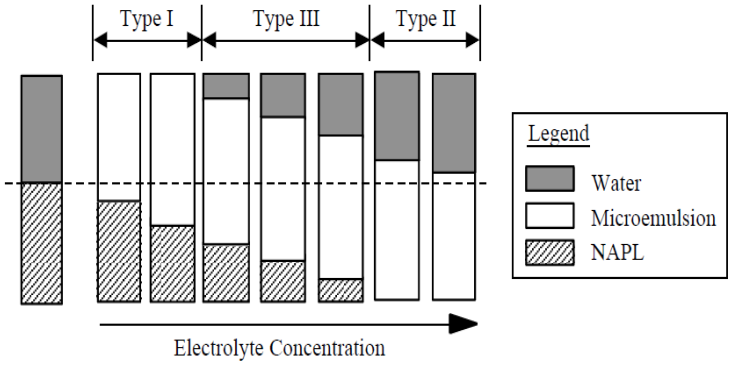

Figure 3.2: An example of different microemulsion systems obtained with increasing electrolyte concentration (UTCHEM Technical Documentation, 2010)

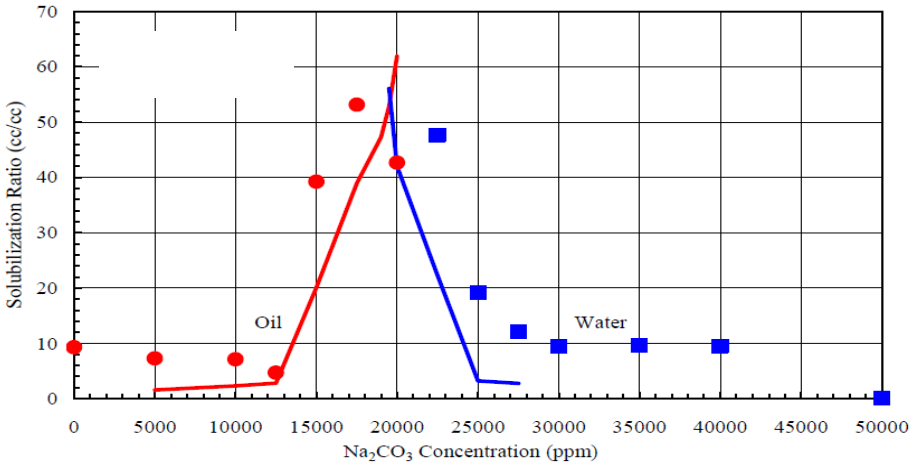

Figure 3.3: An example of oil and water solubilization ratios with increasing alkali concentration (Mohammadi *et.al.* 2008)

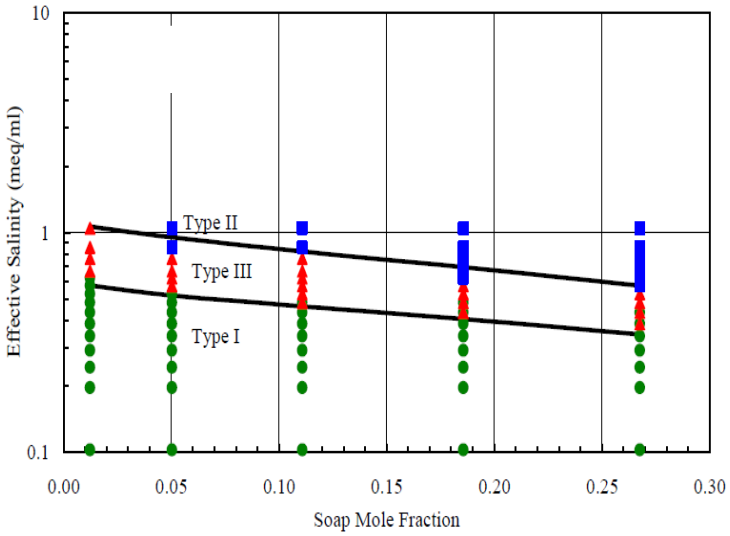

Figure 3.4: An example of the activity diagram with increasing soap mole fraction (Mohammadi *et.al.* 2008)

3.3.3 Sand pack floods in a thin steel tube

Sand pack floods were conducted in order to assess the surfactant system and identify the parameters governing the oil recovery.

Preparing the Sand pack

In order to prepare the sand pack, the target reservoir sand was washed and wet packed in a thin 3 feet long steel tube having an inside diameter of 2/3 inches. Brine water and the water wetted sand were alternatively poured inside the steel tube. Excess water was drained from the bottom outlet of the sand pack. This procedure ensured that no air gets trapped inside during packing. The sand pack was tapped regularly from outside for maximizing the packing of the sand grains. After packing the sand, the top cap was tightened and brine was injected from the bottom end to ensure that any residual air is removed. It is to be noted that the sand packs prepared were water-wet in nature as they were not aged with oil for substantial amount of time at high temperature.

Brine tracer test

For determining the pore volume of the sand pack, a brine tracer test was conducted. The sand pack was saturated with a brine of a particular salinity. Thereafter a brine of different salinity was injected in the sand pack at 5ml/min and the effluent samples were collected using a fraction collector. The salinity response at the outlet gives a measure of the pore volume.

Permeability test

The absolute permeability of the pack was determined by flowing brine through it and measuring the pressure drop across the pack using a Honeywell pressure transducer. Brine was injected at flow rates of 5-20 ml/min. The brine injection was continued until the pressure drop across the pack reached a steady state value. Absolute permeability of the pack was determined by fitting the data to the Darcy equation.

Oil flooding

Saturating the pack with oil is the next step. To speed up the process, the oil saturation was conducted at the high temperature of 80^{o}C. A steady pressure drop of ~400 psi was applied and the process was continued until no more water was produced at the outlet. From the mass balance Soi was calculated.

The sand pack was then allowed to cool down for 2-3 days for temperature to drop to 75F. Oil flood was again commenced, this time at the room temperature and at a steady flow rate of 0.018 ml/min. The chosen flow rate is equivalent to the frontal velocity of ~ 1ft/D. The steady state pressure drop was measured and end point oil relative permeability kro^{o} was calculated.

Waterflooding

Waterflooding was conducted for 3-4 PV as a secondary recovery process at a frontal velocity of 1ft/D. For the heavy oil, we did not continued the waterflood till the residual oil saturation was reached because that would require a large number of PVs of water to be injected which is not practical in the field. The oil cuts were about 2% when we stopped the wateflooding. The effluent was collected periodically using a fraction collector and the pressure drop across the pack was recorded at an interval of 1s. After the waterflood, the cumulative oil recovery as a function of PVs injected was calculated. Sorw was calculated from the mass balance. From the pressure drop data an approximate value of krw^{o} was determined.

Chemical flood

Chemical flood was commenced after the waterflood for tertiary oil recovery. The concentration of the chemicals such as alkali and surfactant was fixed from the test tube experiments. In some experiments chemical flood was conducted in the secondary mode

before the waterflood. Depending on the process different slug sizes and chemical concentrations were tested. For the heavy oil the NaCl salinity was a primary variable in the chemical solution. From the test tube experiments it was found that salinity impacts the emulsion type and the emulsion behavior. The impact of this difference was tested in the sand pack floods by conducting these at different salinities. Slugs of alkali and surfactant were injected directly from the ISCO pump whereas the slugs containing polymer was injected via the fluid transfer vessels called accumulators. The effluent samples were collected using the fraction collector and any emulsions or microemulsions at the outlet were broken down to yield pure oil, the volume of which was used to calculate the oil recovery curve.

Effluent analysis

The effluent from the waterflood and the chemical floods were analyzed for generating oil recovery curves. After every waterflood the sample tubes were capped and heated at 70-80C for 2-3 hours in convection oven. They were then centrifuged. The treatment ensured that oil and water phases get separated thoroughly before their volumes are read.

Similar treatment was conducted for chemical flood with an additional step which involved breaking down the emulsions and microemulsions to yield pure oil. Different methods were used to break W/O than O/W emulsions. For O/W emulsions, the samples were concentrated with a high amount of NaCl salt. The high salt content destabilized the O/W emulsions. In order to break the W/O emulsions, TEGBE alcohol was added to the test tubes. The alcohol makes the total surfactant environment hydrophilic in nature. These samples were subsequently heated and centrifuged for completer phase separation.

Analysis of the pressure drop data

The pressure data was recorded in a spreadsheet file in the form of voltage values. To convert these into pressure drop values, a calibration curve between applied pressure drop and voltage response was generated before starting any experiment. Figure 2.5 gives an example of such curve. This curve was then used to calculate the pressure drop values from the voltage readings.

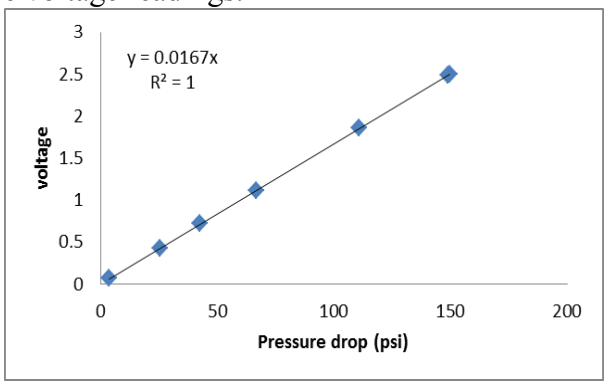

Figure 3.4: Calibration curve between voltage response and applied pressure drop

3.3.4 Sand pack floods in a 2D cell

Sand pack floods conducted in a 2D cell followed very similar steps as those conducted in the steel tube. This section talks about some of the differences in the manner of packing sand and methods used to calculate the sand pack properties. Two kinds of 2D cells were used; one with plastic material of construction and the other with the steel material.

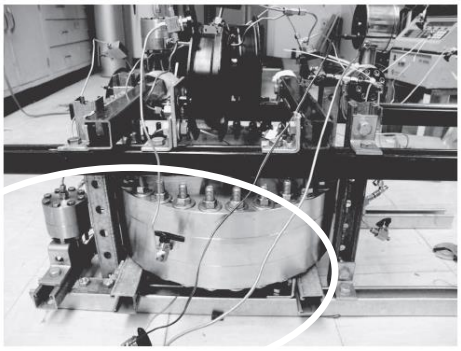

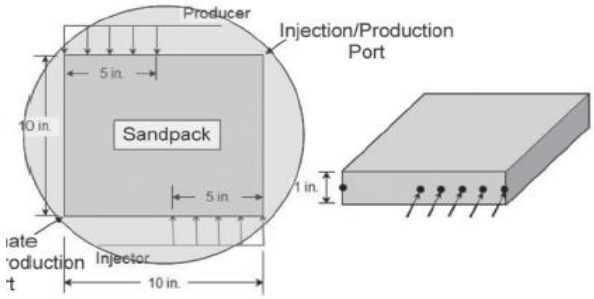

Figure 3.5: Steel 2D cell

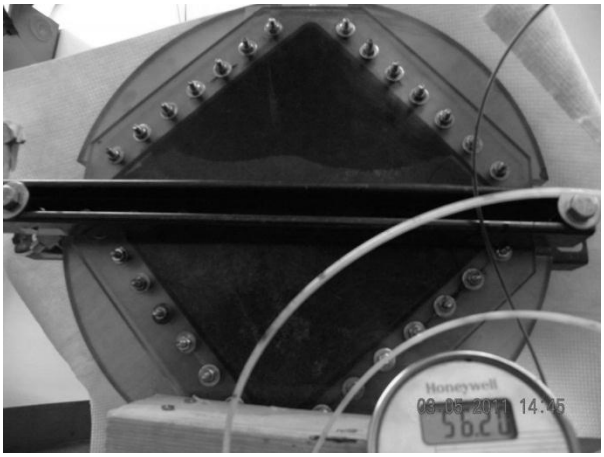

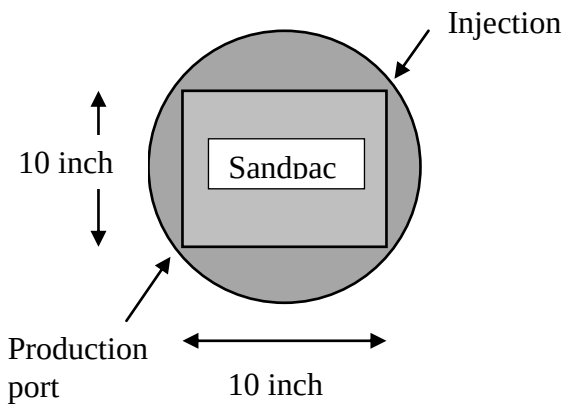

Figure 3.6: Plastic 2D cell

Preparing the Sand pack

Different sand pack preparation methods were used for the plastic and the steel 2D cell. Sand was packed in the dry state in the plastic model. Dry packing enabled us to determine the air porosity and permeability. However a very loose pack resulting in a very high porosity was obtained. On pressurizing the pack to 30-40 psi some gaps were observed because of which the sand pack had to be unscrewed and opened again and more sand has to be filled in. This process was continued until even after pressurizing, no more gaps were observed. This kind of operation was not possible in the steel model as it takes a few days to put it together and reopen it. Hence a wet packing procedure was followed. The first step is to wet the sand sufficiently with a known volume of the brine water. The water wetted sand is then spread in the square shaped slot in such a manner that there is always a small quantity of extra water taking care that no air gets trapped inside. The extra sand was scraped off the surface. A circular rubber sheet was put on the sand and the top plate was subsequently screwed on. The rubber sheet was used to

provide a good seal and also for preventing the overburden fluid in coming in contact with the sand. The last step is to provide overburden pressure. For this purpose the top and the bottom plates are equipped with two ports. The overburden liquid (water in this case) is injected from the top plate all the way to the bottom plate. The liquid fills in the space between the rubber sheets and the inside surface of the plates. 1800 psi of overburden pressure was applied. The overburden pressure keeps the sand from moving inside and also compresses the sand so that a tighter pack is obtained. The compression of the sand released some water which was collected from the side ports.

Porosity determination

The determination of pore volume in the plastic model involved the following steps; determine the air porosity of the sand pack, apply a vacuum on it and then flow brine through it to calculate the brine porosity. The sand was packed in the wet state in the steel model and hence it was not possible to calculate the air porosity. The rough estimate of the pore volume was gotten by subtracting the volume of water expelled from the pack on applying the overburden pressure from the amount of water used to wet the sand. Another accurate method of measuring the porosity was to conduct a tracer test on the sand pack. The measurements gave close estimations of the pore volume but the one calculated from the tracer test was considered the final one.

Permeability determination

To measure the permeability of the sand pack, brine was injected at different flow rates and the pressure drop across the pack was recorded. Simple Darcy equation could not be used because of the nonlinear geometry. The quarter 5 spot was modeled in the CMG STARS reservoir simulator. The grid model was fully saturated with water. Water injection was simulated at different flow rates. The pressure drop predicted by the

simulator was matched with that measured during the water injection experiment by adjusting the absolute permeability of the sand pack. The value which could match the two pressure drop values fairly well was considered the actual absolute permeability of the sand pack.

Waterflood and chemical flood

Waterflood and chemical flood was conducted at a flow rate of 0.1 ml/min. The method of analyzing the data was same as the floods conducted in the steel tubes.

3.4 CALCULATIONS AND EQUATIONS

3.4.1 Emulsion quality calculation

Emulsion quality is defined as the volume fraction of the droplet phase contained within the emulsion. Dilute emulsions are the ones with a low emulsion quality whereas concentrated emulsions can have the quality close to 50% or even more. Mathematically,

$$Q = \frac{V_{drop}}{V_{em}} \tag{3.1}$$

Where Vdrop is the volume of the droplet phase

Vem is the total volume of the emulsion phase.

3.4.2 Microemulsion phase behavior calculations

Solubilization plots

The microemulsion phase behavior in the case of the low viscosity oil was interpreted in terms of the solubilization ratios. The oil solubilization ratio is defined as the volume of oil solubilized in the microemulsion normalized by the volume of the total surfactant in the microemulsion. For simplicity it is usually assumed that the all the surfactant (soap and external surfactant) resides in the microemulsion phase only. The oil

solubilization is found out by measuring the difference in the oil volumes between the initial state and the final equilibrium state. On the similar lines the water solubilization value is calculated.

$$\sigma_o = \frac{V_o}{V_s} \tag{3.2}$$

$$\sigma_w = \frac{V_w}{V_s} \tag{3.3}$$

The solubilization plot is generated by calculating the oil and water solubilization ratios at different salinities.

It is to be noted that for the Type I and Type II microemulsions, only the oil solubilization ratio and water solubilization ratio is calculated respectively. For the Type III microemulsion both the oil and water solubilization ratios are calculated.

3.4.3 Sand pack flood calculations

Pore volume estimation in a 1D flood

The pore volume of the sand pack was calculated by conducting a brine tracer test on the sand pack. A step change in the brine salinity is given at the inlet and the response is measured at the outlet. The salinity of the outlet is normalized by the following equation

$$C_D = \frac{C - C_J}{C_I - C_J} \tag{3.4}$$

Where, C_D = Normalized salinity of the fluid at the outlet

C_J = Initial salinity in the sand pack

C_I = Injected salinity

The normalized salinity at the outlet is plotted with respect to the cumulative volume of the fluid injected (or produced) (V_f). The plot is an S shaped curve and value

of the cumulative fluid volume at the mid-point salinity is read from the curve. In theory this gives the pore volume of the sand pack. Figure 3.7 gives an example of such a curve.

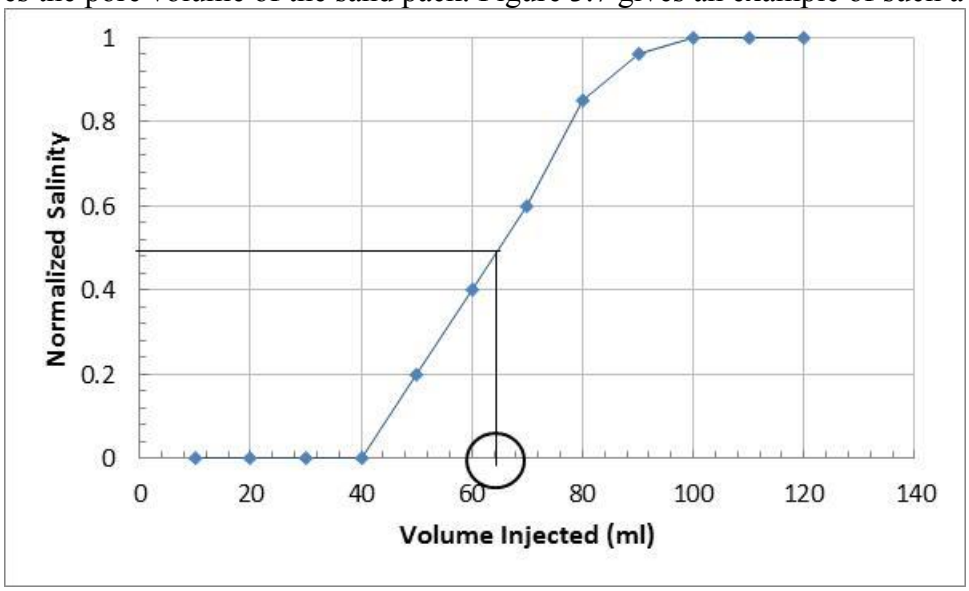

Figure 3.7: Estimation of pore volume by tracer test

Pore volume estimation in a 2D flood

A preliminary estimation of the pore volume could be had by subtracting the water expelled by the five spot after applying the overburden pressure from the initial water volume used for wetting the sand. For a more accurate estimation a tracer test was conducted on the 2D sand pack. The method of conducting the test was similar as the 1D sand pack; the analysis of the results is different. The effluent salinity was normalized by equation 3.4 to yield C_D. Next the areal sweep efficiency was computed by

$$E_A = \int_0^{t_D} \left(1 - \frac{C_D}{C_{Do}}\right) dt_D \qquad (3.5)$$

Where E_A = Sweep efficiency

C_D = Normalized salinity at the outlet

C_{Do} = Normalized salinity at the inlet = 1

Sweep efficiency at breakthrough (E_{Abt}) is read from the curve. Brigham and Smith (1965) conducted a tracer test calculation on a 5 spot pattern and calculated that the breakthrough of the tracer occurs at 0.72 PVs injection. Also 100% sweep by the tracer occurs at an injected volume of 2.4 PV. Correspondingly the breakthrough sweep efficiency (E_{Abt}) is 0.72 and E_{Afinal} is 1.0 at 2.4 PV.

An initial estimate of the pore volume was used to calculate the E_A and E_{Abt}. Later the pore volume value was adjusted until the E_{Abt} was 0.72 and the E_{Afinal} was close to 1.0.

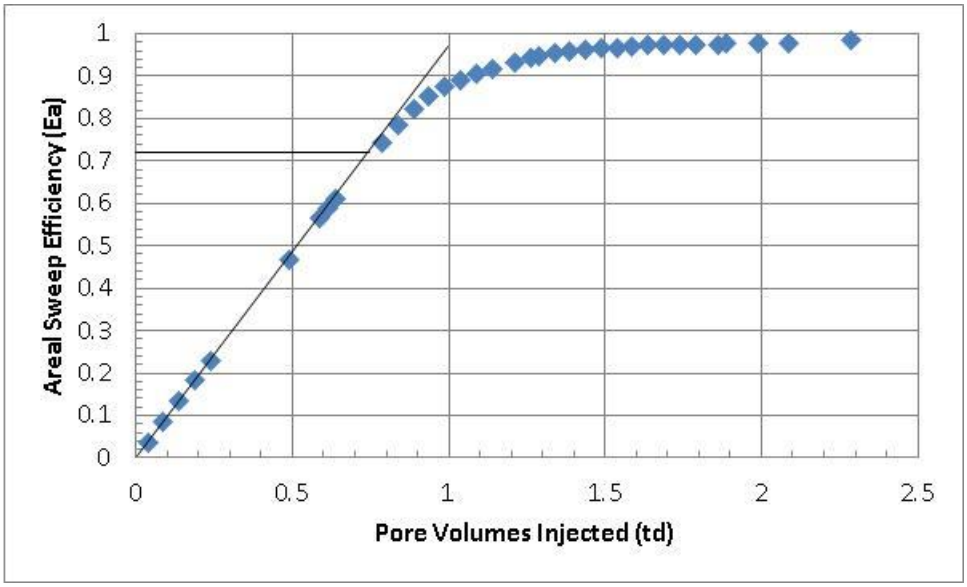

Figure 3.8: An example showing the graphical determination of breakthrough E_A.

Permeability calculation in a 1D flood

Darcy equation was used to calculate the permeability of the 1D sand pack. The steady state pressure drop was recorded for different flow rates. Darcy equation is given by:

$$q = \frac{kA}{\mu L}\Delta P \qquad (3.6)$$

Permeability calculation in a 2D flood

The permeability of the 2D sand pack was calculated by taking help of the reservoir simulator CMG. Brine was injected at different flow rates and the pressure drop across the 2D sand pack was measured. The same process was then simulated in CMG. The quarter 5 spot model was simulated in CMG with a 10 × 10 × 5 cartesian grid structure. Two aqueous components were defined having the viscosity of 1 cp.

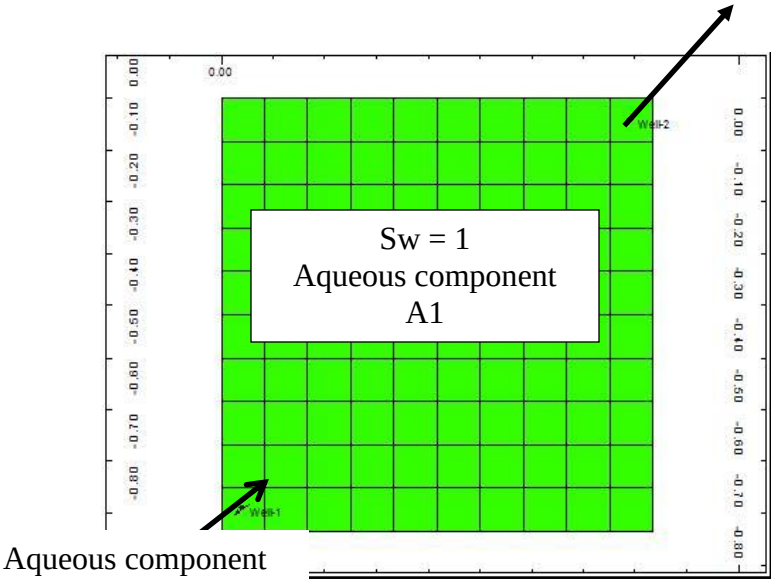

Figure 3.9: Grid model of the quarter 5 spot used in CMG STARS

The model was initialized with the water saturation equal to 1. This water consisted of the component A1. We simulated the water injection from the injection well and compared the pressure drop predicted by the simulator with the pressure drop measured from the experiments. The absolute permeability of the sand pack was varied until a good match between the simulated and the experimental pressure drop was achieved. The absolute

permeability calculated by this method was compared with the permeability calculated from the formula developed for 5 spot flows:

$$q = \frac{k\Delta P\pi}{\mu\left(\ln\left(\frac{d}{r_w}\right) - 0.6190\right)} \quad \text{(Muskat, 1982)} \qquad (3.7)$$

The calculated permeability was found to differ from that estimated from CMG simulations by 20%.

End point relative permeability calculation

The end point relative permeability of a phase is calculated by invoking the Darcy equation. During this calculation, it can be safely assumed that the other phase is immobile.

$$q_j = \frac{kk_{rj}A}{\mu_j}\frac{\Delta P_j}{L} \qquad (3.8)$$

Where qj = flow rate of phase 'j'

k = absolute brine permeability

krj = relative permeability of phase 'j'

μj = viscosity of phase 'j'

ΔPj = Pressure drop in the phase 'j'

Initial oil saturation

The initial oil saturation was calculated by noting the volume of water produced during the oil saturation process. By mass balance, this volume is equal to the volume of the oil residing in the sand pack. Thus the initial water saturation can be calculated as:

$$Soi = \frac{Vo}{Vp} \qquad (3.9)$$

Where Soi = Initial oil saturation

Vo = volume of oil in the sand pack = volume of water produced

Vp = Pore volume

Cumulative oil recovery

The cumulative oil recovery from an experiment was calculated as a function of time by summing over the effluent oil volumes. Division by the pore volume gave the oil recovery in the units of pore volumes.

$$Np = \frac{\sum Vo}{Vp} \qquad (3.10)$$

Where Np = Cumulative oil recovery

Vo = Effluent oil volume as a function of time

Vp = Pore volume

Oil Cut

Oil cut at the outlet was calculated by fraction of the oil produced at the outlet. Mathematically, oil cut 'fo' can be defined by

$$f_o = \frac{V_o}{V_o + V_w} \qquad (3.11)$$

Where fo = Oil cut

Vo = Effluent oil volume as a function of time

Vw = Effluent water volume as a function of time

CHAPTER 4: EXPERIMENTAL RESULTS

The following chapter describes the results of the design and the performance analysis of the chemicals such as alkali, surfactant and polymer in improving the recovery of the heavy oil. The chapter is divided into 2 major sections. The first section deals with the results of chemical design and the sand pack floods of the 10,000 cp oil (Oil A). In the second section, similar results are presented for the 330 cp oil (Oil B).

4.1 CHEMICAL SCREENING AND SAND PACK EXPERIMENTS FOR OIL A

The section describes the test tube experiments used to identify the appropriate combination of the chemicals which could generate the oil and water emulsions. The properties of the emulsions; their type and viscosity characteristics are also described. From the test tube experiments it was possible to draw some conclusions on the dependence of emulsion type on salinity, Water to Oil ratio (WOR) and alkali and surfactant concentrations. It is to be noted that these controlling parameters may vary in position and time as the displacement proceeds due to dispersion, mixing, etc. and hence it is essential to undertake such a study. Next, sand pack floods using the chemicals are described where the salinity and the flow rate of the flow experiments were varied.

4.1.1 Chemical screening tests

Identification of the alkali surfactant system

The initial chemical screening tests were conducted to check whether a combination of alkali and surfactant can generate low viscosity O/W emulsions. These emulsions were deemed to be the desired emulsions due to their low viscosity and the ease of flow. In each set of experiments surfactant type/concentration, salt concentration, and WOR were kept constant and the alkali concentration was varied from 0 to 1.5 wt %. These studies were carried out at the room temperature of 75^{o}F. Figure 4.1 shows the emulsion

behavior for the mixture of 0.1 wt% TDA 30 EO in 20,000 ppm NaCl and oil at a WOR of 9:1 after 1 week of equilibration. The high WOR was adopted to enhance the chances of oil-in-water emulsions. Formation of O/W emulsion was observed in samples with 0.1 and 0.5 wt% alkali. At alkali concentration of 0% the oil-water emulsion separates into two distinct phases within 1 hour. The emulsion in the sample with 0.5 wt% alkali had a viscosity of 2.7 cp. Because of the favorable properties (low viscosity O/W emulsion formation and ample supply in our laboratory) the combination of TDA 30EO surfactant with 0.5% alkali was chosen for additional emulsion studies. These studies were performed in order to observe any changes in the emulsion behavior with different conditions such as WOR and salinity.

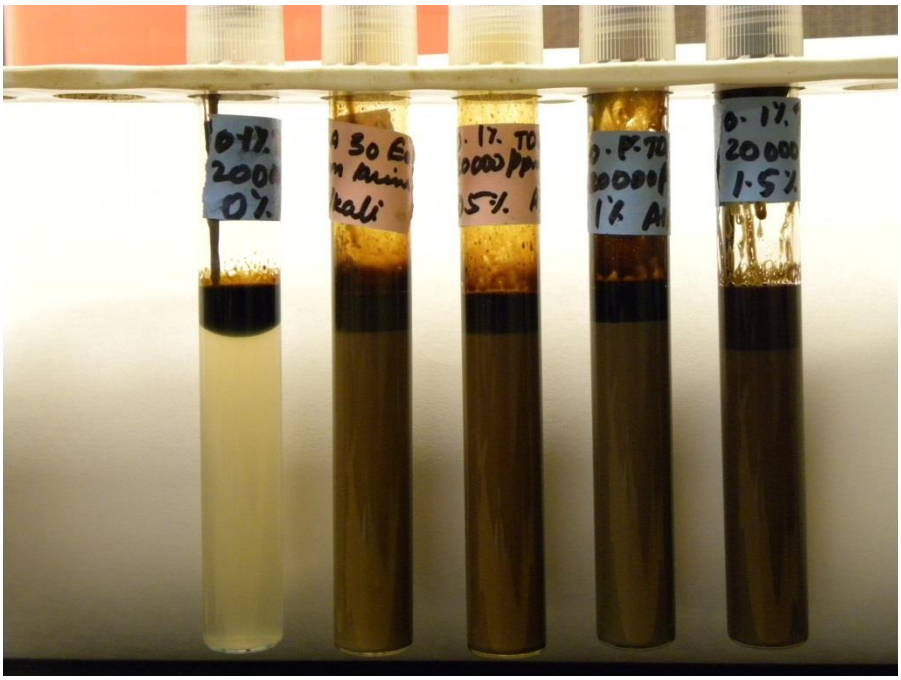

Figure 4.1: Emulsions formed by 0.1 wt% TDA 30 EO; 20,000 ppm NaCl and alkali concentration varying from 0 wt% on the left to 1.5 wt% to the right, after 1 week

Change of emulsion behavior with WOR

The preliminary emulsion study was conducted at a high WOR of 9:1. In the next part of the study, the alkali and surfactant concentrations were kept constant (0.1 wt% TDA 30EO and 0.5 wt% alkali), but the WOR was varied. Figure 4.2 shows the emulsion behavior when the WOR was decreased from 9:1 to 7:3 with 20,000 ppm NaCl brine. The O/W emulsion was observed at high WORs, the emulsion changed to high-viscosity water-in-oil (W/O) emulsion at lower WOR (right two samples). The viscosity of the W/O emulsions was measured at 0.6 s^{-1} shear rate and is shown in figure 4.2 (b). As the WOR decreases, more soap is generated which makes the soap-surfactant mixture more hydrophobic and destabilizes the O/W emulsions.

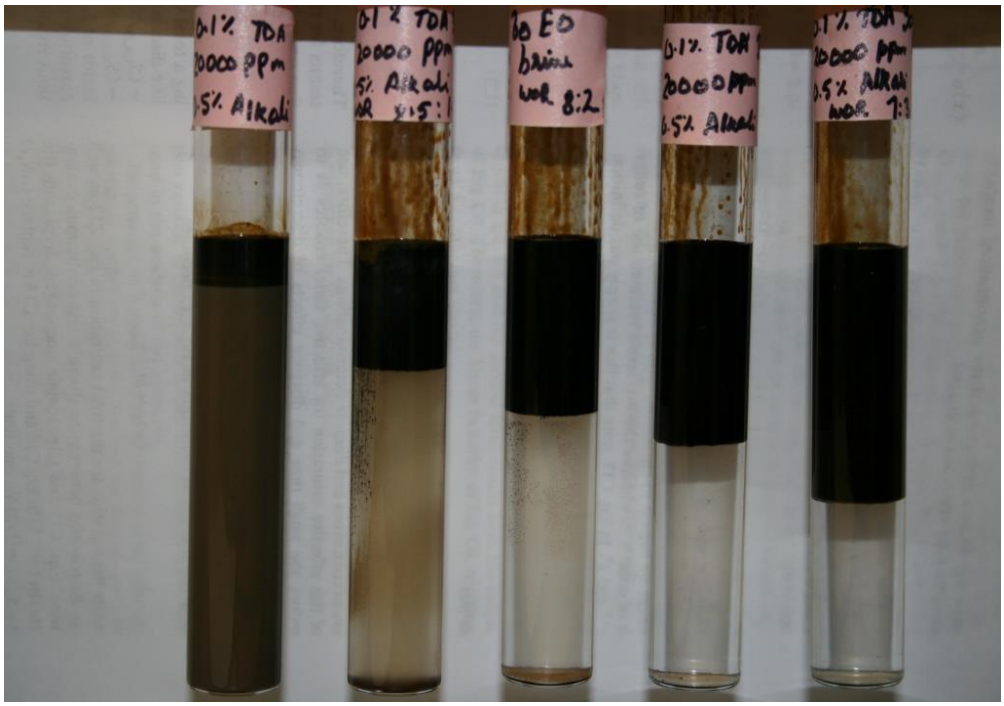

Figure 4.2 (a): Emulsions with 0.1 wt% TDA 30EO, 0.5 wt% alkali and 20,000 ppm NaCl with WOR varying from 9:1 (left) to 7:3 (right)

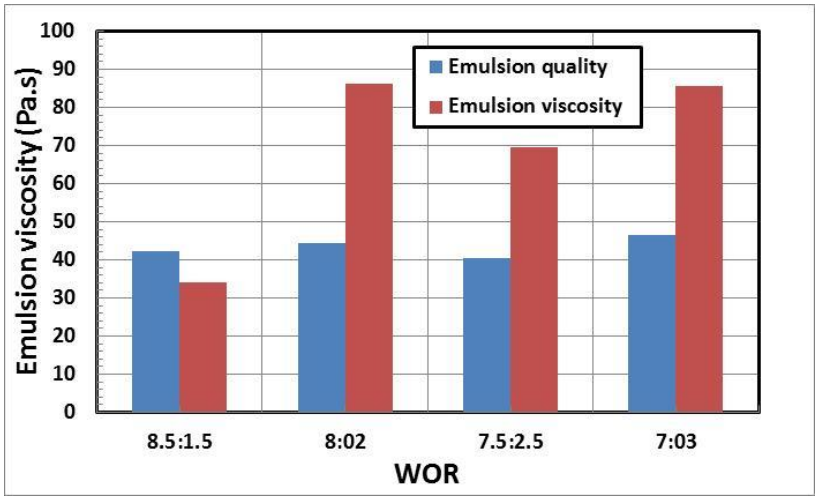

Figure 4.2 (b): Properties of the emulsions generated with 0.1 wt% TDA 30EO, 0.5 wt% alkali and 20,000 ppm NaCl and different WORs.

Figure 4.3 (a) shows the emulsion behavior with WOR variation for 0 ppm NaCl. All the samples showed O/W emulsions. Detailed analysis was conducted for emulsions with varying alkali concentration at WOR of 5:5. The results are presented in figure 4.3 (b). The viscosity of those emulsions was measured and is shown in figure 4.4. From figure 4.3 (a), it can be seen that for all the WORs tested and at a concentration of 0.5 wt% alkali the oil is solubilized easily into the aqueous phase. After emulsification, only a single phase could be seen in all the test tubes. A drop of this phase readily dissolved in DI water but did not dissolve in an organic solvent such as toluene. The test confirms the fact that the generated emulsion is O/W type. Figure 4.3 (b) shows the emulsion type generated for WOR of 5:5 (1:1) and different alkali concentrations. It can be seen that for alkali concentrations in excess of 0.3 wt%, all the oil is emulsified. Below this concentration very little oil was solubilized. Figure 4.4 shows the viscosity of this emulsion for alkali concentrations 0.3 wt% and higher. A shear thinning behavior is exhibited with plateau viscosities of 5.5 Pa.s (5500 cp) for shear rates lower than 1 s^{-1}.

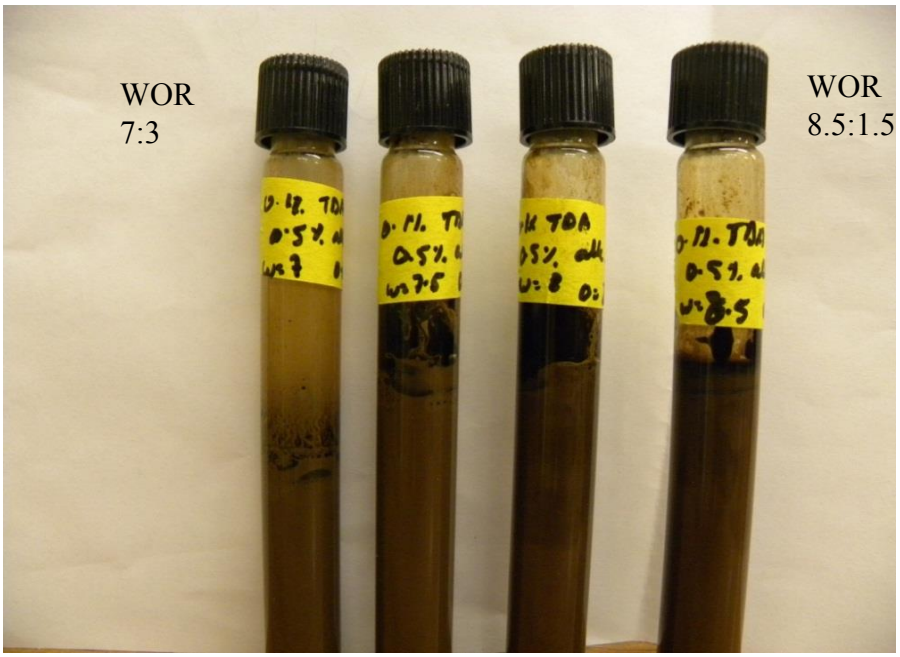

Figure 4.3 (a): Emulsions with 0.1 wt% TDA 30EO, 0.5 wt% alkali and 0 ppm NaCl with WOR varying from 7:3 (left) to 8.5:1.5 (right).

Figure 4.3 (b) Emulsions with 0.1 wt% TDA 30EO, 0 ppm NaCl, WOR 5:5 with alkali concentration varying from 0 wt% (left) to 0.5 wt% (right).

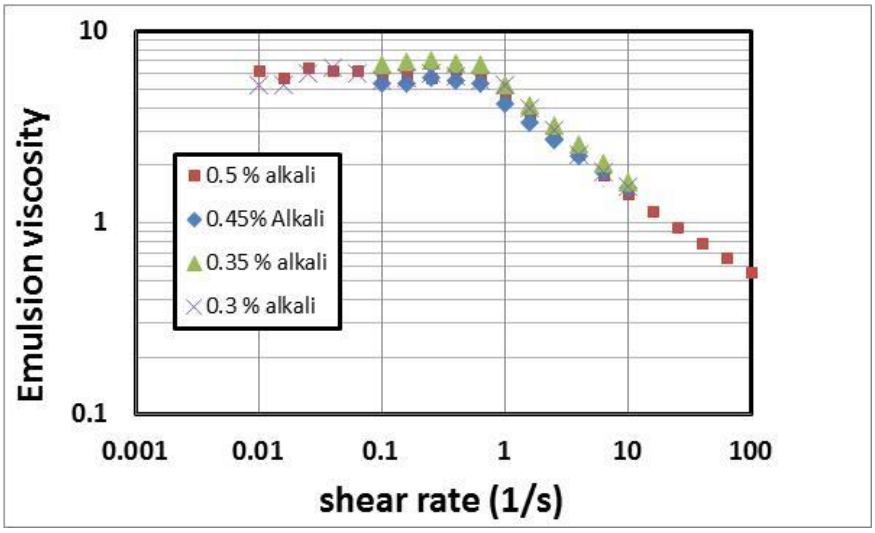

Figure 4.4: Viscosity of the emulsion at WOR = 1:1. Emulsion viscosity is in Pa.s

Change in emulsion behavior with salinity

From the above two tests, it was concluded that the emulsion behavior depends on salinity of the brine as well as the WOR. A salinity scan was performed at a WOR of 7:3 to determine the salinity at which a transition takes place from O/W emulsions to W/O emulsions. Figure 4.5 shows the state of the emulsion with increasing salinity from left to right. At low salinities, O/W emulsions appear at the bottom with their light brown color. As the salinity is increased to about 7500 ppm the O/W emulsions changed to W/O emulsions with dark brown phases appearing at the top of the aqueous phase. Rosen (2004) has shown that as the salinity increases, the electrostatic repulsion between oil drops decreases and O/W emulsions become unstable. As the WOR decreases, the ratio of soap to surfactant increases. Soap is relatively lipophilic and the TDA 30EO is hydrophilic. It can be expected that the microemulsion phase behavior may transition from Winsor I to Winsor II as the WOR decreases [Liu, *et al.*, 2008]. Lower phase microemulsions lead to O/W macroemulsions and vice versa. Therefore the

macroemulsions also transition from oil-in-water to water-in-oil as the WOR is decreased.

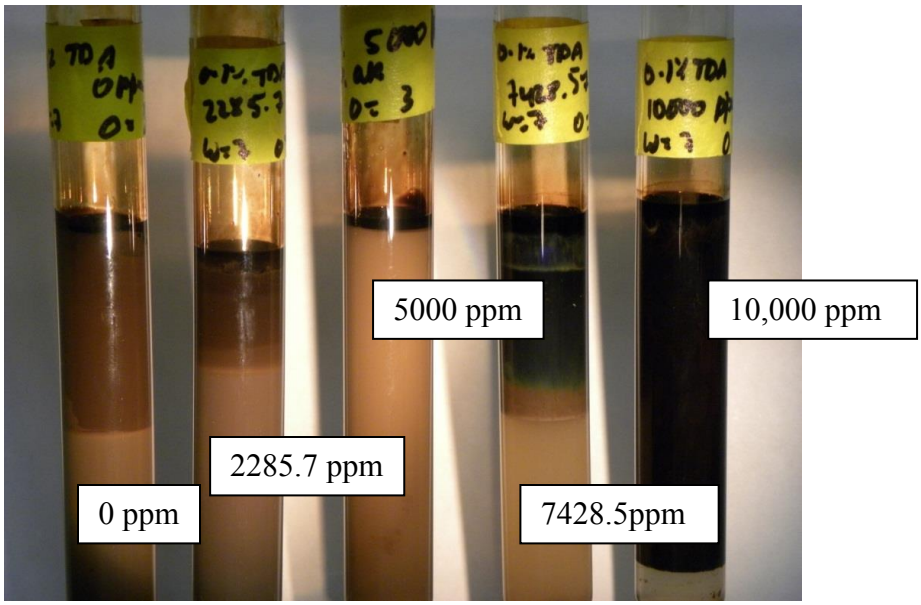

Figure 4.5: Emulsions with 0.1% TDA 30EO, 0.5wt% alkali and salinity increasing from 0ppm (left) to 10,000ppm (right)

The surfactant phase behavior studies showed that emulsion behavior depends on salinity, alkali concentration and WOR. It was possible to form O/W emulsions under lower salinity and higher WOR for TDA 30EO. Sand pack floods were then conducted to study the effect of salinity on the oil recovery by alkali surfactant flooding.

4.1.2 Sand Pack Floods with alkali surfactant

Table 4.1 provides the properties of the sand packs used for the flood experiment. These sand packs were prepared by the procedures outlined before in the methodology section. We varied the salt concentration and velocity, but kept the alkali-surfactant type and concentration constant. The goal was to evaluate oil recovery in alkaline surfactant floods, associated pressure drops, and the type of emulsions produced.

Sand pack properties	Flood 1	Flood 2	Flood 3	Flood 4	Flood 5
Permeability(Darcy)	28.56	28.56	20.40	20.40	20.40
Porosity (%)	35.0	37.50	36.40	43.70	41.50
Swi (%)	10.00	10.00	10.70	10.00	9.64
NaCl salinity (ppm)	20,000	0	8,900	20,000	20,000
Injection velocity (ft/D)	1	1	1	5	1
AS used	0.1% TDA 30EO, 0.5% alkali	0.1% TDA 30EO, 0.5% alkali	0.1% TDA 30EO, 0.5% alkali	0.1% TDA 30EO, 0.5% alkali	0.1% TDA 30EO, 0.5% alkali
Surfactant injection mode	Tertiary	Tertiary	Tertiary	Tertiary	Tertiary

Table 4.1: Properties of the sand packs used for the flood experiments

Flood 1: Injection of 20,000 ppm brine followed by alkaline surfactant at 0.018 ml/min (1ft/D)

Both the brine flood and the alkaline surfactant flood are conducted here with 20,000 ppm NaCl brine. The injection rate was chosen to be 0.018 ml/min, which corresponds to 1ft/D superficial velocity. Figure 4.6 shows the cumulative oil recovery and the pressure profile for the brine and surfactant floods at a relatively low rate. Before the brine injection, there was no flow in the sand pack and the pressure was ambient. Brine injection was continued for 3.65 PV. The water flood could recover 42% of oil, which is low, compared to the waterflood recovery of low viscosity oils. The pressure drop increases from zero, reaches a maximum of 44 psi at 0.2 PV water injection and then decreases. The pressure drop would have been 88 psi for only oil flow at this flow rate (permeability ~ 20D). The pressure drop should have increased to 88 psi instantaneously

and then decreased as water enters the pore space if the system was incompressible. The slow initial increase in the pressure drop and not reaching 88 psi indicate some compressibility in the system, perhaps due to the unconsolidated nature of the sand pack. The flood is marked by the early breakthrough (<0.1 PV) of the water phase. The pressure drop falls as the water fingers pass through the sand pack, subsequent recovery is due to incremental growth of the water finger along the sides of the fingers. The alkaline surfactant (AS) slug injection starts at 3.65 PV and ends at 8 PV. During the injection of AS slug, the pressure drop increases to 43 psi and then decreases. At the time of high pressure, significant amounts of additional oil are mobilized and emulsions are generated in situ. The oil recovery increases to 82% at the end of the AS flood, which is an incremental oil recovery of 40% due to alkaline surfactant injection.

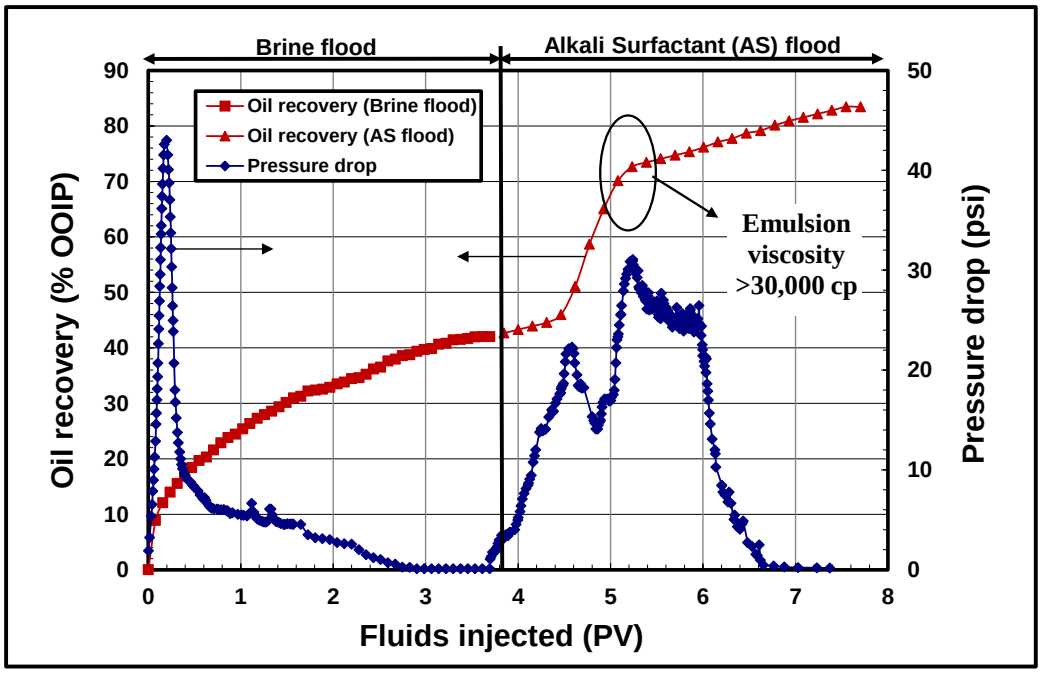

Figure 4.6: Oil recovery and pressure drop for 20,000ppm brine flood at 0.018ml/min followed by the surfactant (0.1 wt% TDA 30EO, 0.5 wt% alkali and 20,000 ppm NaCl) injection

Figure 4.7 plots the fractional flow of oil, W/O emulsion phase and O/W emulsion phase during Flood 1. The pressure drop is also shown. During the brine flood, only water and oil are produced. Oil cut decreases as the flood proceeds. After the alkaline surfactant injection starts, for about 1.35 PV only water and oil are produced, but the oil cut increases. Then the effluent changes to W/O emulsion and excess water, at about 5 PV injected. At about 6.6 PV injected, the effluent changes to O/W emulsion. Peaks in oil or W/O emulsion cut follow the peaks in pressure drop. Both oil and W/O emulsion are viscous. Produced W/O emulsion viscosity reaches higher than 30,000 cp. The pressure drop is very low at the end of the flood when only low viscosity O/W emulsion is observed at the outlet. Oil recovery is high if the W/O emulsion forms, but so is the pressure gradient (about 20-30 psi per 3 ft at 0.018 ml/min flow rate). This kind of pressure gradient is easy to handle in a 1-D laboratory flood, but is too high for field operations. As noted earlier, the type of emulsion depends on the hydrophilicity of surfactants, salinity, and water-oil ratio (WOR). We can control the first two in the injection fluid, but not the WOR. It develops inside the core depending on the transport of the fluid phases. We need to develop a better understanding of this transport before optimizing this process.

The emulsions were broken to separate the oil and water components and the component oil cut was measured. Figure 4.8 plots the surface tension of the aqueous phase and the oil concentration in effluent phases. The surface tension of the produced aqueous phase was 53 dynes/cm during the waterflood. The surface tension of the injected brine was measured to be 72 dynes/cm, hence it is evident that the produced brine had some dissolved component from the oil, which was responsible for lowering its surface tension. The surface tension of the produced fluid decreased further when the surfactant was produced at the outlet. The base value of the surfactant slug surface tension was

measured to be 39 dynes/cm. The graph shows that it took almost a pore volume for the surfactant to break through. This is because the surfactant is reacting with the oil inside the porous medium and forming emulsions rather than just flowing through the viscous fingers. The concentration of the oil component in the oil phase shows a distinct decrease, once W/O emulsions are formed. These W/O emulsions have a lot of water emulsified in them. After about 6.6 PV only O/W emulsion is produced. There was a very small concentration of oil in this emulsion phase. It is suspected that alkaline surfactant flow in the water fingers generates O/W emulsions at the surface of the fingers. Oil is drawn into the fingers while the finger width grows. As O/W emulsion flows through porous media, oil accumulates and transforms to W/O emulsions and thus the effluent is W/O emulsion soon after alkaline surfactant injection. Towards the end of the experiment, little oil is mobile, thus O/W emulsion is produced with low oil content and pressure drop. The generation of W/O high viscosity emulsions can definitely pose problems of injectivity. It is important to figure out the conditions under which W/O emulsions form and how to avoid them.

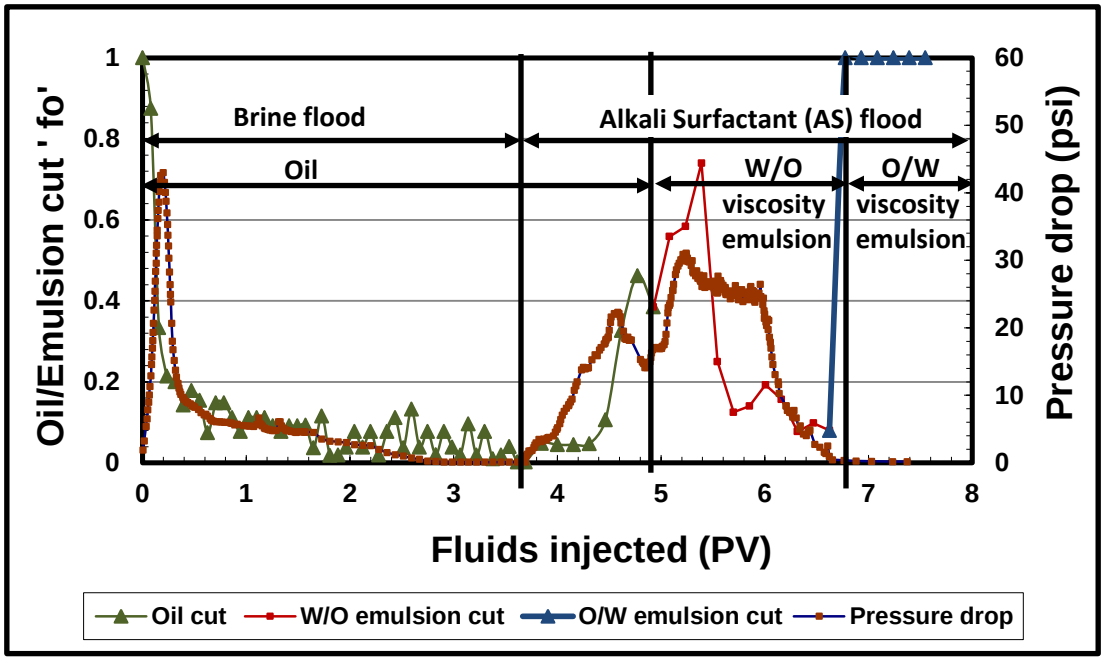

Figure 4.7: Oil cut and pressure drop in Flood 1

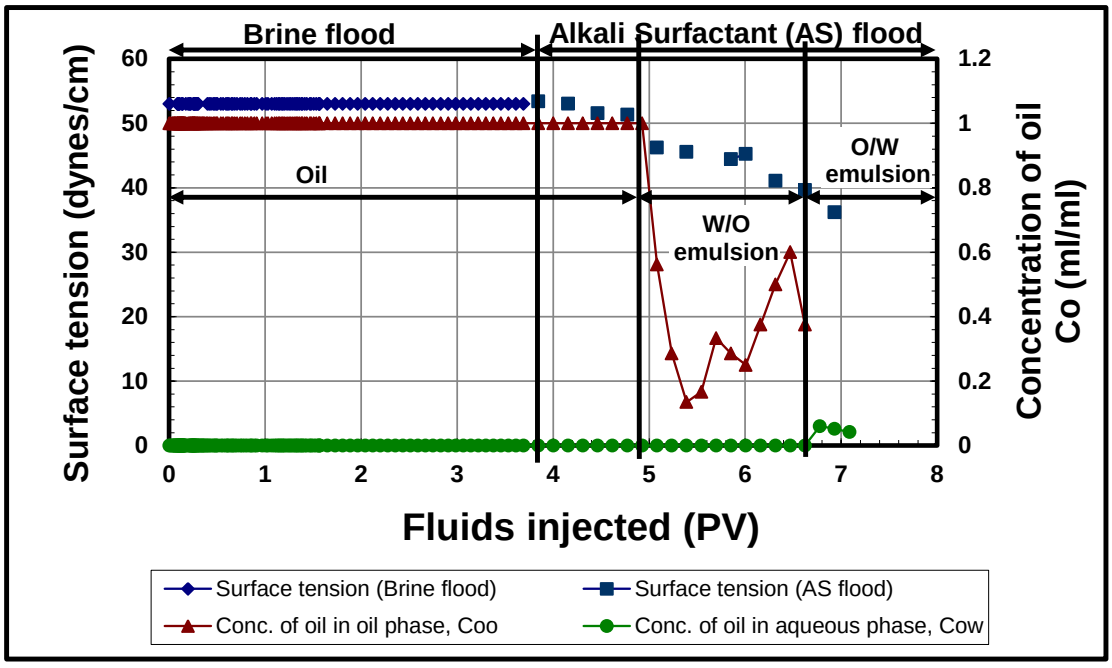

Figure 4.8: Surface tension and oil concentration in different phases in Flood 1

Flood 2: Injection of 8900 ppm brine followed by alkaline surfactant at 0.018 ml/min

Figure 4.9 shows the oil recovery and pressure drop obtained by injecting 8900 ppm brine followed by alkaline surfactant injection at the same low flow rate. This experiment is identical to the last experiment, except that the brine and alkaline surfactant salinity is reduced to 8900 ppm. 2.2 PV of brine injection produced about 28% of oil; the subsequent alkaline surfactant flood produced 42 % of oil giving a total of 70% of oil. High viscosities W/O emulsions were observed at the outlet as the oil cut increased after alkaline surfactant injection.

Flood 3: Injection of deionized (DI) water followed by alkaline surfactant at 0.018 ml/min

Figure 4.10 shows the oil recovery and the pressure drop when DI water was injected followed by alkaline surfactant injection. This flood was performed at the same flow rate of 0.018 ml/min as the last two experiments, the only difference being the salinity. The oil recovery is 42% of oil in about 3 PV water injection, this recovery is very similar to the first experiment. The pressure drop maximum was about 50 psi, which is also similar to the first experiment. The oil recovery during the alkaline surfactant flood was about 20%, not as high as the earlier experiments. This time low viscosity O/W emulsions were observed at the outlet. These emulsions can flow easily at low pressure drops but do not contain as much oil as W/O emulsions. The pressure drop stayed below 10 psi. The possible mechanism of oil recovery is the entrainment of oil from the sides of the fingers into the flowing aqueous solution, but lack of conversion to a W/O emulsion. It may be possible that the low salinity stabilized the oil emulsion droplets and prevented them from coalescing.

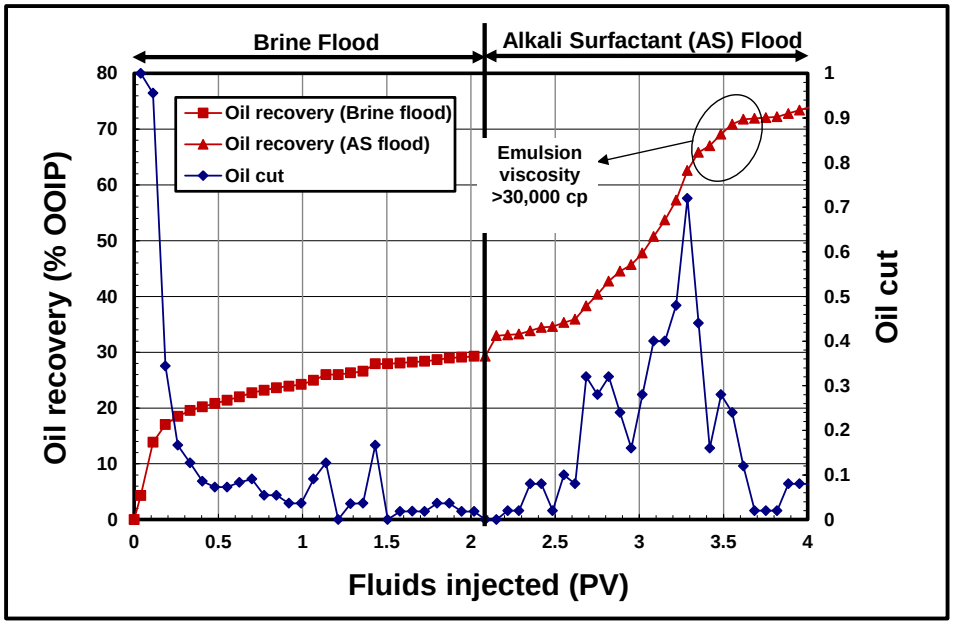

Figure 4.9: Oil recovery and pressure drop for 8900 ppm brine flood followed by the alkali surfactant (0.1 wt% TDA 30EO, 0.5 wt% alkali, and 8900 ppm NaCl water) injection

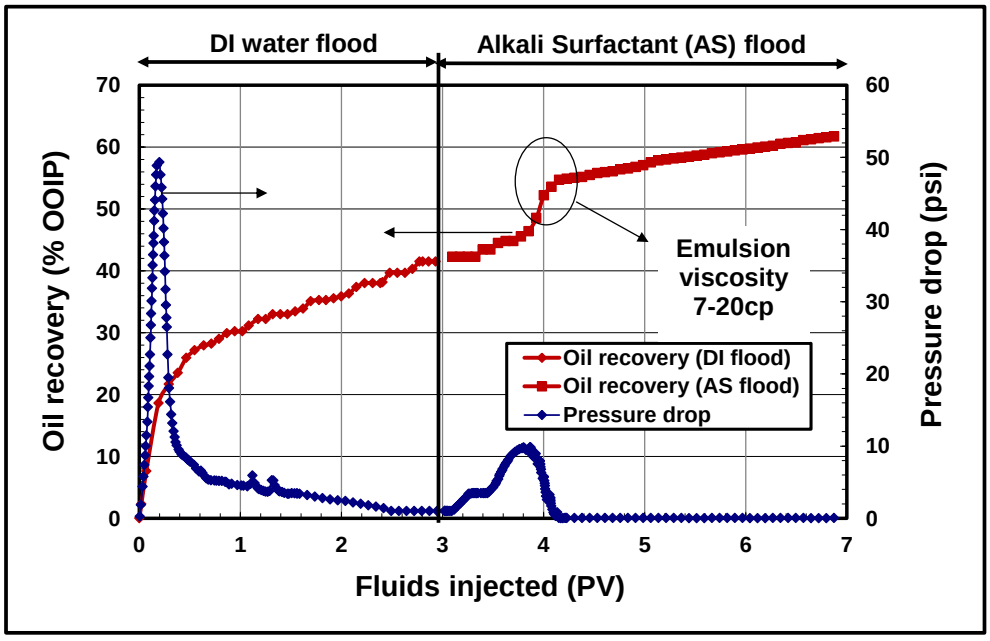

Figure 4.10: Oil recovery and pressure drop for DI water flood followed by the surfactant (0.1 wt% TDA 30EO, 0.5 wt% alkali, and 0 ppm NaCl water) injection

Flood 4: Injection of 20,000 ppm brine followed by alkaline surfactant at 0.1 ml/min

This experiment was conducted with the same fluids as in Flood 1 (20,000 ppm brine), but the flow rate was about 5.5 times faster. Figure 4.11 shows the cumulative oil recovery and the pressure profile for the brine and alkaline surfactant floods at this relatively high rate. Brine injection was continued for 3.65 PV. The water flood recovery is 25%, which is quite low, compared to waterflood recovery of first experiment (42%). The maximum pressure drop during waterflood decreases from 44 psi (in the first experiment) to 30 psi (in this experiment), even though the flow rate was 5.5 times higher. The displacement front during the high flow rate water flood is more unstable which is evident by the faster water breakthrough. The oil left behind at the end of water flood is larger in this case compared with the first experiment. The alkaline surfactant (AS) injection starts at 3.65 PV and ends at 5 PV. During the injection of AS slug, the pressure drop increases to 110 psi and then decreases. At the time of high pressure, significant amounts of additional oil are mobilized and emulsions are generated in situ. The oil recovery increases to 50% at the end of the AS flood. The incremental oil recovery is 25 % at this high flow rate compared to 40% for the first experiment. The generation of viscous W/O emulsion is verified by the viscosity observed at the outlet. The emulsions had a viscosity ranging from 17,000 – 21,000 cp. Oil is possibly mobilized by emulsification. The mobilized emulsion fills the waterflood fingers to give high pressure drops.

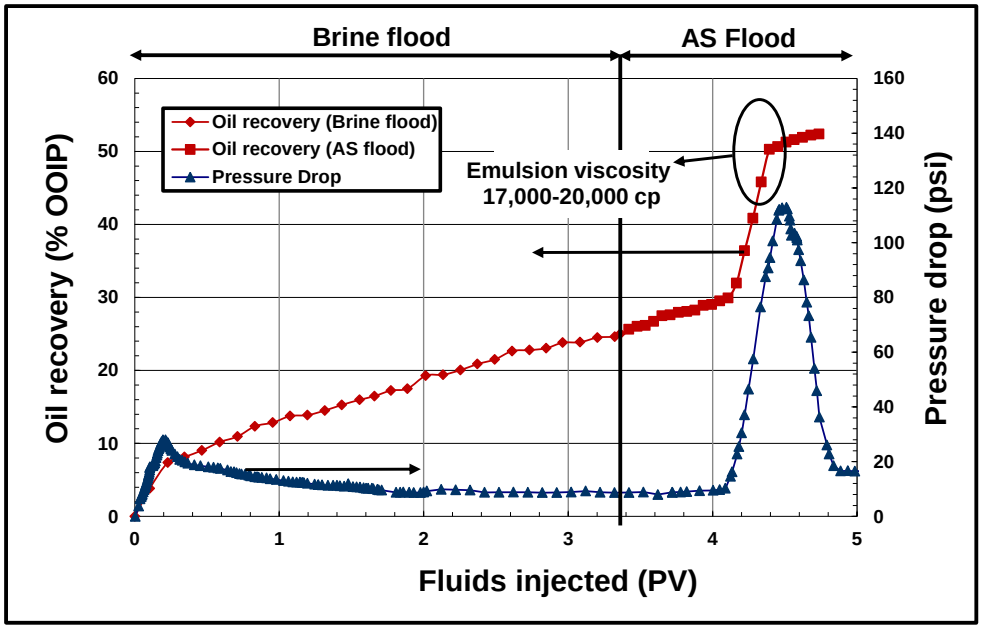

Figure 4.11: Oil recovery and pressure drop for 20,000 ppm brine flood followed by alkaline surfactant (0.1 wt% TDA 30EO, 0.5 wt% alkali and 20,000 ppm NaCl brine) injection at 0.1 ml/min

Flood 5: Injection of 20,000 ppm brine at 0.018ml/min to check the repeatability of the waterflood

This flood was conducted in order to check the repeatability of the waterflood. It is a replication of Flood 1 except for the initial condition. After saturating the sand pack with oil, the oil was injected at the particular flow rate until the pressure drop reached a steady state value. This steady state value corresponds to the flow of oil at the connate water saturation and was equal to 105 psi. Water reservoir was pressurized to this value and water injection was started at this pressure. This is a different initial condition from the previous floods in which water injection was started at a 0 psi pressure and it took some time for the flow to build up. Figure 4.12 shows the comparison of the oil recovery and pressure drop for this flood with that of flood 1. The oil recovery results are very similar for Floods 1 and 5 after the breakthrough. The breakthrough was earlier for flood 1. This waterflood was stopped at 2PV. The oil recovery after 2PV was 40%. The inital pressure

drop was 105 psi which dropped to around 5psi near the breakthrough point. After breakthrough, the pressure drop attained very low values because of the formation of water channels. However, even after breakthrough about 20% of oil was recovered by the brine. Post breakthrough pressure drop is almost similar in both the floods indicating that approximately same amount of oil was recovered during this time and hence similar pattern of viscous fingers was present.

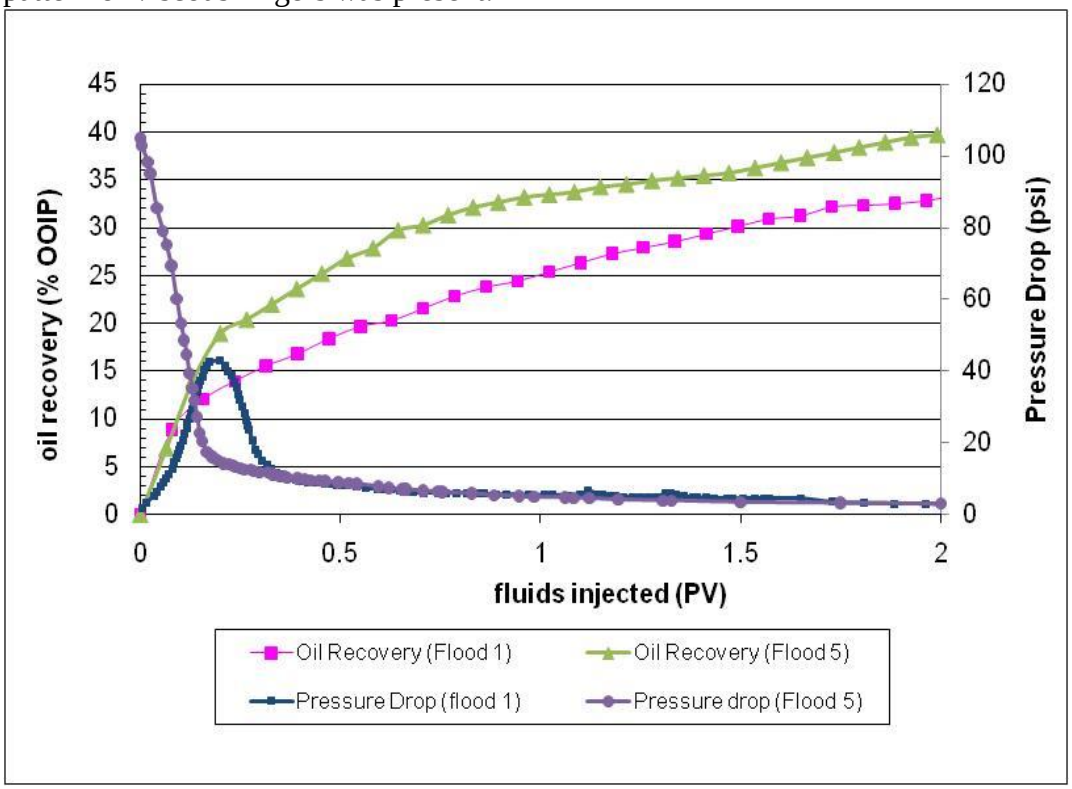

Figure 4.12: Comparison of the waterfloods of Flood 1 and Flood 5.

4.1.3 Sand pack flood with polymer solution

It is well known that during waterflood of the heavy oil, severe viscous fingering does occur in almost all the cases which cause early water breakthrough and low oil recovery rates. The results can be worse in fields where heterogeneities hamper the efficiency of waterflood. So far we have explored the potential application of alkali and surfactant

chemicals in improving the oil recovery over waterflood. In further experiments we aim to use polymers as viscosifying agents in the aqueous phase. Polymers have been used extensively in the oil industry to make the mobility ratio between oil and water more favorable. Most of these studies are focused on the application for light oils where a low polymer concentration is sufficient to make the aqueous slug of the desired viscosity.

The next set of experiments aims to demonstrate that the using polymers in the aqueous phase can improve the recovery of the heavy oil as well. Polymer concentration was chosen such that the viscosity of the aqueous phase increased to 100 cp. Due to the high permeability of the sand pack, it was safe to use a high molecular weight polymer (Flopaam 3630S). Table 4.2 gives the details of the flow experiments.

Sand pack properties	**Flood 1**	**Flood 2**
Length of the sandpack (ft)	3	3
Diameter (inches)	0.67	0.55
Permeability (Darcy)	29.65	24.18
Porosity (%)	47.61	42.06
Swi (%)	8.16	13.33
NaCl salinity (ppm)	20,000	20,000
Flow velocity (ft/D)	1	1
Polymer concentration (ppm)	2200	2200
Polymer viscosity (cp)	100	100
Polymer injection mode	Tertiary	Secondary

Table 4.2: Properties of the sand packs used for polymer flooding

Flood 1: Injection of 20,000 ppm brine followed by 2200 ppm of polymer slug

This experiment was conducted with 1 PV of brine slug followed by 1 PV of polymer slug. Figure 4.13 shows the cumulative oil recovery and the pressure drop for this flood. Brine flood conducted for 1 PV recovered 29% of the oil with breakthrough at 0.1 PVs injection. The pressure drop during the brine flood increased to 105 psi and started decreasing as the brine injection proceeded. The final pressure drop at the end of the brine flood was close to 4.0 psi. Polymer injected commenced after the brine flood. The sand pack responded with an increase in pressure drop to 40 psi and an improvement of over 20% in oil recovery.

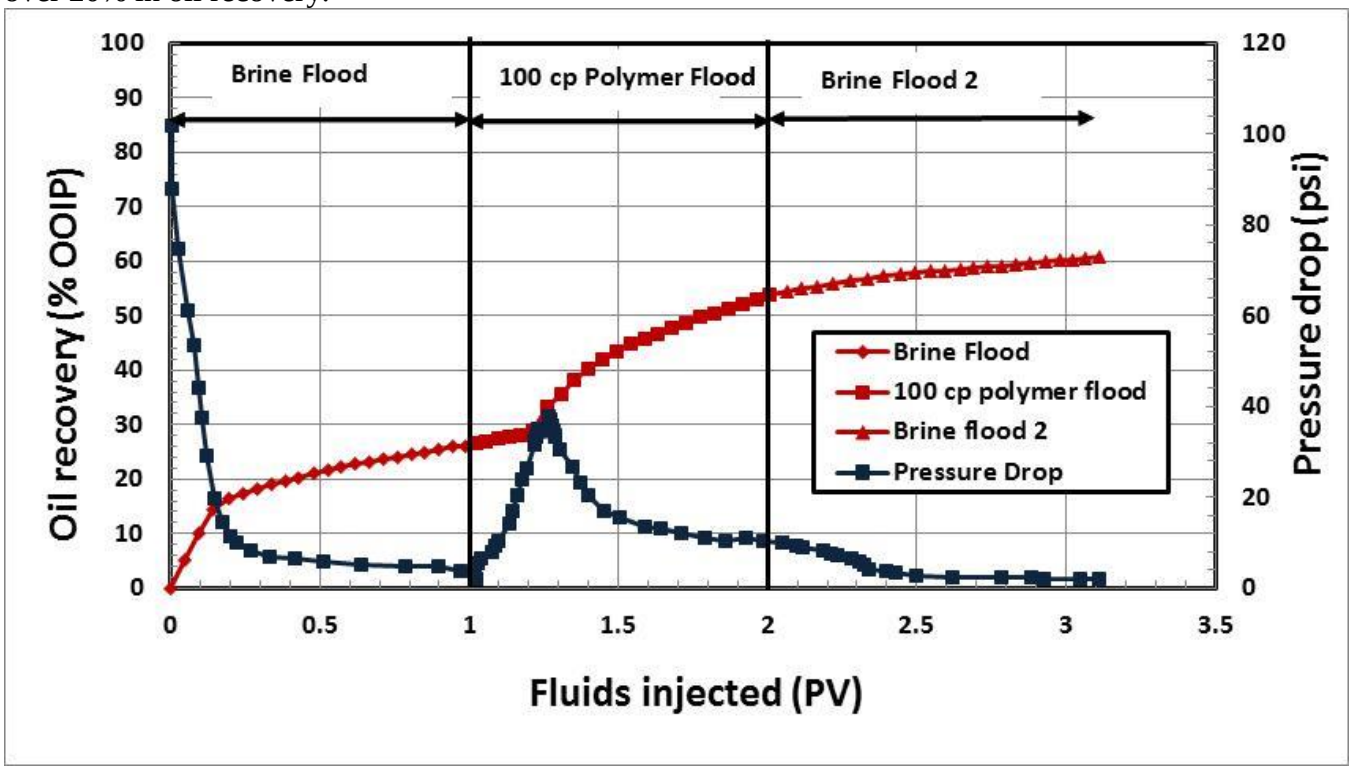

Figure 4.13: Oil recovery and pressure drop for brine flood followed by polymer flood (2200 ppm Flopaam 3630S)

About 50% of oil was recovered after the polymer flood and the pressure drop was close to 10 psi. To limit the use of polymer, a second brine slug was injected after the polymer slug. Final oil recovery was close to 60% of OOIP.

Flood 2: Injection of 2200 ppm polymer slug followed by brine injection

In the second experiment, the polymer slug was injected in the secondary mode. Figure 4.14 presents the oil recovery and pressure drop for this experiment. This experiment was conducted in order to check which injection mode (secondary or tertiary) has a higher oil recovery potential. Polymer injection was conducted for 1 PV followed by 1 PV of brine flood. 42% of oil was recovered after 1 PV of polymer injection with pressure drop close to 20 psi. The initial pressure drop in this experiment was higher than the previous experiment. The reason is a smaller internal diameter (0.55 inches) as compared to the previous one (0.67 inches).

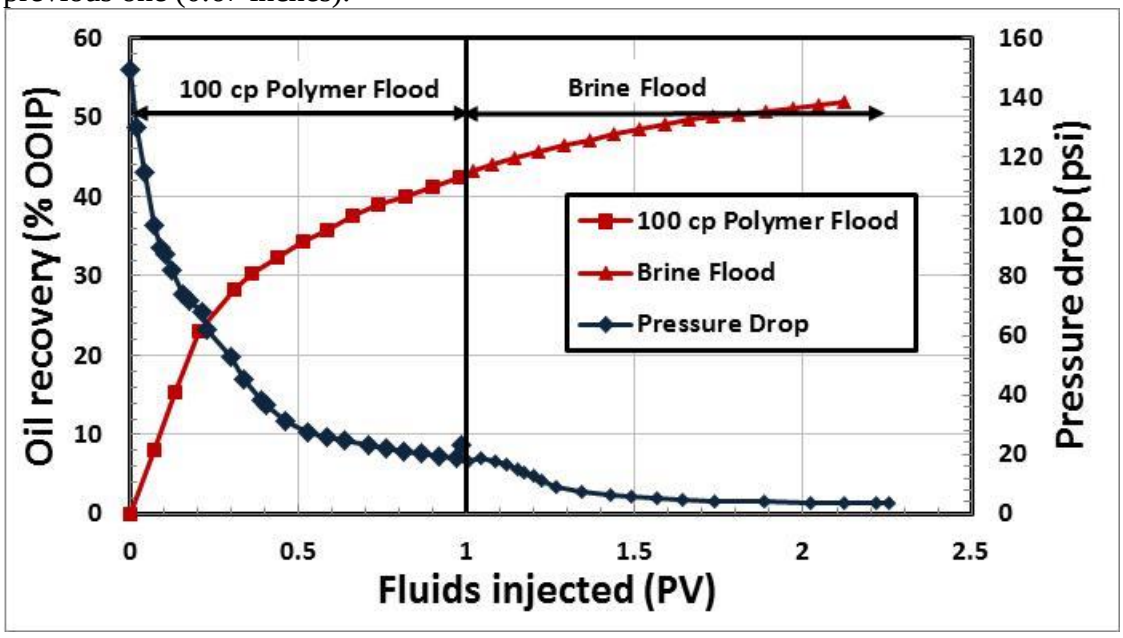

Figure 4.14: Oil recovery and pressure drop for polymer flood (2200 ppm Flopaam 3630S) followed by brine flood

After 1 PV of brine flood 50% of oil was recovered with pressure drop being 3.6 psi. The total oil recovery of 50% after 2 PV of injection was very similar to that obtained from the first experiment, though there were some differences in the properties of the sand packs. Polymer injection in the secondary mode does result in higher initial oil recovery rates than the waterflood.

4.1.4 2D sand pack floods

After conducting the flow experiments in a near 1D system it was found out that the use of chemicals alkali, surfactant and polymer can improve the oil recovery over waterflood. However it was also recognized that because of the adverse viscosity ratio, the viscous fingering phenomenon should be impacting the oil recovery. As noted by Ferer *et.al* (1995), when viscous fingering flows are conducted in a long narrow geometry, the confines of the geometry may curb the growth of a large number of viscous fingers. This may lead to misleading results and hence it was decided to utilize the quarter 5 spot geometry for conducting the sandpack floods. For this purpose a 2D cell measuring 10' by 10' by 1' was used. The injection and the production wells were placed on the opposite ends of the diagonal. The wider geometry of the 2D cell will not curb the growth of the viscous fingers and hence can represent such flows better.

The pore volume and the permeability of the 2D sand packs were evaluated by the procedures outlined in the methodology section. The details of the 2D experiments are given in the table 4.3.

	Flood 1	Flood 2	Flood 3	Flood 4
Permeability (Darcy)	18.8	11.1	11.1	7.38
Porosity (%)	53.17	24.4	24.4	25.63
Swi (%)	14.2	10	10	9.1
NaCl salinity of the secondary flood (ppm)	20,000	20,000	20,000	100 cp polymer @ 20,000
Flow rate (ml/min)	0.1	0.1	0.1	0.1
AS used	0.1% TDA 30EO 0.5% alkali, 20,000ppm brine	0.1% TDA 30EO 0.5% alkali, 20,000ppm brine	0.1% TDA 30EO 0.5% alkali, 0 ppm brine	0.1% TDA 30EO,0.5% alkali 20,000 ppm brine
Surfactant flood mode	Tertiary	Tertiary	Tertiary	Tertiary

Table 4.3: Properties of the 2D cell

Figure 4.15 shows the experimental setup for the 2D sand pack flood. The ISCO pump was used to pump brine and alkali-surfactant solution into the sand pack. Fluid accumulators were introduced into the setup for injecting oil and polymer solution. These accumulators had a floating Teflon piston inside. A mineral oil called Soltrol was injected from the ISCO pump to one side of the floating piston. This in turn would push the same amount of injection fluid from the other side into the sand pack. The piston seal ensured that the two fluids do not come in contact with each other.

Porosity and permeability were determined by the procedure outlined in the previous chapter in the methodology section. Oil saturation process was similar to the one adopted for the 1D sand packs.

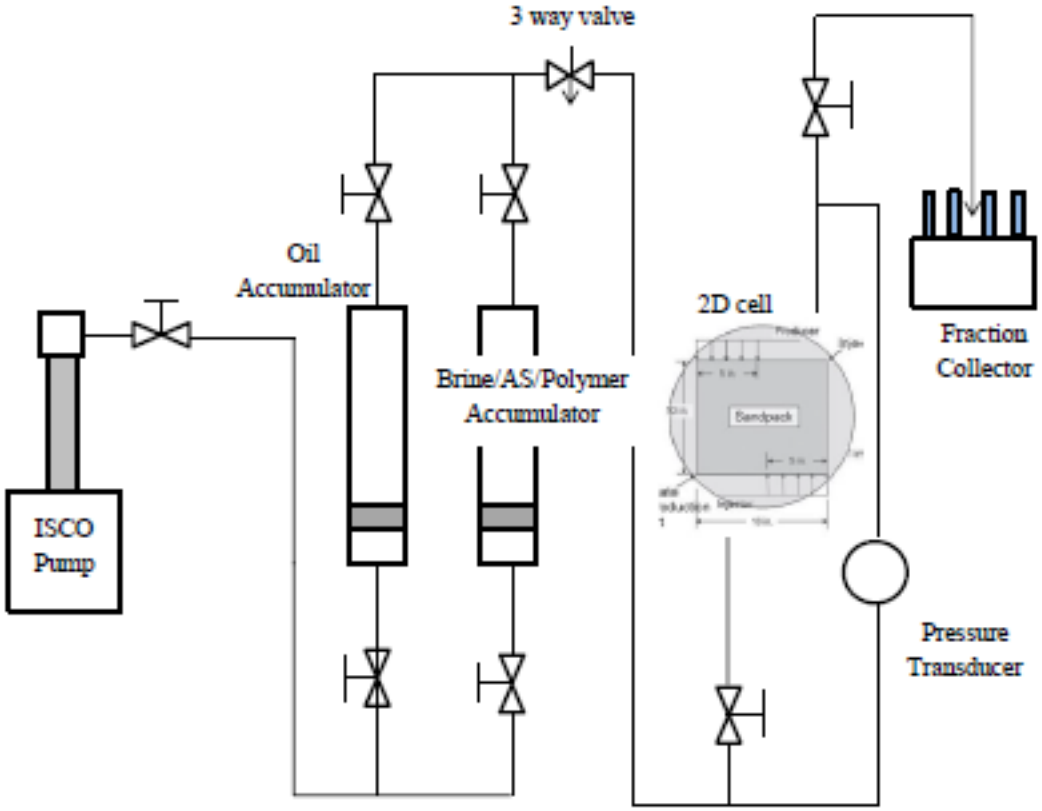

Figure 4.15: Experimental setup

First experiment was conducted in a plastic 2D cell where it was possible to visually observe the fluid fronts. Second experiment is a repetition of the first in a steel 2D cell. The advantages and disadvantages of the steel cell over the plastic cell are discussed in Chapter 2.

Injection of 20,000 ppm brine followed by the AS flood at the same salinity (Plastic cell)

This flood was conducted in the plastic 2D cell. A constant NaCl concentration of 20,000 ppm was used for the brine flood and the AS flood. Figure 4.16 shows the resultant oil

recovery and the oil cut behavior. The oil recovery during the brine flood is about 35% of OOIP. Breakthrough occurred at about 0.04 PV of brine injection. The low value of the breakthrough PV gives an indication that the displacement process is unstable and that viscous fingering dominates the flow behavior. Significant amount of oil is recovered after breakthrough. Our previous study (Kumar and Mohanty, 2010) had indicated that post-breakthrough oil recovery in a linear core was proportional to the square root of the time. The oil recovery had a significant increment soon after starting the AS injection. The increment in the oil recovery is due to the mobilization of residual oil from the water fingers and from the bypassed region. The initial production of oil during the AS flood was followed by the production of emulsions. These emulsions were then demulsified to measure the oil recovery. The oil cut also increased to almost 1 for a short duration. The incremental oil recovery due to the AS flood was about 18% of OOIP.

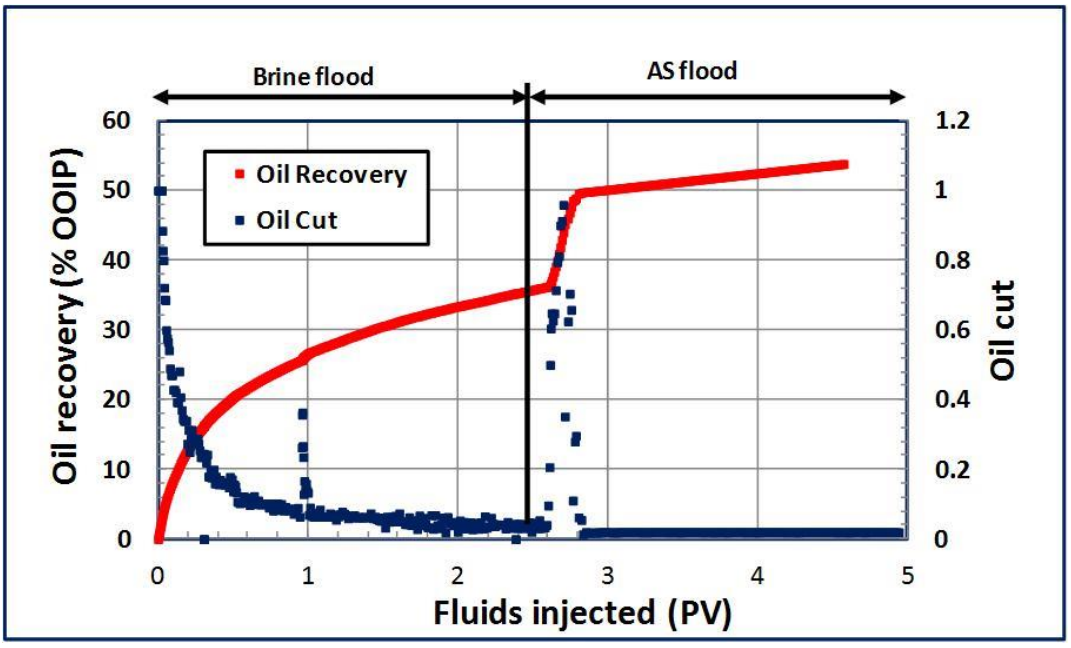

Figure 4.16: Oil recovery and oil cut for 20,000 ppm brine flood followed by alkali-surfactant injection with 20,000 ppm NaCl brine (Plastic 2D cell)

Figure 4.17 shows the pressure drop response of the sandpack during the experiment. The experiment was started from a 'no flow' initial condition (0 psi pressure drop). The pressure drop increased from 0 to 50 psi as the injected brine fingers push out the oil. After the brine breakthrough, it fell sharply to about 2 psi. Injection of the AS solution increased the pressure drop to 15 psi. The corresponding oil cut reached to 1. The cumulative oil recovery curve showed an increase of around 15% of OOIP during the pressure spike. Oil and W/O emulsions were produced in this region. After this spike, oil cut dropped once again. Most of the extra oil had already been produced. O/W low viscosity emulsions were now observed at the outlet. These emulsions have a low oil concentration (< 2% by volume) and a low viscosity (1-2 cp). The result is lower increments in the oil recovery and a fall in the pressure drop.

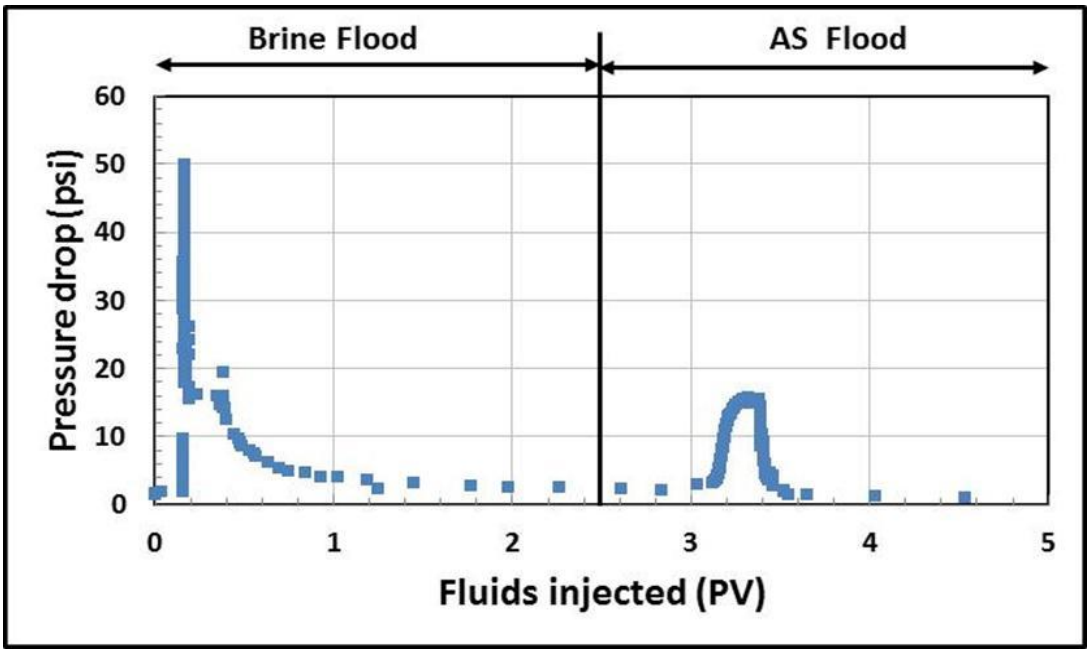

Figure 4.17: Pressure drop for 20,000 ppm brine flood followed by alkali-surfactant injection with 20,000 ppm NaCl brine (Plastic 2D cell)

Figure 4.18 shows the state of the 2D cell after the waterflood. The injection port was at the top corner; the production port was at the bottom corner. The lighter region represents water invaded pores on the top of the model. Distinct viscous fingers were not observed possibly because the oil adhered to the plastic plate and the pack was truly three-dimensional. However, patches of dark (oil) and light (water) regions can be seen throughout the sand pack. This picture gives an indication that the water fingers formed in the entire region and a large amount of oil was unswept.

Figure 4.18: State of the 2D cell after the waterflood

Figure 4.19 shows the state of the 2D cell during the AS flood. Injection of the AS solution increased the oil recovery beyond that of the waterflood. A distinct finger was observed during alkaline-surfactant flood. The AS solution removed the oil from the top plastic plate of the cell where the finger went through. It mobilized the trapped oil within the fingers and the oil adjacent to the fingers (at least near the injection section of the pack). The mobilized oil reacted with the AS solution to form high viscosity W/O

emulsions at conditions of low WOR. The high viscosity of the emulsions aided in the effective displacement of oil. We observed patches of water filled pore getting resaturated with oil indicating the formation of an oil bank. The pore-scale water fingers disappeared and the AS solution got a chance to flow laterally and thus improve the sweep efficiency of the process. Thus the AS solution, in addition to improving the displacement efficiency by mobilizing the trapped oil, also was helpful in improving the sweep efficiency of the flood. Finally, AS solution itself formed its own large fingers due to its low viscosity and produced low viscosity O/W emulsions by entrainment of small volumes of oil from the sides of the finger.

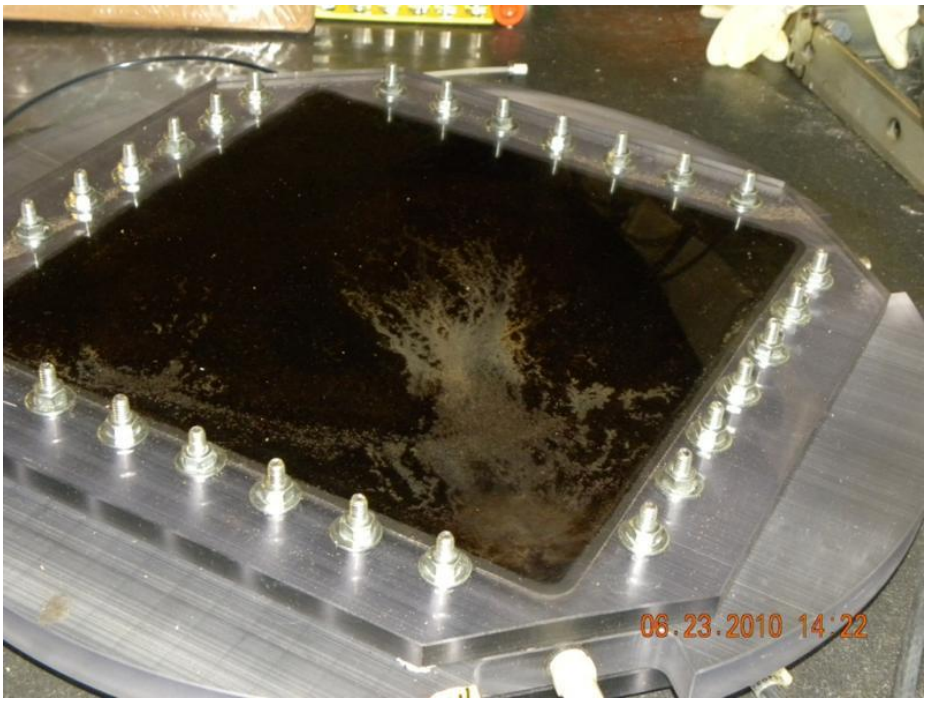

Figure 4.19: State of the 2D cell during the AS flood

The oil recovery increased from 35% after the waterflood to 53% after the AS flood. The next step was to repeat the same experiment in the steel 2D cell. The changes in porosity

and permeability of the two sandpacks were expected to bring about changes in the oil recovery and the pressure drop profile.

Injection of 20,000 ppm brine followed by the AS flood at the same salinity (Steel cell)

This flood was conducted in the steel 2D cell. Same concentrations of brine and the AS slug were used as in the first experiment. Figure 4.20 plots the oil recovery and the oil cut response for the experiment. The pressure drop response is plotted in figure 4.21. This flood had a different starting condition than the previous flood. Before starting the water flood, oil was injected into the pack at a constant flow rate of 0.1 ml/min until a steady pressure was reached. The water pump was pressurized to the same pressure and the injection was then switched from oil to water. This is the reason why the pressure drop in the Figure 4.21 starts from a high value of 180 psi (rather than from 0 psi as in the previous flood). The pressure drop fell quickly as the injected water fingers through the oil and the oil cut decreases.

The oil recovery by brine flood reached to 30% OOIP. Breakthrough occurred at 0.075PV of water injection. The oil cut progressively decreased from 100% to 2-3% as the water channels were formed post breakthrough. The pressure drop plotted in figure 4.21 also demonstrated a sharp fall from 100 psi to about 4 psi after breakthrough for the same reason. Injection of the AS solution increased the recovery to 55% with oil cuts reaching to 40-50%. Production of extra oil is followed by the production of W/O emulsions having a high viscosity and a high oil concentration. The viscosity of the produced emulsion was measured to be ~51,000 cp by the AR G2 Rheometer at 25^{o}C and for shear rates ranging from 0.1 to 1 s^{-1}. This viscosity is five times higher than the oil viscosity (10,000 cp) and the high viscosity W/O emulsions could be providing a mobility control to the displacement process. The droplet sizes of the emulsions were

measured by an optical microscope. Figure 4.22 shows the picture of W/O emulsion with a 40X magnification. The lighter colored droplets and the dark colored continuous phase reinforces the fact that the emulsion is W/O type. We found the droplet sizes ranging from 5-10 µm. Corresponding pressure drop, as shown in figure 4.21 increased to 60 psi and remained almost constant for a pore volume. After the production of the extra oil and the high viscosity emulsion low viscosity O/W emulsions with a lower viscosity and a low oil concentration were produced. The low oil concentration resulted in lower increments in the oil recovery curve thereafter and a lower viscosity lead to a fall in the pressure drop from 60 psi to 2 psi.

Figure 4.20: Oil recovery and oil cut for 20,000 ppm brine flood followed by alkaline-surfactant injection with 20,000 ppm NaCl brine (Steel 2D cell)

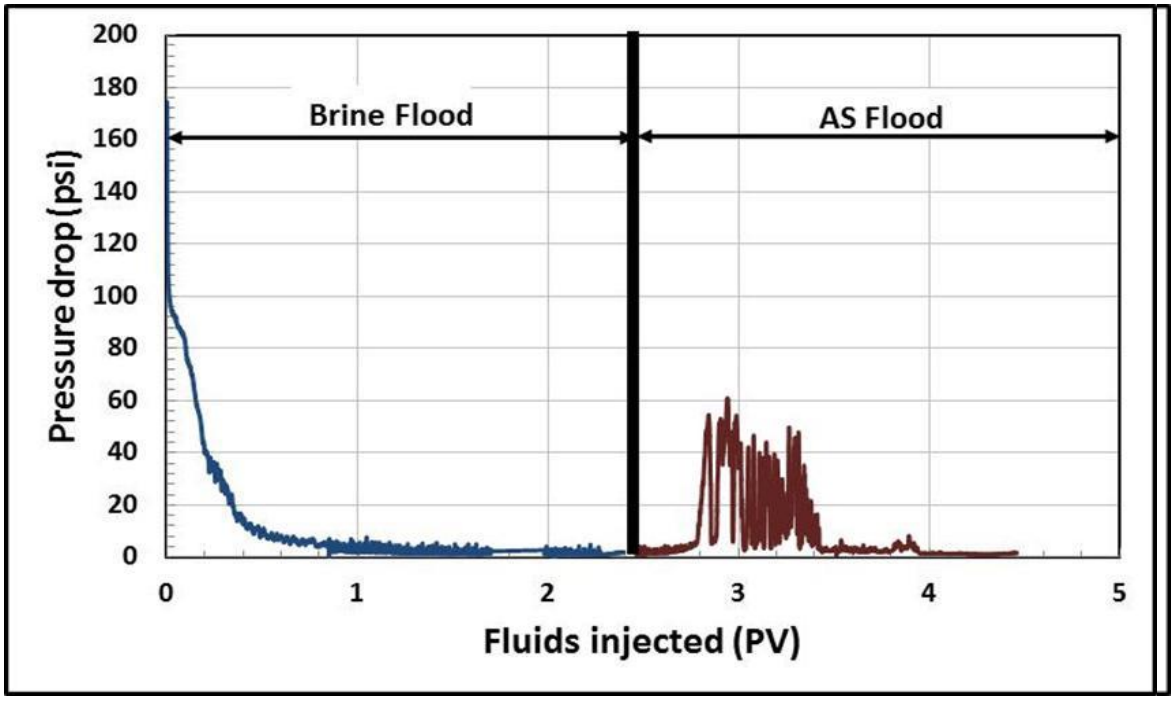

Figure 4.21: Pressure drop for 20,000 ppm brine flood followed by alkali-surfactant injection with 20,000 ppm NaCl brine (Steel 2D cell)

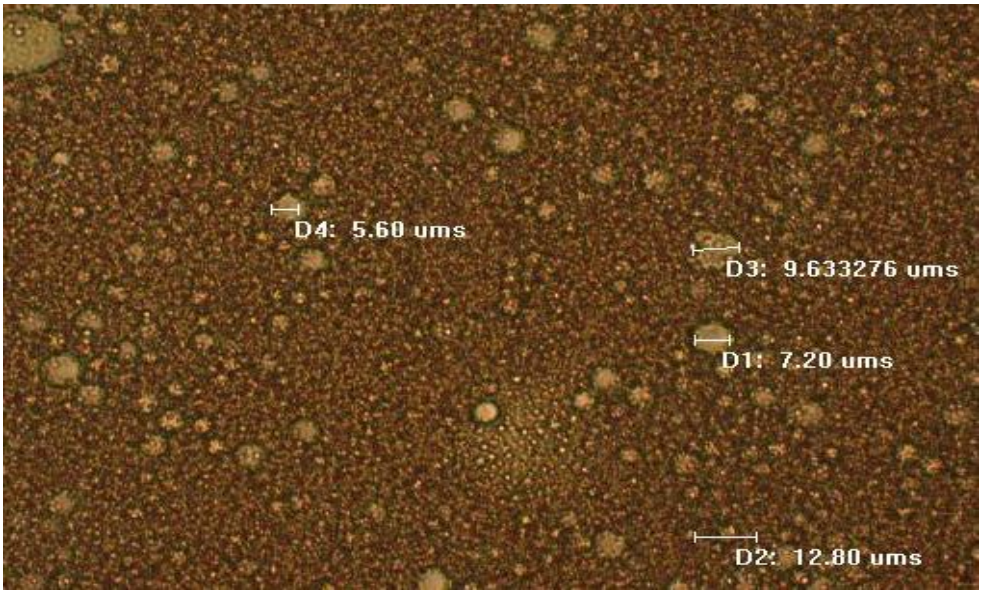

Figure 4.22: Microscopic picture of W/O emulsion

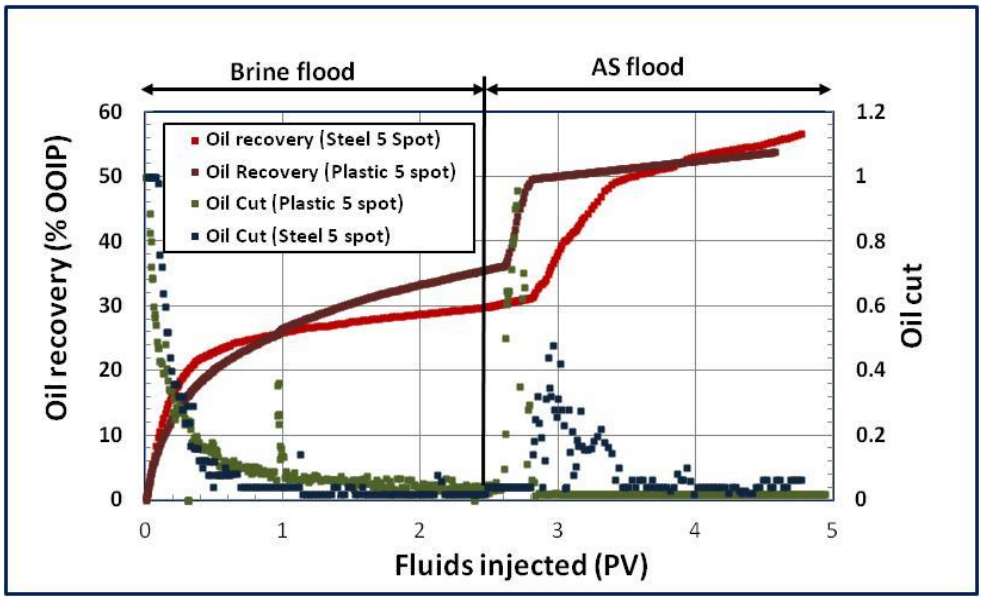

Figure 4.23: Comparison of oil recovery and oil cut for 20,000 ppm brine flood followed by alkaline-surfactant injection with 20,000 ppm NaCl brine (Plastic vs. Steel 2D cell)

Injection of 20,000 ppm brine followed by the AS flood at 0ppm salinity

This flood was conducted in sand pack # 3. After conducting the AS floods at a high brine salinity, we wanted to look into the effect of introducing the AS slug at low salinity. The brine injection was performed at a higher salinity of 20,000 ppm brine and the AS solution was injected at 0 ppm brine.

Figure 4.24 shows the oil recovery and the oil cut during the flood. The waterflood recovery is same as in the second flood due to the same properties of the pack. The pressure drop profile was also identical for the same reason and hence is not plotted. The oil recovery during the AS flood did not show any appreciable jump and the oil cuts remained low (under 10%) during the entire course of the flood. This behavior indicates that the emulsion behavior at least near the outlet is almost entirely controlled by the AS brine and the mixing had a negligible effect on oil recovery. The final oil recovery was only about 51% OOIP which is much lower than the previous flood experiments.

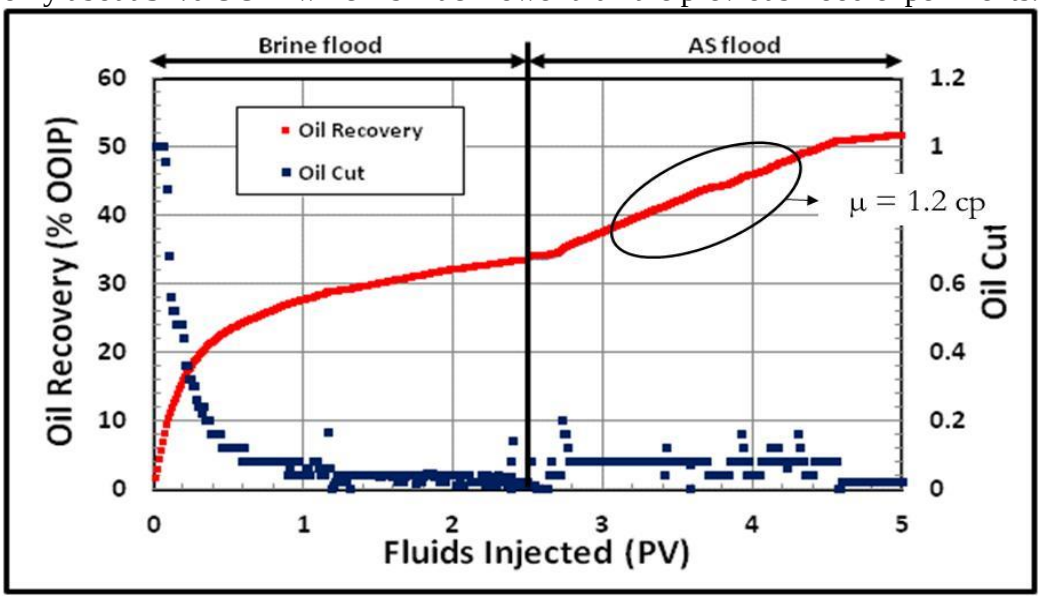

Figure 4.24: Oil recovery and oil cut for 20,000 ppm brine flood followed by alkaline-surfactant injection at 0 ppm NaCl brine

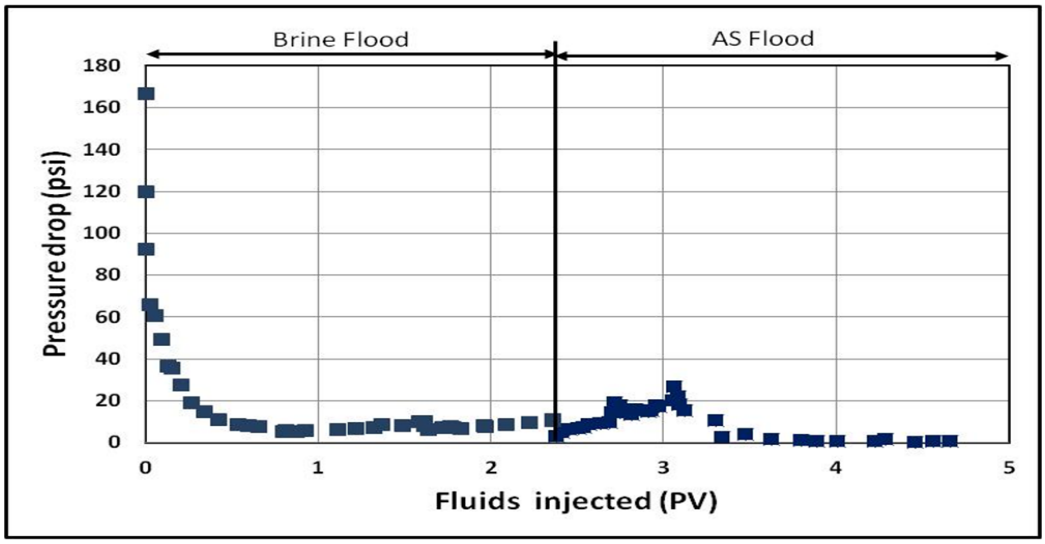

Figure 4.25: Pressure drop for 20,000 ppm brine flood followed by alkali-surfactant injection with 0 ppm NaCl brine (Steel 2D cell)

Figure 4.25 shows the pressure drop during the flood. During the brine flood the pressure drop reduced from 170 psi to about 10 psi after 2.5 PVs of injection. Injection of the AS flood led to an increase of pressure drop to about 20 psi. The lower increase in pressure drop is attributed to the generation of low viscosity O/W emulsions inside the sand pack.

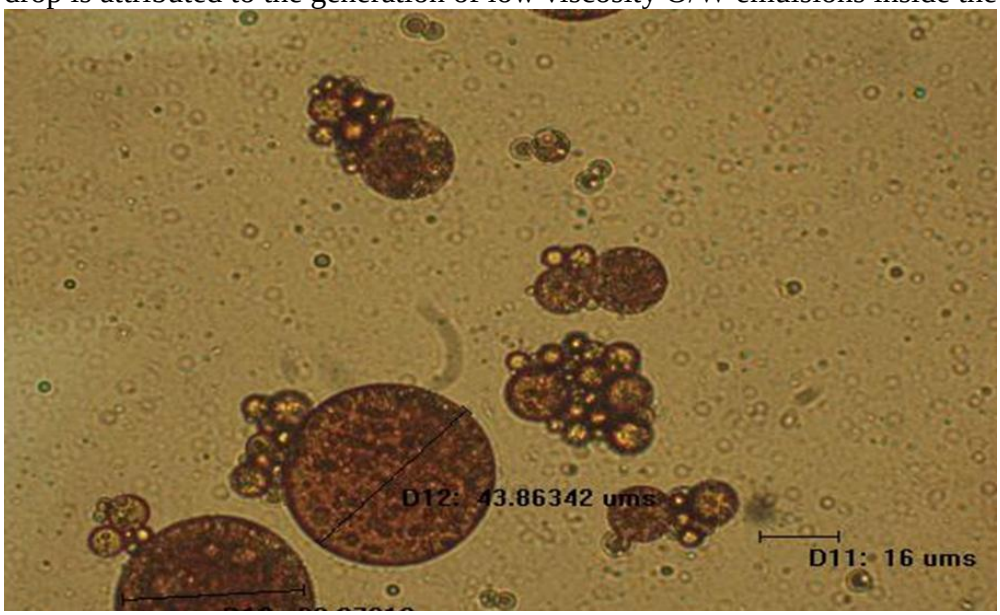

Figure 4.26: Microscope picture of O/W emulsion

Figure 4.26 shows a microscopic image of the produced O/W emulsions. The lighter external phase and the darker droplet phase is a characteristic of an O/W emulsion. Most of the emulsion droplets were in the size range of 15 µmm however we also observed a few bigger droplets of 30-40 µm in sizes.

Figure 4.27 compares the cumulative oil recovery in these three floods. The oil recovery after brine flood ranges from 30-35% in all the experiments. There was a significant change in the AS flood oil recovery behavior with the salinity of the injection solution. Alkaline-surfactant flood at the high salinity flood lead to a sharper increase in the oil recovery. As the salinity of the AS solution is decreased, the oil recovery becomes more gradual. The difference in this behavior arises due to the difference in the emulsion behavior inside the pack. The high viscosity W/O emulsions are generated at high salinities whereas O/W low viscosity emulsions are generated at low salinities.

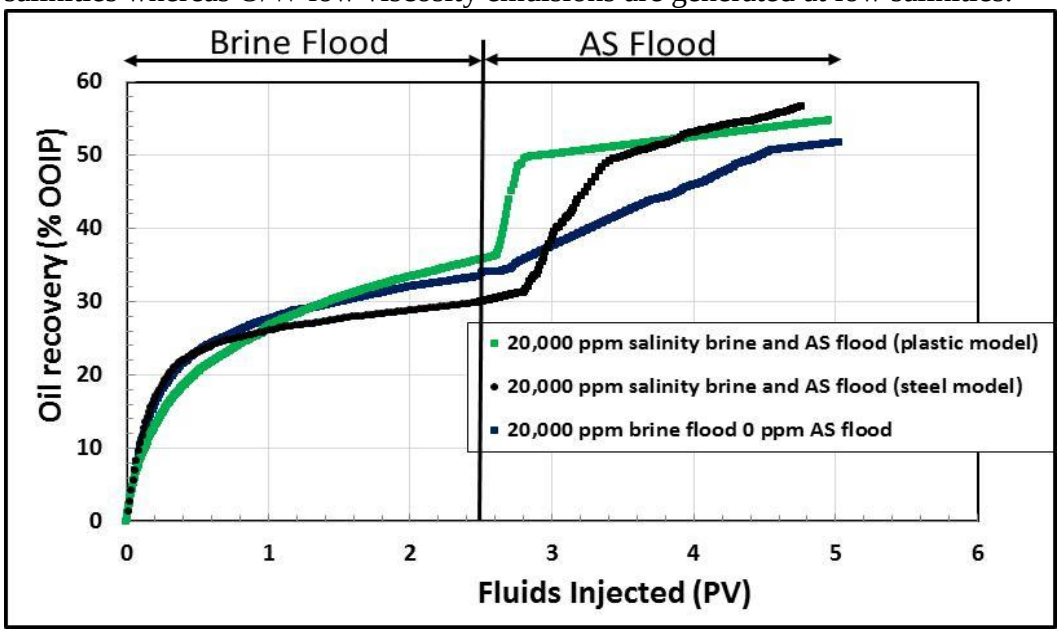

Figure 4.27: Comparison of floods at different salinities

Injection of 100 cp polymer followed by AS flood at 20,000 ppm

This experiment was conducted in the sandpack #4. The 1D experiments demonstrated that polymer injected in either the secondary or the tertiary mode has the capability to improve the oil recovery over water flood. It was stipulated that polymer injection improves the sweep efficiency over waterflood. Thus we decided to conduct the polymer flood in the steel 2D cell. A secondary polymer flood followed by AS flood was conducted. The polymer slug was made in 20,000 ppm salinity brine. The salinity of the AS solution was also 20,000 ppm.

Figure 4.28 shows the oil recovery and the oil cut behavior for this flood.

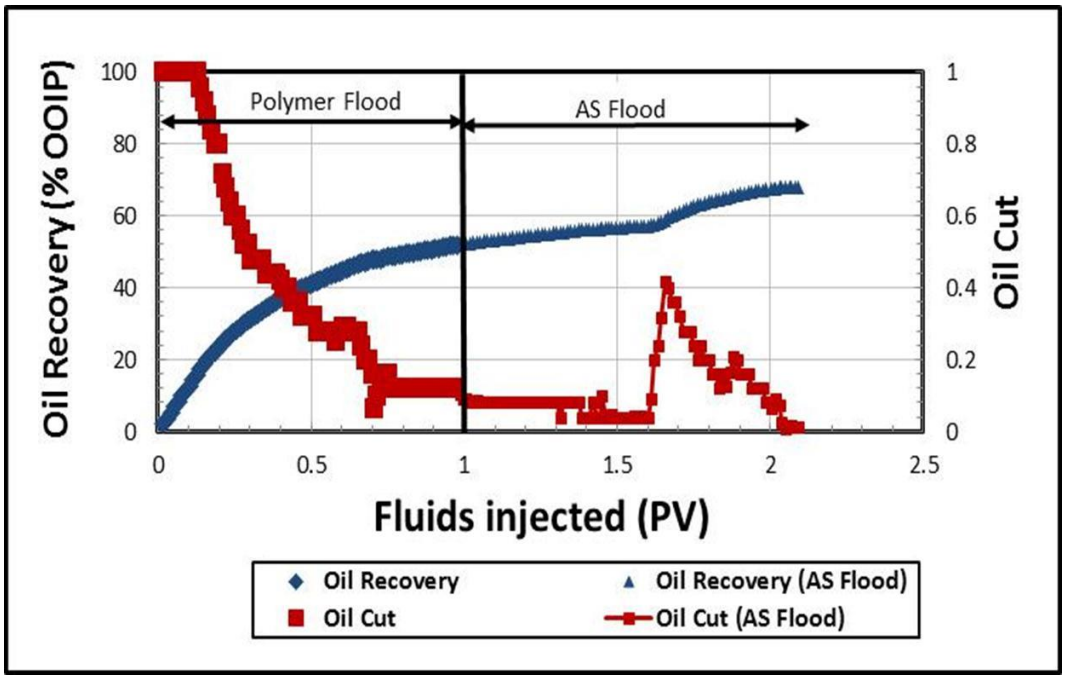

Figure 4.28: Oil recovery and oil cut for 100 cp polymer flood followed by alkaline-surfactant injection at 20,000 ppm NaCl brine

The polymer slug was injected for 1 PV only in this experiment. The oil recovery was about 50% OOIP after about 1 PV of polymer injection with breakthrough occurring at

0.2 PV. The oil recovery showed a marked improvement over water flood (~35% OOIP after 2.5 PVs injection).

However the AS flood after the polymer flood could not improve the oil recovery appreciably over the polymer flood. The oil recovery took a long time to respond possibly because of the fact that the polymer flood by itself had taken out most of the oil and formed a broader viscous finger inside the sand pack. Now, when the AS solution was injected it had a low oil saturation in the finger to target and emulsify. Figure 4.29 shows the pressure drop response of the experiment.

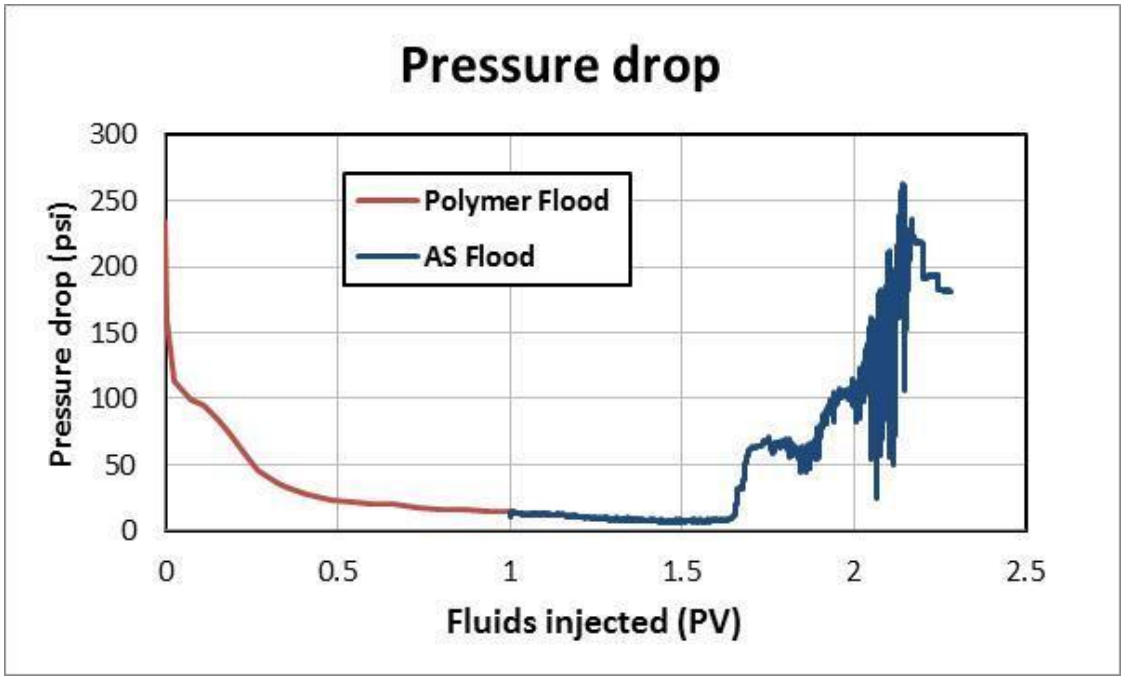

Figure 4.29: Pressure drop for 100 cp polymer flood followed by alkaline-surfactant injection at 20,000 ppm NaCl brine

The initial pressure drop was higher and reduced to about 20 psi towards the end of the polymer flood. On switching to AS injection the pressure drop took almost the same time (~0.7 PV) to respond as the oil recovery. The late response of the pressure drop also

indicates the fact that the AS solution finds its way through the low oil saturation finger. The pressure drop rose to higher than 200 psi when the emulsions are generated in the system. It should be noticed that the pressure drop increase is much higher than the AS injection after the waterflood. The prime reason is the generation of very high viscosity emulsions inside the system as figure 4.30 indicates. Emulsion viscosity as high as 100,000 cp was observed at the outlet. The emulsions generated in the previous flood experiments had a maximum viscosity of 50,000 cp.

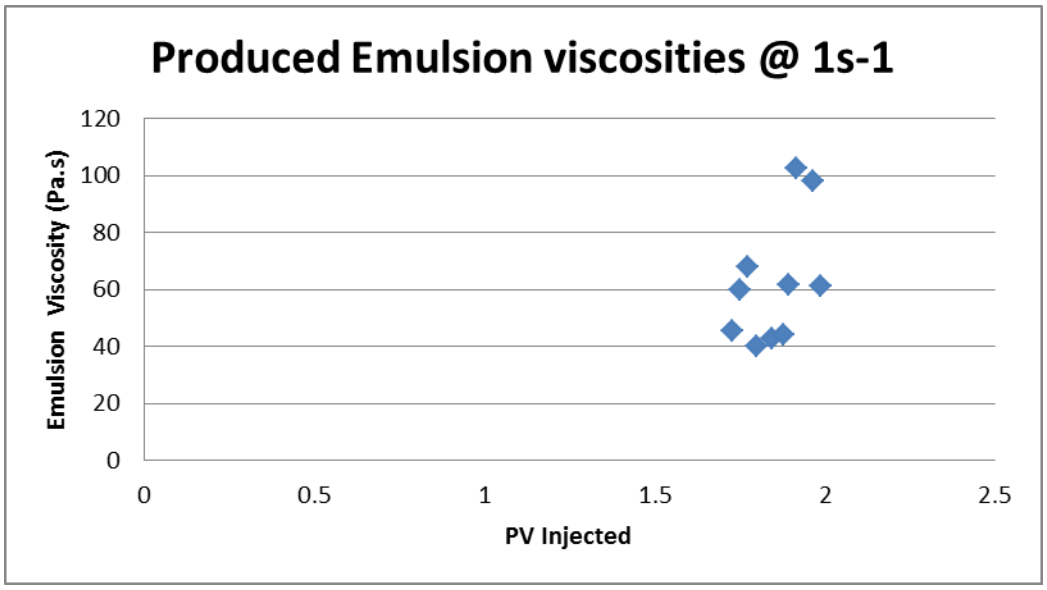

Figure 4.30: Viscosity of the effluent emulsions.

The high pressure drops in conjunction with the late response of oil recovery makes the AS injection after a polymer flood unsuitable from EOR perspective.

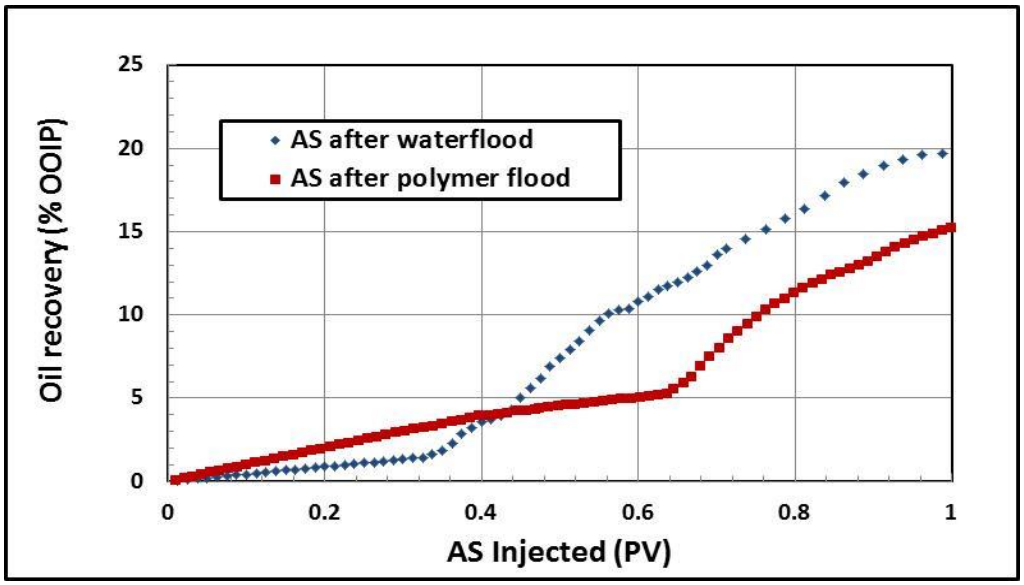

Figure 4.31: Comparison of the oil recovery by AS solution when it is injected after the polymer with the case when AS is injected the waterflood

Figure 4.31 compares the additional oil recovery by AS flood after waterflood and polymer flood. The incremental oil recovery by AS after waterflood was 20% compared with 15% after polymer flood. The oil recovery response is late and total additional oil recovery is poor in the case of polymer flood.

Thus it can be concluded that polymer flood provides the benefit of improving the sweep efficiency over waterflood when conducted in the secondary or the tertiary mode. However, the process performance is poor when the alkali surfactant is used along with the polymer flood.

4.2 CHEMICAL SCREENING AND SAND PACK EXPERIMENTS FOR OIL B

In this section chemical methods for a 330 cp oil are developed. This oil will be called Oil B to distinguish it from Oil A (10,000 cp). Chemical screening tests also known as phase behavior tests were conducted in order to search for an alkali surfactant

system which could generate a thermodynamically stable microemulsion phase with the oil. Due to the high acid number (1.47 mg KOH/100 gm oil) sodium carbonate was used as an alkali to generate soap with the oil. The soap acts as an in situ hydrophobic surfactant. A relatively hydrophilic surfactant was added to achieve the hydrophilic hydrophobic balance in the total surfactant mixture. A Type III microemulsion with optimum solubilization ratio and optimum IFT occurs when this balance occurs. A robust system with the Type III microemulsion occurring over a wide range of salinity together with high solubilization ratios (greater than 10) was desired for the low enough IFT. Chemical systems which generated viscous emulsions were discarded. Due to the high oil viscosity and low temperature (~75 F), the systems took a long time to equilibrate and separate out into individual phases. The phase behavior was conducted for different alkali concentrations and WORs.

4.2.1 Chemical screening tests

These screening tests were conducted to select the appropriate concentration of alkali and surfactant chemicals. The first test was conducted by fixing the alkali concentration to 0.5 wt% and changing the surfactant concentration starting from 0 to 0.9 wt%. The surfactant tested was TDA 30EO which is a hydrophilic surfactant with 30 ethoxylate groups. At low surfactant concentrations, the system is expected to exhibit a hydrophobic behavior due to a larger concentration of soap. The results are displayed in figure 4.32.

The samples with 0 and 0.1 wt% surfactant showed viscous emulsions at the bottom of the oil phase. This was confirmed because the lower phase did not move when the tubes were tilted. On the other hand, the samples with higher amounts of the surfactant did not show the presence of any viscous emulsion. Samples with 0.3% and

0.4% surfactant started to show a thin layer of the third phase. On tilting the tubes, all the phases showed good fluidity. Samples with higher surfactant concentration showed higher volumes of the 3rd phase. This surfactant also acts as a cosolvent and gives fluidity to the middle phase.

Figure 4.32: Phase behavior with 0.5 wt% alkali and 20,000 ppm brine with varying surfactant concentration in steps of 0.1 wt% from 0 wt % on the left to 0.9 wt% on the right

From the first phase behavior results, a surfactant concentration of 0.4 wt% was chosen for further studies. The phase behavior with 0.5 wt% alkali showed a dark bottom phase with a thin layer of middle phase. Figure 4.33 shows the phase behavior of samples with 0.4 wt% (high) surfactant and 20,000ppm NaCl brine at a WOR of 1:1 and 25 °C. The test tubes were allowed to stand for almost a year. This time was deemed appropriate to allow the phases to come to equilibrium and the mixture to separate out into individual phases. The alkali concentration is varied from 0 wt% to 0.9 wt% in the increments of 0.1 wt%. Figure 4.34 shows samples with alkali concentration from 0.9-1.5 wt%. The

aqueous phase is almost clear in the left most tube with 0 wt% alkali; oil solubilization is small with only the synthetic surfactant at 20,000 ppm NaCl. As the alkali concentration increases, the amount of soap generated increases. As a result the total amount of surfactant (soap + synthetic surfactant) in the system increases giving rise to higher oil solubilization. Three phases form giving rise to Type III behavior. Higher alkali concentrations also mean higher salinity for the system. Typical microemulsion systems tend to generate Type II systems instead of Type III for higher salinities. However in this system the higher concentration of alkali (~ 1.5 wt%) did not drive the system to Type II.

Figure 4.33: Phase behavior of 0.4 wt% surfactant and 20,000 ppm NaCl with varying alkali concentrations (0 wt% on the left to 0.9 wt% on the right)

Due to the dark color of the bottom and a very dark brown color of the middle phase in most of the test tubes, it was not possible to observe the phase boundaries clearly under the normal white light. In these cases an Ultra Violet light source was used to read

the phase volumes. An example is shown in figure 4.35 where the phase boundaries are marked as were read using the UV light. After reading the phase boundaries oil and water solubilization ratios were calculated and plotted against the salinity (alkali concentration).

Based on the read volumes of the individual phases, oil and water solubilization ratios were plotted as shown in figure 4.36. The calculation steps are outlined in the methodology chapter. Oil solubilization ratio increases with salinity whereas the water solubilization ratio decreases with salinity. The plot also shows a Type III phase behavior for almost the entire salinity spectrum. Since the phases were very dark in color, direct measurement of IFT was not possible. The raw data from the lab was matched with the UTCHEM phase behavior algorithm. The curve shows such a match. The parameters extracted were used in UTCHEM simulations to history match the oil recovery and the pressure drop curves.

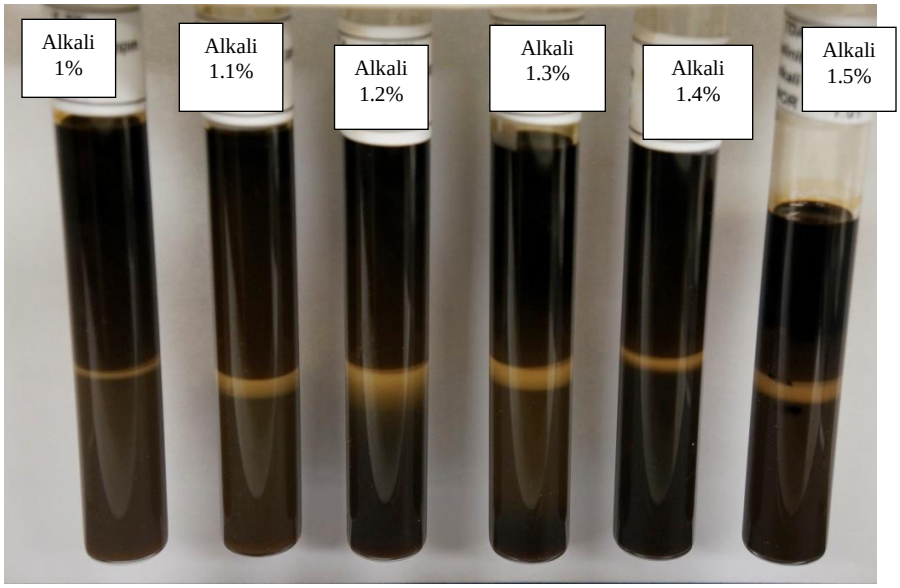

Figure 4.34: Phase behavior of 0.4 wt% surfactant and 20,000 ppm NaCl with varying alkali concentrations (1 wt% on the left to 1.5 wt% on the right)

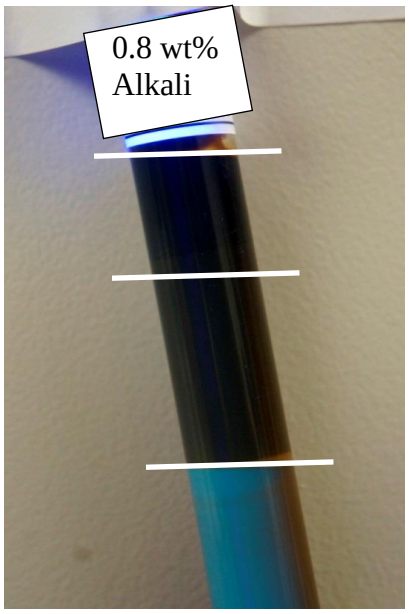

Figure 4.35: Sample with 0.8 wt% alkali under the UV light

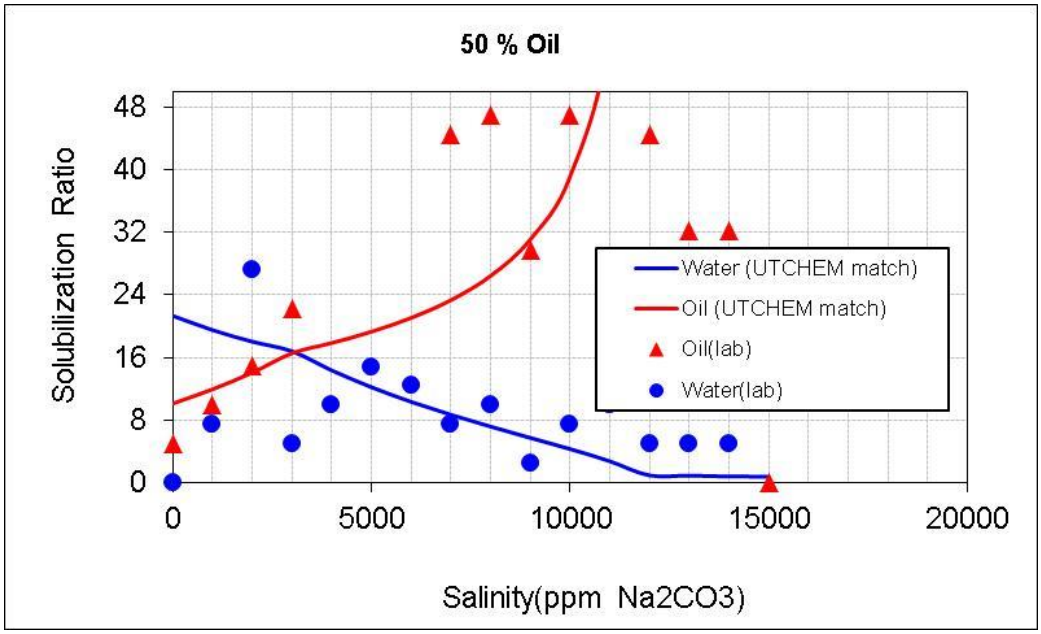

Figure 4.36: Oil and Water solubilization ratios (age of the samples is 1 year)

4.2.2 Sand Pack Floods

Sand pack floods were performed in order to determine the effectiveness of the alkali surfactant polymer formulations in a 1D flooding system. Table 4.4 gives the

properties of the sand packs used for different experiments. The injection scheme is given in separate tables. The length and diameter are slightly different across different sand packs but this difference is not expected to bring about any significant changes in the oil recovery behavior.

Experimental Data	Flood 1	Flood 2	Flood 3
Permeability (Darcy)	22.6	26.17	25.65
Porosity (%)	42.3	43.72	45.5
Initial Water Saturation (S_{wi})	8.6%	13%	20%
Length (ft)	2	3	3
Diameter (inches)	0.67	0.67	0.56

Table 4.4: Properties of the sand packs

Flood 1: Injection of ASP in the tertiary mode followed by graded polymer slugs

Table 4.5 gives the injection scheme for this experiment. The polymer viscosities are reported at the estimated apparent shear rate of $0.6s^{-1}$ inside the sandpack.

Figure 4.37 shows the oil recovery and the oil cut for the brine flood and ASP flood. The oil recovery reached 70% OOIP after 3PV of brine flood. Breakthrough occurs at 0.4PV of brine injection. Oil cut drops to 0.1 at the end of the brine flood. After brine flood the remaining 30% of the oil is recovered by ASP and subsequent polymer slugs. The size of the ASP slug was about 0.5 PV. The flood responded to the ASP slug in about 0.5 PV.

Fluid Injected	PV injected	Viscosity
20,000 ppm brine	3 PV	1 cp
ASP slug 0.4 wt% surfactant 20,000 ppm brine, 1.5 wt% alkali, 0.48 wt% polymer	0.5PV	800 cp (shear rate = 0.6 s^{-1})
Polymer slug 20,000 ppm brine, 0.48 wt% polymer	1PV	1100 cp (shear rate = 0.6 s^{-1})
Polymer slug 20,000 ppm brine, 0.38 wt% polymer	0.5PV	500 cp (shear rate = 0.6 s^{-1})
Polymer slug 20,000 ppm brine, 0.29 wt% polymer	0.5PV	200 cp (shear rate = 0.6 s^{-1})
20,000 ppm brine	0.5PV	1 cp

Table 4.5: Injection scheme for Flood 1

Oil cut increased to about 0.6 and then decreased. High oil cut persisted for another 0.5 PV. The ASP slug was followed by the tapered polymer slug. The polymer slug provided mobility control and displaced the oil bank in a stable manner.

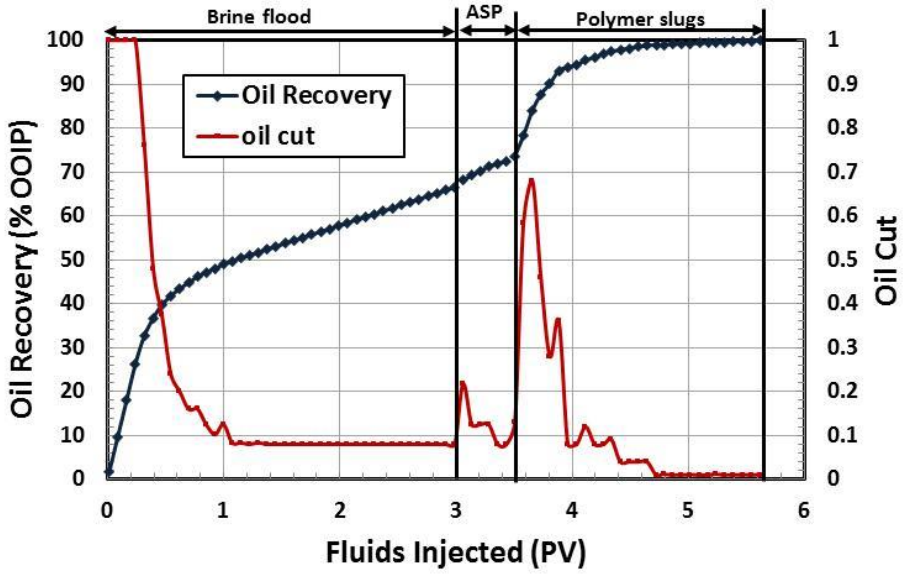

Figure 4.37: Cumulative oil recovery and oil cut for a tertiary ASP flood

Figure 4.38 shows the pressure drop during the waterflood and the subsequent alkaline surfactant polymer flood. Initially oil was flowing through the system at the steady state at a pressure drop of 1.4 psi. When the injection port was switched to the water side, the pressure drop declined from 1.4 psi to very close to 0 psi at the end of the waterflood. The pressure drop picked up again when the alkaline-surfactant-polymer slug was injected. The pressure drop increased to a maximum of about 4 psi (a pressure gradient of 2 psi/ft) and, as expected, began to decline when the tapered polymer slugs were injected. The final pressure drop after the end of the flood was about 0.5 psi. During the entire flood the pressure drops did not rise to very high values. This indicated that there were no viscous emulsions in the system. Thus the alkali surfactant polymer flood was able to recover most of the oil at a reasonable pressure drop.

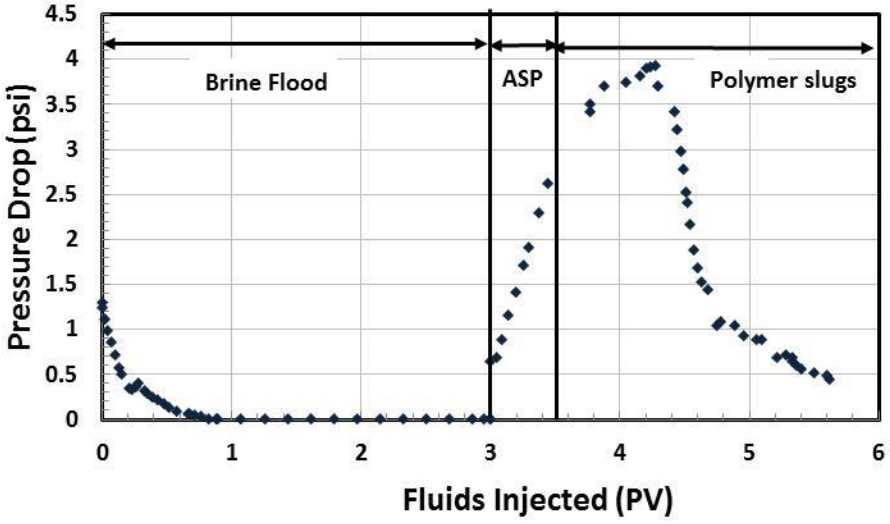

Figure 4.38: Pressure drop during waterflood and alkaline surfactant polymer flood

Flood 2: injection of polymer slug in the secondary mode

In the above experiment, it was found out that the waterflood could alone recover close to 70% oil in 3PV of injection. The high oil recovery also indicates that the flood front is stable. Thus it makes sense to study the effect of a secondary polymer flood on the oil recovery. The secondary polymer flood will be able to recover the same oil (70% OIP) with faster recovery rates. Figure 4.39 and figure 4.40 plot the oil recovery and pressure drop for these experiments.

Fluid Injected	**PV injected**	**Viscosity**
Polymer 20,000 ppm brine, 0.48 wt% polymer	1.3	1100 cp (shear rate = 0.6 s^{-1})
20,000 ppm brine	0.67	1 cp

Table 4.6: Injection scheme for Flood 2

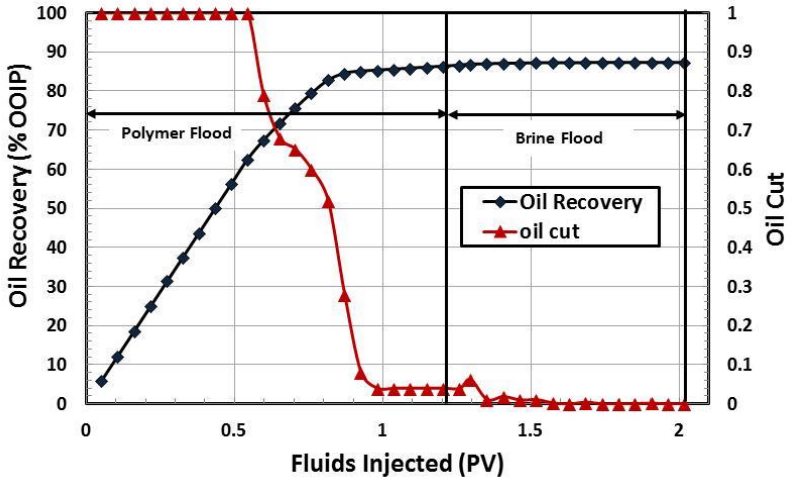

Figure 4.39: Cumulative oil recovery and oil cut for the secondary polymer flood

Figure 4.39 indicates that almost 90% of the oil in place (OIP) is recovered by the secondary polymer flood. The behavior of the oil recovery curve indicates that a piston like displacement was achieved owing to the high viscosity (~3 times of oil) of the polymer solution. The data of this experiment can give an estimate of the residual oil after a secondary flood. The calculations show that this value is 0.12 and can be used for history matching the brine flood experiments as well.

Figure 4.40 shows a pressure drop increase from about 2 psi to 4.5 psi due to the high viscosity polymer injection and sweep out of the 330 cp oil. However as expected during the brine injection, the pressure drop reduced to 0.5 psi, very close to the final pressure drop obtained after the Flood 1.

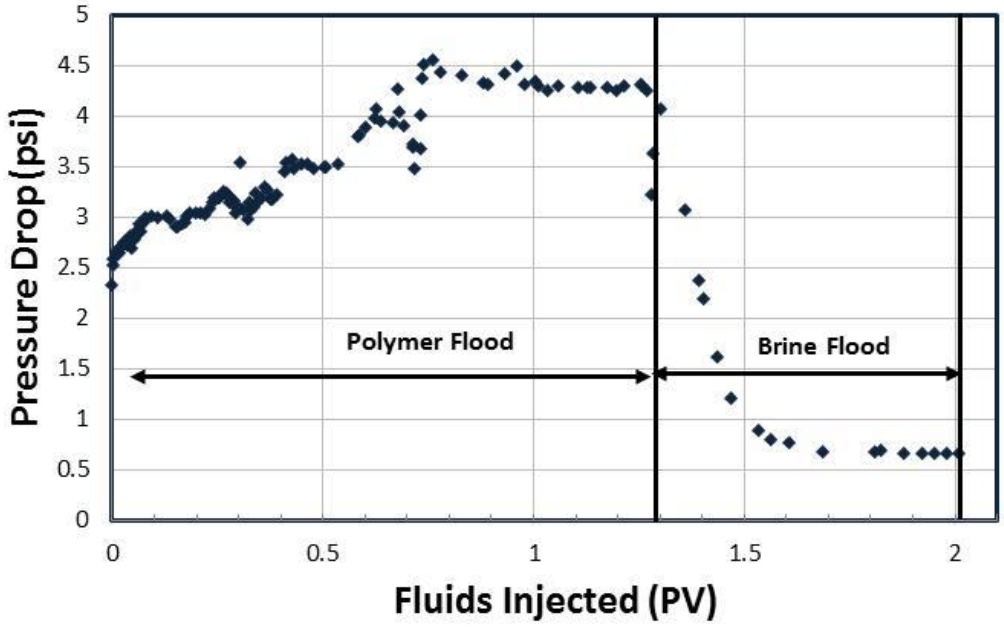

Figure 4.40: Pressure drop during the secondary polymer flood

Flood 3: Injection of a low viscosity ASP slugs in the tertiary mode followed by graded polymer slugs

This experiment is very similar to the first experiement in that an ASP slug is followed by polymer slugs. However in this experiment we wanted to study the impact of reducing the polymer viscosity. The injection scheme is given in Table 4.7. It is to be noticed that due to a pump error, only 0.3 PV of ASP slug was injected instead of the intended 0.5 PV. The polymer concentration in the ASP slug has been reduced to 0.38 wt%. The viscosity of the ASP slug was measured to be 350 cp which is comparable to that of oil. The polymer concentration in the polymer slug was also curtailed from 0.48 wt% to 0.38 wt%. Figure 4.41 and figure 4.42 plot the oil recovery and pressure drop for this experiment.

Fluid Injected	**PV injected**	**Viscosity**
20,000 ppm brine	3.3 PV	1 cp
ASP slug 0.4 wt% surfactant 20,000 ppm brine, 1.5 wt% alkali, 0.38 wt% polymer	0.3PV	350 cp (shear rate = 0.6 s^{-1})
Polymer slug 20,000 ppm brine, 0.38 wt% polymer	1PV	500 cp (shear rate = 0.6 s^{-1})
Polymer slug 20,000 ppm brine, 0.29 wt% polymer	0.5PV	200 cp (shear rate = 0.6 s^{-1})
Polymer slug 20,000 ppm brine, 0.2 wt% polymer	0.3PV	65 cp (shear rate = 0.6 s^{-1})
20,000 ppm brine	0.4PV	1 cp

Table 4.7: Injection scheme of Flood 3

Brine flood could recover 62% of oil in 3.3 PV of injection. Water breakthrough occurred at 0.4PV after which oil recovery proceeded with decreasing oil cuts. The oil cut reduced to 0.05 at the end of the waterflood. During the brine flood the pressure drop in the system declined from 5 psi to close to 0.8 psi. The initial pressure for this experiment (5 psi) is higher than the last two. The reason is the larger length of the steel tube used than the first experiment and the smallest tube diameter used than the other two experiments. However we do not expect the profile of oil recovery to change significantly with the tube diameter.

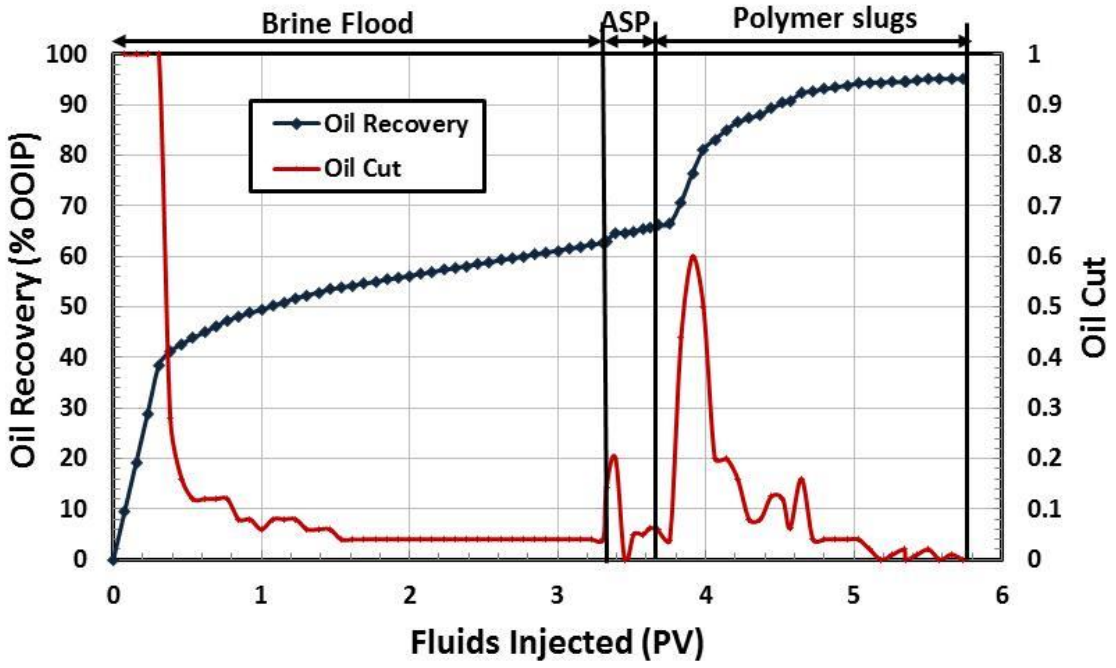

Figure 4.41: Cumulative oil recovery and oil cut for a tertiary ASP flood

Upon injection of the viscous ASP slug, the system responded with a build-up of pressure. As the pressure buildup took place the fluid produced was mainly water. However, once the pressure buildup reached to 6 psi, oil cuts increased the cumulative oil

recovery improved. Final oil recovery was 95% with an improvement of 33% in recovery after waterflooding. Due to malfunctioning of the pressure recording system we could record data upto only 4.5 PV. Till this time most of the extra oil had already been produced and pressure drop across the sandpack started to decline simultaneously.

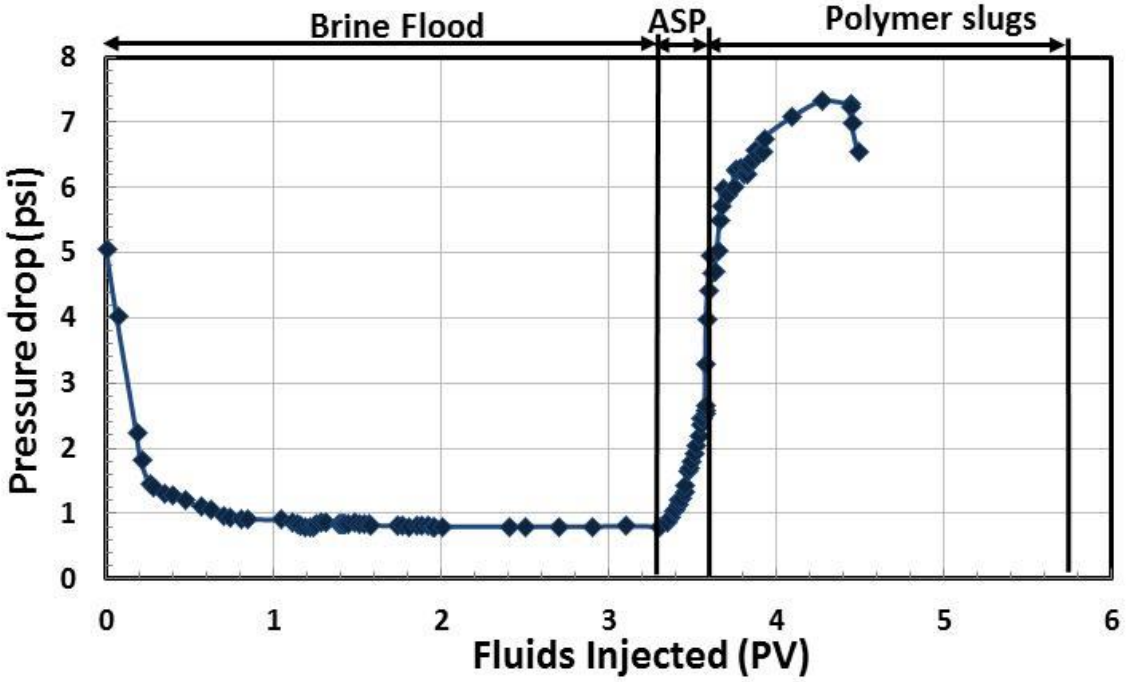

Figure 4.42: Pressure drop during waterflood and alkaline surfactant polymer flood

CHAPTER 5: MODELLING AND SIMULATION

This chapter describes the models developed and the simulations undertaken to match the experimental results from the laboratory sand pack floods. The modeling of waterflood, polymer flood and alkali surfactant flood are described in separate sections for the 10,000 cp oil (Oil A) and 330 cp oil (Oil B).

5.1 WATERFLOOD AND CHEMICAL FLOOD SIMULATION FOR 10,000 CP OIL (OIL A)

5.1.1 Modeling and simulation of the waterflood for 10,000 cp oil

The modeling and simulation of the waterflood for the 10,000 cp oil was attempted by two methods.

1) Fine grid simulations
2) Heuristic viscous fingering model

Fine grid simulations

Fine grid simulations were deemed necessary to generate viscous fingers in the simulations. Although such simulations require a lot of computational power, they can still be undertaken for the laboratory scale experiments. The details of the simulation setup are described next.

Grid Structure

1D sand pack flood experiments were simulated using the CMG STARS simulator. The porosity and permeability of the model were set at 35% and 20.4 Darcy respectively. The model was represented by 80×1×100 grids. The injection well was located at the bottom of the model and the production well was placed at the top. To generate fingers in the model, the permeability was perturbed randomly around the mean value with a standard deviation of 10%. Figure 5.1 shows the grid structure and permeability distribution used in the simulations.

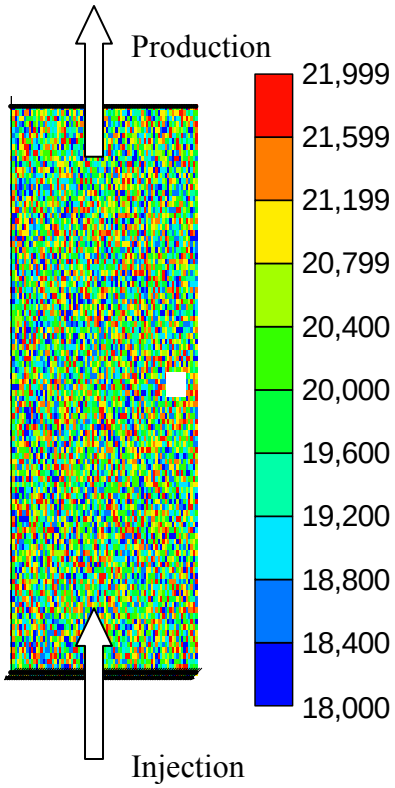

Figure 5.1: Grid structure and permeability distribution used in the waterflood simulations

Component definition in CMG STARS

Two components (oil and water) were defined to be present in the oleic and the aqueous phase respectively, in CMG STARS. The viscosity of these components was set as 10,000 cp and 1 cp, respectively.

Simulation results

Fine grid simulations were aimed at generating viscous fingers inside the porous media and at the same time successfully history matching the oil recovery and the pressure drop behavior of the experiment. The oil-water relative permeability curves were tweaked until a good match was attained. Figure 5.2 shows the relative permeability curves which could match the experimental results.

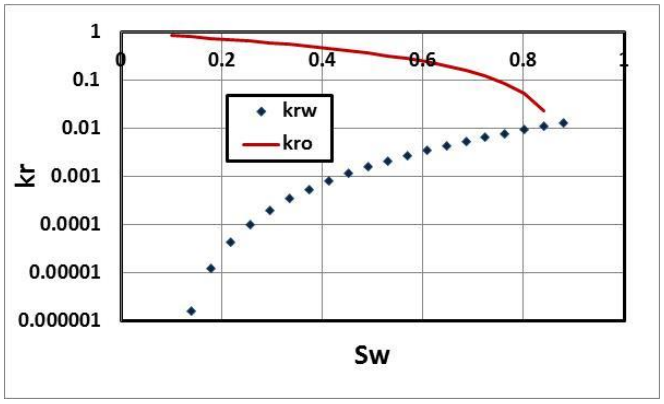

Figure 5.2: Oil water relative permeability curves used in water flood simulations

Figure 5.3 shows the viscous fingers generated in the system by the simulations. It should be noted that because we did not conduct a visual analysis of the fingers in the experiments, the simulations do not aim to match the viscous fingering patterns from the experiments.

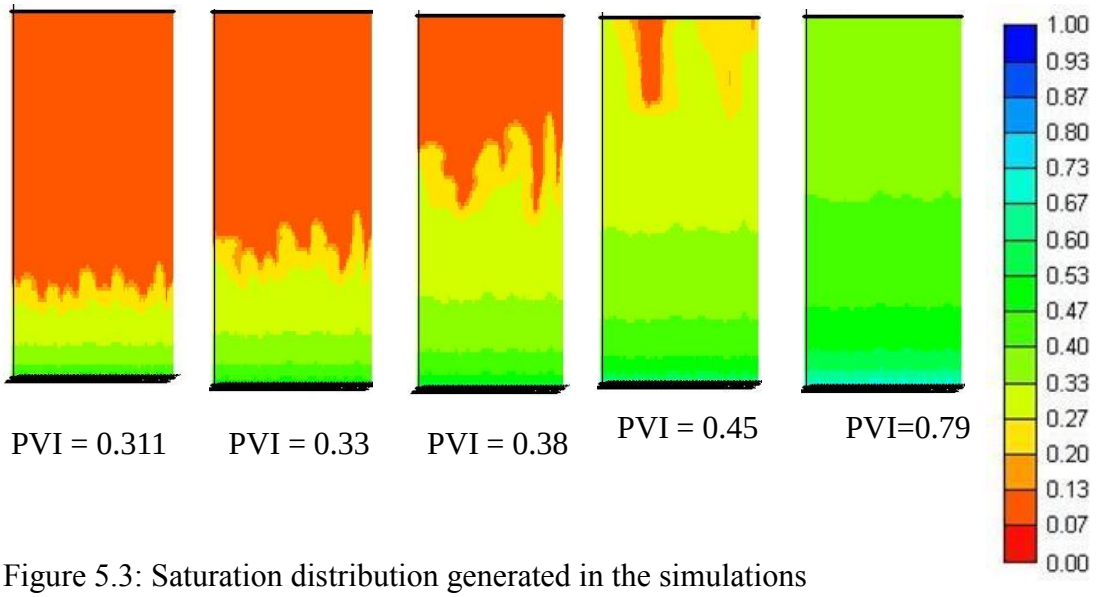

Figure 5.3: Saturation distribution generated in the simulations

At earlier times when the water saturations are low, water fingers through the oil phase. In the simulations this occurred until 0.45 PVs injection. However, once the water

saturation was high (0.4-0.5 in the figure), no further fingers were formed. Figures 5.4 and 5.5 present the results on the history match of the oil recovery and the pressure drop.

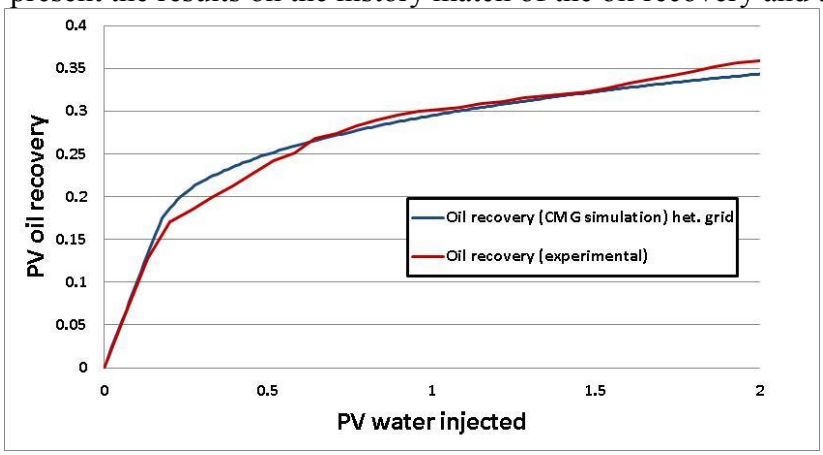

Figure 5.4: History match of the oil production data

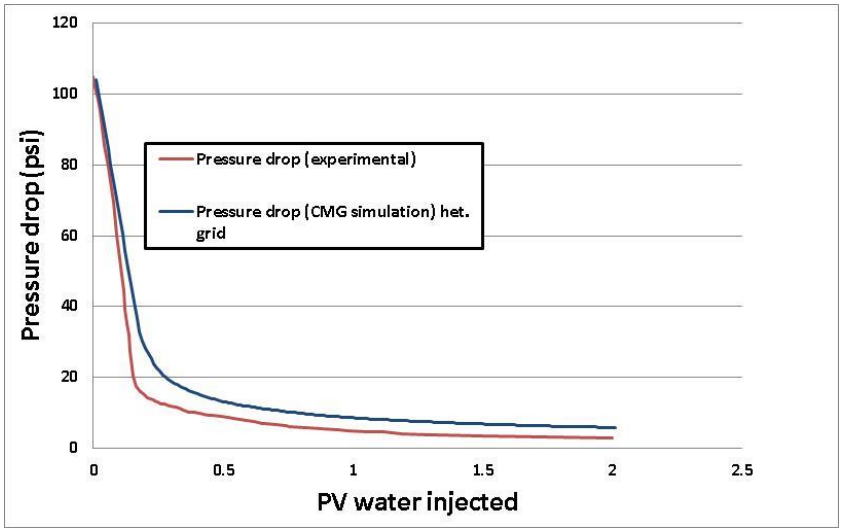

Figure 5.5: History match of the pressure drop data

Figures 5.4 and 5.5 display a good agreement between the experimental and simulated oil recovery and the pressure drop data. From Figure 5.2, it can be noticed that the end point water relative permeability is close to 0.01, a value very low as compared to the usual range of 0.1-0.2 for water end point relative permeability used for sandstone

reservoirs with light oils. Tang and Kovscek (1995) noticed a decrease in the end point steady state water relative permeability value when the high oil viscosity of 155 cp was used. Doorwar and Mohanty (2011) conducted waterflood experiments on the heavy oil in a micro-model and observed that viscous fingers formed had a fractal structure. Moreover, the main water finger developed side branches which do not propagate to long distances. In other words, even though water resides in the side branches it does not contribute to the flow. This means that for the same water saturation, the water relative permeability tends to be lower than that without viscous fingering.

Heuristic viscous fingering model

When viscous oil is displaced from a porous medium by a low viscosity brine, the oil-water interface becomes unstable and breaks up into fingers. These fingers are called viscous fingers owing their formation to the presence of large viscosity ratio (μo/μw >1,000). A different approach is needed to model the waterfloods which are dominated by the viscous fingers. Here we present some models which were used to match the results of a linear sandpack heavy oil waterflood.

Koval (1963) developed a model to describe the average behavior of an unstable miscible flooding phenomenon. The model did not aim to predict the growth, size or the shape of the fingers. The model developed for the miscible displacement is here modified to represent the unstable immiscible displacement. Next, we give the necessary equations and present results on applying the model.

$$f_w = \frac{k_{rw}{}^{o}\left(Sw^{*}\right)^{Ew} \Big/ \mu_w}{k_{rw}{}^{o}\left(Sw^{*}\right)^{Ew} \Big/ \mu_w + k_{ro}{}^{o}(1-Sw^{*})^{Eo} \Big/ \mu_o} \qquad (5.1)$$

Where $Sw^{*} = \dfrac{Sw - Swi}{1 - Swi - Sorw}$ (5.2)

fw = fractional flow of water

krw^o = end point relative permaeability to water

kro^o = end point relative permeability to oil

Ew = water relative permeability exponent

Eo = oil relative permeability exponent

Swi = initial water saturation

Sorw = residual oil saturation

Which can be rewritten as:

$$fw = \frac{(Sw^*)^{Ew}}{(Sw^*)^{Ew} + \frac{(1-Sw^*)^{Eo}}{M}} \qquad (5.3)$$

Where $M = \frac{k_{rw}\mu_o}{k_{ro}\mu_w}$

Applying the Koval theory, we modify the factor M (mobility ratio) with the koval factor K. Also for simplicity, we also specify the water and oil exponents as 1. The equation of water fractional flow now reads as:

$$fw = \frac{KSw^*}{1+Sw^*(K-1)} \qquad (5.4)$$

where K is the koval factor

The equation derived above is very similar to the one developed by Koval for the miscible fingering case. Equivalently, the oil recovery in pore volumes can be written as:

$$Np = \left(\frac{2(K*PVI)^{1/2} - 1 - PVI}{(K-1)} \right)(1-Swi-Sorw) \qquad (5.5)$$

Where Np = cumulative oil recovery (PV)

PVI = water injected (PV)

The equation was used to calculate the oil recovery and match it with the experimental data. Figure 5.6 shows the results of such a match.

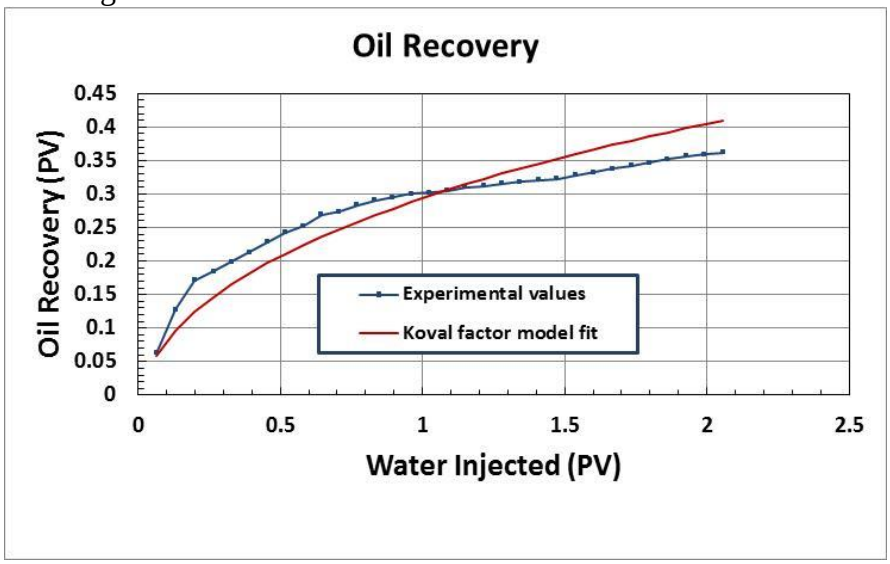

Figure 5.6: History match of the experimental oil recovery data by Koval theory

Table 5.1 shows the model fit parameters.

Parameter	Value
K (Koval factor)	25
Swi	0.1
Sorw	0.12

Table 5.1: Parameters used in the Koval model

The equivalent koval model could not match the experimental oil recovery data accurately. Possible reason is that it is a one parameter model and we probably need more parameters to represent average behavior of the phenomenon.

Another method to represent the immiscible viscous fingering was used after limited success with the koval model. This method was developed on the basis of the

basis of empirical miscible viscous fingering model of Fayers and Newly (1988). Following are the assumptions of the model:

1) The flow can be described as the displacement of the bypassed oil by the fingering liquid.
2) Different fingers can be lumped together into a single equivalent finger.
3) The equivalent viscous finger does not exchange fluids (oil or water) with the bypassed zone.
4) The fractional width, λ, occupied by the finger grows away from the leading edge of the finger.
5) Single phase oil flow occurs in the bypassed zone. Two phase flow occurs in the viscous finger.

With the assumptions listed above, the viscous fingering inside the porous medium can be represented by the schematic shown in figure 5.7. The picture can also be referred as the physical model of the viscous fingering phenomenon. Figure 5.8 shows the mathematical model which results from the assumptions of Fayers and Newly (1988).

Figure 5.7: Physical model of the viscous fingering phenomenon

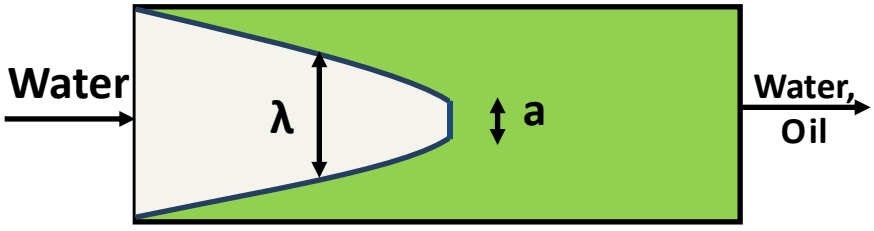

Figure 5.8: Mathematical model considered for representing viscous fingering phenomenon

Based on the assumptions listed above, a fingering function was developed which describes the fractional width of the finger away from the leading edge. The model, originally developed for the miscible flood process, defines the fingering width as a growing function of solvent concentration. Similarly, for the immiscible process the fingering width is defined as a growing function of the normalized saturation Swf.

$$Swf = \frac{(S_w - S_{wi})}{(1 - S_{wi} - S_{orw})} \tag{5.6}$$

$$\lambda = a + bS_{wf}{}^{\alpha} \tag{5.7}$$

where, λ = finger width

Sw = water saturation inside the finger

Swi = initial water saturation of the sand pack

Sorw = residual oil saturation

a, b and α = fitting parameters.

The finger fractional width defines the region in which the 2 phase flow is allowed to occur. Everywhere outside the finger it is assumed that only oil can flow at initial water saturation. In other words the relative permeabilities are defined for fluid flow only inside the finger region.

$$q_w = \frac{kk_{rw}\lambda A}{\mu_w}\left(-\frac{\partial P}{\partial x}\right) \tag{5.8}$$

$$q_o = \frac{kk_{ro}\lambda A}{\mu_o}\left(-\frac{\partial P}{\partial x}\right) + \frac{kk_{ro}{}^{0}(1-\lambda)A}{\mu_o}\left(-\frac{\partial P}{\partial x}\right) \tag{5.9}$$

$$k_{ro} = k_{ro}{}^{o}\left(\frac{1-S_w-S_{wi}}{1-S_{wi}-S_{orw}}\right)^{Eo} \qquad (5.10)$$

$$k_{rw} = k_{rw}{}^{o}\left(\frac{S_w-S_{wi}}{1-S_{wi}-S_{orw}}\right)^{Ew} \qquad (5.11)$$

where, krw^{o} = end point relative permeability of the water phase

Ew = exponent for the water phase relative permeability

kro^{o} = end point relative permeability of the oil phase

Eo = exponent for the oil phase relative permeability

A = Area of cross section of the porous media

μ_w = water phase viscosity

μ_o = oil phase viscosity

$-\frac{\partial P}{\partial x}$ = pressure gradient.

The fractional flow of water through the entire cross section can now be calculated as:

$$f_w = \frac{q_w}{q_w + q_o} \qquad (5.12)$$

Similar to the cross sectional water fractional flow, the cross sectional averaged water saturation can be calculated as:

$$\overline{S_w} = S_w\lambda + (1-S_{wi})(1-\lambda) \qquad (5.13)$$

Upon using the above correlation the 1D problem can easily be solved using the Buckley-Leverett formulation. From the model, it is also possible to derive relationships for the apparent water and oil relative permeabilities as follows.

From $q_w = \frac{kk_{rw}\lambda A}{\mu_w}\left(-\frac{\partial P}{\partial x}\right)$

$$k_{rwapp} = k_{rw}\lambda = f1(S_w) = g1(\overline{S_w}) \qquad (5.14)$$

From $q_o = \frac{kk_{ro}\lambda A}{\mu_o}\left(-\frac{\partial P}{\partial x}\right) + \frac{kk_{ro}{}^{0}(1-\lambda)A}{\mu_o}\left(-\frac{\partial P}{\partial x}\right)$

$$q_o = \frac{kA}{\mu_o}\left[k_{ro}\lambda + k_{ro}{}^{o}(1-\lambda)\right]\left(-\frac{\partial P}{\partial x}\right)$$

$$k_{roapp} = k_{ro}\lambda + k_{ro}{}^{o}(1-\lambda) = f2(S_w) = g2(\overline{S_w}) \qquad (5.15)$$

The advantage of calculating the apparent relative permeabilities is that these functions can now be used directly in a reservoir simulator to predict the oil recovery and the pressure drop behavior.

History matching of 1D waterflood

The above model was used to conduct the history matching of the 1D waterflood of the heavy oil. For this purpose, experimental data from Chapter 4 was used. Figure 5.9 shows the results of the history match of the cumulative oil production data. Figure 5.10 shows the match of the pressure drop data. The model predicted the early water breakthrough (0.15 PV) as compared to 0.18 PV from the experiment. However the post breakthrough oil recovery was matched fairly well. The match of the pressure drop data showed slight deviations from the experimental values, though good agreement with the overall trend was achieved. Figure 5.11 shows the apparent oil and water relative permeabilities calculated from the model. The end point relative permeability of water is fairly low. Table 5.2 lists the oil-water intrinsic relative permeability parameters used for the calculations. It is to be noted that the relative permeability parameters along with the fingering function together influence the final apparent oil and water relative permeability.

The fingering function for this case was calculated to be $\lambda = 0.1 + 0.9S_{wf}^{0.7}$ indicating that finger occupies the entire cross sectional area at the inlet where Swf is always equal to 1.

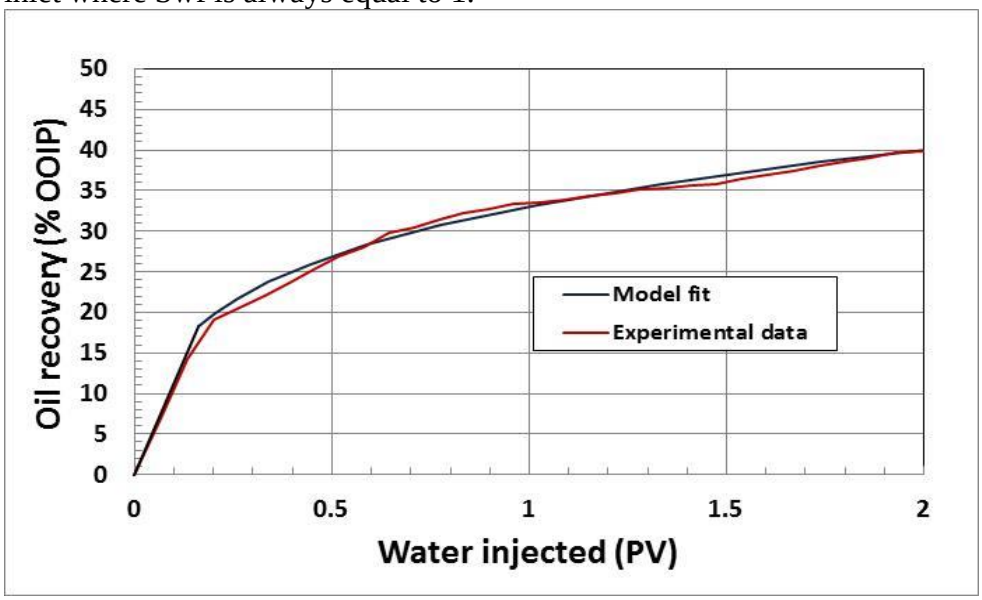

Figure 5.9: History match of the 1D oil production data

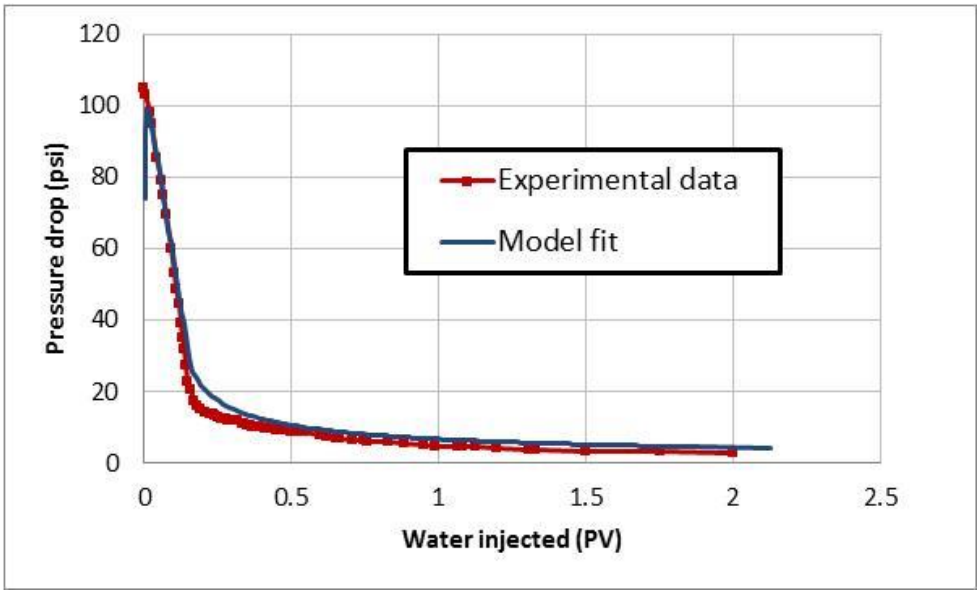

Figure 5.10: History match of the 1D pressure drop data

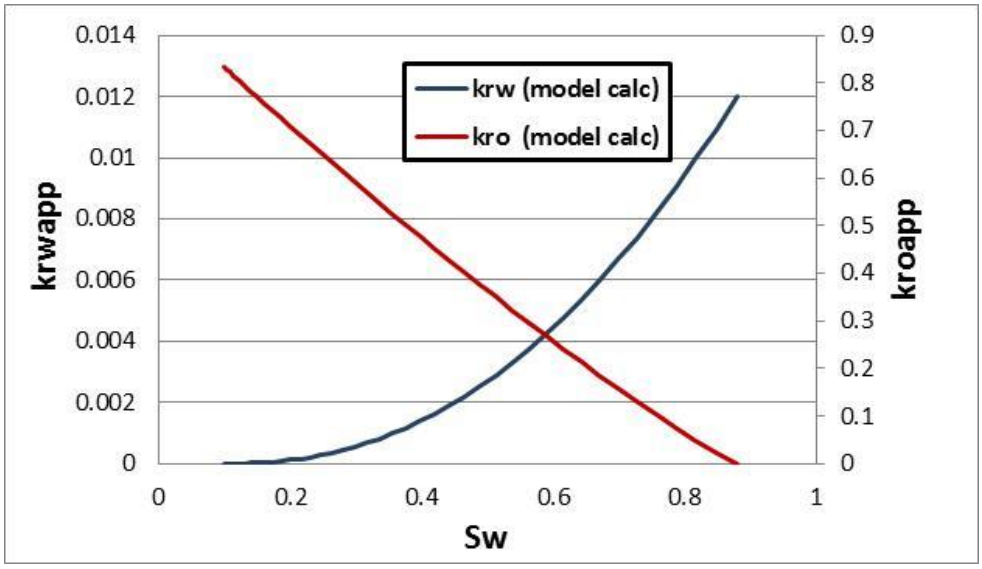

Figure 5.11: Apparent oil and water relative permeabilities calculated from the model

krw^o	0.012
kro^o	0.833
S_{wi}	0.1
S_{orw}	0.12
Ew	3
Eo	1.2

Table 5.2: Intrinsic oil and water relative permeability parameters

History matching of the 2D waterflood

The similar structure of the relative permeability curves were used to match the oil production and the pressure drop curves. Figure 5.12 and 5.13 show the match of the oil recovery and the pressure drop data, respectively. The simulated oil recovery shows a good agreement with the experimental data. The simulated pressure drop does not agree

with the experimental values at earlier times. However after 0.4 PVs of injection, the simulated values and the experimental data agree well.

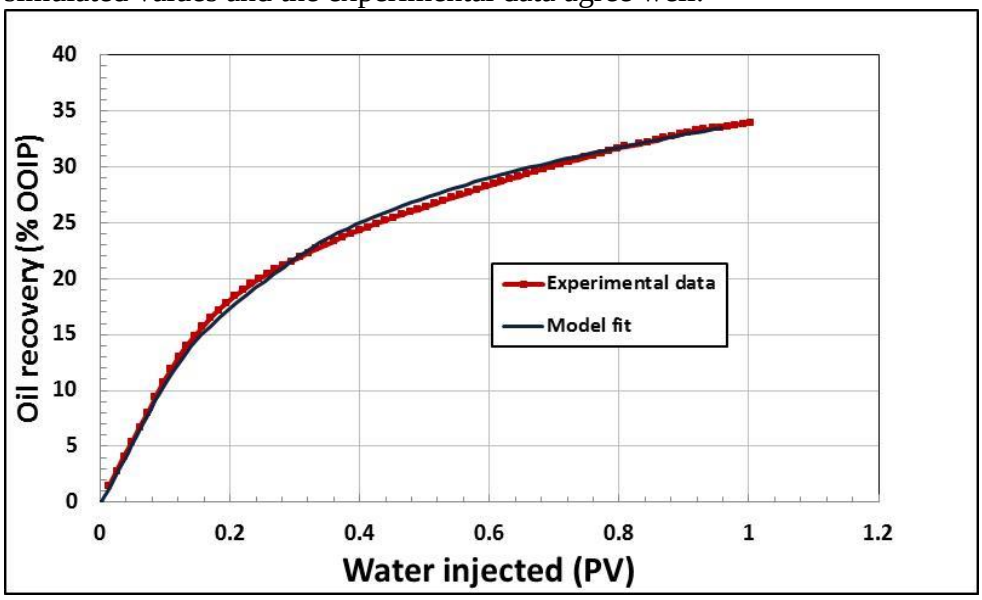

Figure 5.12: History match of the 2D oil production data

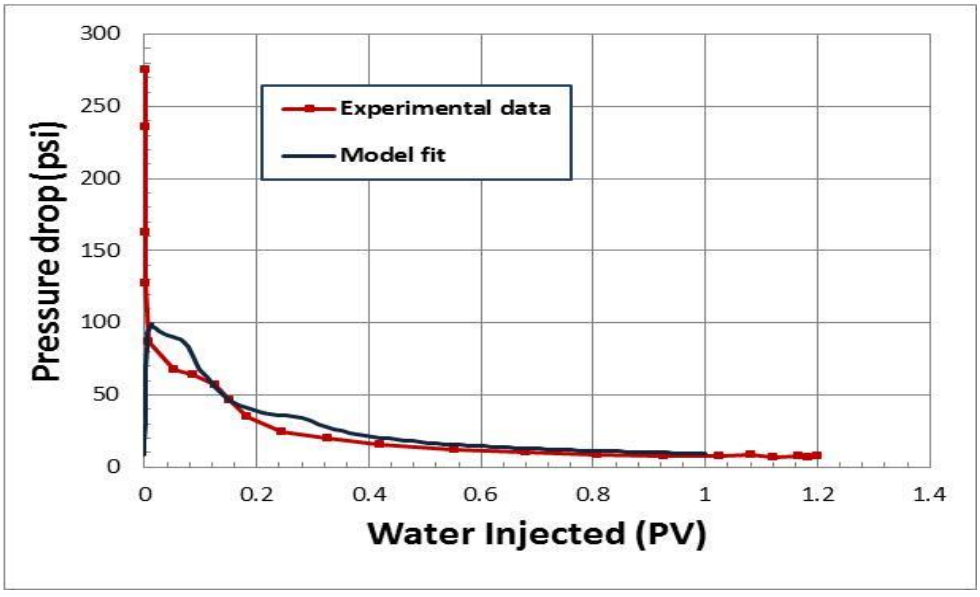

Figure 5.13: History match of the 2D pressure drop data

Figures 5.14 (a) and 5.14 (b) show the saturation map of the waterflood from the 2D simulations. The simulations were conducted on a 20×20×5 grid blocks. The simulation was not intended to reproduce the viscous fingering inside the porous media but to match the average behavior of the waterflood, in other words to match the oil recovery and the pressure drop response.

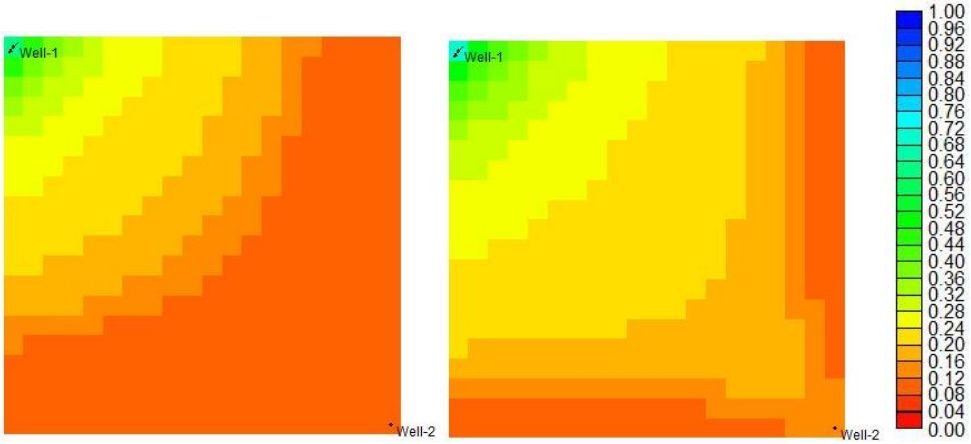

Figure 5.14: Water saturation at (a) 0.37 PV and (b) 0.57 PV

Figure 5.15 gives the apparent relative permeability curves used for the history matches. The relative permeability curves were calculated by an equivalent 1D model where the fingering function was specified as $\lambda = 0.1 + 0.9 S_{wf}^{\ 2}$. Table 5.3 lists the intrinsic oil and water relative permeability parameters.

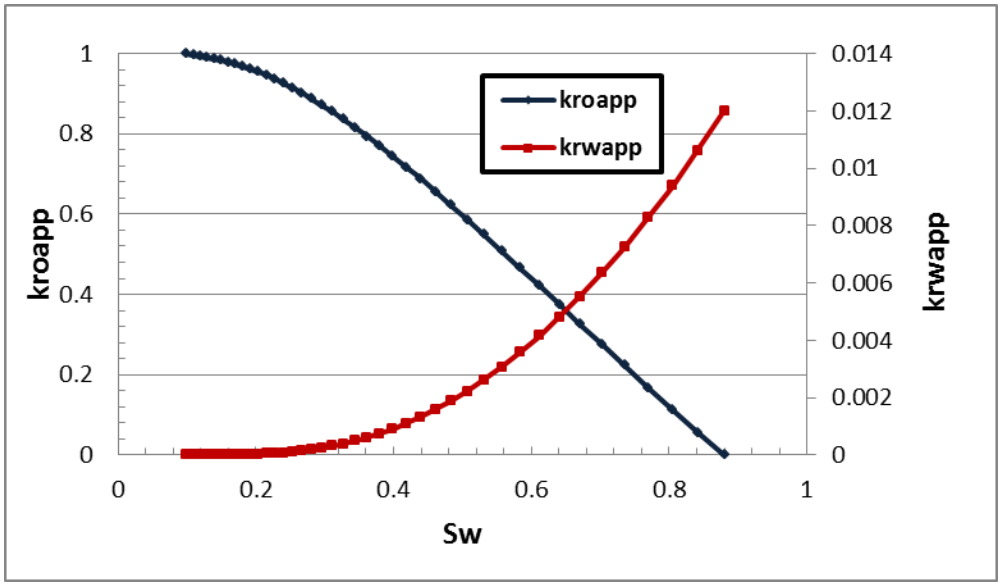

Figure 5.15: Apparent oil and water relative permeabilities for history matching of the 2D floods

krw^o	0.012
kro^o	1.0
S_{wi}	0.1
S_{orw}	0.12
Ew	3
Eo	1.2

Table 5.3: Intrinsic oil and water relative permeability parameters

5.1.2 Modeling and simulation of the polymer flood for 10,000 cp oil

Experimental data indicated that application of the polymer flood could give improved oil recovery rates over waterflood both in the secondary mode as well as the tertiary mode. In this section, the experimental data of the polymer flood is matched

using the commercially available multicomponent multiphase reservoir simulator CMG STARS.

Components

Polymer and water components were defined in the aqueous phase and the oil component was defined in the oleic phase. Table 5.4 gives the properties of different components.

Component	Phase	MW (gm/gmole)
Water	Aqueous	18
Polymer	Aqueous	22 million
Oil	Oleic	420

Table 5.4: Components defined for the polymer flood simulation

Grid structure

For the purpose of simulation a Cartesian grid structure was used. The sand pack was divided into 100 grids in the direction of fluid flow. Because the sand pack was homogenous, grid properties such as permeability, porosity and initial water saturation were uniform throughout. Figure 5.16 gives the grid properties defined at the start of the simulation.

Figure 5.16: Grid Structure used for simulations in CMG

Model for polymer properties

The laboratory experiments indicate that the polymer viscosity is a function of shear rate in the porous medium, polymer concentration, temperature, and the brine salinity. Since the brine salinity (20,000 ppm NaCl) and temperature (25°C) was kept constant throughout the experiment, shear rate and polymer concentration were the only factors governing the viscosity of the polymer solution.

To model the effect of shear rate the method outlined by Canella *et al.* (1988) is used. The first step was to determine the bulk polymer rheology. Figure 5.17 shows the shear rate dependence for a 4000 ppm Flopaam 3630S solution.

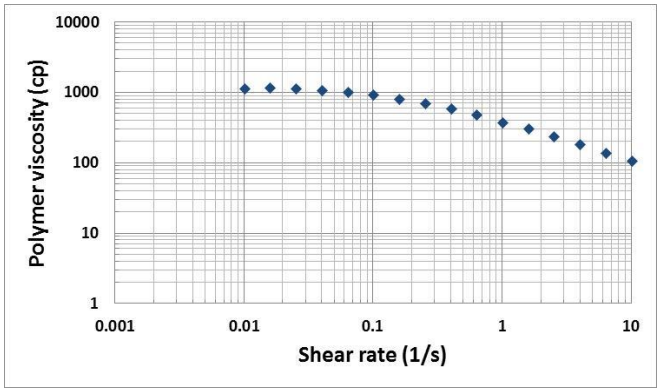

Figure 5.17: Bulk viscosity-shear rate dependence of the polymer solution

The viscosity data is then fitted with the Carreau viscosity model. The governing equation of this model is:

$$\frac{\mu-\mu_\infty}{\mu_o-\mu_\infty}=\left(1+\left(\frac{K}{\mu_o}\right)^{\left(\frac{2}{n-1}\right)}.\,\gamma^{2}\right)^{\left(\frac{n-1}{2}\right)} \qquad (5.16)$$

where K is the consistency index and n is the power law exponent.

For moderate to high shear rates the equation reduces to the power law equation

$$\mu = K\dot{\gamma}^{n-1} \quad . \qquad (5.17)$$

Model fitting gives the values of K and n as K = 20.77 cp $s^{0.4823}$ and n = 1.4823.

The next step is to calculate the equivalent shear rate and the apparent polymer viscosity in the porous media. For this purpose the polymer solution is injected in a sand pack at different flow rates and the pressure drop is recorded for every injection rate. Table 5.5 lists the sand pack properties.

Sand pack properties	
Permeability (Darcy)	32.0
Porosity (%)	43.7

Table 5.5: Properties of the sand pack used for evaluating the equivalent shear rate

The single phase Darcy's law is then used to calculate the apparent viscosity of polymer in the porous media, i.e.,

$$\mu_p = \frac{qL}{KA}\Delta P \, . \qquad (5.18)$$

The equivalent shear rate in the porous media is given by:

$$\dot{\gamma}_{app} = C\left(\frac{3n+1}{4n}\right)^{\left(\frac{n}{n-1}\right)} \frac{u}{\sqrt{K\phi}}, \qquad (5.19)$$

where n: power law exponent used from the bulk viscosity data

C: parameter depending on the type of the polymer

u: superficial velocity in the sand pack

K: Permeability of the sand pack

Φ: porosity of the sand pack.

The parameter 'C' is varied until good agreement is obtained between the curves of shear rate vs. viscosity of the bulk solution to that exhibited inside the porous medium. Figure 5.18 shows the result of such a curve fitting procedure.

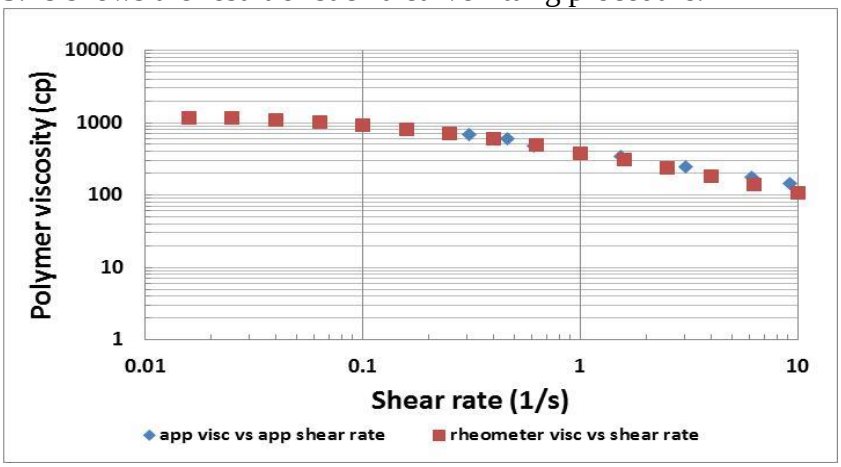

Figure 5.18: Apparent viscosity vs. shear rate compared with the values from bulk measurements

The experimental procedure described above is useful for determining the parameters of the necessary equations. CMG STARS defines the shear thinning model in the following manner.

$$\mu_{app} = \mu_{l,p} \quad \text{for } u < u_{lower}$$

$$\mu_{app} = \mu_{l,p} \left[\frac{u_l}{u_{lower}} \right]^{(n-1)} \quad \text{for } u_{lower} < u < u_{upper} \qquad (5.20)$$

$$\mu_{app} = \mu_{l,0} \quad \text{for } u > u_{upper}$$

where u: superficial velocity of the aqueous phase containing polymer

n: power law exponent

$\mu_{l,p}$: polymer viscosity at zero shear rate

$\mu_{l,0}$: fluid viscosity in the absence of polymer = water viscosity

u_{lower}: velocity of the aqueous phase where $\mu_{app} = \mu_{l,p}$.

Figure 5.19 shows how u_{lower} was determined. In order to convert the shear rates into velocities, equation 5.14 was used with the value of 'C' as 2 and 'n' as 1.483.

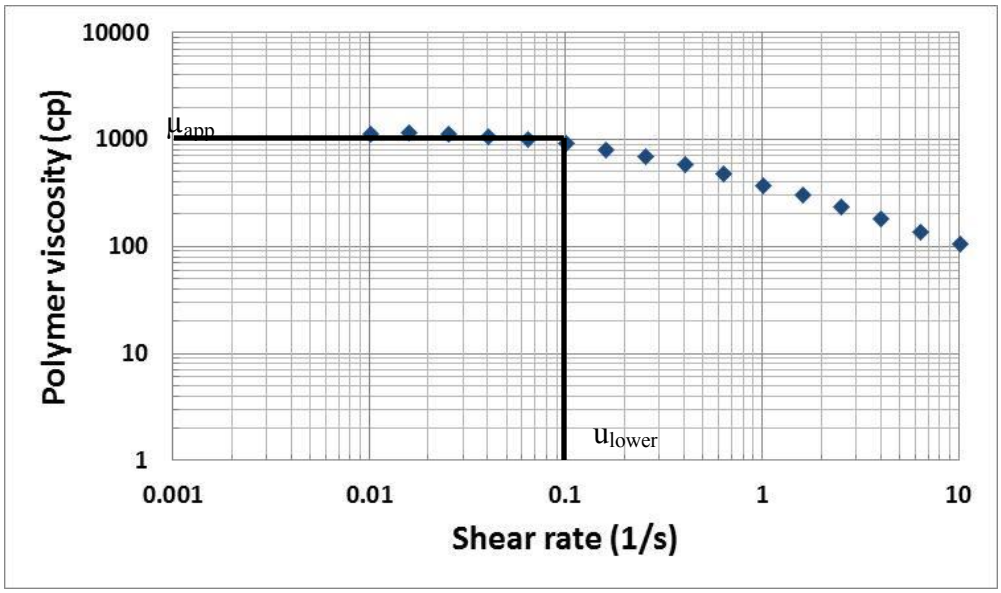

Figure 5.19: Determining u_{lower} and μ_{app}

The effect of polymer concentration on viscosity was modeled in CMG STARS using the viscosity mixing models. Laboratory experiments were conducted to determine the polymer viscosity at a shear rate of 0 s^{-1} at different concentrations.

A non-linear viscosity mixing rule was used to model the variation of viscosity with polymer mole (or mass) fraction in the aqueous phase. Equation 5.16 is the equation used by the simulator.

$$\ln(\mu_i) = f(x_a)\ln(\mu_a) + (1 - f(x_a))\ln(\mu_b) \qquad (5.21)$$

Where μ_i: viscosity of the polymer and water mixture

μ_a: viscosity of the highest concentration of polymer solution

μ_b: viscosity of aqueous phase without any polymer present

$f(x_a)$: non-linear function to account for non-linear mixing

Figure 5.20 depicts the procedure to determine the values of $f(x_a)$ from the lab data. It is to be noted that the values of $f(x_a)$ or x_a are to be determined either in terms of mole fraction or in terms of mass fraction as per the simulator.

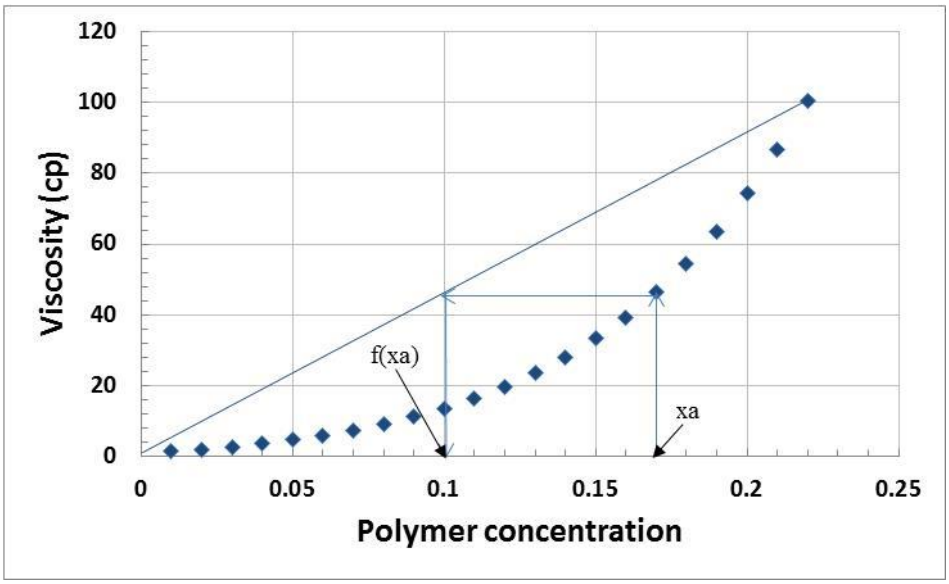

Figure 5.20: Procedure to determine the non-linear mixing function f(xa)

History matching of 1D polymer flood

The experimental data for history match was taken from Chapter 4. In the 1D system polymer was injected in the secondary as well as the tertiary mode. Injection of the polymer improved the sweep efficiency over the waterflood. Figure 5.21 shows the history match of the oil recovery and the pressure drop for the tertiary polymer flood. The simulated values show reasonable agreement with the experimental data. During the polymer flood, the simulated oil recovery showed an earlier response than the experimental values. Correspondingly the pressure response also peaked out earlier than what the simulation predicted. The total oil recovery predicted by the simulator shows a good agreement with that of the experiment. The simulated pressure drop was higher than

the experimental data values during the entire course of the polymer flood. Figure 5.22 shows the history match of the oil recovery and the pressure drop for the secondary polymer flood. Good agreement was obtained between the experimental and simulated values.

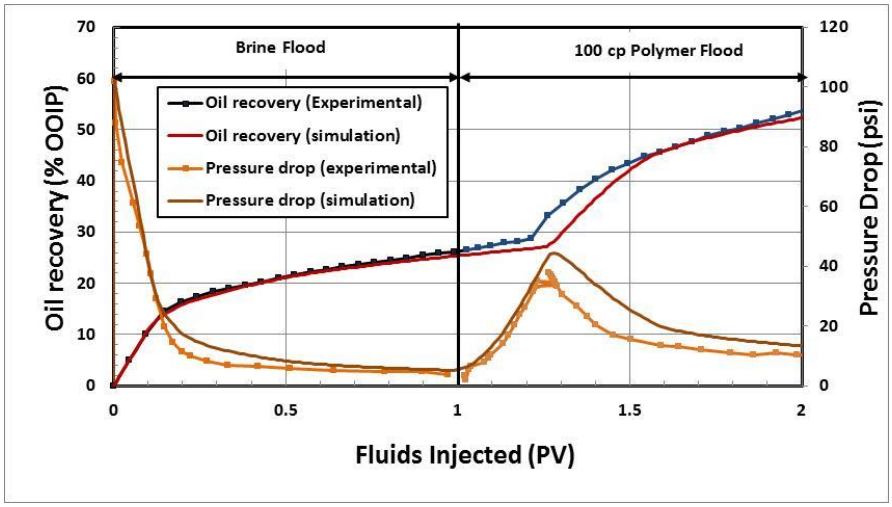

Figure 5.21: History match of the oil recovery and the pressure drop data (tertiary polymer flood)

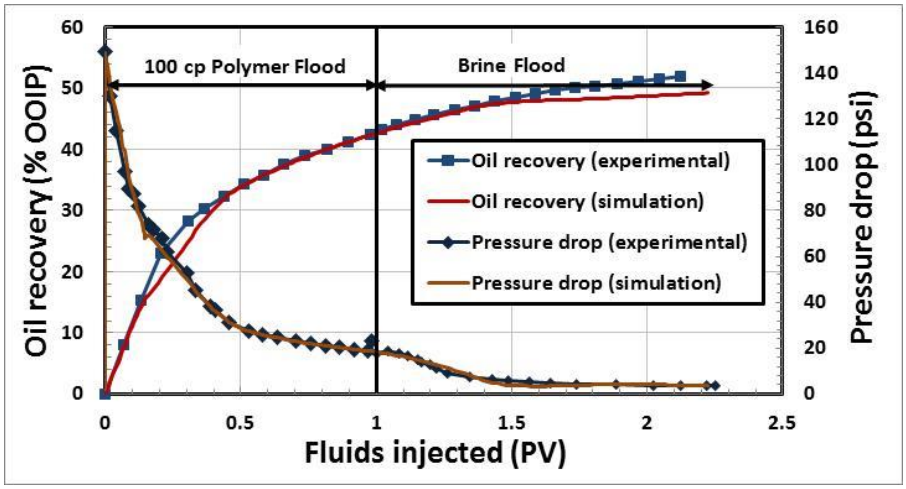

Figure 5.22: History match of the oil recovery and the pressure drop data (secondary polymer flood)

Figure 5.23 depicts the oil and water relative permeabilities used for matching the oil recovery and the pressure drop data. A different set of oil-water relative permeabilities was needed to match the experimental data during the polymer flood than during the waterflood. It should be noted here that although the fingering function model was not used for matching the waterflood, the relative permeabilities used are the apparent relative permeabilities due to the presence of the viscous fingering in the porous medium. Because the viscosity of the polymer is about 100 times higher than the water, the viscosity ratio of oil to water is reduced from 10,000 to 100. The relative permeabilities used to match the polymer flood seem to be intrinsic and not the apparent relative permeabilities.

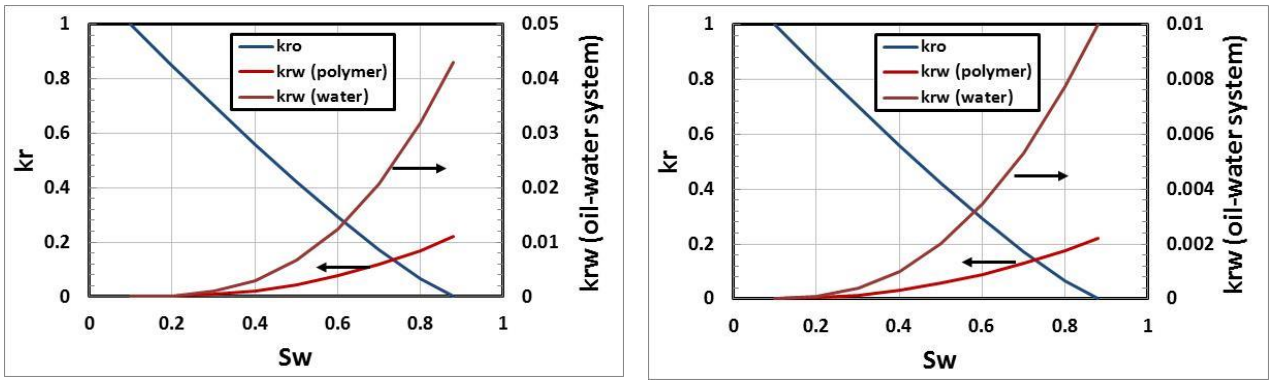

Figure 5.23: Oil and water relative permeabilities used for history matching the polymer flood data. (a) tertiary polymer flood (b) secondary polymer flood

History matching of 2D polymer flood

Polymer injection in the 2D cell was undertaken in the secondary mode. Higher oil recovery than waterflood was obtained as a result of the polymer injection. Figure 5.24 shows the history match of the secondary polymer flood. The predicted oil recovery by simulation was in close agreement with the experimental values. The pressure drop could not be exactly matched, although the simulated values were fairly close to the

experimental data. Very close to 0.8 PV of polymer injection some numerical instability arose in the simulations because of which the simulated data of the pressure drop show various spikes.

Figure 5.25 represents the relative permeability curves used for history matching the secondary polymer flood. End point water relative permeability was 0.2. End point oil relative permeability of 0.8 was used to history match the results as opposed to the value of 1.0 used for 1D simulation.

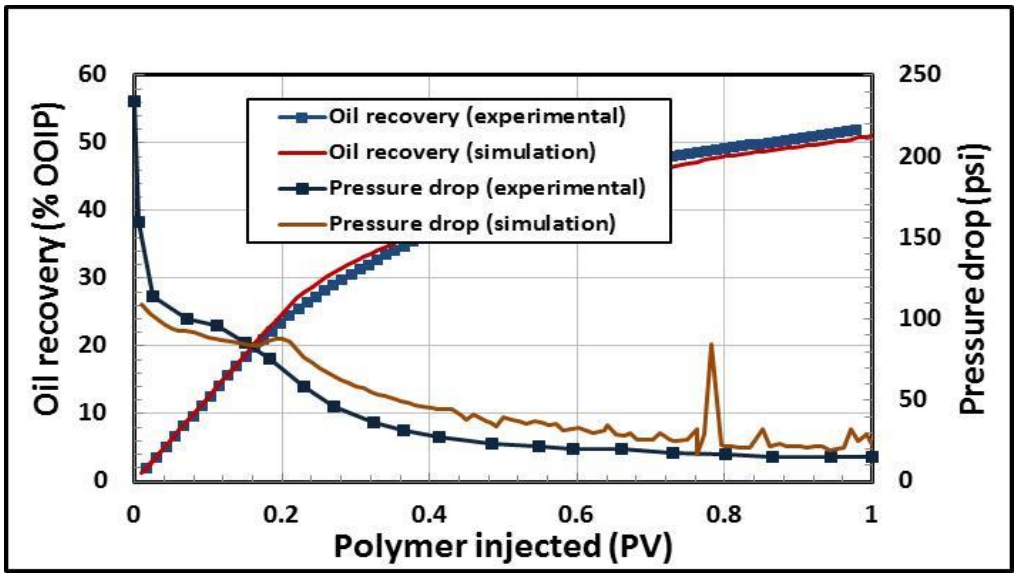

Figure 5.24: History match of the secondary polymer flood in a 2D cell

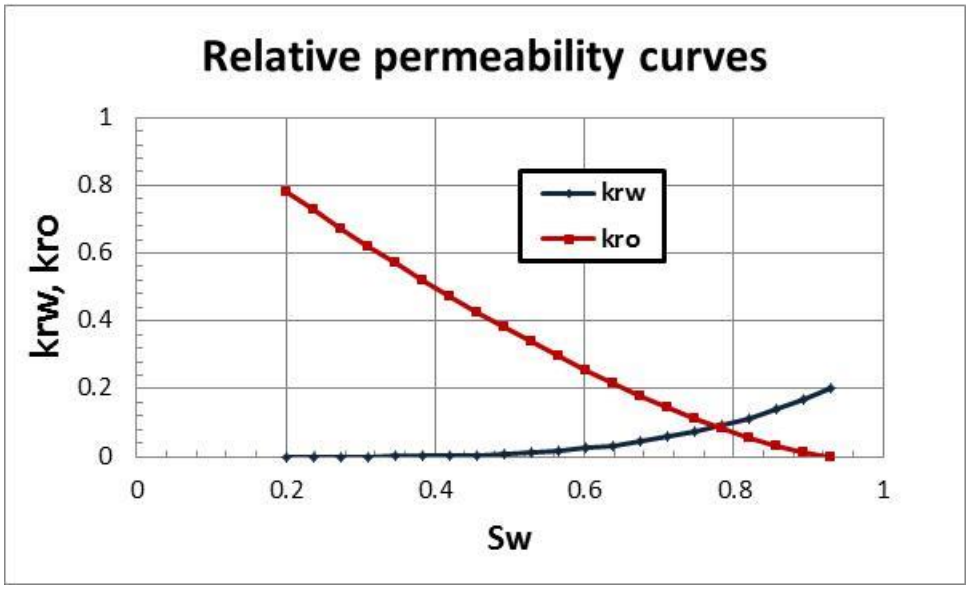

Figure 5.25: Relative permeability curves used for history matching the 2D polymer flood.

Summary of the modeling and simulation results

Table 5.6 lists summarize the oil-water relative permeabilities used to match the waterflood in both the 1D and 2D geometry. The parameters of the intrinsic relative permeabilities are listed along with the fingering function of the respective 1D or the 2D case. The difference in the fingering function used for the 1D and the 2D geometry indicates the difference in the average finger shape for different geometries.

Table 5.7 lists the oil-polymer relative permeability parameters used to history match the polymer floods. It is to be noted that the relative permeabilities used to simulate the 2D polymer flood are markedly different from those used to model the 1D polymer floods. The results indicate that there are some key mechanism which might be different in 1D and 2D geometry. Proper understanding and modeling of these mechanisms may help in improving the history matching results.

	1D waterflood	1D waterflood (before polymerflood)	1D waterflood (after polymerflood)	2D waterflood
Swi	0.1	0.1	0.1	0.2
Sorw	0.12	0.12	0.12	0.12
krw^o	0.012	0.043	0.01	0.012
kro^o	0.833	1.0	1.0	1.0
Ew	3	2.8	2.4	3
Eo	1.2	1.2	1.2	1.2
Fingering Function	$\lambda = 0.1 + 0.9 S_{wf}^{0.7}$	-	-	$\lambda = 0.1 + 0.9 S_{wf}^{2}$

Table 5.6: Summary of relative permeability parameters used for history matching the waterfloods

	1D polymerflood (Tertiary mode)	1D polymerflood (Secondary mode)	2D polymerflood (Secondary mode)
Swi	0.1	0.1	0.2
Sorw	0.12	0.12	0.07
krw^o	0.22	0.22	0.2
kro^o	1.0	1.0	0.8
Ew	2.4	2	3.5
Eo	1.2	1.2	1.4

Table 5.7: Summary of oil-polymer relative permeability parameters used for history matching the polymer floods.

The fingering function developed from the heuristic model presents a possible method to derive the apparent relative permeability curves using the same intrinsic oil-water relative permeability for the 1D and the 2D geometry.

We have not conducted the study to scale-up the waterflood and the polymer flood for the field scale but here we propose a possible method of doing so. For up-scaling the heavy oil waterflood, we can take the help of simulations. It was shown that fine grid simulations using the intrinsic oil-water relative permeability curves were able to reproduce viscous fingers inside the porous media. However it will be computationally expensive to conduct such simulations for a scale much bigger than the laboratory scale. For such scales, we propose to conduct coarse grid simulations by using the apparent relative permeability curves determined from the heuristic model. A good choice of the model size will be the size of a typical reservoir grid. The predictions of the average behavior (oil recovery and pressure drop) of the model from the coarse grid simulations can be benchmarked with those from the fine grid simulations. If the two are found to be very similar, we can go ahead and use the apparent relative permeability curves for conducting pilot scale and field scale simulations.

5.1.3 Modeling and simulation of the Alkali Surfactant (AS) flood for 10,000 cp oil

The present section describes the modeling and simulation of the AS flood for the heavy oil. The AS solution generated low viscosity Oil in Water (O/W) emulsion in the system at a salinity of 0 ppm brine. The in situ generation of emulsion in the system led to an improvement in oil recovery. The filtration model developed by Soo and Radke (1984) for describing the flow of stable, dilute emulsions in the porous media was used in the simulations. Following are the key features of the model.

1. The dispersed oil droplets can be captured in the pore constrictions and the pore walls by both straining and interception. This restricts the mobility of the dispersion (emulsion).
2. Once captured there is a negligible particle re-entrainments.

The model development and the history matching results are given next. The simulations were conducted using the compositional reservoir simulator CMG STARS. The CMG STARS model of the AS flooding captures the following mechanisms:

1. Lowering of IFT by the action of alkali and surfactant
2. Generation of O/W emulsions in situ by a reaction between water, alkali, surfactant and heavy oil.
3. Flow of O/W emulsion having oil entrained in the flowing aqueous phase.
4. Trapping of the emulsion droplets caused by the clogging on the pore constrictions and pore walls
5. The reduction of the local water phase mobility when the emulsified oil droplets get trapped. Trapping also diverts the injected water to un-swept regions.

The mechanism modeled here is called the entrapment mechanism and is responsible for increase in pressure drop and improvement in oil recovery.

Components

A total of 6 components were used in the simulations. 4 components in the aqueous phase: water, surfactant, alkali and O/W emulsion. One component 'Heavy Oil' was defined in the oil phase and a component 'Trapped Oil' was defined in the solid phase. Table 5.8 lists the properties of the individual components.

Name	Phase	MW (g/gmole)	Viscosity (cp)	Mole density (gmole/m^3)
Water	Water	18	1	55555.6
Alkali	Water	106	1	55555.6
Surfactant	Water	1520	1	55555.6
OW Em	Water	184	5500 @ 0.6 s^{-1}	5434.78
Heavy Oil	Oil	350	10,000	2857.14
Trapped Oil	Solid	350	-	2857.14

Table 5.8: Properties of the different components

The O/W emulsion was found to exhibit the non-Newtonian behavior. At the shear rate of 0.6 s^{-1} (estimated by the apparent shear rate test on HPAM polymer) the viscosity was close to 5500 cp. Figure 5.26 shows the rheology of the O/W emulsion.

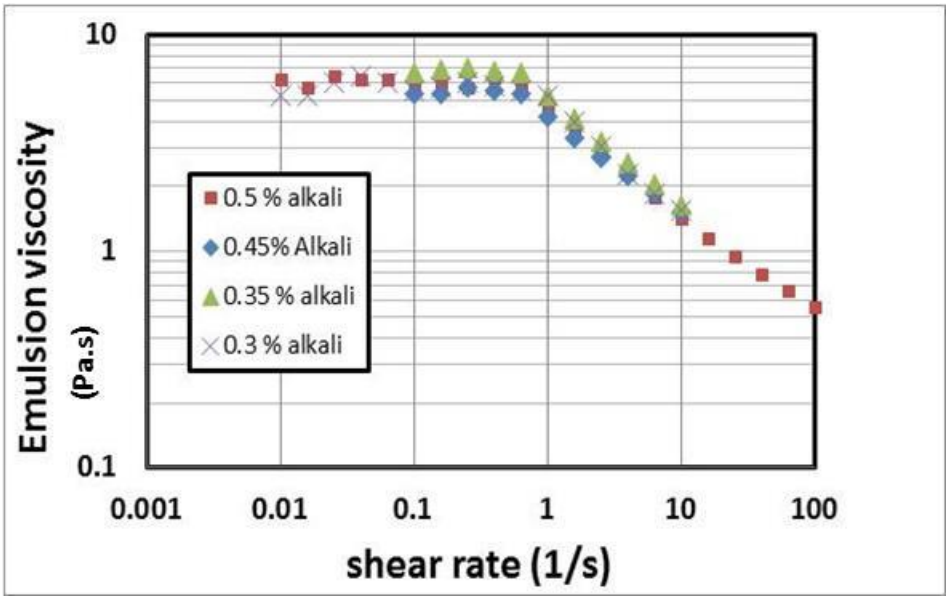

Figure 5.26: Non Newtonian viscosity behavior of O/W emulsion

Next, we discuss the different mechanisms modeled for conducting the simulations.

IFT lowering by the action of alkali and surfactant

The lowering of IFT by the action of alkali and surfactant is important for the generation and sustenance of emulsions in the porous media. For this particular case, the chemical screening studies were conducted at a fixed surfactant concentration of 0.1 wt % and NaCl brine salinity of 0 ppm. The WOR for fixed at 1:1. On increasing the alkali concentration from 0 wt% to 0.5 wt%, significant solubilization of oil could be observed as shown in figure 5.27.

Figure 5.27: Emulsion screening tests with alkali and surfactant at WOR 1:1 and 0 ppm brine salinity

The IFT at different alkali concentrations was measured. Figure 5.28 shows the result. The IFT value at 0 wt% alkali is higher as also evident by the round curvature of the oil water interface. Addition of alkali brings down the IFT to about 0.03 dynes/cm. Notice that the IFT values could not be measured for higher than 0.2 wt % alkali as in these samples, the entire water and oil phase was converted to emulsion.

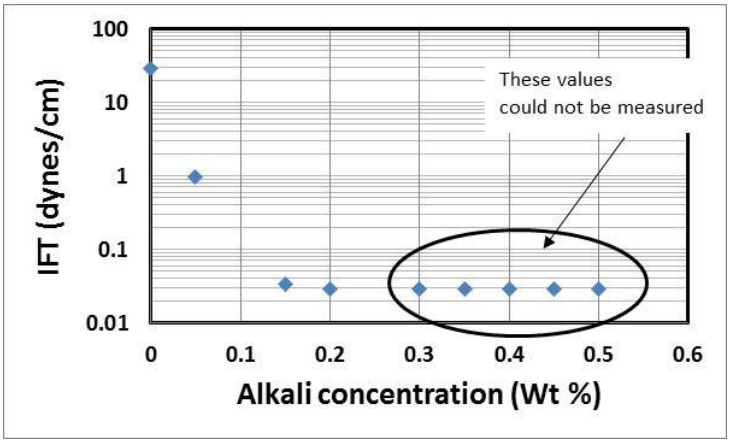

Figure 5.28: Lowering of IFT with alkali concentration

The above data was used directly in the model.

Generation of O/W emulsion in situ

The O/W emulsion was generated in situ by a reaction between water, alkali, surfactant and heavy oil. The reaction coefficients were decided based on the quality of the emulsion desired and the fact that the total mass on the reactant side should be equal to the total mass on the product side.

The reaction can be presented as:

$$W\ water + A\ alkali + S\ surf. + HvyOil \xrightarrow{k1} E\ O\_WEm \ldots\ldots(1)$$

where the coefficients W, A, S and E represent the stoichiometric coefficients of the reaction.

From the emulsion tests, for high alkali concentration it was seen that all the oil and water got converted into the emulsion component. Because we started with 5 ml each of oil and water in the test tube, the final emulsion quality is:

$$q = \frac{Vo}{Vem} = \frac{5}{10} = 50\% \qquad (5.22)$$

Hence 5 ml of oil gets converted to 10 ml of emulsion.

To determine the stoichiometric coefficients the volumes were converted to moles using the mole densities.

Moles of oil reacted = $5*2857.14*10^{-6} = 0.0142857$

Moles of em formed = $10*5434.78*10^{-6} = 0.0543478$

According to the reaction stoichiometry, 1 mole of heavy oil gives E moles of emulsion

Hence,

$\frac{1}{E} = \frac{0.0142857}{0.0543478}$ giving **E = 3.8**

On the similar lines we can say that the 5 ml of water are converted to 10 ml of emulsion

Moles of water reacted = $5*55555.6*10^{-6} = 0.277778$

Stoichiometry states that W moles of water are converted to E moles of emulsion,

$\frac{W}{E} = \frac{0.277778}{0.0543478}$

W = 19.42.

Also from the emulsion tests, it was seen that for alkali concentration below 0.35 wt%, the lower phase does become darker but the oil emulsification was not very significant. In other words, the 50% emulsion existed for alkali concentration higher than 0.35 wt% only. Thus the particular concentration is a limiting concentration for alkali. This fact was used to decide the stoichiometric coefficient of alkali component as presented below.

Number of moles of alkali in a 0.35 wt% of 5 ml (= ~5gm) solution

$= \frac{0.35}{100} \times 5 \times \frac{1}{106} = 1.65*10^{-4}$ moles

Water moles as calculated earlier = 0.277778

Because 0.35 wt% is a limiting alkali concentration, it can be safely assumed that the moles of alkali are fully consumed by the reaction.

According to the stoichiometry W moles of water react with A moles of alkali. Hence,

$$\frac{W}{A} = \frac{0.277778}{1.65\times10^{-4}}$$

A = 0.0115

After determining the stoichiometric coefficients of water, alkali, heavy oil and emulsion, a weight balance on the reactants and products was conducted to calculate the coefficient for surfactant. The results are summarized in table 5.9.

Component	Stoichiometric coefficient
Water	19.42
Alkali	0.0115
Surfactant	0.0001
Heavy Oil	1
O_W Emulsion	3.8

Table 5.9: Stoichiometric coefficients of different components

Capture of emulsion drops by the porous media

The capture of the emulsion droplets in the porous media is represented by the following reactions:

$$1.902\ O\_WEm \xrightarrow{k2} trapped\ oil \quad \text{..... (2)}$$

The stoichiometric coefficients were decided so that the total mass on the left hand side remains equal to the total mass on the right hand side.

In addition a reverse reaction was also defined as:

$$1.902\ O\_WEm + trapped\ oil \xrightarrow{k3} 3.804\ O\_WEm \quad \text{.....(3)}$$

The reversible reaction was defined because physically, all the O/W emulsion cannot be converted into the trapped oil. The reversible reaction serves to put an upper limit on the amount of trapped oil that can be generated. It is to be noted that the 3rd reaction is not a

re-entrainment reaction. The trapped oil occurs in the solid phase and does not contribute to the flow of the fluids anymore.

Reduction in the local water permeability

Water relative permeability was reduced in the grid cells during the simulation where the trapped oil was generated. A non-equilibrium blockage factor was defined in the CMG STARS to represent the blockage. The water relative permeability was reduced on the basis of the following equation:

$$kw_{eff} = \frac{k_{abs} krw}{RF} \qquad (5.23)$$

where kweff : Effective permeability of the water phase

kabs: Absolute permeability of the porous media

krw: Relative permeability of water phase

RF: Permeability reduction factor

$$RF = 1 + BF \times Cs \qquad (5.24)$$

where BF: Blockage factor (input in the simulation)

Cs: Concentration of the trapped oil on the solid phase.

Surfactant and alkali adsorption

The adsorption of alkali and surfactant was defined by Langmuir adsorption isotherms in the simulator. CMG STARS defines the adsorption isotherm by:

$$\mathrm{ad} = \frac{(\mathrm{tad1} + \mathrm{tad2} * \mathrm{xnacl}) * \mathrm{ca}}{(1 + \mathrm{tad3} * \mathrm{ca})} \qquad (5.25)$$

where tad1: First coefficient in the Langmuir Isotherm expression

tad2: Second coefficient in the Langmuir Isotherm expression associated with salinity effects

tad 3: Third parameter in the Langmuir expression

ca: Mole fraction of a species

Table 5.10 gives the parameters that were used in the simulations for alkali and surfactant chemicals. The maximum possible alkali adsorption was specified at 0.02 gmole/m^3 and that of surfactant was 0.28 gmole/m^3.

Component	tad1 (gmole/m^3)	tad 2 (gmole/m^3)	tad 3	Max ads. (gmole/m^3)
Alkali	20	0	1000	0.02
Surfactant	270	0	1000	0.28

Table 5.10: Adsorption parameters for alkali and surfactants

History match of the AS flood

The present section describes the results of the history match of the AS flood. The reaction rate constants and the blockage factor were used as the history match parameters. The relative permeabilities were specified for the high and low IFT (correspondingly high and low capillary numbers).

From the simulation, the total oil produced was calculated by adding the quantity of the free oil and the oil produced as the O/W emulsion (50% oil volume).

Net Oil recovery = Free Oil recovery + 0.50 * (O/W emulsion recovery)

Figure 5.29 and figure 5.30 show the history match of the oil recovery and the pressure drop data. Good matches could not be obtained for either of these. However, the simulation could match the oil recovery fairly close. The final oil recovery predicted by the simulation was close to 23% OOIP as opposed to 20% obtained from the experiments. Figure 5.22 shows the simulation match for the pressure drop. The pressure drop peak predicted by the simulation was 12 psi, fairly close to the peak of 10 psi from the experiments. There is a large disagreement between the simulated and the

experimental pressure drops after 0.8 PV. The final pressure drop from the simulation is about 4 psi and the experimental pressure drop was almost 0 psi.

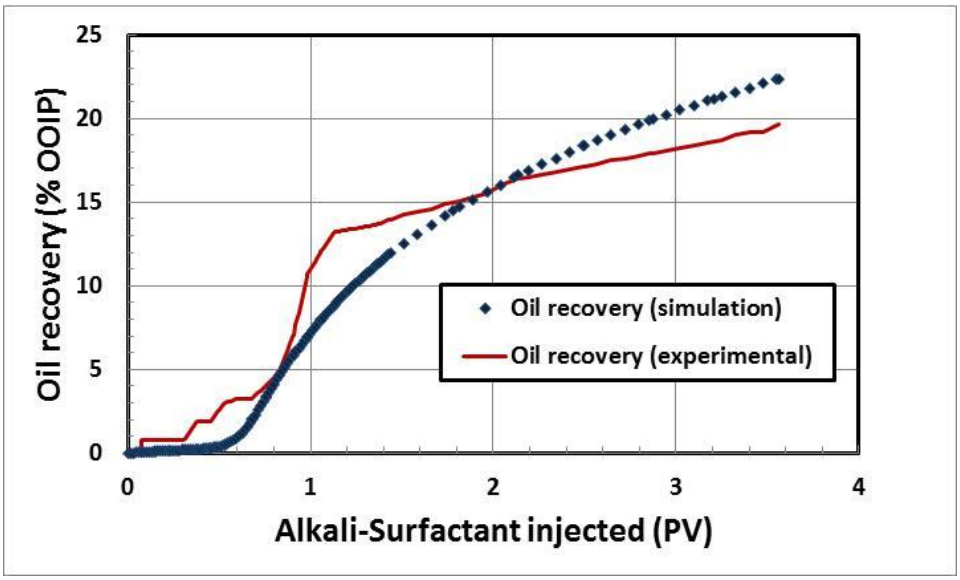

Figure 5.29: History match of the oil recovery for AS flood of 10,000 cp oil

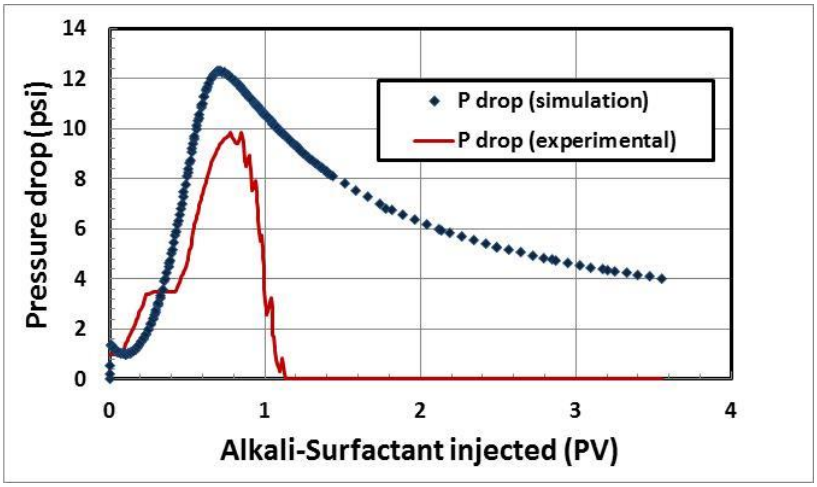

Figure 5.30: History match of the pressure drop for AS flood of 10,000 cp oil

Figure 5.31 gives the two sets of relative permeabilities used to match the AS flood. To represent the effect of IFT reduction on two-phase flow, the relative permeability was interpolated as a function of capillary number. The low capillary number corresponding to waterflood was set as 6.48×10^{-6} and the high capillary number was set as 2.7×10^{-1}. It can be seen that both oil and water relative increased during AS flooding as a result of IFT lowering.

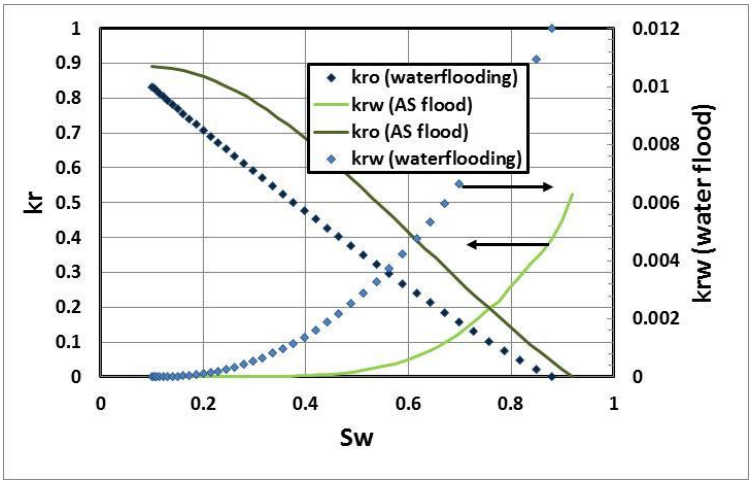

Figure 5.31: Relative permeabilities used to history match the AS flood

The water phase relative permeability was locally reduced in the grid blocks in which the emulsified oil drops were trapped by including a water phase blockage factor. The reaction rates, relative permeabililties and the blockage factor were the tuning parameters during the history match process. Table 5.11 lists the reaction rates and the blockage factor for the present history matching.

The tuning parameters are not unique in this simulation. There can be a number of other combinations of the tuning parameters which will produce the same simulation results.

k1 (emulsion generation reaction)	0.003
k2 (formation of trapped oil)	0.007
k3 (reversible reaction of rxn. 2)	0.2
Blockage	610

Table 5.11: Tuning parameters for history matching the AS flood

5.2 ASP FLOOD SIMULATION OF 330 CP OIL (OIL B)

The present section describes the modeling and simulation of ASP process for the lower viscosity 330 cp oil (Oil B). UTCHEM simulator developed at the University of Texas at Austin was used for the simulations. UTCHEM is a three-dimensional, multi-component, multi-phase, and compositional model for chemical flooding processes (Pope, Delshad and Sepehrnoori, 1996). The simulator accounts for the complex phase behavior of oil, water and surfactant mixture. It is capable of modeling the flow of three liquid phases namely oil, water and microemulsion. The generation of the microemulsion phase is modeled by reaction between the crude oil and the chemical species present in the water such as alkali and surfactant. Phase behavior signifying the effect of salinity on the microemulsion phase is modeled by using Hand's rule (Pope and Nelson, 1978). In addition, it also takes into account the change of oil and water relative permeabilities with the reduction in interfacial tension (IFT). The simulator has the capability of handling the dependence of polymer viscosity on the brine salinity, concentration, and shear rate. The adsorptions of polymer and surfactant are also included.

The UTCHEM model of ASP process captures the following aspects of the process:

1. Generation of soap based on acid number and water-to-oil ratio
2. Effect of soap on optimal salinity and solubilization ratio at the optimal salinity

3. Hydrogen ion concentration (pH)
4. Alkali consumption
5. Reduction of synthetic surfactant adsorption as a function of pH
6. Ion exchange on clay

The mass balance equations are solved for the following (simplified) ASP species:

a) Water
b) Oil
c) Surfactant
d) Polymer
e) Total anions (in the units of equivalents of chloride)
f) Total divalent cations (in the units of equivalents of calcium)
g) Sodium
h) Hydrogen
i) Alkali (carbonate)
j) Soap

5.2.1 UTCHEM model for ASP process

In situ soap generation

In situ soap generation is based on an input total acid number (TAN) in the unit of mg KOH/g oil for the crude oil. It is assumed that acid is either fully or partially converted to soap using an acid conversion factor (K_s) only when there is co-presence of alkali and oil. The generated soap in mole/L water is computed using

$$C_{soap} = \frac{K_s TAN S_2 \rho_2}{S_1 (MW_{KOH})} \tag{5.26}$$

where S2,ρ2, S1 and MW_{KOH} are oil saturation, oil density, water saturation and molecular weight of KOH respectively.

Phase behavior modeling

Oil, brine and surfactant phase behavior mechanisms (Pope and Nelson, 1978; Satoh, 1984; Camilleri *et. al.* 1987) are modeled by using Hand's rule (Hand, 1939). The surfactant mixture consists of the added surfactant (TDA 30EO in this study) and the in situ generated soap. The optimal salinity of the mixture of surfactant and soap is given by a non-linear mixing rule (Salager *et. al.*, 1979; Bhuyan, 1989), i.e.

$$\ln (S_M^*) = X_{Soap}.\ln(S^*_{Soap}) + X_{Surfactant}.\ln(S^*_{Surfactant}) \quad (5.27)$$

where S_M^*, S^*_{Soap},$S^*_{Surfactant}$ are the optimal salinities of the mixture, soap and surfactant, respectively. Soap and surfactant mole fractions are X_{Soap} and $X_{Surfactant}$. The optimal salinity of the in situ generated soap is lower than that of the surfactant (Nelson *et. al.* 1984) and thus as the ratio of soap to surfactant increases, the optimal salinity decreases and approaches that of the soap.

The phase behavior data suggests that the optimal solubilization ratio follows a linear mixing rule as follows (Mohammadi *et.al.*, 2009):

$$\sigma_M^* = X_{soap}.\ \sigma_{soap}^* + Xs_{urfactant}\ .\sigma_{surfactant}^* \qquad (5.28)$$

where σ_M^*, σ_{soap}^* and $\sigma_{surfactant}^*$ are the optimum solubilization ratio of the mixture, soap and surfactant, respectively.

Alkali consumption

Alkali consumption due to soap reactions, ion exchange, and aqueous reactions are lumped as an adsorption term using a Langmuir isotherm.

$$\hat{C}_{alk} = \min\left[\tilde{C}_{alk}, \frac{a_{alk}(\tilde{C}_{alk} - \hat{C}_{alk})}{1 + b_{alk}(\tilde{C}_{alk} - \hat{C}_{alk})}\right] \qquad (5.29)$$

where a_{alk} and b_{alk} are alkaline adsorption parameters, $\hat{C}_{alk}$ is the adsorbed alkaline concentration and $\tilde{C}_{alk}$ is the total concentration. The adsorption of the surfactant is reduced by a constant input variable if the alkali concentration is above some value.

Surfactant adsorption

The effect of alkali (high pH) on the injected surfactant adsorption is given by

$$\hat{C}_3 = \frac{a_3 k_{pH} C_3}{1 + b_3 C_3} \tag{5.30}$$

where $\hat{C}_3$ is the adsorbed surfactant concentration and C_3 is the surfactant concentration in the aqueous phase. k_{pH} is the constant adsorption reduction factor.

Polymer viscosity model

UTCHEM has the capability of modeling the effect of effective salinity, polymer concentration and shear rate on polymer viscosity. The specific models available in UTCHEM for this function are presented in the following section.

The viscosity of a polymer solution is dependent on both polymer concentration and salinity. UTCHEM uses a modified Flory-Huggins equation, which in addition accounts for variation in salinity as presented in Eq. 5.26:

$$\mu_p = \mu_w[1 + (A_{p1} C_{41} + A_{p2} C_{41}^{\,2} + A_{p3} C_{41}^{\,3}) C_{sep}^{\,S_p}] \tag{5.31}$$

where Ap1 , Ap2 , and Ap3 are parameters for calculating polymer viscosity at zero shear rate as a function of both polymer and electrolyte concentrations. C_{sep} is the effective salinity for polymer. It takes into account both the anion and divalent ion concentrations, i.e.,

$$C_{sep} = \frac{C_{51} + (\beta_p - 1) C_{61}}{C_{11}} \tag{5.32}$$

where C51 is the total anion concentration in water, C61 is the total divalent ion concentration in water and C11 is the total water concentration in the aqueous phase in volume fraction. β_p is an input parameter. S_p is the slope of viscosity versus effective salinity on a log-log plot.

The overall behavior of a polymer solution in a wide range of shear-rates may be modeled by the Meter Eq. 5.27

$$\mu_{app} = \mu_w + \frac{\mu_p^{\,o} - \mu_w}{1 + \left(\frac{\dot{\gamma}_{eff}}{\dot{\gamma}_{1/2}} \right)^{P_\alpha - 1}} \qquad (5.33)$$

where $\dot{\gamma}_{1/2}$ is the shear rate at which the viscosity is the average of $\mu_p^{\,0}$ and μ_w. P_α is an empirical coefficient. The effective shear rate in the porous media $\dot{\gamma}_{eff}$ is calculated using

$$\gamma_{eff} = C\left[\frac{3n+1}{4n}\right]^{n/(n-1)}\left[\frac{u_w}{\sqrt{kk_{rw}S_w\phi}}\right] \qquad (5.34)$$

where $\mu_p^{\,0}$ is the shear thinning plateau viscosity computed as a function of salinity and concentration using equation 5.26.

5.2.2 UTCHEM model matches

UTCHEM phase behavior model match

Chapter 4 gives the experimental data used to model the ASP process on the oil in question. The phase behavior data presented in Figure 4.36 was modeled with the UTCHEM phase behavior parameters. This was done before conducting the flow simulation. Figure 5.32 shows such a match. The oil and water solubilization ratios were calculated by measuring the volumes of oil and water solubilized in the microemulsion phase (Vo and Vw) and normalizing them to the total surfactant volume (Vs) present. All

surfactant was assumed to partition into the microemulsion phase. Two solubilization ratios (Vw/Vs and Vo/Vs) were measured and matched using UTCHEM parameters. The region where both oil and water solubilization curves exists represent the Type III region and the point of intersection gives the opimal salinity with optimal solubilization ratio.

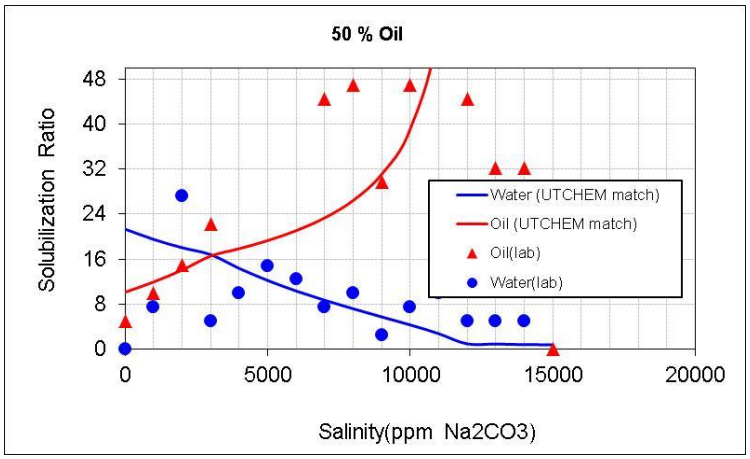

Figure 5.32: UTCHEM match of the experimental phase behavior

From the match of the phase behavior, salinity of 3,000 ppm alkali concentration is the optimal salinity for the system with the optimum solubilization ratio of 16.

Match of the polymer viscosity model

The experimental data of the polymer viscosity was matched with the UTCHEM models. The effective salinity was calculated by adding the equivalents of the alkali (Na_2CO_3) to the brine salinity.

Figure 5.33 shows the determination of the parameter Sp obtained by matching the polymer viscosity at different salinities to the model. Figure 5.34 shows the match of the polymer viscosity with the polymer concentration. Based on this match the UTCHEM parameters were estimated as:

Ap1	14.6683
Ap2	0
Ap3	3655.01

Table 5.12: Parameters for polymer viscosity match

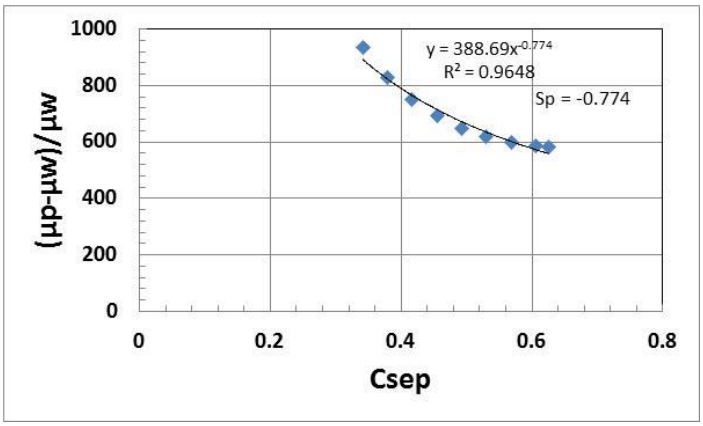

Figure 5.33: Determination of the parameter Sp

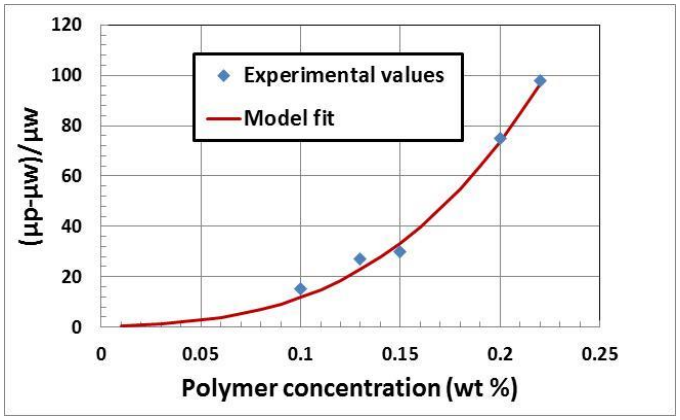

Figure 5.34: Match of the experimental polymer viscosity vs. concentration values with UTCHEM model

Match of the experimental oil recovery and pressure drop data

The next step was to match the oil recovery and the pressure drop data. Experimental data was taken from section 4.2.2. The results of the history matching of

the ‘Flood 3’are shown in this section. Figure 5.35 shows the history match of the oil recovery and the oil cut data. The simulated oil recovery during the waterflood displayed a good agreement with the experimental data. However, during the ASP and the polymer slug injection, the simulated oil recovery displayed a steeper increase than the experimental values. The overall oil recovery was predicted to be about 95% OOIP, which is in good agreement with the experiment.

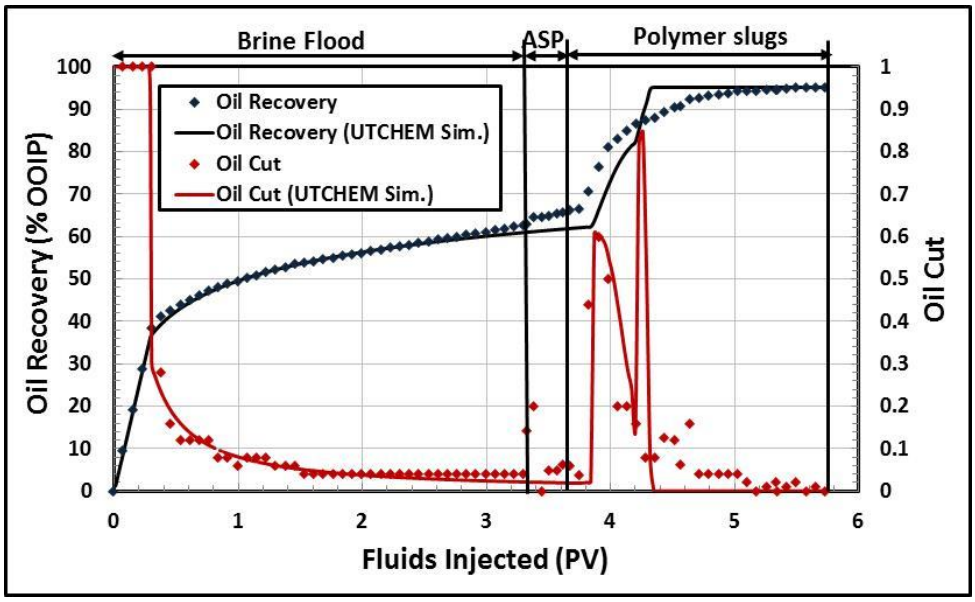

Figure 5.35: Match of the experimental oil recovery and the oil cut data

The match of the pressure drop is shown in figure 5.36. The pressure drop showed a good agreement with the experimental data during the waterflood as well during ASP and polymer slug injections. In the final stages of the experiment (after 4.2 PV), due to the device malfunction the pressure drop data could not be recorded. Simulation shows a steady decline in the pressure drop. The oil saturation inside the porous medium had been reduced to ultra-low value and the injection was then switched to lower viscosity tapered polymer slugs.

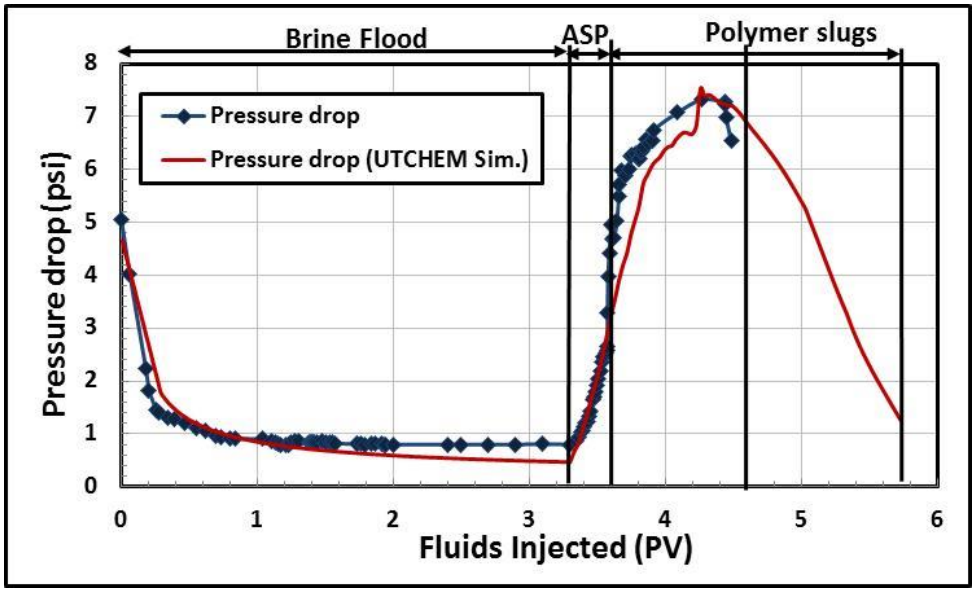

Figure 5.36: Match of the experimental pressure drop data

CHAPTER 6: CONCLUSIONS AND RECOMMENDATIONS

This study is aimed at improving the recovery of heavy oil without injecting any heat into the reservoir. The experiments were conducted in both 1D and 2D geometries. 2D geometry is a better representation of the system where viscous fingering has a dominant effect. Two viscous oils were used: oil A with a viscosity of 10,000 cp and oil B with a viscosity of 330 cp. The experiments were conducted in a sand pack at a temperature of 25^{o}C and 20,000 ppm NaCl brine salinity without any divalent ions present.

6.1 CONCLUSIONS

Based on the experimental and numerical studies, following conclusions were drawn:

1. For a fixed concentration of alkali and surfactant chemicals, it was possible to generate emulsions of the heavy oil (Oil A) and water. In general high viscosity W/O were generated at high brine salinity and low WOR. At conditions of low salinity and high WOR, low viscosity O/W emulsions were generated.
2. In this study, displacements were conducted at a constant velocity of approximately 1 ft./d. Pressure drops at the start of the injection processes (waterflood, polymer flood and AS flood) were high (e.g.105 psi for a 3ft sandpack). The resulting pressure gradient at early times is close to 35 psi/ft. However, the typical pressure gradients in the field are of the order of 1 psi/ft. To reduce the pressure gradients, the injection should be conducted at slower rates than used in the experiments in this study. Another approach one can adopt is to inject the fluids at a constant pressure gradient of 1 psi/ft.
3. Sand pack floods conducted with alkali-surfactant solutions on the Oil A at different conditions of salinity showed improvements in cumulative oil recovery and oil

recovery rates over waterflooding. At low brine salinity, low viscosity O/W emulsions were generated in situ. In the 1D system, the oil recovery improved from 40 % OOIP after the waterflood to 55% after 1PV injection of AS solution. However in the 2D system, the change was more gradual. Oil recovery improved from 35% after the waterflood to 40% after 1PV of AS flood. The difference in the oil recovery rates observed in the 1D and 2D system justifies the experimental studies in different geometries.

4. At high brine salinities, high viscosity W/O emulsions were generated in situ. These emulsions tend to block the water flowing in the water channels and lower the water phase mobility. In the 1D system, oil recovery increased from 40% after the waterflood to 70% after 1PV of AS injection, an improvement of 30% OOIP. The improvement in the oil recovery was also accompanied by an increase in the pressure drop across the porous medium. The generation and flow of the viscous emulsions together with the improved sweep of the oil were responsible for higher pressure drops. The oil recovery was found to be geometry dependent giving an increase of 20% OOIP over waterflood in a 2D system.
5. Injecting the AS solution at high salinity after the waterflood gave a marked improvement in oil recovery albeit at high pressure drops. However, the injection of the same AS solution after a polymer flood did not have any benefit. Ultra high viscosity emulsions were produced in the system. The oil recovery took a very long time to respond and the improvement was 10 % after 1 PV of AS injection. The pressure drop rose much higher than the earlier case.
6. Application of a 100 cp viscosity polymer solution could improve the sweep efficiency of the heavy oil (Oil A) over waterflood in 1D and 2D geometry. In the 1D geometry both secondary and tertiary polymer injection performed equally well with

a total of 50% OOIP recovery after 1PV of water injection and 1PV of polymer injection. The presence of the mobile oil left after the waterflood was the key reason for the success of the tertiary polymer flood. Oil recovery in a 2D geometry was found to be very similar, about 50 % after 1 PV of polymer injection.

7. For the 330 cp oil (Oil B) a combination of alkali and a hydrophilic non-ionic surfactant could produce microemulsions in the system. The microemulsions had a high solubilization ratio indicating ultra-low IFTs. Sand pack floods conducted using alkali-surfactant along with polymer could recover almost all the oil from the system. The pressure drop in the system was quite reasonable (~ 2 psi/ft) as the oil recovery improved from 60% after the waterflood to 95% after 0.5 PV of ASP slug and following it subsequently with tapered polymer slugs.
8. Unlike the conventional light oils, different set of relative permeabilities were needed to match the oil recovery and pressure drop from the experiments on waterflood and polymer flood. Water end point relative permeability was found to be almost an order of magnitude lower for waterflood than for the polymer flood. Possible explanation is the flow of water in the thin viscous fingers rather than through the entire cross section.
9. A linear viscous fingering model was developed to match the unstable waterfloods in a 1D and 2D system. The model calculates a fingering function which can be used along with the Corey relative permeabilities to calculate the effective relative permeabilities. A different fingering function was needed to match the 1D and the 2D waterfloods. The effective oil relative permeability was found to be higher for the 2D system.

10. UTCHEM reservoir simulator was able to simulate the ASP process for Oil B (330 cp) oil. The reason is that for Oil B, the displacement is stable and the adverse effect of viscous fingering is not present.
11. For modeling the AS flood for the heavy oil, the use of the filtration theory developed by Soo and Radke (1984) was found to model the improvement in oil recovery due to the generation and flow of O/W emulsions in the porous media.

6.2 RECOMMENDATIONS

Based on the present study, further research in the following area is recommended:

1. Conduct experiments in lower permeability field cores and at the reservoir conditions of the net overburden pressure to obtain more representative data.
2. Explore the possibility of conducting the laboratory experiments at a constant pressure gradient. It is recommended that a pressure gradient of 1 psi/ft be chosen for such experiments. This will be more representative of the actual field operations.
3. Conduct the waterflood experiments for a wider range of permeability and porosity to make the modeling more robust. It is also recommended that the heavy oil-water relative permeability curves be determined from the steady state experiments to minimize the effect of viscous fingering on relative permeability.
4. Conduct these experiments in an oil-wet sandpack. All the experiments conducted in this study are for water-wet reservoirs. However, the impact of the wettability change should also be explored.

5. It is important to characterize the adsorption of the non-ionic surfactant on the sand surface for the proper design of the AS process. Such experiments should be conducted in the future. Also the use of an anionic surfactant should be explored for the emulsification tests with the heavy oil.
6. Conduct experiments for different polymer viscosities to find an optimum polymer viscosity and flow rate.
7. Make the model of AS flood more representative by incorporating the emulsion viscosities and qualities at different chemical concentrations, brine salinity and WORs.
8. Conduct experiments to determine the parameters of the filtration model more accurately.
9. An alkali co-solvent (ACP) process can be developed in the future for the heavy oil. Similar to the ASP process developed in this study, the co-solvent can be used as a substitute for the non-ionic surfactant to impart the hydrophilic character.

APPENDIX A: DATA SETS USED FOR SIMULATIONS

The input files used in the simulations are given here. The first section gives the input file used for simulating an unstable waterflood for the Oil A (10,000 cp) using fine grid simulations. The second section gives the input file used to simulate a tertiary polymer process and in the third section input file used to simulate the AS process for 10,000 cp oil is given. The last section gives the input file used to simulate the ASP process for the 330 cp oil.

A.1 WATERFLOOD SIMULATION OF THE 10,000 CP OIL

The simulation was conducted using CMG STARS simulator. Fine grid simulations with permeability heterogeneity were conducted.

```
** 2013-01-07, 4:59:40 PM, rk7522
RESULTS SIMULATOR STARS 200900
INUNIT FIELD
WSRF WELL TIME
WSRF GRID TIME
WSRF SECTOR TIME
OUTSRF GRID ALL
OUTSRF GRID PRES SG SO SW TEMP VISO VISW
OUTSRF WELL COMPONENT ALL
WPRN GRID 0
OUTPRN GRID NONE
OUTPRN RES NONE
**$  Distance units: m
RESULTS XOFFSET         0.0000
RESULTS YOFFSET         0.0000
RESULTS ROTATION          0.0000  **$  (DEGREES)
RESULTS AXES-DIRECTIONS 1.0 -1.0 1.0
**$  Distance units: m
RESULTS XOFFSET         0.0000
RESULTS YOFFSET         0.0000
RESULTS ROTATION          0.0000  **$  (DEGREES)
RESULTS AXES-DIRECTIONS 1.0 -1.0 1.0
**$ ************************************************************************
**$ Definition of fundamental cartesian grid
**$ ************************************************************************
GRID VARI 80 1 100
KDIR DOWN
```

```
DI IVAR
80*0.0006152
DJ JVAR
0.0492126
DK ALL
 8000*0.03
DTOP
80*0

**$ Property: NULL Blocks  Max: 1  Min: 1
**$  0 = null block, 1 = active block
NULL CON           1
**$ Property: NULL Blocks  Max: 1  Min: 1
**$ Property: Porosity  Max: 0.35  Min: 0.35
POR CON         0.364
**$ Property: Permeability I (md)   Max: 28560  Min: 28560
INCLUDE 'PERMI_large_change.dat'
**PERMI CON 20400
PERMJ EQUALSI
PERMK EQUALSI
**$ Property: Pinchout Array  Max: 1  Min: 1
**$  0 = pinched block, 1 = active block
PINCHOUTARRAY CON           1

END-GRID
**$ Model and number of components
MODEL 2 2 2 1
COMPNAME 'H2O' 'HVYOIL'
CMM
.018 .350
PCRIT
0 0
TCRIT
0 0
KVTABLIM 14.7 100000 10 100
**$ Gas-liquid K Value tables
KVTABLE 'H2O'
**$
         0        0
         0        0
**$ Gas-liquid K Value tables
KVTABLE 'HVYOIL'
**$
         0        0
         0        0
PRSR 14.7
TEMR 80
PSURF 14.7
TSURF 80
MASSDEN
```

```
62.3655 62.3655
AVISC
1 10000
BVISC
0 0

ROCKFLUID
RPT 1 WATWET
**$       Sw          krw       krow
SWT
        0.1           0       0.833
    0.14875  1.52588e-006    0.732129
     0.1975  2.44141e-005    0.637766
    0.24625   0.000123596     0.54991
      0.295   0.000390625    0.468562
    0.34375   0.000953674    0.393723
     0.3925    0.00197754    0.325391
    0.44125    0.00366364    0.263566
       0.49       0.00625     0.20825
    0.53875     0.0100113    0.159441
     0.5875     0.0152588    0.117141
    0.63625     0.0223404   0.0813477
      0.685     0.0316406   0.0520625
    0.73375     0.0435806   0.0292852
     0.7825     0.0586182   0.0130156
    0.83125     0.0772476  0.00325391
       0.88           0.1           0
**$       Sl       krg       krog
SLT
        0.1         1         0
    0.15625    0.9375  0.0520625
     0.2125     0.875   0.104125
    0.26875    0.8125   0.156187
      0.325      0.75    0.20825
    0.38125    0.6875   0.260313
     0.4375     0.625   0.312375
    0.49375    0.5625   0.364437
       0.55       0.5     0.4165
    0.60625    0.4375   0.468562
     0.6625     0.375   0.520625
    0.71875    0.3125   0.572688
      0.775      0.25    0.62475
    0.83125    0.1875   0.676812
     0.8875     0.125   0.728875
    0.94375    0.0625   0.780937
          1         0      0.833

INITIAL
VERTICAL OFF
```

```
INITREGION 1
**$ Property: Pressure (kPa)   Max: 101.3  Min: 101.3
PRES CON        14.7
**$ Property: Pressure (kPa)   Max: 101.3  Min: 101.3
PRES CON        14.7
**$ Property: Water Saturation  Max: 0.48  Min: 0.48
SW CON         0.1
**$ Property: Oil Saturation  Max: 0.52  Min: 0.52
SO CON         0.9
**$ Property: Water Mole Fraction(H2O)  Max: 1  Min: 1
MFRAC_WAT 'H2O' CON            1
**$ Property: Oil Mole Fraction(HVYOIL)  Max: 1  Min: 1
MFRAC_OIL 'HVYOIL' CON            1
NUMERICAL
NORM PRESS 20 SATUR 0.05 X 0.05 W 0.05 ZO 0.05 ZAQ 0.05
DTMIN 1e-20
MAXSTEPS 1000000000
NEWTONCYC 30
NORTH 150
SDEGREE 3
ITERMAX 300
SOLVER PARASOL
RUN
DATE 1901 1 1
DTWELL 1e-007
**$
WELL  'Well-1'
INJECTOR UNWEIGHT 'Well-1'
INCOMP  WATER  1.  0.
TINJW  80.
OPERATE  MAX  STW  0.000163  CONT
**$ UBA    ff  Status  Connection
**$ UBA     ff  Status  Connection
**$         rad  geofac  wfrac  skin
GEOMETRY  K  0.00086  0.249  1.  0.
PERF  GEOA  'Well-1'
**$ UBA       ff  Status  Connection
   1 1 100   1.  OPEN    FLOW-FROM  'SURFACE'  REFLAYER
   2 1 100   1.  OPEN    FLOW-FROM  1
   3 1 100   1.  OPEN    FLOW-FROM  2
   4 1 100   1.  OPEN    FLOW-FROM  3
   5 1 100   1.  OPEN    FLOW-FROM  4
   6 1 100   1.  OPEN    FLOW-FROM  5
   7 1 100   1.  OPEN    FLOW-FROM  6
   8 1 100   1.  OPEN    FLOW-FROM  7
   9 1 100   1.  OPEN    FLOW-FROM  8
   10 1 100  1.  OPEN    FLOW-FROM  9
   11 1 100  1.  OPEN    FLOW-FROM  10
   12 1 100  1.  OPEN    FLOW-FROM  11
   13 1 100  1.  OPEN    FLOW-FROM  12
```

14 1 100 1. OPEN FLOW-FROM 13
15 1 100 1. OPEN FLOW-FROM 14
16 1 100 1. OPEN FLOW-FROM 15
17 1 100 1. OPEN FLOW-FROM 16
18 1 100 1. OPEN FLOW-FROM 17
19 1 100 1. OPEN FLOW-FROM 18
20 1 100 1. OPEN FLOW-FROM 19
21 1 100 1. OPEN FLOW-FROM 20
22 1 100 1. OPEN FLOW-FROM 21
23 1 100 1. OPEN FLOW-FROM 22
24 1 100 1. OPEN FLOW-FROM 23
25 1 100 1. OPEN FLOW-FROM 24
26 1 100 1. OPEN FLOW-FROM 25
27 1 100 1. OPEN FLOW-FROM 26
28 1 100 1. OPEN FLOW-FROM 27
29 1 100 1. OPEN FLOW-FROM 28
30 1 100 1. OPEN FLOW-FROM 29
31 1 100 1. OPEN FLOW-FROM 30
32 1 100 1. OPEN FLOW-FROM 31
33 1 100 1. OPEN FLOW-FROM 32
34 1 100 1. OPEN FLOW-FROM 33
35 1 100 1. OPEN FLOW-FROM 34
36 1 100 1. OPEN FLOW-FROM 35
37 1 100 1. OPEN FLOW-FROM 36
38 1 100 1. OPEN FLOW-FROM 37
39 1 100 1. OPEN FLOW-FROM 38
40 1 100 1. OPEN FLOW-FROM 39
41 1 100 1. OPEN FLOW-FROM 40
42 1 100 1. OPEN FLOW-FROM 41
43 1 100 1. OPEN FLOW-FROM 42
44 1 100 1. OPEN FLOW-FROM 43
45 1 100 1. OPEN FLOW-FROM 44
46 1 100 1. OPEN FLOW-FROM 45
47 1 100 1. OPEN FLOW-FROM 46
48 1 100 1. OPEN FLOW-FROM 47
49 1 100 1. OPEN FLOW-FROM 48
50 1 100 1. OPEN FLOW-FROM 49
51 1 100 1. OPEN FLOW-FROM 50
52 1 100 1. OPEN FLOW-FROM 51
53 1 100 1. OPEN FLOW-FROM 52
54 1 100 1. OPEN FLOW-FROM 53
55 1 100 1. OPEN FLOW-FROM 54
56 1 100 1. OPEN FLOW-FROM 55
57 1 100 1. OPEN FLOW-FROM 56
58 1 100 1. OPEN FLOW-FROM 57
59 1 100 1. OPEN FLOW-FROM 58
60 1 100 1. OPEN FLOW-FROM 59
61 1 100 1. OPEN FLOW-FROM 60
62 1 100 1. OPEN FLOW-FROM 61
63 1 100 1. OPEN FLOW-FROM 62

```
   64 1 100  1.  OPEN    FLOW-FROM  63
   65 1 100  1.  OPEN    FLOW-FROM  64
   66 1 100  1.  OPEN    FLOW-FROM  65
   67 1 100  1.  OPEN    FLOW-FROM  66
   68 1 100  1.  OPEN    FLOW-FROM  67
   69 1 100  1.  OPEN    FLOW-FROM  68
   70 1 100  1.  OPEN    FLOW-FROM  69
   71 1 100  1.  OPEN    FLOW-FROM  70
   72 1 100  1.  OPEN    FLOW-FROM  71
   73 1 100  1.  OPEN    FLOW-FROM  72
   74 1 100  1.  OPEN    FLOW-FROM  73
   75 1 100  1.  OPEN    FLOW-FROM  74
   76 1 100  1.  OPEN    FLOW-FROM  75
   77 1 100  1.  OPEN    FLOW-FROM  76
   78 1 100  1.  OPEN    FLOW-FROM  77
   79 1 100  1.  OPEN    FLOW-FROM  78
   80 1 100  1.  OPEN    FLOW-FROM  79

**$
WELL  'Well-2'
PRODUCER 'Well-2'
OPERATE  MIN  BHP  14.7  CONT
**$ UBA       ff  Status  Connection
**$          rad  geofac  wfrac  skin
GEOMETRY  K  0.00086  0.249  1.  0.
PERF  GEOA  'Well-2'
**$ UBA     ff  Status  Connection
   1 1 1   1.  OPEN    FLOW-TO  'SURFACE'  REFLAYER
   2 1 1   1.  OPEN    FLOW-TO  1
   3 1 1   1.  OPEN    FLOW-TO  2
   4 1 1   1.  OPEN    FLOW-TO  3
   5 1 1   1.  OPEN    FLOW-TO  4
   6 1 1   1.  OPEN    FLOW-TO  5
   7 1 1   1.  OPEN    FLOW-TO  6
   8 1 1   1.  OPEN    FLOW-TO  7
   9 1 1   1.  OPEN    FLOW-TO  8
   10 1 1  1.  OPEN    FLOW-TO  9
   11 1 1  1.  OPEN    FLOW-TO  10
   12 1 1  1.  OPEN    FLOW-TO  11
   13 1 1  1.  OPEN    FLOW-TO  12
   14 1 1  1.  OPEN    FLOW-TO  13
   15 1 1  1.  OPEN    FLOW-TO  14
   16 1 1  1.  OPEN    FLOW-TO  15
   17 1 1  1.  OPEN    FLOW-TO  16
   18 1 1  1.  OPEN    FLOW-TO  17
   19 1 1  1.  OPEN    FLOW-TO  18
   20 1 1  1.  OPEN    FLOW-TO  19
   21 1 1  1.  OPEN    FLOW-TO  20
   22 1 1  1.  OPEN    FLOW-TO  21
   23 1 1  1.  OPEN    FLOW-TO  22
```

24 1 1 1. OPEN FLOW-TO 23
25 1 1 1. OPEN FLOW-TO 24
26 1 1 1. OPEN FLOW-TO 25
27 1 1 1. OPEN FLOW-TO 26
28 1 1 1. OPEN FLOW-TO 27
29 1 1 1. OPEN FLOW-TO 28
30 1 1 1. OPEN FLOW-TO 29
31 1 1 1. OPEN FLOW-TO 30
32 1 1 1. OPEN FLOW-TO 31
33 1 1 1. OPEN FLOW-TO 32
34 1 1 1. OPEN FLOW-TO 33
35 1 1 1. OPEN FLOW-TO 34
36 1 1 1. OPEN FLOW-TO 35
37 1 1 1. OPEN FLOW-TO 36
38 1 1 1. OPEN FLOW-TO 37
39 1 1 1. OPEN FLOW-TO 38
40 1 1 1. OPEN FLOW-TO 39
41 1 1 1. OPEN FLOW-TO 40
42 1 1 1. OPEN FLOW-TO 41
43 1 1 1. OPEN FLOW-TO 42
44 1 1 1. OPEN FLOW-TO 43
45 1 1 1. OPEN FLOW-TO 44
46 1 1 1. OPEN FLOW-TO 45
47 1 1 1. OPEN FLOW-TO 46
48 1 1 1. OPEN FLOW-TO 47
49 1 1 1. OPEN FLOW-TO 48
50 1 1 1. OPEN FLOW-TO 49
51 1 1 1. OPEN FLOW-TO 50
52 1 1 1. OPEN FLOW-TO 51
53 1 1 1. OPEN FLOW-TO 52
54 1 1 1. OPEN FLOW-TO 53
55 1 1 1. OPEN FLOW-TO 54
56 1 1 1. OPEN FLOW-TO 55
57 1 1 1. OPEN FLOW-TO 56
58 1 1 1. OPEN FLOW-TO 57
59 1 1 1. OPEN FLOW-TO 58
60 1 1 1. OPEN FLOW-TO 59
61 1 1 1. OPEN FLOW-TO 60
62 1 1 1. OPEN FLOW-TO 61
63 1 1 1. OPEN FLOW-TO 62
64 1 1 1. OPEN FLOW-TO 63
65 1 1 1. OPEN FLOW-TO 64
66 1 1 1. OPEN FLOW-TO 65
67 1 1 1. OPEN FLOW-TO 66
68 1 1 1. OPEN FLOW-TO 67
69 1 1 1. OPEN FLOW-TO 68
70 1 1 1. OPEN FLOW-TO 69
71 1 1 1. OPEN FLOW-TO 70
72 1 1 1. OPEN FLOW-TO 71
73 1 1 1. OPEN FLOW-TO 72

```
 74 1 1  1.  OPEN    FLOW-TO  73
 75 1 1  1.  OPEN    FLOW-TO  74
 76 1 1  1.  OPEN    FLOW-TO  75
 77 1 1  1.  OPEN    FLOW-TO  76
 78 1 1  1.  OPEN    FLOW-TO  77
 79 1 1  1.  OPEN    FLOW-TO  78
 80 1 1  1.  OPEN    FLOW-TO  79



DATE 1901 1  1.04167
DATE 1901 1  1.50000
DATE 1901 1  2.29167
DATE 1901 1  2.33333
DATE 1901 1  2.37500
DATE 1901 1  2.41667
DATE 1901 1  2.83333
DATE 1901 1  3.83333
DATE 1901 1  3.87500
DATE 1901 1  3.91667
DATE 1901 1  3.95833
DATE 1901 1  4.00000
DATE 1901 1  4.04167
DATE 1901 1  4.87500
DATE 1901 1  4.91667
DATE 1901 1  4.95833
DATE 1901 1  5.00000
DATE 1901 1  6.33333
DATE 1901 1  6.37500
DATE 1901 1  7.00000
DATE 1901 1  7.66667
DATE 1901 1  8.37500
DATE 1901 1  8.41667
DATE 1901 1  8.45833
DATE 1901 1  9.00000
DATE 1901 1  9.45833
DATE 1901 1  9.50000
DATE 1901 1  9.54167
DATE 1901 1  10.00000

STOP
```

A.2 TERTIARY POLYMER FLOOD SIMULATION OF THE 10,000 CP OIL

This section gives the input file used for the fine grid CMG STARS simulation of a tertiary polymer flood. To model the experimental data water injection is simulated for 1PV followed by polymer flood simulation for another 1PV. To initiate viscous fingers, the permeability was randomly distributed around the mean value with a standard deviation of ± 10%.

```
RESULTS SIMULATOR STARS 200900
INTERRUPT *STOP
** ============== INPUT/OUTPUT CONTROL ========================
TITLE1 'STARS Fluid Model'
TITLE2 'model the tertiary polymer flood in a heterogenous grid'
INUNIT LAB
OUTUNIT LAB
MASSBASIS
WPRN GRID TIME
OUTPRN GRID PRES SW SO SG W X VISW VISO
OUTPRN WELL ALL
WPRN ITER TIME
OUTPRN ITER NEWTON
WSRF WELL 1
WSRF GRID TIME
WSRF SECTOR 1
OUTSRF GRID MASS ADSORP PPM ADSPCMP KRO KRW MASDENO MASDENW MOLDENO
MOLDENW PRES RFO RFW  SG SHEARG SHEARO SHEARSTRSG SHEARSTRSO SHEARSTRSW
SHEARW SO SW VISCVELG VISCVELO VISCVELW VISO VISW VPOROS W X Y OUTSRF WELL
MASS COMPONENT ALL

**$  Distance units: cm
RESULTS XOFFSET         0.0000
RESULTS YOFFSET         0.0000
RESULTS ROTATION          0.0000  **$  (DEGREES)
RESULTS AXES-DIRECTIONS 1.0 -1.0 1.0
** ========= RESERVOIR DESCRIPTION ===================================
GRID CART 80 1 100
KDIR DOWN
DI CON 0.01875
DJ CON   1.5
DK CON   .93
DTOP     80*1000
**$ Property: NULL Blocks  Max: 1  Min: 1       (0 = null block, 1 = active block)
NULL CON           1
**$ Property: Porosity
```

```
POR CON        0.476                  **  sandpack porosity
*INCLUDE 'PERMI.dat'
PERMJ EQUALSI
PERMK EQUALSI
**$ Property: Pinchout Array  Max: 1  Min: 1
**$  0 = pinched block, 1 = active block
PINCHOUTARRAY CON           1
END-GRID
** ============== COMPONENT PROPERTIES ==================================
** ncomp = numy = numx = 3, numw = 2
MODEL 3 3 3 2
**          ----- Aqueous -----   ---- Oleic ----
COMPNAME 'Water' 'Polymer' 'Dead_Oil'
**kg/mol
CMM
0.018 22000 0.42
**kPa
PCRIT
0.0 0 0
TCRIT
0.0 0 0
**  Reference Conditions
PRSR 101.1
TEMR 25
PSURF 101.1
**kg/cm3
MASSDEN
0.001 0.001 0.00081
AVISC
1 100 16500.0
BVISC
0 0 0
VSMIXCOMP 'Polymer'
** 2000 MG/L
VSMIXENDP 0 2.0E-3
VSMIXFUNC 0 0.155 .3 .425 .55 .6 .7 .75 .825 .905 1.0
** Add shear thinning of power index n= 0.6 and reference velocity of .0375 cm/min
*SHEARTHIN 0.4823   0.015
** ================= ROCK-FLUID PROPERTIES ==========================
ROCKFLUID
RPT 1 WATWET
INTCOMP 'Polymer' *WATER
KRINTRP 1
DTRAPW 0
**$       Sw          krw       krow
SWT
        0.1           0         1
     0.14875   1.0498e-005   0.925477
      0.1975  8.39844e-005   0.851941
     0.24625   0.000283447    0.77945
```

```
      0.295   0.000671875   0.708066
    0.34375    0.00131226   0.637863
     0.3925    0.00226758   0.568926
    0.44125    0.00360083   0.501357
       0.49      0.005375   0.435275
    0.53875    0.00765308   0.370829
     0.5875     0.010498   0.308203
    0.63625     0.0139729    0.24764
      0.685     0.0181406   0.189465
    0.73375     0.0230642   0.134153
     0.7825     0.0288066  0.0824692
    0.83125     0.0354309  0.0358968
       0.88         0.043          0
**NOSWC
** Sl     Krg       Krog
**$       Sl       krg      krog
SLT
        0.1         1         0
    0.15625    0.9375    0.0625
     0.2125     0.875     0.125
    0.26875    0.8125    0.1875
      0.325      0.75      0.25
    0.38125    0.6875    0.3125
     0.4375     0.625     0.375
    0.49375    0.5625    0.4375
       0.55       0.5       0.5
    0.60625    0.4375    0.5625
     0.6625     0.375     0.625
    0.71875    0.3125    0.6875
      0.775      0.25      0.75
    0.83125    0.1875    0.8125
     0.8875     0.125     0.875
    0.94375    0.0625    0.9375
          1         0         1
KRINTRP 2
DTRAPW 0.0022
**$       Sw       krw         krow

SWT
        0.1           0         1
    0.14875  0.000162821   0.925477
     0.1975  0.000987163   0.851941
    0.24625   0.00283287    0.77945
      0.295   0.00598504   0.708066
    0.34375    0.0106914   0.637863
     0.3925    0.0171753   0.568926
    0.44125    0.0256428   0.501357
       0.49    0.0362865   0.435275
    0.53875     0.049288   0.370829
     0.5875    0.0648203   0.308203
```

```
    0.63625    0.0830485    0.24764
     0.685     0.104131   0.189465
    0.73375     0.128222   0.134153
     0.7825     0.155469  0.0824692
    0.83125     0.186015  0.0358968
       0.88         0.22          0
**$        Sl       krg       krog
SLT
        0.1         1         0
    0.15625    0.9375    0.0625
     0.2125     0.875     0.125
    0.26875    0.8125    0.1875
      0.325      0.75      0.25
    0.38125    0.6875    0.3125
     0.4375     0.625     0.375
    0.49375    0.5625    0.4375
       0.55       0.5       0.5
    0.60625    0.4375    0.5625
     0.6625     0.375     0.625
    0.71875    0.3125    0.6875
      0.775      0.25      0.75
    0.83125    0.1875    0.8125
     0.8875     0.125     0.875
    0.94375    0.0625    0.9375
          1         0         1

**ADSCOMP 'Polymer' WATER
**ADSTABLE
  ** 0      0.00
   **0.4E-3 0.1     ** 400 ppm
  **2.0E-3 0.2
**ADMAXT    0.5
**ADRT      0
**RRFT  1.2
**PORFT  .7
** ============== INITIALIZATION ==================================
INITIAL
VERTICAL OFF
INITREGION 1
**$ Property: Pressure (kPa)
*PRES CON         101.3
**vertical *depth_ave
**REFPRES 101.3
**REFDEPTH 1000.
SW CON .1
**$ Property: Temperature (C)
TEMP CON          25
**$ Property: Water Mole Fraction(Water)  Max: 1  Min: 1
MFRAC_WAT 'Water' CON           1
**$ Property: Water Mole Fraction(Polymer)  Max: 0  Min: 0
```

```
MFRAC_WAT 'Polymer' CON           0
** ============  NUMERICAL CONTROL ================================
NUMERICAL
NORM PRESS 100 SATUR 0.05 ZAQ 2e-005
CONVERGE ZAQ 2e-005
DTMIN 1.44e-17
MAXSTEPS 10000000
TFORM ZT
ISOTHERMAL
MATBALITER 30
MATBALTOL 1E-7
NORTH 200
ITERMAX 300
NCUTS 30
RUN
** ============  RECURRENT DATA  ==================================
TIME 0.0
DTWELL 2e-017
WELL  'Injector'
**COMPNAME      'Water'       'Polymer'      'Dead_Oil'
                                ** ML/MIN
INJECTOR MOBWEIGHT EXPLICIT 'Injector'
INCOMP  WATER  1.  0.  0.
OPERATE  MAX  STW  0.018  CONT
OPERATE  MAX  BHP  5.025e+006  CONT
**$ UBA    ff  Status  Connection
**$         rad  geofac  wfrac  skin
GEOMETRY  K  0.000212  0.2  1.  0.
PERF  GEO  'Injector'
**$ UBA       ff  Status  Connection
   1 1 100   1.  OPEN    FLOW-FROM  'SURFACE'  REFLAYER
   2 1 100   1.  OPEN    FLOW-FROM  1
   3 1 100   1.  OPEN    FLOW-FROM  2
   4 1 100   1.  OPEN    FLOW-FROM  3
   5 1 100   1.  OPEN    FLOW-FROM  4
   6 1 100   1.  OPEN    FLOW-FROM  5
   7 1 100   1.  OPEN    FLOW-FROM  6
   8 1 100   1.  OPEN    FLOW-FROM  7
   9 1 100   1.  OPEN    FLOW-FROM  8
   10 1 100  1.  OPEN    FLOW-FROM  9
   11 1 100  1.  OPEN    FLOW-FROM  10
   12 1 100  1.  OPEN    FLOW-FROM  11
   13 1 100  1.  OPEN    FLOW-FROM  12
   14 1 100  1.  OPEN    FLOW-FROM  13
   15 1 100  1.  OPEN    FLOW-FROM  14
   16 1 100  1.  OPEN    FLOW-FROM  15
   17 1 100  1.  OPEN    FLOW-FROM  16
   18 1 100  1.  OPEN    FLOW-FROM  17
   19 1 100  1.  OPEN    FLOW-FROM  18
   20 1 100  1.  OPEN    FLOW-FROM  19
```

21 1 100 1. OPEN FLOW-FROM 20
22 1 100 1. OPEN FLOW-FROM 21
23 1 100 1. OPEN FLOW-FROM 22
24 1 100 1. OPEN FLOW-FROM 23
25 1 100 1. OPEN FLOW-FROM 24
26 1 100 1. OPEN FLOW-FROM 25
27 1 100 1. OPEN FLOW-FROM 26
28 1 100 1. OPEN FLOW-FROM 27
29 1 100 1. OPEN FLOW-FROM 28
30 1 100 1. OPEN FLOW-FROM 29
31 1 100 1. OPEN FLOW-FROM 30
32 1 100 1. OPEN FLOW-FROM 31
33 1 100 1. OPEN FLOW-FROM 32
34 1 100 1. OPEN FLOW-FROM 33
35 1 100 1. OPEN FLOW-FROM 34
36 1 100 1. OPEN FLOW-FROM 35
37 1 100 1. OPEN FLOW-FROM 36
38 1 100 1. OPEN FLOW-FROM 37
39 1 100 1. OPEN FLOW-FROM 38
40 1 100 1. OPEN FLOW-FROM 39
41 1 100 1. OPEN FLOW-FROM 40
42 1 100 1. OPEN FLOW-FROM 41
43 1 100 1. OPEN FLOW-FROM 42
44 1 100 1. OPEN FLOW-FROM 43
45 1 100 1. OPEN FLOW-FROM 44
46 1 100 1. OPEN FLOW-FROM 45
47 1 100 1. OPEN FLOW-FROM 46
48 1 100 1. OPEN FLOW-FROM 47
49 1 100 1. OPEN FLOW-FROM 48
50 1 100 1. OPEN FLOW-FROM 49
51 1 100 1. OPEN FLOW-FROM 50
52 1 100 1. OPEN FLOW-FROM 51
53 1 100 1. OPEN FLOW-FROM 52
54 1 100 1. OPEN FLOW-FROM 53
55 1 100 1. OPEN FLOW-FROM 54
56 1 100 1. OPEN FLOW-FROM 55
57 1 100 1. OPEN FLOW-FROM 56
58 1 100 1. OPEN FLOW-FROM 57
59 1 100 1. OPEN FLOW-FROM 58
60 1 100 1. OPEN FLOW-FROM 59
61 1 100 1. OPEN FLOW-FROM 60
62 1 100 1. OPEN FLOW-FROM 61
63 1 100 1. OPEN FLOW-FROM 62
64 1 100 1. OPEN FLOW-FROM 63
65 1 100 1. OPEN FLOW-FROM 64
66 1 100 1. OPEN FLOW-FROM 65
67 1 100 1. OPEN FLOW-FROM 66
68 1 100 1. OPEN FLOW-FROM 67
69 1 100 1. OPEN FLOW-FROM 68
70 1 100 1. OPEN FLOW-FROM 69

```
   71 1 100  1.  OPEN    FLOW-FROM  70
   72 1 100  1.  OPEN    FLOW-FROM  71
   73 1 100  1.  OPEN    FLOW-FROM  72
   74 1 100  1.  OPEN    FLOW-FROM  73
   75 1 100  1.  OPEN    FLOW-FROM  74
   76 1 100  1.  OPEN    FLOW-FROM  75
   77 1 100  1.  OPEN    FLOW-FROM  76
   78 1 100  1.  OPEN    FLOW-FROM  77
   79 1 100  1.  OPEN    FLOW-FROM  78
   80 1 100  1.  OPEN    FLOW-FROM  79


WELL  'Producer1'
PRODUCER 'Producer1'
OPERATE  MIN  BHP  101.3  CONT
 **$ UBA     ff  Status  Connection
**$ UBA     ff  Status  Connection
**$         rad  geofac  wfrac  skin
GEOMETRY  K  0.00075  0.2  1.  0.
PERF  GEO  'Producer1'
**$ UBA     ff  Status  Connection
   1 1 1   1.  OPEN    FLOW-TO  'SURFACE'  REFLAYER
   2 1 1   1.  OPEN    FLOW-TO  1
   3 1 1   1.  OPEN    FLOW-TO  2
   4 1 1   1.  OPEN    FLOW-TO  3
   5 1 1   1.  OPEN    FLOW-TO  4
   6 1 1   1.  OPEN    FLOW-TO  5
   7 1 1   1.  OPEN    FLOW-TO  6
   8 1 1   1.  OPEN    FLOW-TO  7
   9 1 1   1.  OPEN    FLOW-TO  8
   10 1 1  1.  OPEN    FLOW-TO  9
   11 1 1  1.  OPEN    FLOW-TO  10
   12 1 1  1.  OPEN    FLOW-TO  11
   13 1 1  1.  OPEN    FLOW-TO  12
   14 1 1  1.  OPEN    FLOW-TO  13
   15 1 1  1.  OPEN    FLOW-TO  14
   16 1 1  1.  OPEN    FLOW-TO  15
   17 1 1  1.  OPEN    FLOW-TO  16
   18 1 1  1.  OPEN    FLOW-TO  17
   19 1 1  1.  OPEN    FLOW-TO  18
   20 1 1  1.  OPEN    FLOW-TO  19
   21 1 1  1.  OPEN    FLOW-TO  20
   22 1 1  1.  OPEN    FLOW-TO  21
   23 1 1  1.  OPEN    FLOW-TO  22
   24 1 1  1.  OPEN    FLOW-TO  23
   25 1 1  1.  OPEN    FLOW-TO  24
   26 1 1  1.  OPEN    FLOW-TO  25
   27 1 1  1.  OPEN    FLOW-TO  26
   28 1 1  1.  OPEN    FLOW-TO  27
   29 1 1  1.  OPEN    FLOW-TO  28
```

30 1 1 1. OPEN FLOW-TO 29
31 1 1 1. OPEN FLOW-TO 30
32 1 1 1. OPEN FLOW-TO 31
33 1 1 1. OPEN FLOW-TO 32
34 1 1 1. OPEN FLOW-TO 33
35 1 1 1. OPEN FLOW-TO 34
36 1 1 1. OPEN FLOW-TO 35
37 1 1 1. OPEN FLOW-TO 36
38 1 1 1. OPEN FLOW-TO 37
39 1 1 1. OPEN FLOW-TO 38
40 1 1 1. OPEN FLOW-TO 39
41 1 1 1. OPEN FLOW-TO 40
42 1 1 1. OPEN FLOW-TO 41
43 1 1 1. OPEN FLOW-TO 42
44 1 1 1. OPEN FLOW-TO 43
45 1 1 1. OPEN FLOW-TO 44
46 1 1 1. OPEN FLOW-TO 45
47 1 1 1. OPEN FLOW-TO 46
48 1 1 1. OPEN FLOW-TO 47
49 1 1 1. OPEN FLOW-TO 48
50 1 1 1. OPEN FLOW-TO 49
51 1 1 1. OPEN FLOW-TO 50
52 1 1 1. OPEN FLOW-TO 51
53 1 1 1. OPEN FLOW-TO 52
54 1 1 1. OPEN FLOW-TO 53
55 1 1 1. OPEN FLOW-TO 54
56 1 1 1. OPEN FLOW-TO 55
57 1 1 1. OPEN FLOW-TO 56
58 1 1 1. OPEN FLOW-TO 57
59 1 1 1. OPEN FLOW-TO 58
60 1 1 1. OPEN FLOW-TO 59
61 1 1 1. OPEN FLOW-TO 60
62 1 1 1. OPEN FLOW-TO 61
63 1 1 1. OPEN FLOW-TO 62
64 1 1 1. OPEN FLOW-TO 63
65 1 1 1. OPEN FLOW-TO 64
66 1 1 1. OPEN FLOW-TO 65
67 1 1 1. OPEN FLOW-TO 66
68 1 1 1. OPEN FLOW-TO 67
69 1 1 1. OPEN FLOW-TO 68
70 1 1 1. OPEN FLOW-TO 69
71 1 1 1. OPEN FLOW-TO 70
72 1 1 1. OPEN FLOW-TO 71
73 1 1 1. OPEN FLOW-TO 72
74 1 1 1. OPEN FLOW-TO 73
75 1 1 1. OPEN FLOW-TO 74
76 1 1 1. OPEN FLOW-TO 75
77 1 1 1. OPEN FLOW-TO 76
78 1 1 1. OPEN FLOW-TO 77
79 1 1 1. OPEN FLOW-TO 78

80 1 1 1. OPEN FLOW-TO 79

**SHUTIN 'Injector' 'Producer1'
TIME 60
TIME 120
TIME 180
TIME 240
TIME 780
TIME 840
1320

TIME 1337.98 **$ water Injection
TIME 1380
TIME 1440
TIME 1500
TIME 1560
TIME 1620
TIME 1680
TIME 1740
TIME 1800
TIME 1860

TIME 1915.45
TIME 1920
TIME 1980
TIME 2040
TIME 2100
TIME 2160
TIME 2220
TIME 2280
TIME 2340
TIME 2400
TIME 2460
TIME 2520
TIME 2580
TIME 2640
TIME 2700
TIME 2760
TIME 2820
TIME 2880
TIME 2940
TIME 3000
TIME 3060
TIME 3120
TIME 3180
TIME 3240
TIME 4860
TIME 4920
TIME 4980
TIME 5040

```
TIME 5100
TIME 5160
TIME 5220
TIME 5280
TIME 5340
TIME 5400
TIME 5443.18
**COMPNAME       'Water' 'Polymer''Dead_Oil'
                                ** ML/MIN
INJECTOR MOBWEIGHT EXPLICIT 'Injector'
INCOMP  WATER  0.9978   0.0022    0.
OPERATE  MAX  STW  0.018  CONT
OPERATE  MAX  BHP  502500.  CONT
TIME 5444
TIME 5445
TIME 5446
TIME 5447
TIME 5448
TIME 5449
TIME 5450
TIME 5451
TIME 6660
TIME 6720
TIME 6780
TIME 6840
TIME 6900
TIME 6960
TIME 7020
TIME 7080
TIME 7140
TIME 7200
TIME  10680.0
TIME  10740.0
TIME  10800.0
TIME  10860.0
TIME  10920.0
**COMPNAME       'Water' 'Polymer''Dead_Oil'
                                ** ML/MIN
INJECTOR MOBWEIGHT EXPLICIT 'Injector'
INCOMP  WATER  1.  0.  0.
OPERATE  MAX  STW  0.018  CONT
OPERATE  MAX  BHP  5.025e+006  CONT
TIME  10980.0
TIME  11040.0
TIME  11100
TIME  18180.0
TIME  18240.0
TIME  18300.0
TIME  18360.0
TIME  18420.0
```

TIME 18480.0
TIME 18540.0
TIME 18600.0
TIME 18660.0
TIME 18720.0
TIME 18780.0
TIME 18840.0
TIME 18900.0
TIME 18960.0
TIME 19020.0
TIME 19080.0
TIME 19140.0
STOP

A.3 TERTIARY ALKALI-SURFACTANT FLOOD SIMULATION OF THE 10,000 CP OIL

This section gives the input file used for simulating the AS flood of the 10,000 cp oil.

```
** 2013-01-07, 4:59:40 PM, rk7522
RESULTS SIMULATOR STARS 200900

INUNIT SI
WSRF WELL TIME
WSRF GRID TIME
WSRF SECTOR TIME
OUTSRF GRID ALL
OUTSRF GRID PRES SG SO SW TEMP VISO VISW
OUTSRF WELL COMPONENT ALL
WPRN GRID 0
OUTPRN GRID NONE
OUTPRN RES NONE
**$  Distance units: m
RESULTS XOFFSET         0.0000
RESULTS YOFFSET         0.0000
RESULTS ROTATION          0.0000  **$  (DEGREES)
RESULTS AXES-DIRECTIONS 1.0 -1.0 1.0
**$  Distance units: m
RESULTS XOFFSET         0.0000
RESULTS YOFFSET         0.0000
RESULTS ROTATION          0.0000  **$  (DEGREES)
RESULTS AXES-DIRECTIONS 1.0 -1.0 1.0
**$ ************************************************************************
**$ Definition of fundamental cartesian grid
**$ ************************************************************************
GRID VARI 80 1 100
KDIR DOWN
DI IVAR
80*0.0001875
DJ JVAR
0.015
DK ALL
 8000*0.009144
DTOP
 80*1000

**$ Property: NULL Blocks  Max: 1  Min: 1
**$  0 = null block, 1 = active block
NULL CON           1
**$ Property: NULL Blocks  Max: 1  Min: 1
**$ Property: Porosity  Max: 0.35  Min: 0.35
```

```
POR CON         0.364
**$ Property: Permeability I (md)   Max: 28560  Min: 28560
INCLUDE 'PERMI.DAT'
**PERMI CON         20400
**$ Property: Permeability I (md)   Max: 28560  Min: 28560
PERMJ EQUALSI
**$ Property: Permeability J (md)   Max: 28560  Min: 28560
PERMK EQUALSI
**$ Property: Pinchout Array  Max: 1  Min: 1
**$  0 = pinched block, 1 = active block
PINCHOUTARRAY CON           1

END-GRID
**$ Model and number of components
MODEL 6 5 5 4
COMPNAME 'H2O' 'SURF' 'ALK' 'O_W EM' 'HVYOIL' 'trapoil'
CMM
.018 1.520 .106 .184 .350 0.35
PCRIT
0 0 0 0 0
TCRIT
0 0 0 0 0
KVTABLIM 101.3 100000 10 100
**$
**$ Gas-liquid K Value tables
KVTABLE 'H2O'
**$
        0       0
        0       0
**$
**$ Gas-liquid K Value tables
KVTABLE 'SURF'
**$
        0       0
        0       0
**$
**$ Gas-liquid K Value tables
KVTABLE 'ALK'
**$
        0       0
        0       0
**$
**$ Gas-liquid K Value tables
KVTABLE 'HVYOIL'
**$
        0       0
        0       0
PRSR 101.3
TSURF 25
SOLID_DEN 'trapoil' 999.99 0 0
```

```
** oil = 1/10 water for easier mol -> vol
MOLDEN
55555.56 55555.56 55555.56 5434.78 2857.142857
AVISC
1 1 1 9222 10000
BVISC
0 0 0 0 0

*VSMIXCOMP 'O_W EM'
SHEARTHIN 0.5606 4.15E-02

**$    effplt     rrsft
**$ Non-equilibrium blockage
BLOCKAGE W 'trapoil'
**$    effplt     rrsft
       20400       600
       21000       610
**$ Reaction specification
**$ Reaction specification
STOREAC
19.586 1.0117 1.0001 0 1 0
STOPROD
0 1 1 3.89 0 0
RPHASE
1 1 1 0 2 0
RORDER
0 1 1 1 1 0
FREQFAC .003
**$ Reaction specification
**$ Reaction specification
STOREAC
0 0 0 1.902 0 0
STOPROD
0 0 0 0 0 1
RORDER
0 0 0 1 0 1
FREQFAC 0.007
**$ Reaction specification
**$ Reaction specification
STOREAC
0 0 0 1.902 0 1
STOPROD
0 0 0 3.804 0 0
RORDER
0 0 0 1 0 1
FREQFAC .2



** High IFT
```

```
ROCKFLUID
RPT 1 WATWET
INTCOMP 'ALK' *MAX
IFTTABLE
**$  Composition of component/phase  Interfacial tension
**$  Composition of component/phase  Interfacial tension
**$  Composition of component/phase  Interfacial tension
                    0                30
              8.5025E-05               1
              0.000170121              0.08
              0.000255287              .035
              0.000340525              .03
              0.000425833              .01
              0.000511212              .01
              0.000596663              .01
              0.000682185              .01
              0.000767778              .01
INTLOG
KRINTRP 1 WATWET
DTRAPW -6.188

SWT
         0.1          0       0.833
    0.103276891  3.15086E-08  0.828811108
     0.10821108  3.15811E-07  0.822530517
    0.114438973  1.24953E-06  0.814637554
    0.121806741  3.35488E-06  0.805341092
    0.130218411  7.26404E-06  0.794775132
    0.139605657  1.37097E-05   0.78303787
    0.149916179  2.35182E-05  0.770206773
    0.161108037  3.76049E-05  0.756345963
    0.173146492  5.69699E-05  0.741510357
    0.186002064  8.26943E-05  0.725748225
    0.199649269  0.000115938  0.709102872
    0.214065747  0.000157937  0.691613808
    0.229231647  0.000210001  0.673317599
    0.245129162  0.000273513  0.654248509
    0.261742187  0.000349923  0.634438999
    0.279056049  0.000440753  0.613920132
    0.297057299  0.000547592  0.592721909
    0.315733537  0.000672093  0.570873562
    0.335073279  0.000815976  0.548403807
    0.355065845  0.000981022  0.525341089
    0.375701258  0.001169079  0.501713807
    0.396970174  0.001382054   0.47755055
    0.418863808  0.001621913  0.452880328
    0.441373882  0.001890686  0.427732838
    0.464492571   0.00219046  0.402138744
    0.488212466  0.002523381  0.376130011
    0.512526531  0.002891652  0.349740303
```

```
   0.537428075  0.003297535  0.323005468
   0.562910722  0.003743345  0.295964149
   0.588968384  0.004231457  0.268658592
   0.615595241  0.004764298  0.241135718
   0.642785721  0.005344352  0.213448627
   0.670534479  0.005974154  0.185658772
   0.698836385  0.006656297  0.157839268
   0.727686505  0.007393423  0.130080214
   0.757080093  0.008188229   0.10249799
   0.787012573  0.009043464  0.075253263
   0.817479533  0.009961927  0.048592043
   0.848476714  0.010946472  0.022970077
         0.88        0.012            0
**$        Sl       krg       krog
SLT
        0.1         1         0
    0.15625    0.9375    0.0625
     0.2125     0.875     0.125
    0.26875    0.8125    0.1875
      0.325      0.75      0.25
    0.38125    0.6875    0.3125
     0.4375     0.625     0.375
    0.49375    0.5625    0.4375
       0.55        0.5       0.5
    0.60625    0.4375    0.5625
     0.6625     0.375     0.625
    0.71875    0.3125    0.6875
      0.775      0.25      0.75
    0.83125    0.1875    0.8125
     0.8875     0.125       .82
    0.94375    0.0625       .83
          1         0      .833
KRINTRP 2 WATWET
DTRAPW -0.565
**$        Sw           krw          krow
SWT
        0.1            0         0.89
     0.1205  5.85938e-009  0.888794576
      0.141    1.875e-007  0.885251356
     0.1615  1.42383e-006  0.879479352
      0.182        6e-006  0.871586805
     0.2025  1.83105e-005  0.861681159
      0.223  4.55625e-005  0.849869042
     0.2435  9.84785e-005  0.836256241
      0.264      0.000192  0.820947677
     0.2845    0.00034599  0.804047379
      0.305   0.000585938  0.785658453
     0.3255   0.000943658  0.765883052
      0.346      0.001458  0.744822343
     0.3665   0.002175545  0.722576472
```

```
      0.387   0.003151313  0.699244522
     0.4075   0.004449463  0.674924473
      0.428      0.006144  0.649713159
     0.4485   0.008319475  0.623706212
      0.469   0.011071688  0.596998013
     0.4895   0.014508393   0.56968163
       0.51       0.01875   0.54184875
     0.5305   0.023930279  0.513589608
      0.551   0.030197063  0.484992902
     0.5715   0.037712947  0.456145702
      0.592      0.046656  0.427133346
     0.6125   0.057220459  0.398039317
      0.633   0.069617437  0.368945109
     0.6535   0.084075627  0.339930066
      0.674      0.100842  0.311071193
     0.6945   0.120182514  0.282442934
      0.715   0.142382813    0.2541169
     0.7355   0.167748932  0.226161541
      0.756      0.196608  0.198641725
     0.7765  0.2182211538    0.1716182
      0.797  0.2545913462  0.145146883
     0.8175  0.2866826923  0.119277866
      0.838  0.3230528846  0.094053968
     0.8585  0.3572836538  0.069508459
      0.879  0.3957932692  0.045661041
     0.8995  0.4471394231  0.022509336
       0.92  0.5241586538            0
**$        Sl       krg       krog
SLT
        0.1         1         0
    0.15625    0.9375    0.0625
     0.2125     0.875     0.125
    0.26875    0.8125    0.1875
      0.325      0.75      0.25
    0.38125    0.6875    0.3125
     0.4375     0.625     0.375
    0.49375    0.5625    0.4375
       0.55       0.5       0.5
    0.60625    0.4375    0.5625
     0.6625     0.375     0.625
    0.71875    0.3125    0.6875
      0.775      0.25      0.75
    0.83125    0.1875    0.8125
     0.8875     0.125       .82
    0.94375    0.0625       .83
          1         0       .89


SWR 0.1
SWCRIT 0.1
```

```
SORW 0.12
SOIRW 0.12
KRWRO .6
KRWIRO .6
KROCW  .89

ADSCOMP 'SURF' WATER
ADSLANG 270 0 1000
ADMAXT .28
ADSCOMP 'ALK' WATER
ADSLANG 20 0 1000
ADMAXT .02
INITIAL
VERTICAL OFF

INITREGION 1
**$ Property: Pressure (kPa)   Max: 101.3  Min: 101.3
PRES CON        101.3
**$ Property: Pressure (kPa)   Max: 101.3  Min: 101.3
PRES CON        101.3
**$ Property: Water Saturation  Max: 0.48  Min: 0.48
SW CON         0.48
**$ Property: Oil Saturation  Max: 0.52  Min: 0.52
SO CON         0.52
**$ Property: Water Mole Fraction(ALK)  Max: 0  Min: 0
MFRAC_WAT 'ALK' CON           0
**$ Property: Water Mole Fraction(H2O)  Max: 1  Min: 1
MFRAC_WAT 'H2O' CON           1
**$ Property: Water Mole Fraction(SURF)  Max: 0  Min: 0
MFRAC_WAT 'SURF' CON           0
**$ Property: Oil Mole Fraction(HVYOIL)  Max: 1  Min: 1
MFRAC_OIL 'HVYOIL' CON           1
NUMERICAL
NORM PRESS 10 SATUR 0.05 Y 0.05 X 0.05 W 0.05 ZO 0.05 ZNCG 0.05 ZAQ 0.05
DTMIN 1e-20
MATBALITER 30
NEWTONCYC 30
NORTH 200
ITERMAX 100
MINPRES .01
NCUTS 20
RUN
DATE 1901 1 1
DTWELL 1e-007
**$
WELL  'Well-1'
INJECTOR UNWEIGHT 'Well-1'
INCOMP  WATER  0.999134654  1.19033e-005  0.000853443  0.  0.
TINJW  25.
OPERATE  MAX  STW  2.592e-005  CONT
```

```
**$ UBA    ff  Status  Connection
**$ UBA      ff  Status  Connection
**$         rad  geofac  wfrac  skin
GEOMETRY  K  0.00086  0.249  1.  0.
PERF  GEOA  'Well-1'
**$ UBA     ff  Status  Connection
   1 1 100   1.  OPEN    FLOW-FROM  'SURFACE'  REFLAYER
   2 1 100   1.  OPEN    FLOW-FROM  1
   3 1 100   1.  OPEN    FLOW-FROM  2
   4 1 100   1.  OPEN    FLOW-FROM  3
   5 1 100   1.  OPEN    FLOW-FROM  4
   6 1 100   1.  OPEN    FLOW-FROM  5
   7 1 100   1.  OPEN    FLOW-FROM  6
   8 1 100   1.  OPEN    FLOW-FROM  7
   9 1 100   1.  OPEN    FLOW-FROM  8
   10 1 100  1.  OPEN    FLOW-FROM  9
   11 1 100  1.  OPEN    FLOW-FROM  10
   12 1 100  1.  OPEN    FLOW-FROM  11
   13 1 100  1.  OPEN    FLOW-FROM  12
   14 1 100  1.  OPEN    FLOW-FROM  13
   15 1 100  1.  OPEN    FLOW-FROM  14
   16 1 100  1.  OPEN    FLOW-FROM  15
   17 1 100  1.  OPEN    FLOW-FROM  16
   18 1 100  1.  OPEN    FLOW-FROM  17
   19 1 100  1.  OPEN    FLOW-FROM  18
   20 1 100  1.  OPEN    FLOW-FROM  19
   21 1 100  1.  OPEN    FLOW-FROM  20
   22 1 100  1.  OPEN    FLOW-FROM  21
   23 1 100  1.  OPEN    FLOW-FROM  22
   24 1 100  1.  OPEN    FLOW-FROM  23
   25 1 100  1.  OPEN    FLOW-FROM  24
   26 1 100  1.  OPEN    FLOW-FROM  25
   27 1 100  1.  OPEN    FLOW-FROM  26
   28 1 100  1.  OPEN    FLOW-FROM  27
   29 1 100  1.  OPEN    FLOW-FROM  28
   30 1 100  1.  OPEN    FLOW-FROM  29
   31 1 100  1.  OPEN    FLOW-FROM  30
   32 1 100  1.  OPEN    FLOW-FROM  31
   33 1 100  1.  OPEN    FLOW-FROM  32
   34 1 100  1.  OPEN    FLOW-FROM  33
   35 1 100  1.  OPEN    FLOW-FROM  34
   36 1 100  1.  OPEN    FLOW-FROM  35
   37 1 100  1.  OPEN    FLOW-FROM  36
   38 1 100  1.  OPEN    FLOW-FROM  37
   39 1 100  1.  OPEN    FLOW-FROM  38
   40 1 100  1.  OPEN    FLOW-FROM  39
   41 1 100  1.  OPEN    FLOW-FROM  40
   42 1 100  1.  OPEN    FLOW-FROM  41
   43 1 100  1.  OPEN    FLOW-FROM  42
   44 1 100  1.  OPEN    FLOW-FROM  43
```

```
   45 1 100  1.  OPEN    FLOW-FROM  44
   46 1 100  1.  OPEN    FLOW-FROM  45
   47 1 100  1.  OPEN    FLOW-FROM  46
   48 1 100  1.  OPEN    FLOW-FROM  47
   49 1 100  1.  OPEN    FLOW-FROM  48
   50 1 100  1.  OPEN    FLOW-FROM  49
   51 1 100  1.  OPEN    FLOW-FROM  50
   52 1 100  1.  OPEN    FLOW-FROM  51
   53 1 100  1.  OPEN    FLOW-FROM  52
   54 1 100  1.  OPEN    FLOW-FROM  53
   55 1 100  1.  OPEN    FLOW-FROM  54
   56 1 100  1.  OPEN    FLOW-FROM  55
   57 1 100  1.  OPEN    FLOW-FROM  56
   58 1 100  1.  OPEN    FLOW-FROM  57
   59 1 100  1.  OPEN    FLOW-FROM  58
   60 1 100  1.  OPEN    FLOW-FROM  59
   61 1 100  1.  OPEN    FLOW-FROM  60
   62 1 100  1.  OPEN    FLOW-FROM  61
   63 1 100  1.  OPEN    FLOW-FROM  62
   64 1 100  1.  OPEN    FLOW-FROM  63
   65 1 100  1.  OPEN    FLOW-FROM  64
   66 1 100  1.  OPEN    FLOW-FROM  65
   67 1 100  1.  OPEN    FLOW-FROM  66
   68 1 100  1.  OPEN    FLOW-FROM  67
   69 1 100  1.  OPEN    FLOW-FROM  68
   70 1 100  1.  OPEN    FLOW-FROM  69
   71 1 100  1.  OPEN    FLOW-FROM  70
   72 1 100  1.  OPEN    FLOW-FROM  71
   73 1 100  1.  OPEN    FLOW-FROM  72
   74 1 100  1.  OPEN    FLOW-FROM  73
   75 1 100  1.  OPEN    FLOW-FROM  74
   76 1 100  1.  OPEN    FLOW-FROM  75
   77 1 100  1.  OPEN    FLOW-FROM  76
   78 1 100  1.  OPEN    FLOW-FROM  77
   79 1 100  1.  OPEN    FLOW-FROM  78
   80 1 100  1.  OPEN    FLOW-FROM  79
**$
WELL  'Well-2'
PRODUCER 'Well-2'
OPERATE  MIN  BHP  101.3  CONT
**$ UBA     ff  Status  Connection
**$         rad  geofac  wfrac  skin
GEOMETRY  K  0.00086  0.249  1.  0.
PERF  GEOA  'Well-2'
**$ UBA       ff  Status  Connection
   1 1 1   1.  OPEN    FLOW-TO  'SURFACE'  REFLAYER
   2 1 1   1.  OPEN    FLOW-TO  1
   3 1 1   1.  OPEN    FLOW-TO  2
   4 1 1   1.  OPEN    FLOW-TO  3
   5 1 1   1.  OPEN    FLOW-TO  4
```

6 1 1 1. OPEN FLOW-TO 5
7 1 1 1. OPEN FLOW-TO 6
8 1 1 1. OPEN FLOW-TO 7
9 1 1 1. OPEN FLOW-TO 8
10 1 1 1. OPEN FLOW-TO 9
11 1 1 1. OPEN FLOW-TO 10
12 1 1 1. OPEN FLOW-TO 11
13 1 1 1. OPEN FLOW-TO 12
14 1 1 1. OPEN FLOW-TO 13
15 1 1 1. OPEN FLOW-TO 14
16 1 1 1. OPEN FLOW-TO 15
17 1 1 1. OPEN FLOW-TO 16
18 1 1 1. OPEN FLOW-TO 17
19 1 1 1. OPEN FLOW-TO 18
20 1 1 1. OPEN FLOW-TO 19
21 1 1 1. OPEN FLOW-TO 20
22 1 1 1. OPEN FLOW-TO 21
23 1 1 1. OPEN FLOW-TO 22
24 1 1 1. OPEN FLOW-TO 23
25 1 1 1. OPEN FLOW-TO 24
26 1 1 1. OPEN FLOW-TO 25
27 1 1 1. OPEN FLOW-TO 26
28 1 1 1. OPEN FLOW-TO 27
29 1 1 1. OPEN FLOW-TO 28
30 1 1 1. OPEN FLOW-TO 29
31 1 1 1. OPEN FLOW-TO 30
32 1 1 1. OPEN FLOW-TO 31
33 1 1 1. OPEN FLOW-TO 32
34 1 1 1. OPEN FLOW-TO 33
35 1 1 1. OPEN FLOW-TO 34
36 1 1 1. OPEN FLOW-TO 35
37 1 1 1. OPEN FLOW-TO 36
38 1 1 1. OPEN FLOW-TO 37
39 1 1 1. OPEN FLOW-TO 38
40 1 1 1. OPEN FLOW-TO 39
41 1 1 1. OPEN FLOW-TO 40
42 1 1 1. OPEN FLOW-TO 41
43 1 1 1. OPEN FLOW-TO 42
44 1 1 1. OPEN FLOW-TO 43
45 1 1 1. OPEN FLOW-TO 44
46 1 1 1. OPEN FLOW-TO 45
47 1 1 1. OPEN FLOW-TO 46
48 1 1 1. OPEN FLOW-TO 47
49 1 1 1. OPEN FLOW-TO 48
50 1 1 1. OPEN FLOW-TO 49
51 1 1 1. OPEN FLOW-TO 50
52 1 1 1. OPEN FLOW-TO 51
53 1 1 1. OPEN FLOW-TO 52
54 1 1 1. OPEN FLOW-TO 53
55 1 1 1. OPEN FLOW-TO 54

```
   56 1 1  1.  OPEN    FLOW-TO  55
   57 1 1  1.  OPEN    FLOW-TO  56
   58 1 1  1.  OPEN    FLOW-TO  57
   59 1 1  1.  OPEN    FLOW-TO  58
   60 1 1  1.  OPEN    FLOW-TO  59
   61 1 1  1.  OPEN    FLOW-TO  60
   62 1 1  1.  OPEN    FLOW-TO  61
   63 1 1  1.  OPEN    FLOW-TO  62
   64 1 1  1.  OPEN    FLOW-TO  63
   65 1 1  1.  OPEN    FLOW-TO  64
   66 1 1  1.  OPEN    FLOW-TO  65
   67 1 1  1.  OPEN    FLOW-TO  66
   68 1 1  1.  OPEN    FLOW-TO  67
   69 1 1  1.  OPEN    FLOW-TO  68
   70 1 1  1.  OPEN    FLOW-TO  69
   71 1 1  1.  OPEN    FLOW-TO  70
   72 1 1  1.  OPEN    FLOW-TO  71
   73 1 1  1.  OPEN    FLOW-TO  72
   74 1 1  1.  OPEN    FLOW-TO  73
   75 1 1  1.  OPEN    FLOW-TO  74
   76 1 1  1.  OPEN    FLOW-TO  75
   77 1 1  1.  OPEN    FLOW-TO  76
   78 1 1  1.  OPEN    FLOW-TO  77
   79 1 1  1.  OPEN    FLOW-TO  78
   80 1 1  1.  OPEN    FLOW-TO  79
**$
**WLISTSHUT 'Well-1'
DATE 1901 1  1.04167
DATE 1901 1  2.58333
DATE 1901 1  2.62500
DATE 1901 1  2.66667
DATE 1901 1  2.70833
DATE 1901 1  2.75000
DATE 1901 1  2.79167
DATE 1901 1  4.79167
DATE 1901 1  4.83333
DATE 1901 1  4.87500
DATE 1901 1  4.91667
DATE 1901 1  4.95833
DATE 1901 1  5.00000
DATE 1901 1  6.00000
DATE 1901 1  7.00000
DATE 1901 1  8.00000
DATE 1901 1  9.00000
DATE 1901 1  10.00000

WELL  'Well-1'
INJECTOR UNWEIGHT 'Well-1'
INCOMP  WATER  0.999134654  1.19033e-005  0.000853443  0.  0.
TINJW  25.
```

```
OPERATE  MAX  STW  2.592e-005  CONT

DATE 1901 1  11.00000
DATE 1901 1  12.00000
DATE 1901 1  13.00000
DATE 1901 1  14.00000
DATE 1901 1  15.00000
DATE 1901 1  16.00000
DATE 1901 1  17.00000
DATE 1901 1  18.00000

STOP
```

A.4 ASP FLOOD SIMULATION OF THE 330 CP OIL

The ASP flood simulations were conducted using the UTCHEM simulator. This section gives the input file for the simulations.

```
CC*************************************************************************
CC                                                                       *
CC   BRIEF DESCRIPTION OF DATA SET : UTCHEM (VERSION 2011_7)      *
CC                                                                       *
CC*************************************************************************
CC                                                                       *
CC  SURFACTANT POLYMER   FLOODING                                *
CC                                                                       *
CC  LENGTH (FT) :               PROCESS : A/S/P FLOODING       *
CC  THICKNESS (FT) :             INJ. PRESSURE (PSI) :          *
CC  WIDTH (FT) : 100.            COORDINATES : CARTESIAN        *
CC  POROSITY :                                  *
CC  GRID BLOCKS : 100X1X1                                *
CC  DATE :                                    *
CC                                                                       *
CC*************************************************************************
CC
CC*************************************************************************
CC                                                                       *
CC   RESERVOIR DESCRIPTION                                *
CC                                                                       *
CC*************************************************************************
CC
CC
*----RUNNO
ALs-01
CC
CC
*----HEADER
 sandpackflood  ALS-1
Experiment  25 C   using simple ASP with UTCHEM2011_7
*************************************************************
CC
CC SIMULATION FLAGS
*---- IMODE IMES IDISPC ICWM ICAP IREACT IBIO ICOORD ITREAC ITC IGAS IENG
      1  4   3     0   0    5     0   1    0     0   0  0
CC
CC  NUMBER  OF  GRID  BLOCKS  AND  FLAG  SPECIFIES  CONSTANT  OR  VARIABLE
GRID SIZE
*----NX   NY  NZ  IDXYZ  IUNIT
    100   1  1  0      1
CC
CC  CONSTANT GRID BLOCK SIZE IN X, Y, AND Z
*----DX        DY        DZ
```

```
   0.009144    0.0125      0.0125
CC
CC TOTAL NO. OF COMPONENTS, NO. OF TRACERS, NO. OF GEL COMPONENTS
*----N   no NTw nta ngc  ng  noth
   12    0 0   0 4    0    0
CC
CC
*---- SPNAME(I),I=1,N
WATER
OIL
SURFACTANT
POLYMER
ANION
CALCIUM
alc1
alc2
SODIUM
hydrogen
alkali
HAo
CC
CC FLAG INDICATING IF THE COMPONENT IS INCLUDED IN CALCULATIONS OR
NOT
*----ICF(KC) FOR KC=1,N
   1  1  1  1  1  0   0  0  1  0   1  0
CC
CC**********************************************************************
CC                                          *
CC    OUTPUT OPTIONS                                *
CC                                          *
CC**********************************************************************
CC
CC
CC  FLAG FOR PV OR DAYS FOR OUTPUT AND STOP THE RUN
*----ICUMTM  ISTOP   IOUTGMS  IS3G
      1       1    0      0
CC
CC FLAG INDICATING IF THE PROFILE OF KCTH COMPONENT SHOULD BE WRITTEN
*----IPRFLG(KC),KC=1,N
   1  1  1  1  1  0  0  0  1  0  1  0
CC
CC  FLAG  FOR  PRES,SAT.,TOTAL  CONC.,TRACER  CONC.,CAP.,GEL,  ALKALINE
PROFILES
*----IPPRES IPSAT IPCTOT IPBIO IPCAP IPGEL IPALK ITEMP    IPOBS
    1     1     1     0     0     0   1     0       0
CC
CC FLAG FOR WRITING SEVERAL PROPERTIES
*----ICKL IVIS IPER ICNM  ICSE IFOAM IHYST  INONEQ
    1     1    1    1    1    0     0      0
CC
CC FLAG FOR WRITING SEVERAL PROPERTIES TO PROF
*----IADS  IVEL IRKF IPHSE
```

```
    1    0    1    1
CC
CC*********************************************************************
CC                                        *
CC   RESERVOIR PROPERTIES                                 *
CC                                        *
CC*********************************************************************
CC
CC
CC MAX. SIMULATION TIME ( PV)
*---- TMAX
    5.735
CC
CC ROCK COMPRESSIBILITY (1/PSI), STAND. PRESSURE(PSIA)
*----COMPR   PSTAND
    0.      0.
CC
CC  FLAGS  INDICATING  CONSTANT  OR  VARIABLE  POROSITY,  X,Y,AND  Z
PERMEABILITY
*----IPOR1 IPERMX IPERMY IPERMZ  IMOD   ITRANZ  INTG
     0     0    3     3     0      0      0
CC
CC CONSTANT POROSITY
*----PORC1
   .456
CC
CC CONSTANT X-PERMEABILITY (MILIDARCY) FOR LAYER K = 1,NZ
*----PERMX
   25650
CC
CC Y DIRECTION PERMEABILITY IS DEPENDENT ON X DIRECTION PERMEABILITY
*---- CONSTANT PERMEABILITY MULTIPLIER FOR Y DIRECTION PERMEABILITY
      1
CC
CC Z DIRECTION PERMEABILITY IS DEPENDENT ON X DIRECTION PERMEABILITY
*---- CONSTANT PERMEABILITY MULTIPLIER FOR Z DIRECTION PERMEABILITY
      1
CC
CC FLAG FOR CONSTANT OR VARIABLE DEPTH, PRESSURE, WATER SATURATION
*----IDEPTH  IPRESS  ISWI  ICWI
    0       0      0    -1
CC
CC CONSTANT DEPTH (FT)
*----D111
   0.
CC
CC INITIAL PRESSURE (PSIA)
*----PINIT   DEPTH
   101.3    0.0
CC
CC CONSTANT INITIAL WATER SATURATION (residual oil)
*----SWI
```

```
  0.2
CC
CC CONSTANT CHLORIDE AND CALCIUM CONCENTRATIONS (MEQ/ML)
*----C50      C60
  0.3419    0.0
CC
CC*********************************************************************
CC                                        *
CC   PHYSICAL PROPERTY DATA                          *
CC                                        *
CC*********************************************************************
CC
CC 3.4.1 OIL CONC. AT PLAIT POINT FOR TYPE II(+)AND TYPE II(-), CMC
CC               CMC
*---- c2plc  c2prc   epsme   ihand
      0     1    0.001    0
CC
CC 3.4.2 flag indicating type of phase behavior parameters
*---- ifghbn=0 for input height of binodal curve; =1 for input sol. ratio
      0
CC 3.4.3 SLOPE AND INTERCEPT OF BINODAL CURVE AT ZERO, OPT., AND 2XOPT
SALINITY
CC FOR ALCOHOL 1
*---- hbns70   hbnc70   hbns71   hbnc71   hbns72   hbnc72
      0   0.05      0.35    0.03    0    0.05
CC 3.4.5 SLOPE AND INTERCEPT OF BINODAL CURVE AT ZERO, OPT., AND 2XOPT
SALINITY
CC FOR ALCOHOL 2
*---- hbns80  hbnc80  hbns81  hbnc81  hbns82  hbnc82
      0      0.05      0   0.025      0   0.05
CC
CC 3.4.6 LOWER AND UPPER EFFECTIVE SALINITY FOR ALCOHOL 1 AND ALCOHOL
2
*---- csel7   cseu7   csel8   cseu8
     0.3   0.6    0.05   0.4
CC 3.4.7 THE CSE SLOPE PARAMETER FOR CALCIUM AND ALCOHOL 1 AND
ALCOHOL 2
CC   Ca    Alcohol#1  Alcohol#2
*---- beta6    beta7    beta8
      0       0       0
CC
CC 3.4.8 FLAG FOR ALCOHOL PART. MODEL AND PARTITION COEFFICIENTS
*---- ialc   opsk7o   opsk7s   opsk8o   opsk8s
      0     0       0       0       0
CC  these are used only for alcohol partitioning in a two alcohol system:
CC 3.4.9 NO. OF ITERATIONS, AND TOLERANCE
*---- nalmax     epsalc
      20       0.0001
CC 3.4.10 ALCOHOL 1 PARTITIONING PARAMETERS IF IALC=1
CC   aq-oleic   aq-oleic  surf-oleic
*---- akwc7     akws7     akm7      ak7      pt7
     4.671    1.79      48      35.31    0.222
```

```
CC
CC 3.4.11 ALCOHOL 2 PARTITIONING PARAMETERS IF IALC=1
*---- akwc8     akws8    akm8    ak8     pt8
      0         0        0       0       0
CC
CC 3.4.22 ift model flag
*----  ift=0 for Healy&Reed; =1 for Chun Huh correl.
       1
CC 3.4.24 INTERFACIAL TENSION PARAMETERS
CC    typ=.1-.35   typ=5-20
*---- chuh         ahuh
     0.3           10
CC 3.4.25 LOG10 OF OIL/WATER INTERFACIAL TENSION
CC     units of log 10 dynes/cm = mN/m
*---- xiftw
      1.3
CC 3.4.26 ORGANIC MASS TRANSFER FLAG
CC    imass=0 for no oil sol. in water.  icorr=0 for constant MTC
*---- imass   icor
      0       0
cc
cc
*---  iwalt   iwalf
      0       0
CC 3.4.31 CAPILLARY DESATURATION PARAMETERS FOR PHASE 1, 2, AND 3 dont
increase t22, dont decrease t33
CC              AQ     OLEIC     ME
*---- itrap      t11      t22      t33
      2        1065     2030     5420
CC
CC  3.4.32 FLAG FOR RELATIVE PERMEABILITY AND CAPILLARY PRESSURE MODEL
*---- iperm=0 for constant; =1 varies by layer; =2 varies by gridblock
      0       0
CC
CC 3.4.35 FLAG FOR CONSTANT OR VARIABLE REL. PERM. PARAMETERS
*---- isrw    iprw    iew
      0       0       0
CC
CC CONSTANT RES. SATURATION OF PHASES 1,2,AND 3 AT LOW CAPILLARY NO.
*----S1RWC  S2RWC  S3RWC
     0.2     0.12    .3
CC
CC CONSTANT ENDPOINT REL. PERM. OF PHASES 1,2,AND 3 AT LOW CAPILLARY
NO.
*----P1RW  P2RW  P3RW
     0.06   0.7   .3
CC
CC CONSTANT REL. PERM. EXPONENT OF PHASES 1,2,AND 3 AT LOW CAPILLARY
NO.
*----E1W     E2W  E3W
    3.3     2.0   2
CC
```

```
CC  RES. SATURATION OF PHASES 1,2,AND 3 AT HIGH CAPILLARY NO.
*----S1RC  S2RC  S3RC
  .042   .0  .0
CC
CC ENDPOINT REL. PERM. OF PHASES 1,2,AND 3 AT HIGH CAPILLARY NO.
*----P1RC    P2RC  P3RC
   1    1.0  1.0
CC
CC REL. PERM. EXPONENT OF PHASES 1,2,AND 3 AT HIGH CAPILLARY NO.
*----E13CW  E23C  E31C
  1.0      1.0   1.0
CC 3.4.61 WATER AND OIL VISCOSITY , RESERVOIR TEMPERATURE
CC   water     oil       =0 for isothermal modeling
*---- VIS1     VIS2   TSTAND
     1     330      0
CC
CC 3.4.80 COMPOSITIONAL PHASE VISCOSITY PARAMETERS for microemulsion
*----   ALPHAV1   ALPHAV2   ALPHAV3   ALPHAV4  ALPHAV5
       0     0     0.       0     0
CC
CC  3.4.81  PARAMETERS  TO  CALCULATE  POLYMER  VISCOSITY  AT  ZERO  SHEAR
RATE
*---- AP1      AP2      AP3
    14.6683   0      3655.01
CC
CC 3.4.82 PARAMETER TO COMPUTE CSEP,MIN. CSEP, AND SLOPE OF LOG VIS. VS.
LOG CSEP
*---- BETAP    CSE1     SSLOPE
     1      0.01      -0.774
CC
CC 3.4.83 PARAMETER FOR SHEAR RATE DEPENDENCE OF POLYMER VISCOSITY
*---- GAMMAC   GAMHF   POWN  IPMOD  ishear  rweff  gamhf2
     0.0585     0.7    1.8   0      0       0.    0.0
CC
CC 3.4.84  FLAG FOR POLYMER PARTITIONING, PERM. REDUCTION PARAMETERS
*---- IPOLYM    EPHI3    EPHI4    BRK     CRK     rkcut
      0       1.0      1.0     10.0      0.01   0
CC 3.4.85 SPECIFIC WEIGHT FOR COMPONENTS 1,2,3,7,8 ,Coeffient of oil and GRAVITY
FLAG
CC   if IDEN=1 ignore gravity effect; =2 then include gravity effect
*---- DEN1     DEN2      DEN23     DEN3     DEN7    DEN8    IDEN
     1    1  0.4065     0.42     0.346   0       1
CC   ISTB=0:BOTTOMHOLE CONDITION , 1: STOCK TANK
CC 3.4.93 FLAG FOR CHOICE OF UNITS when printing
*----- ISTB
       1
CC  3.4.94 FORMATION VOLUME FACTOR - may set all these to 1.0 and just factor in post-
proc
CC       water   oil        me
*----- FVF(I), I=1 TO MXP (IGAS=0 MXP=3,IGAS=1 MXP=4)
         1.0        1.0        1
CC
```

```
CC 3.4.95 COMPRESSIBILITY FOR VOL. OCCUPYING COMPONENTS 1,2,3,7,AND 8
*----  COMPC(1)        COMPC(2)    COMPC(3)  COMPC(7)  COMPC(8)
       0.0      0.0        0        0        0
CC  IOW=0 water wet, =1 oil wet, =2 mixed wet
CC 3.4.99 CONSTANT OR VARIABLE PC PARAM., WATER-WET OR OIL-WET PC CURVE FLAG
*---- ICPC    IEPC   IOW
     0      0     0
CC
CC 3.4.100 CAPILLARY PRESSURE PARAMETER, CPC0
*---- CPC0
     0.0
CC
CC 3.4.103 CAPILLARY PRESSURE PARAMETER, EPC0
*---- EPC0
     0.0
CC
CC 3.4.117 MOLECULAR DIFFUSION COEF. KCTH COMPONENT IN PHASE 1
*---- D(KC,1),KC=1,N
      0       0       0       0       0       0       0       0       0       0       0       0
CC
CC 3.4.118 MOLECULAR DIFFUSION COEF. KCTH COMPONENT IN PHASE 2
*---- D(KC,2),KC=1,N
      0       0       0       0       0       0       0       0       0       0       0       0
CC
CC 3.4.119 MOLECULAR DIFFUSION COEF. KCTH COMPONENT IN PHASE 3
*---- D(KC,3),KC=1,N
      0       0       0       0       0       0       0       0       0       0       0       0
CC
CC 3.4.121 LONGITUDINAL AND TRANSVERSE DISPERSIVITY OF PHASE 1
*---- ALPHAL(1)     ALPHAT(1)
      0.01          0.001
CC
CC 3.4.122 LONGITUDINAL AND TRANSVERSE DISPERSIVITY OF PHASE 2
*---- ALPHAL(2)     ALPHAT(2)
      0.01          0.001
CC
CC 3.4.124 LONGITUDINAL AND TRANSVERSE DISPERSIVITY OF PHASE 3
*---- ALPHAL(3)     ALPHAT(3)
      0.01          0.001
CC
CC 3.4.125 flag to specify organic adsorption calculation
*---- iadso=0 if organic adsorption is not considered
     0
CC
CC 3.4.130 SURFACTANT AND POLYMER ADSORPTION PARAMETERS
*---- AD31    AD32     B3D    AD41    AD42   B4D   IADK  IADS1   FADS   REFK
    0.16     0.1    1000     0.     0.1     10    0     0      0      50
 cc
 cc
 *---  acid number EQW   phtol   soapk
     1.47         1520   8.5      0.02
```

```
cc
cc
*--- cselp, cseup, EQWSP
    0.05    0.4   500
cc
cc
*--- imix
    0
cc
cc
*---  c160    iphad
    8       1
cc
cc
*--- 7   13   13  0.1
    0.1
cc
cc
*---  cna      calk    alkcrit
    0.34188    0.0    0.01
cc
cc  Need to estimate for carbonate adsorption
*---   alkad   alkbd
     5      1000
cc
cc
*----  icatex
     0
CC
CC**********************************************************************
CC                                          *
CC    WELL DATA                                     *
CC                                          *
CC**********************************************************************
CC
CC
CC FLAG FOR PRESSURE CONST. BOUNDARIES
*---- IBOUND  IZONE
    0    0
CC
CC TOTAL NUMBER OF WELLS, WELL RADIUS FLAG, FLAG FOR TIME OR COURANT
NO.
*----NWELL   IRO   ITIME  NWREL
    2     2     1     2
CC
CC WELL ID,LOCATIONS,AND FLAG FOR SPECIFYING WELL TYPE, WELL RADIUS,
SKIN
*----IDW   IW    JW    IFLAG    RW     SWELL  IDIR   IFIRST  ILAST  IPRF
    1   1     1     1   .003      0.    3     1    1    0
CC
CC WELL NAME
*---- WELNAM
```

```
INJECTOR
CC
CC ICHEK MAX. AND MIN. ALLOWABLE BOTTOMHOLE PRESSURE AND RATE
*----ICHEK   PWFMIN   PWFMAX  QTMIN   QTMAX
    0    0.0    5000.  0.0    50000.
CC
CC WELL ID, LOCATION, AND FLAG FOR SPECIFYING WELL TYPE, WELL RADIUS,
SKIN
*----IDW  IW   JW   IFLAG   RW    SWELL  IDIR  IFIRST   ILAST   IPRF
   2   100    1    2      .003    0.     3    1      1      0
CC
CC WELL NAME
*---- WELNAM
PRODUCER
CC
CC MAX. AND MIN. ALLOWABLE BOTTOMHOLE PRESSURE AND RATE
*----ICHEK  PWFMIN   PWFMAX  QTMIN   QTMAX
    0    0.0    5000.  0.0    50000.
CC
CC ID,INJ. RATE AND INJ. COMP. FOR RATE CONS. WELLS FOR EACH PHASE (L=1,3)
*----ID   QI(M,L)   C(M,KC,L)   2.75 wt% Sodium carbonate, 1.3 ft/d   cl   ca na    hydrogen
carbonate  pH
     1   0.00002592   1  0.  0.0   0.  0.3419  0.  0.   0.   0.3419  8      0.   0.0
     1      0.   0.   0.  0.    0.       0.    0.   0.   0.      0.   0.    0.   0.
     1      0.   0.   0.  0.    0.       0.    0.   0.   0.      0.   0.    0.   0.
CC
CC ID,
*----ID   PWF
   2   101.3
CC
CC CUM. INJ. TIME , AND INTERVALS (PV OR DAY) FOR WRITING TO OUTPUT FILES
*----TINJ   CUMPR1  CUMHI1   WRHPV  WRPRF    RSTC
   3.3      0.01     0.01      0.01   0.01     0.3
CC
CC FOR IMES=2 ,THE INI. TIME STEP,CONC. TOLERANCE,MAX.,MIN. COURANT NO.
*----DT     DCLIM    CNMAX   CNMIN
   0.0001   12*0.01    0.1    0.01
CC******    INJECT surfactant **********************
CC FLAG FOR INDICATING BOUNDARY CHANGE
*---- IBMOD
      0
CC
CC  IRO, ITIME, NEW FLAGS FOR ALL THE WELLS
*----  IRO   ITIME    IFLAG
      2      1       1  2
CC
CC  NUMBER OF WELLS CHANGES IN LOCATION OR SKIN OR PWF
*----  NWEL1
       0
CC
CC  NUMBER OF WELLS WITH RATE CHANGES, ID
*---- NWEL2    ID
```

```
      1       1
CC
CC  ID,INJ. RATE AND INJ. COMP. FOR RATE CONS. WELLS FOR EACH PHASE (L=1,3)
*---- ID      QI(M,L) water oil  surf polymer Chlor divalent  cl          ca                  na       pH
carbonate  hAo
      1   0.00002592  0.996   0.  0.004   0.38    0.3419  0. 0.    0.  0.625   11   0.283     0
      1      0.   0.   0.  0.    0.       0.    0.   0.   0.      0.   0.    0.   0.
      1      0.   0.   0.  0.    0.       0.    0.   0.   0.      0.   0.    0.   0.
CC
CC  CUM. INJ. TIME , AND INTERVALS (PV) FOR WRITING TO OUTPUT FILES
*---- TINJ          CUMPR1         CUMHI1      WRHPV      WRPRF     RSTC
     3.57          0.03      0.03       0.03    0.03       2.0
CC
CC  FOR IMES=4 ,THE INI. TIME STEP,CONC. TOLERANCE,MAX.,MIN. TIME STEPS
*---- DT           DCLIM       CNMAX      CNMIN
      0.0001       12*0.01      0.1         0.01
CC******    INJECT surfactant **********************
CC FLAG FOR INDICATING BOUNDARY CHANGE
*---- IBMOD
      0
CC
CC  IRO, ITIME, NEW FLAGS FOR ALL THE WELLS
*---- IRO    ITIME     IFLAG
      2      1        1  2
CC
CC  NUMBER OF WELLS CHANGES IN LOCATION OR SKIN OR PWF
*----  NWEL1
       0
CC
CC  NUMBER OF WELLS WITH RATE CHANGES, ID
*---- NWEL2     ID
      1       1
CC
CC  ID,INJ. RATE AND INJ. COMP. FOR RATE CONS. WELLS FOR EACH PHASE (L=1,3)
*----  ID      QI(M,L) water oil  surf polymer Chlor divalent  cl          ca                  na       pH
carbonate  hAo
      1   0.00002592  1.0   0.  0.0   0.38   0.3419  0. 0.    0.  0.3419   8   0.0     0
      1      0.   0.   0.  0.    0.       0.    0.   0.   0.      0.   0.    0.   0.
      1      0.   0.   0.  0.    0.       0.    0.   0.   0.      0.   0.    0.   0.
CC
CC  CUM. INJ. TIME , AND INTERVALS (PV) FOR WRITING TO OUTPUT FILES
*---- TINJ          CUMPR1         CUMHI1      WRHPV      WRPRF     RSTC
     4.52          0.03      0.03       0.03    0.03       2.0
CC
CC  FOR IMES=4 ,THE INI. TIME STEP,CONC. TOLERANCE,MAX.,MIN. TIME STEPS
*---- DT           DCLIM       CNMAX      CNMIN
      0.0001       12*0.01      0.1         0.01
CC******    INJECT surfactant **********************
CC FLAG FOR INDICATING BOUNDARY CHANGE
*---- IBMOD
      0
CC
```

```
CC  IRO, ITIME, NEW FLAGS FOR ALL THE WELLS
*---- IRO   ITIME    IFLAG
      2      1       1 2
CC
CC  NUMBER OF WELLS CHANGES IN LOCATION OR SKIN OR PWF
*----  NWEL1
       0
CC
CC  NUMBER OF WELLS WITH RATE CHANGES, ID
*---- NWEL2    ID
      1       1
CC
CC  ID,INJ. RATE AND INJ. COMP. FOR RATE CONS. WELLS FOR EACH PHASE (L=1,3)
*----  ID      QI(M,L) water oil  surf polymer Chlor divalent  cl          ca                  na       pH
carbonate  hAo
      1   0.00002592  1.0   0.  0.0   0.29    0.3419  0. 0.    0.  0.3419   8   0.0     0
      1      0.    0.    0.   0.     0.        0.     0.    0.    0.       0.    0.     0.    0.
      1      0.    0.    0.   0.     0.        0.     0.    0.    0.       0.    0.     0.    0.
CC
CC  CUM. INJ. TIME , AND INTERVALS (PV) FOR WRITING TO OUTPUT FILES
*---- TINJ          CUMPR1         CUMHI1     WRHPV     WRPRF     RSTC
     5.0307         0.03      0.03       0.03    0.03       2.0
CC
CC  FOR IMES=4 ,THE INI. TIME STEP,CONC. TOLERANCE,MAX.,MIN. TIME STEPS
*----  DT          DCLIM       CNMAX      CNMIN
       0.0001      12*0.01     0.1        0.01
CC******     INJECT surfactant **********************
CC FLAG FOR INDICATING BOUNDARY CHANGE
*---- IBMOD
       0
CC
CC  IRO, ITIME, NEW FLAGS FOR ALL THE WELLS
*---- IRO   ITIME    IFLAG
      2      1       1 2
CC
CC  NUMBER OF WELLS CHANGES IN LOCATION OR SKIN OR PWF
*----  NWEL1
       0
CC
CC  NUMBER OF WELLS WITH RATE CHANGES, ID
*---- NWEL2    ID
      1       1
CC
CC  ID,INJ. RATE AND INJ. COMP. FOR RATE CONS. WELLS FOR EACH PHASE (L=1,3)
*----  ID      QI(M,L) water oil  surf polymer Chlor divalent  cl          ca                  na       pH
carbonate  hAo
      1   0.00002592  1.0   0.  0.0   0.2    0.3419  0. 0.    0.  0.3419   8   0.0     0
      1      0.    0.    0.   0.     0.        0.     0.    0.    0.       0.    0.     0.    0.
      1      0.    0.    0.   0.     0.        0.     0.    0.    0.       0.    0.     0.    0.
CC
CC  CUM. INJ. TIME , AND INTERVALS (PV) FOR WRITING TO OUTPUT FILES
*---- TINJ          CUMPR1         CUMHI1     WRHPV     WRPRF     RSTC
```

```
          5.34          0.03      0.03       0.03    0.03        2.0
        CC
        CC  FOR IMES=4 ,THE INI. TIME STEP,CONC. TOLERANCE,MAX.,MIN. TIME STEPS
        *----  DT           DCLIM       CNMAX      CNMIN
             0.0001       12*0.01      0.1         0.01
        CC******     INJECT surfactant **********************
        CC FLAG FOR INDICATING BOUNDARY CHANGE
        *---- IBMOD
             0
        CC
        CC  IRO, ITIME, NEW FLAGS FOR ALL THE WELLS
        *----  IRO    ITIME     IFLAG
             2       1        1  2
        CC
        CC  NUMBER OF WELLS CHANGES IN LOCATION OR SKIN OR PWF
        *----  NWEL1
              0
        CC
        CC  NUMBER OF WELLS WITH RATE CHANGES, ID
        *---- NWEL2     ID
             1        1
        CC
        CC  ID,INJ. RATE AND INJ. COMP. FOR RATE CONS. WELLS FOR EACH PHASE (L=1,3)
        *----  ID      QI(M,L) water oil  surf polymer Chlor divalent  cl            ca                    na       pH
carbonate  hAo
             1    0.00002592  1.0   0.  0.0   0.    0.3419  0. 0.    0.  0.3419   8   0.0     0
             1      0.    0.    0.   0.    0.        0.    0.    0.    0.      0.    0.     0.    0.
             1      0.    0.    0.   0.    0.        0.    0.    0.    0.      0.    0.     0.    0.
        CC
        CC  CUM. INJ. TIME , AND INTERVALS (PV) FOR WRITING TO OUTPUT FILES
        *---- TINJ          CUMPR1         CUMHI1      WRHPV      WRPRF     RSTC
            5.735          0.03      0.03       0.03    0.03        2.0
        CC
        CC  FOR IMES=4 ,THE INI. TIME STEP,CONC. TOLERANCE,MAX.,MIN. TIME STEPS
        *----  DT           DCLIM       CNMAX      CNMIN
      0.0001       12*0.01      0.1         0.01
```

REFERENCES

Adkins S., Liyanage P., Pinnawala Arachchilage G. W. P., Mudiyanselage T., Weerasooriya U., and Pope G.. 2010. A New Process for Manufacturing and Stabilizing High-Performance EOR Surfactants at Low Cost for High-Temperature, High-Salinity Oil Reservoirs. Proceedings of SPE Improved Oil Recovery Symposium.

Adibhatla, B. & Mohanty, K.K. 2008. Oil Recovery from Fractured Carbonates by Surfactant Aided Gravity Drainage: Laboratory Experiments and Mechanistic Simulations. *SPE Res Eval & Eng*, **11**(1): 119-130. SPE 99773-PA. doi: 10.2118/99773-PA

Alvarado, D. A. and Marsden, S. S. Jr. 1979. Flow of Oil-in-Water Emulsions through Tubes and Porous Media, *Soc. Pet. Eng. J.*, 369–377.

Ameafule, J.O. and Handy, L.L.: "The Effect of Interfacial Tensions on Relative Oil Water Permeabilities of Consolidated Porous Media," paper SPE 9783 presented at the 1981 SPE/DOE Enhanced Oil Recovery Symposium, Tulsa, April 2-5.

Aronofsky, J. S., 1952. Mobility ratio—its influence on flood patterns during water encroachment, *Trans.*, AIME, **195**, 15-24.

Atkinson, H. 1927. Recovery of Petroleum from Oil Bearing Sands. U.S. Patent no. 1,651,311

Avnir, D., Farin, D. and Pfeiffer, P. 1984. *Nature* **308**, 261-263.

Barnes, A. L., 1962. The use of a viscous slug to improve waterflood efficiency in a reservoir partially invaded by bottom water, *J. Pet., Tech*., 1147-1153.

Bhuyan, D. 1989. Development of an Alkali/Surfactant/Polymer Compositional Reservoir Simulator. PhD dissertation, University of Texas, Austin, TX USA.

Brady R.M and Ball R.C. 1984. *Nature* **309,** 225-229.

Brigham,W. E and Smith,D. H. 1965.: Prediction of Tracer Behavior in Five-spot Flow. Paper No,1130 presented at the SPE Conference on Production Research and Engineering, Tulsa, OK, USA 3-4 May.

Bryan, J. and Kantzas, A. 2007. Enhanced Oil Recovery by Alkali-Surfactant Flooding. Paper SPE 110738 presented at the SPE Annual Technical Conference and Exhibition, Anaheim, CA USA, 11-14 November. doi: 10.2118/110738-MS.

Bryan, J., Mai, A., Kantzas, A. 2008. Investigation into the Processes Responsible for Heavy Oil Recovery by Alkali-Surfactant Flooding. Paper SPE 113993 presented at the SPE/DOE Symposium on Improved Oil Recovery, Tulsa, Oklahoma, USA, 20-23 April. doi:10.2118/113993-MS

Buckley, S.E. and Leverett, M.C. 1942. Mechanisms of Fluid Displacement in Sands. *Trans* AIME **146**, 107

Camilleri, D., Engelson, S., Lake, L.W., Lin, E.C., Ohnos, T., Pope, G.A., and Sepehrnoori, K. 1987a. Description of an Improved Compositional Micellar/Polymer Simulator. *SPE Res. Eng.* **2** (4): 427-432.

Caudle, B. H. and Witte, M. D. 1959. Production Potential Changes During Sweep-Out in a Fivespot System, *Trans*., AIME, **216**, 446-448.

Cayias J. L., Schechter R. S., and Wade W. H. 1976. Modeling Crude Oils for Low Interfacial Tension. SPE 5813 Paper presented at the SPE/AIME IOR Symposium, Tulsa, Oklahoma. 22-24 March.

Chang, H. L. 1978. Polymer flooding technology—yesterday, today and tomorrow, *J. Pet.Tech*., **30** (8), 1113−1128.

Chouke, L., Van Meurs, P., and Van Der Poel, C. 1959. The instability of slow, immiscible, viscous liquid-liquid displacements in permeable media. *Trans.* AIME **216**, 188 (1959).

Caudle, B.H., Slobod, R.L. and Brownscombe, E.R. 1951. Further Developments in the Laboratory Determination of Relative Permeability. *J Petr Tech* **3**(5).

Claridge, E.L. 1972. Discussion of the Use of Capillary Tube Networks in Reservoir Performance Studies. *SPEl* 352-53.

CMG IMEX 2010 User's Guide, Computer Modelling Group.

CMG STARS 2010 User's Guide, Computer Modelling Group.

Cooper, R.J., 1971. The Effect of Temperature on the Caustic Displacement of Crude Oil. Paper SPE 3685 presented at the SPE AIME 41st Annual California Regional Meeting, Los Angeles, 4-5 November.

Cooke, C. E. Jr., William, R. E. and Kolodzie, P.A., 1974. Oil Recovery by Alkaline Waterflooding, *J. Pet. Tech*., 1365–1374.

Coskuner, G. and Bentsen, R.G. 1987. A New Stability Theory for Designing Graded Viscosity Banks. *J Can. Petr. Tech*. 26-30.

Craig, F. F. Jr., Gefen, T. M. and Morse, R. A. 1955. Oil recovery performance of pattern gas on water injection operations from model tests, *Trans*. AIME, **204**, 7-15.

Craig, F. F. Jr. 1971. The reservoir engineering aspects of waterflooding, Monograph Series. 3, SPE, Richardson, TX.

Christie, M.A. and Bond, D.J. 1987. Detailed Simulation of Unstable Processes in Miscible Flooding. *SPERE* 514-22; *Trans.,* AlME, **283.**

Dawson, R. and Lantz, R. B. 1972. Inaccessible pore volume in polymer flooding, *Soc. Pet.Eng. J*., 448-452.

Detling, K. D.,1944. Process of recovering oil from oil sand, U. S. Patent No. 2,341,500,

Delshad, M., Pope, G.A., and Sepehrnoori, K. 1996. A Compositional Simulator for Modeling Surfactant Enhanced Aquifer Remediation. Journal of Contaminant Hydrology, 23, 303-327.

DOE Office of Petroleum Reserves-Strategic Unconventional Fuels, Fact Sheet: US Heavy Oil Resource Potential, June 2007.

Dranchuk, P. M., Scott, J. D. and Flock, D. L. 1974. Effect of the Addition of Certain chemicals on Oil Recovery during Waterflooding, *J. Can. Pet. Tech*., 27–36.

Dyes, A. B., Caudle, B. H. and Erickson, R. A. 1954. Oil production after breakthrough as influenced by mobility ratio, *Trans.*, AIME, **201**, 81-86.

Ehlrich, R., Hasiba, H. and Raimondi, P. 1974. Alkaline Waterflooding for Wettability Alteration. *J.Pet. Tech.*: 1335-1343.

Engelberts, W.F. and Klinkerberg, L.J.. 1951. Laboratory experiments on the Displacement of Oil by Water from Packs of Granular Material. Proceedings Third World Petr. Congress, Section II, 544-554.

Falls, A.H., Thigpen, D.R., Nelson, R.C., Ciaston, J.W., Lawson, J.B., Good, P.A., Ueber, R.C., Shahin, G.T. 1994. Field Test of Cosurfactant-Enhanced Alkaline Flooding. *SPE Res Eng,* **9**(3): 217-223. SPE 24117-PA. doi: 10.2118/24117-PA

Fayers, FJ. 1988. An Approximate Model With Physically Interpretable Parameters for Representing Miscible Viscous Fingering *SPERE* 551-58; *Trans.,* AIME, **285**.

Fayers, FJ. and Newley, T.M.J. 1988. Detailed Validation of an Empirical Model for Viscous Fingering With Gravity Effects. *SPERE* 542-50; *Trans.,* AIME, **285**.

Flaaten, A.A., Nguyen, Q.P., Zhang, J., Mohammadi, H., and Pope, G.A. 2008. ASP Chemical Flooding Without the Need for Soft Water. Paper SPE 116754 presented at the SPE Annual Technical Conference and Exhibition, Denver, Colorado, 21-24 September. doi: 10.2118/116754-MS.

Flaaten, A.A., Nguyen, Q.P., Zhang, J. and Pope, G.A. 2008. A Systematic Laboratory Approach to Low Cost High Performance Chemical Flooding. Paper SPE 113469 presented at the SPE IOR Symposium, Tulsa, Oklahoma, April 2008.

Ferer M., Sams, W.N., Geidbrecht, R.A. and Smith, D.H. 1995. Fractal Nature of Viscous Fingering in Two Dimensional Pore Level Models. *AICHE J*. **41**(4) 749-763.

Gardner, J.W. and Ypma, J.G.J. 1982. An Investigation of Phase Behavior Macroscopic Bypassing Interaction in CO_2 Flooding. Paper SPE 10686 presented at the SPE IOR Symposium, Tulsa April 4-7.

Green, D. W. and Willhite, G. P. 1988. Enhanced oil recovery, SPE Textbook Series, Volume 6, Society of Petroleum Engineers, Richardson, TX, USA.

Gogarty, W. B., 1967. Mobility control with polymer solutions, *Soc. Pet. Eng. J.*, 161-170.

Giordano, R.M. and Salter, S.J. The Effects of Dispersion and Phase Behavior on Unfavorable Mobility Ratio Displacements. Paper SPE 13165 available at SPE, Richardson, TX.

Hallam, R.J., Plekenbrock, E.J., Abou-Sayed, A.S., Garon, A.M., Putnam, T.W., Weggeland, M.C., Webb, K.J. 1992. Resource Description and Development Potential of the Ugnu Reservoir, North Slope, Alaska. *SPE Form Eval* **7** (3): 211-218. SPE-21779-PA. doi: 10.2118/21779-PA.

Haan, H.J. 1959. Effect of Capillary Forces in the Water-Drive Process. *Proc.,* Fifth World Pet. Cong., New York City (1959) Sec IT, 319-35

Healy, R.N. and Reed, R.L. 1977. Immiscible Microemulsion Flooding. *SPE J.* **17 (**2): 129-139. SPE-5817-PA. doi: 10.2118/5817-PA.

Hand, D.B. 1939. Dineric Distribution of a Consulate Liquid between Two Immiscible Liquids. *J. of Physics and Chemistry*, Volume 34, pp 1961-2000.

Hirasaki, G.J., Miller, C.A., and Puerto, M. 2008. Recent Advances in Surfactant EOR. Paper 115386 presented at the SPE Annual Technical Conference and Exhibition, Denver, Colorado, 21-24 September. doi: 10.2118/115386-MS.

Hoar, T.P and Schulman. J.H. 1943. Transparent Water in Oil Dispersions: the oleopathic hydro-micelle. *Nature* 152. 102-103.

Hsieh W. C., and Shah D. O. 1976. The Effect of Chain Length of Oil and Alcohol As Well as Surfactant to Alcohol Ratio on the Solubllization, Phase Behavior and Interracial Tension of Oil / Brine / Surfactant / Alcohol Systems. *SPEJ* 6594.

Huang A.B, Chikhliwala E.D., and Yortsos Y.C., "Linear stability analysis of immiscible displacements including continuously changing mobility and capillary effects: Part II General basic profiles," SPE Paper 13163, 59th Annual Meeting, Houston, TX (1984).

Hughes, D.S. 1987. An Analytical Model of Unstable Immiscible Flow. Copyright SPE.

Jackson A.C. 2006. Experimental Study of the Benefits of Sodium Carbonate on Surfactants for Enhanced Oil Recovery. M.S. Thesis at the University of Texas at Austin.

Jennings, H.Y. 1966. Waterflood Behavior of High Viscosity Crudes in Preserved Soft and Unconsolidated Cores. *J.Pet. Tech.* **18** (1): 116-120. SPE 1202-PA. doi: 10.2118/1202-PA.

Jennings, H. Y. Jr., Johnson, C. E. Jr., and McAuliffe, C. D., 1974. A Caustic Waterflooding Process for Heavy Oils, J. Pet. Tech., 1344–1352.

Jewett, R. L. and Schurz, G. F. 1970. Polymer flooding—a current appraisal, J. Pet. Tech., 22(6), 675−684.

Johnson, C. E. Jr. 1976. Status of Caustic and Emulsion Methods, J. Pet. Tech. 28 (1): 85-92. SPE 5561-PA.

Jones, S.C and Dreher, K.D. 1976. Co-solvents in Miceller Systems used for Tertiary Oil Recovery, SPEJ 161-167.

Kumar, M., Hoang, V. and Satik, C. 2005. High Mobility Ratio Waterflood Performance Prediction: Challenges and New Insights. SPE Res Eval & Eng 11 (1): 186-196. SPE 97671-PA. doi: 10.2118/97671-PA.

Kokal, S. 2002, Crude Oil Emulsions: A State-Of-The-Art Review. Paper SPE 77497 presented at the SPE Annual Technical Conference and Exhibition, San Antonio, Texas, September 29-October 2.

Koval. E.J. 1963. A Method for Predicting the Perfonnancc of Unstable Miscible Displacement in Heterogeneous Media. SPEJ 145-49; Trans.. AlME. 228.

Levitt, D.B., Jackson, A.C., Heinson, C., Britton, L.N., Malik, T., Dwarakanath, V., Pope, G.A. 2006. Identification and Evaluation of High-Performance EOR Surfactants. SPE Re.s Eng., 12(2): 243-253. SPE 100089-PA. doi: 10.2118/100089-PA

Lake, L. 1989. Enhanced Oil Recovery. Englewood Cliffs, New Jersey: Prentice Hall

Lefebvre de Prey, E.J.: "Factors Affecting Liquid-Liquid Relative Permeabilities of a Consolidated Porous Medium," SPEJ (Feb. 1973) 39-47

LeGuen, S.S. and Kovscek, A.R. 2006. Nonequilibrium Effects During Spontaneous Imbibition, Transport in Porous Media, 63: 127-146.

Lee, S.T., Gary LI, K.M., Culham, W.E. 1984. Stability Analysis of Miscible Displacement Process. SPE/DOE 12531 presented at the SPE/DOE 4th Symposium on Enhanced Oil Recovery, Tulsa, OK, Apr 15-18.

Lenormand, R., Touboul, E. and Zarcone, C. 1988. Numerical models and experiments on immiscible displacements in porous media, J. Fluid Mechanics, 189: 165-187.

Liu, Q., Dong, M., and Ma, S. 2006. Alkaline/Surfactant Flood Potential in Western Canadian Heavy Oil Reservoirs. Paper SPE 99791 presented at the SPE/DOE Symposium on Improved Oil Recovery, Tulsa, Oklahoma, 22-26 April. doi: 10.2118/99791-MS.

Liu, Y. and Buckley, J.S. 1997. Evaluation of Wettability Alteration by Adsorption from Crude Oils, SPE Formation Evaluation 12: 5-12.

Maerker, J. M. 1973. Dependence of polymer retention on flow rate, *J. Pet. Tech*., 1307-1308.

Mai, A. and Kantzas, A. 2008. Improved Heavy Oil Recovery by Low Rate Waterflooding. Paper SPE 117648 presented at the International Thermal Operations and Heavy Oil Symposium, Calgary, Alberta, Canada, 20-23 October. doi: 10.2118/117648-MS.

Maini, B. 1998. Is It Futile to Measure Relative Permeability For Heavy Oil Reservoirs? *J. Canad. Pet. Tech.* **37** (4): 56-62.

Maloy, K.J., Feder, J, and Jossang, T. 1985. Viscous Fingering Fractals in Porous Media. *Phys. Rev. Lett*. **55**, 2688.

Mandelbrot, B.B. 1982. The Fractal Geometry of Nature, Freeman, New York.

Marques, C., Castanier, L.M., and Kovscek, A.R. 2009. Thaw Front Dynamics and Super Insulated Wells for Thermal Recovery in Cold Environments. Paper SPE 121059 presented at the SPE Western Regional Meeting, San Jose, California, 24-26 March. doi: 10.2118/121059-MS.

Martin, F.D. and Oxley, J.C. 1985. Effect of Various Alkaline Chemicals on Phase Behavior of Surfactant/Brine/Oil Mixtures. Paper SPE 13575 presented at the International Symposium on Oilfield and Geothermal Chemistry, Phoenix, AZ, USA, 9-11 April. doi: 10.2118/13575-MS.

Matsushita, M., Sano, M., Hayakawa, Y., Honjo, H. and Sawada, Y. 1984. *Phys Rev. Lett.* **53,** 286-289.

Mattax, C.C. and Kyte, J.R. 1962. Imbibition oil recovery from fractured, water-drive reservoir, *SPE J.,* 2: 177-184.

McAuliffe, C. D., 1973a. Oil-in-Water Emulsions and Their Flow Properties in Porous Media*, J.Pet. Tech*. **25** (6), 727–733.

McAuliffe, C. D., 1973b. Crude Oil-in-Water Emulsions to Improve Fluid Flow in an Oil Reservoir*, J.Pet. Tech*. **25** (6), 721–726.

Meurs, P.V and Poel, C.V. 1958. A Theoretical Description of Water Drive Processes Involving Viscous Fingering. SPE 931-G

Miller, K. A. 1987. EOR pilot review—Husky experience, paper No. 11, presented at the firstannual South Saskatchewan Section, the Petroleum Society of CIM, ReginaSaskatchewan, Canada, October 6−8.

Miller, K.A. 2006. Improving the State of the Art of Western Canadian Heavy Oil Waterflood Technology, *J.Canad. Pet. Tech.* **45** (4): 7-11.

Mohammadi, H., Delshad, M. and Pope, G.A. 2009. Mechanistic Modeling of Alkali/Surfactant/Polymer Floods. *SPE REE*, pp 518-527.

Mungan, N. 1966. Interfacial Effects in Immiscible Liquid-Liquid Displacements in Porous Media. *Soc. Pet. Eng. J*. **237**. 247-253. *Trans. AIME*

Needham, R. B. and Doe P. H. 1987. Polymer flooding review, *J. Pet. Tech*., **39** (12), 1503−1507.

Nelson, R.C. and Pope, G.A. 1978 Phase Relationships in Chemical Flooding. *SPE J*. **18** (5): 325-338. SPE-6773-PA. doi: 10.2118/6773-PA

Nelson, R.C., Lawson, J.B., Thigpen, D.R., Stegemeier, G.L. 1984. Cosurfactant-Enhanced Alkaline Flooding. Paper SPE 12672 presented at the SPE Enhanced Oil Recovery Symposium, Tulsa, Oklahoma, 15-18 April. doi: 10.2118/12672-MS.

Nittmann, J., Daccord, G., and Stanley, H.E. 1985. Fractal Growth of Viscous Fingers: Quantitative Characterization of a Fluid Instability Phenomenon. *Nature*, **314**, 141

Nutting, P. G. 1925. Chemical Problems in the Water-driving of Petroleum Reservoirs, *Ind.Eng. Chem*., **17**, 1035–1036, 1925.

Osaba, J.S., Richardson, J.G., Kerver, J.K., Hafford, J.A. and Blair, P.M. 1951. Laboratory Measurements of Relative Permeability. *J of Petr. Tech.* **3**(2).

Ottewill, R.H., 1967. Effect of nonionic surfactant on the stability of dispersions. In: M. Schick (Editor), Nonionic Surfactant. Marcel Dekker, New York, pp. 627-680.

Palit. S.R., Moghe. V.A., and Biswas, B. 1959. *Trans. Faraday Soc.* 55:463.

Paterson, L. 1984. Diffusion-Limited Aggregation and Two-Fluid Displacements in Porous Media. *Phys. Rev. Lett*. **52**, 1621–1624.

Peaceman, D.W. and Rachford, Jr. H.H. 1962. Numerical Calculation of multidimensional Miscible Displacement. *SPE J.* **2**(4).

Perkins, T.K., Johnston, O.C. and Hoffman, R.N. 1965. Mechanics of Viscous Fingering in Miscible Systems. *SPEJ* 501-17 *Trans.* AIME, **239.**

Perrine, R.L. 1961. The Development of Stability Theory for Miscible Liquid-Liquid Displacement. *SPE J.* 17-25. *Trans.* AIME, **222**

Peters, E.J. and Flock, D.L. 1981. The Onset of Instability during the Two Phase Immiscible Displacements in Porous Media. *SPE J.* 831.

Peters, E.J., Khatanair, S. 1987 The effect of instability on relative permeability curves obtained by the dynamic displacement method. *SPE Formation Evaluation* **2**(4).

Peyton, H.R. 1970. Arctic Engineering. J. Pet. Tech. **22** (9): 1076-1082. SPE-2701-PA. doi:10.2118/2701-PA.

Pope, G.A., Wang, B., Tsaur, K. 1979. A Sensitivity Study of Micellar/Polymer Flooding. *SPE J* **19** (6): 357-368. SPE-7079-PA. doi: 10.2118/7079-PA.

Pope, G.A. and Nelson, R.C. 1978. A Chemical Flooding Compositional Simulator. *SPE J*. **18**(5). 339-354. SPE 6725-PA.

Pye, D. J., 1964. Improved secondary recovery by control of water mobility, *J. Pet. Tech*., **16** (8), 911−916.

Rachford, H.H. 1964. Instability in Water Flooding Oil from Water –Wet Porous Media Containing Connate Water. SPE 684 Paper presented at SPE ATCE, New Orleans Oct 6-9.

Reisberg, J. and Doscher, T.M. 1956. Interfacial Phenomena in Crude Oil Water Systems. Prod Monthly 43-50 (Nov.)

Rekvig, L., Kranenberg, M., Hafskjold, B., Smit, B. 2003. Effect of Surfactant Structure on Interfacial Properties. *Europhysics Letters*. **63** (6) 902-907.

Riaz A. and Tchelepi, H.A. 2005. Numerical Simulation of Immiscible Two-Phase Flow in Porous Media, *Phys. Fluids.* **18.**

Riaz A. and Tchelepi, H.A. 2006. Influence of Relative Permeability on the Stability Characteristics of Immiscible Flow in Porous Media, *Trans. Porous Media* **64**, 315-338

Rosen, M.J. 2004. Surfactants and Interfacial Phenomena. Third edition. New York. John Wiley and Sons.

Ruckenstein, E. 1996. Microemulsions, Macroemulsions, and Bancroft's Rule, Langmuir, 12 (26): 6351-6353.

Saffman, P.G. and Taylor, G. 1958. The Penetration of a Fluid into a Porous Medium or Hele-Shaw Cell Containing a More Viscous Liquid. Proc. R. Soc. Lond. **245** 312-329.

Sahni V., Dean R. M., Britton C., Kim D. H., Weerasooriya U., and Pope A., 2010. The Role of Co-Solvents and Co-Surfactants in Making Chemical Floods Robust. Paper SPE 130007 presented at the SPE Improved Oil Recovery Symposium, Tulsa, Oklahoma 24-28th April 2010.

Salagar, J.L., Morgan, J.C., Schechter, R.S., Wade, W.H., and Vasquez, E. 1979. *SPE J.,* **19**(2): 107-115. SPE 7054-PA. doi: 10.2118/7054-PA

Salager, J-L., Marquez, L., Pena, A.A., Rondon, M., Silva, F. and Tyrode, E. 2000. Current Phenomological Know-How and Modeling of Emulsion Inversion, Ind. Eng. & Chem. Res., 39 (8): 2665-2676.

Sandberg, C.R., Gourney, L.S. and Sippel, R.F. 1958. Effect of Fluid flow rate and viscosity on Laboratory determinations of oil water relative permeabilities. *Trans* AIME **213**, 36-43.

Sandiford, B. B.,1964. Laboratory and field studies of water floods using polymer solutions to increase oil recoveries, *J. Pet. Tech*., **16** (8), 917−922.

Satoh, T. 1984. Treatment of Phase Behavior and Associated Properties used in Micellar-Polymer Flood Simulator. M.S. thesis, University of Texas at Austin, Austin, Texas, U.S.A.

Schembre ,J.M. and Kovscek,A.R 2003. A Technique for Measuring Two Phase Relative Permeability in Porous Media via X-ray CT Measurements. *J. Pet. Sci. & Engg*. **39** (1): 159-174.

Seright, R.S. 2010. Potential for Polymer Flooding Reservoirs With Viscous Oils. Paper presented at the SPE Improved Oil Recovery Symposium, Tulsa, Oklahoma, 24-28 April. doi: 10.2118/129899-MS

Settari, A. and Karcher, B. 1985. Simulation of Enhanced Recovery Projects-the Problems and the Pitfalls of the Current Solutions. *J Can. Pet. Tech*. **24**(6).

Shinoda, K. (Editor), 1967. Solvent Properties of Surfactant Solutions. Marcel Dekker, New York.

Shutang, G., Qiang, G., Lin, J. 2010. Recent Progress and Evaluation of ASP Flooding for EOR in Daqing Oil Field. Paper presented at the SPE EOR conference at Oil and Gas West Asia, Muscat, Oman, 11-13 April. doi: 10.2118/127714-MS

Sigmund, P., Sharma, H., Sheldon, D. and Aziz, K. 1988. Rate Dependence of Unstable Waterfloods. *SPE Res. Engg*. 401-409.

Smith, F. W., 1970. The behaviour of partially hydrolyzed polyacrylamide solution in porous media, *J. Pet. Tech*., 148-156.

Skauge A., and Fotland P. 1990. Effect of Pressure and Temperature on the Phase Behavior of Microemulsions. (November), pp. 601–608.

Squires F., 1917. Method of Recovering Oil and Gas. U.S. Patent No. 1,238,355

Soo, H. and Radke, C. J. 1984. The Flow Mechanism of Dilute, Stable Emulsion in Porous Media, *Ind. Eng. Chem. Fundam*., **23**(3), 342–347.

Solairaj S., Britton C., Lu J., Kim D. H., Weerasooriya U., and Pope A. 2012. New Correlation to Predict the Optimum Surfactant Structure for EOR," SPE 154262 Paper presented at the SPE IOR Symposium in Tulsa, OK. April 14-18.

Stanley, H.E., *Fractals in Statistical Physics*, New York 1985.

Stegemeier, G.L. 1977. *Mechanism of Entrapment and Mobilization of Oil in Porous Media*. New York City: Academic Press.

Sufi, A.S., Ramey, H.R. and Brigham, W.E.: "Temperature Effects on Relative Permeabilities of Oil Water Systems." Paper SPE 11071 presented at the 1982 SPE Annual Conference and Exhibition, New Orleans, Sept 26-29.

Sun, R. and Shook, C.A. 1996. Inversion of Heavy Crude Oil-in-Brine Emulsions. J. Petro. Sc. and Eng. **14.** 169-182.

Subkow, P. 1942. Process for the Removal of Bitumen from Bituminous Deposits. U.S Patent No. 2,288,857.

Symonds, R.W., Farouq Ali, S.M. and Thomas, S. 1991. A Laboratory Study of Caustic Flooding for Two Alberta Crude Oils. *J.Cdn.Pet.Tech*, 3**0** (1).

Szabo, M. T., 1975. Some aspects of polymer retention in porous media using a C14-tagged hydrolyzed polyacrylamide, Soc. Pet. Eng. J., 322-337.

Tan, C.T. and Homsy, G.M. 1986. Stability of miscible displacements in porous media: Rectilinear flow. Phys. Fluids **29**, 3549.

Tan, C.T. and Homsy, G.M. 1988. Simulation of nonlinear viscous fingering in miscible displacement. Phys. Fluids **31**, 1330.

Todd, M.R. and Longstaff, J.W. 1972. The Development, Testing, and Application of a Numerical Simulator for Predicting Miscible Flood Performance *JPT* 874-78; *Trans.,* AIME, **253.**

Thomas, S. and Ali S.M.F. 2001. Miceller Flooding and ASP-Chemical Methods for Enhanced Oil Recovery. *J.Cdn.Pet.Tech*, **40** (2).

UTCHEM .2000. User's Guide, The University of Texas at Austin, Austin, TX U.S.A.

Wang, J., Dong, M. and Asghari, K. 2006. Effect of Oil Viscosity on Heavy-Oil Relative Permeability Curves. Paper SPE 99763 presented at the SPE/DOE Symposium on Improved Oil Recovery, Tulsa, Oklahoma, USA, 22-26 April. doi:10.2118/99763-MS

Wang, J. and Dong, M. 2007. A Laboratory Study of Polymer Flooding for Improving Heavy Oil Recovery, paper presented at the Petroleum Society's 8th Canadian International Petroleum Conference, Calgary, Alberta, Canada, June 12– 14.

Wang, J. and Dong, M. 2009a Optimum effective viscosity of polymer solution for improving heavy oil recovery, Journal of Petroleum Science and Engineering, **67**, 155-158.

Wagner O.R and Leach R.O., 1959. Improving Oil Displacement by Wettability Adjustment. Trans. AIME 216, 65-72.

Wassmuth, F. R., Arnold, W., Green, K., Cameron, N. 2007. Polymer flood application to improve heavy oil recovery at East Bodo, Paper 2007-184, presented at the Petroleum Society's 8th Canadian International Petroleum Conference, Calgary,Albert, Canada, June 12–14.

Willhite, G. P. and Dominguez, J. G. 1976. Mechanisms of polymer retention in porous media, paper presented at the AIChE Symposium on Improved Oil Recovery bySurfactant and Polymer Flooding, Kansas City, KS, U.S.A., April.

Wilson, E.D. 1972. Some Aspects of Arctic Oil Pipe Line Research. Paper SPE 1972-061 presented at the SPE Annual Technical Meeting, Calgary, Alberta, 16–19 May. doi:10.2118/1972-061.

Winsor, P., 1954. Solvent Properties of Amphilic Compounds. Butterworths, London.

Witten, T.A., and Sanders, L.M. 1981 Diffusion Limited Aggregation, a Kinetic Critical Phenomenon. *Phys. Rev. Lett*., **47**, 1400.

Yang, H., Britton, C., Liyanage, P.M., Solairaj, S., Kim, D.H., Nguyen, Q., Weerasooriya, U., Pope, G.A. 2010. Low-Cost, High-Performance Chemicals for Enhanced Oil Recovery. Paper presented at the SPE Improved Oil Recovery Symposium, Tulsa, Oklahoma, 24-28 April. doi: 10.2118/129978-MS

Yorstsos Y.C. and Huang, A.B. 1986. Linear Stability of Immiscible Displacement in Porous Media, *SIAM J*. **49**(3), 730

Zhao P., Jackson A. C., Britton C., Kim D. H., Britton L. N., Levitt D. B., and Pope G., 2008. Development of High-Performance Surfactants for Difficult Oils. SPE 13432 Paper presented at the SPE IOR Symposium, Tulsa, Oklahoma.